



The
University
Of
Sheffield.

**Development of the Conform™ process for the recycling of waste titanium
into wire**

Sarah Anne Smythe

A thesis submitted in partial fulfilment of the requirements for the degree of
Doctor of Philosophy

The University of Sheffield
Faculty of Science and Engineering
Department of Materials Science and Engineering

February 2021

Acknowledgements

I would like to thank my supervisors, Prof. Martin Jackson (The University of Sheffield) and Matt Lunt (DSTL), for all the support and guidance throughout my project, without whom I would not have been able to complete this PhD. Additionally, both EPSRC and DSTL for the funding supplied for the work.

For the work carried out in this thesis, I would like to thank BWE Ltd., Ashford, UK for access to the ConformTM machine and their technical assistance, and Airbus for providing swarf for ConformTM trials.

Thank you, Dr Ben Thomas, for the additional supervision and assistance throughout, and to my colleagues in the STAR research group, thank you for the help and support throughout the project, especially when I was stressed and panicking in the office.

To my fellow PhD students and staff at the University of Sheffield, Stavrina Dimosthenous, Tes Monaghan, Daniel Button and Claire Healey, thank you for letting me rant and complain, taking me for large volumes of coffee and just being incredibly supportive throughout.

And finally, to my family and friends, especially Mum and Andy, Emma, Grandad, Simon, Rebecca and Nafisa, you supported me throughout, you kept me going and I would not have gotten this far without you.

Abstract

The ConformTM process was first established in the early 1970's for the recycling of copper and aluminium rod. Since then, the process has been developed further with the expansion into powder feedstocks and other materials such as titanium, magnesium and zinc. However, there are still significant gaps in the understanding of ConformTM – particularly for high strength feedstocks such as titanium alloys.

This work sets out to develop the ConformTM process for titanium particulate feedstocks including machining swarf, in order to provide scientific insight into the challenges and process parameter requirements for the next stage of industrialisation.

Through the use of discrete element modelling and experimental trials, bespoke toolsets were designed for use in the ConformTM machine and their effectiveness discussed. In this work it was shown that different powder feedstocks require different toolset geometries in order to increase the chance of extruding a consolidated product. This was further influenced by a small-scale testing rig, which assessed the densification and consolidation of powder feedstocks used in the ConformTM process and helped to determine the 'Conform-ability'. This testing rig, known as the Arbitrary Strain Path (ASP) test machine, used bespoke tooling to replicate similar conditions to those found in the ConformTM machine, in that the feedstocks undergo both load and shear during processing.

Large scale trials methods were completed using a ConformTM 350i at BWE Ltd., Ashford, UK. The trials were conducted using bespoke tooling designed for this project and resulted in, in a number of cases, the successful extrusion of a titanium rod product. The experimental data from each trial was recorded and analysed to attempt to show further insight into the ConformTM process and demonstrate how this can influence the parameters used during a trial.

The results showed that the spherical particles require more pressure to consolidate, and when coupled with the results from the simulations and experimental trials, this has shown that the smaller ConformTM toolset is more appropriate. By using the ASP and DEM simulations, there is a significant reduction in the costs of experimental testing, as the large ConformTM toolsets

can cost upwards of £10000, whereas the small-scale testing and computational modelling fall in the £100s.

Large scale extrusion trials were conducted on Ti-6Al-4V swarf and Ti-6Al-4V GA. The microstructure of the products often demonstrated an equiaxed fine-grained structure with grain sizes $< 20 \mu\text{m}$ and limited porosity. This was reflected in the mechanical properties, which, in the case of the extruded CP Ti HDH Gr 2 feedstock, were closer to CP Ti HDH Gr 4. These results would meet requirements for additive manufacturing feedstocks and therefore the wire holds the potential of being used for downstream welding and wire-based additive manufacturing processes. This in turn highlights a potential recycling stream for aerospace waste.

Overall, the thesis provides a novel, small-scale testing method for determining whether a feedstock would be suitable for ConformTM and the conditions under which it should be processed, resulting in significant cost savings. The work also develops understanding of the processing occurring during ConformTM with an insight into the trial data and how this can be analysed to provide details about the optimum extrusion parameters. Finally, the project, for the first time, reports the extrusion of waste titanium feedstocks, including swarf, into a potential product for wire-based additive manufacturing.

Declaration

I, the author, confirm that the Thesis is my own work. I am aware of the University's Guidance on the Use of Unfair Means (www.sheffield.ac.uk/ssid/unfair-means). This work has not previously been presented for an award at this, or any other, university.

Table of Contents

| | |
|---|-------------|
| <i>Acknowledgements</i> | <i>i</i> |
| <i>Abstract</i> | <i>ii</i> |
| <i>Declaration</i> | <i>iii</i> |
| <i>Table of Figures</i> | <i>ix</i> |
| <i>Table of Tables</i> | <i>xvi</i> |
| <i>List of Abbreviations</i> | <i>xvii</i> |
| Chapter 1 : Introduction | 1 |
| 1.1 Aims & Objectives | 4 |
| 1.2 Thesis Structure | 5 |
| Chapter 2 : Literature Review | 7 |
| 2.1 Titanium | 7 |
| 2.1.1 Structure..... | 7 |
| 2.1.2 Extraction..... | 10 |
| 2.1.3 Powder Metallurgy | 13 |
| 2.1.4 Uses | 14 |
| 2.2 Severe Plastic Deformation | 15 |
| 2.2.1 Methods | 16 |
| 2.3 ConformTM | 25 |
| 2.3.1 Conform TM of rod feedstock..... | 27 |
| 2.3.2 Conform TM of particulate feedstocks | 27 |
| 2.3.3 Simulating the Conform TM process..... | 29 |
| 2.3.4 Recycling | 32 |
| 2.4 Powder Metallurgy | 33 |
| 2.4.1 Powder characterisation methods | 34 |
| 2.4.2 Shear Testing..... | 34 |
| 2.4.3 Powder behaviour under shear | 35 |
| 2.5 Wire | 38 |
| 2.5.1 Production..... | 38 |
| 2.5.2 Uses | 39 |
| 2.5.3 Additive manufacturing | 40 |

| | | |
|---|---|-----------|
| 2.6 | Summary..... | 43 |
| Chapter 3 : Materials and Methodologies | | 45 |
| 3.1 | Materials | 45 |
| 3.2 | Powder Characterisation..... | 46 |
| 3.2.1 | Angle of Repose | 46 |
| 3.2.2 | Bulk/Tap Density..... | 47 |
| 3.2.3 | Particle Size Distribution | 48 |
| 3.2.4 | Powder Imaging | 48 |
| 3.3 | Mechanical Testing..... | 48 |
| 3.3.1 | Metallurgical Preparation..... | 48 |
| 3.3.2 | Light Microscopy | 49 |
| 3.3.3 | Tensile Testing | 49 |
| 3.3.4 | Microhardness Indenting..... | 49 |
| 3.4 | Arbitrary Strain Path Machine..... | 49 |
| 3.4.1 | Calibration..... | 51 |
| 3.4.2 | Testing | 52 |
| 3.4.3 | Analysis Method..... | 53 |
| 3.4.4 | Feedstocks..... | 54 |
| 3.5 | ConformTM Process..... | 55 |
| 3.6 | Discrete Element Modelling | 56 |
| 3.6.1 | Particle Development..... | 57 |
| Chapter 4 : Arbitrary Strain Path Testing..... | | 59 |
| 4.1 | Density..... | 61 |
| 4.2 | Displacement versus. Angle..... | 63 |
| 4.3 | Summary..... | 67 |
| Chapter 5 : The ConformTM Process | | 69 |
| 5.1 | Feedstocks | 69 |
| 5.2 | Tool Design | 69 |
| 5.2.1 | Swarf Trials..... | 71 |
| 5.2.2 | Spherical Powder Trials | 74 |
| 5.3 | Changes to the tooling | 74 |
| Chapter 6 : Discrete Element Modelling | | 76 |

| | |
|--|------------|
| Particle Development..... | 76 |
| 6.1 | 76 |
| 6.1.1 CP Ti HDH Gr 2..... | 76 |
| 6.1.2 Ti-6Al-4V GA..... | 80 |
| 6.1.3 Ti-6Al-4V Swarf..... | 82 |
| 6.2 ConformTM Tooling Simulation..... | 84 |
| 6.2.1 CP Ti HDH Gr 2 simulations..... | 86 |
| 6.2.2 Ti-6Al-4V GA simulations..... | 93 |
| 6.2.3 Ti-6Al-4V Swarf..... | 100 |
| 6.2.4 Summary..... | 107 |
| Chapter 7 : Experimental Trials..... | 110 |
| 7.1 Tooling..... | 110 |
| 7.2 Calculations..... | 112 |
| 7.3 Trials..... | 113 |
| 7.3.1 Trial 1..... | 113 |
| 7.3.2 Trial 2..... | 114 |
| 7.3.3 Trial 3..... | 117 |
| 7.3.4 Trial 4..... | 119 |
| 7.3.5 Trial 5..... | 120 |
| 7.3.6 Trial 6..... | 121 |
| 7.3.7 Trial 7..... | 122 |
| 7.3.8 Trial 8..... | 123 |
| 7.3.9 Trial 9..... | 125 |
| 7.3.10 Trial 10..... | 125 |
| 7.4 Comparison..... | 127 |
| 7.5 Optimum Parameters..... | 131 |
| Chapter 8 : Microstructure and Mechanical Properties..... | 132 |
| 8.1 Extruded Rod..... | 132 |
| 8.1.1 Trial 2 and Trial 3..... | 132 |
| 8.1.2 Trial 7..... | 133 |
| 8.1.3 Trial 8..... | 134 |
| 8.1.4 Trial 10..... | 134 |
| 8.2 Microstructural Analysis..... | 135 |
| 8.2.1 Trial 2..... | 136 |
| 8.2.2 Trial 8..... | 137 |

| | | |
|--|--|------------|
| 8.2.3 | Trial 10 | 139 |
| 8.3 | SEM and EDX | 141 |
| 8.3.1 | Trial 8 – Ti-6Al-4V GA | 141 |
| 8.3.2 | Trial 10 – Heat Treatment of Ti-6Al-4V swarf derived rod | 142 |
| 8.4 | Tensile Testing Results | 143 |
| 8.4.1 | Trial 8 | 145 |
| 8.4.2 | Trial 10 | 147 |
| 8.5 | Fractography | 148 |
| 8.6 | Microhardness Results | 151 |
| 8.6.1 | Trial 8 | 151 |
| 8.6.2 | Trial 10 | 153 |
| 8.7 | Summary..... | 154 |
| Chapter 9 : Conclusions..... | | 156 |
| Chapter 10 : Future Work..... | | 160 |
| 10.1 | Conform™ | 160 |
| 10.2 | Simulations..... | 161 |
| 10.3 | Annular Shear Testing..... | 162 |
| Chapter 11 : Bibliography..... | | 163 |
| Appendix 1: Recycling of Titanium Alloy Powders and Swarf through Continuous Extrusion (Conform™) into Affordable Wire for Additive Manufacturing | | 175 |
| 11.1 | Abstract..... | 175 |
| 11.2 | Keywords | 175 |
| 11.3 | Introduction | 176 |
| 11.4 | Materials and Methods..... | 180 |
| 11.4.1 | Powder Characteristics | 180 |
| 11.4.2 | Conform Extrusion..... | 182 |
| 11.4.3 | Cold Drawing | 184 |
| 11.4.4 | Characterisation | 185 |
| 11.5 | Results..... | 186 |
| 11.5.1 | Wiredrawing | 193 |
| 11.6 | Discussion..... | 195 |

| | | |
|-------------|---|------------|
| 11.7 | Conclusions | 197 |
| 11.8 | Acknowledgements | 198 |
| | <i>Appendix 2 CAD Drawings – ASP Tools.....</i> | <i>199</i> |

Table of Figures

| | |
|--|----|
| Figure 1 Schematic from the original 1973 Conform TM patent [1] | 1 |
| Figure 2 The various applications for wire produced with different mechanical property requirements. | 4 |
| Figure 3 Hexagonal Close-Packed (HCP) crystal structure and Body-Centred Cubic (BCC) crystal structure..... | 8 |
| Figure 4 Pseudo phase diagram of titanium taken from [19] | 9 |
| Figure 5 Schematic of the Kroll process. Taken from [24]..... | 11 |
| Figure 6 Schematic of the FFC process. Taken from [25]..... | 12 |
| Figure 7 Schematic of conventional Direct Extrusion taken from [50]..... | 17 |
| Figure 8 Schematic of Hydrostatic Extrusion taken from [50]..... | 18 |
| Figure 9 Schematic of High Pressure Torsion taken from [50]..... | 19 |
| Figure 10 Schematic of ECAP for bulk samples. Taken from [50]..... | 21 |
| Figure 11 Orientation maps for ECAP, showing the appearance of fine grains along old grain boundaries and a relatively coarse microstructure, taken from [67]..... | 22 |
| Figure 12 TEM of a Ti billet processed by ECAP for 8 passes (left) followed by cold rolling to a strain of 55%. (a) Cross-section and (b) longitudinal section. Taken from [68]. | 22 |
| Figure 13 Back-scattered electron images of the microstructure after ECAP and consequent annealing at 120°C taken from [72] White arrows (a) indicate the interface between the chips, yellow arrows (b) show the boundary without pores when white arrows (b) indicate the pores, green arrows (c, d) show the nano-pores at interface, when red arrows (c, d) indicate the submicron pores at interface..... | 23 |
| Figure 14 Bright-field TEM images of CP Ti after 1, 2, and 4 ECAP-C passes in cross and longitudinal sections. Cross section: (a) 1 pass, (c) 2 passes and (e) 4 passes; Longitudinal section: (b) 1 pass, (d) 2 passes and (f) 4 passes. Taken from [73]. | 24 |
| Figure 15 Photograph of a Conform TM machine produced by BWE Ltd., Ashford, UK. Taken from [78] | 25 |
| Figure 16 Schematic of a Conform TM continuous rotary extrusion machine..... | 26 |
| Figure 17 Schematic showing the adjustments made to the Conform TM process to allow for granular feedstocks. Taken from [75]. | 28 |
| Figure 18 Tool and simulation schematic, showing the assumptions made for the wheel as a straight section. Taken from the work of C Stadelmann [2]. | 31 |

| | |
|---|----|
| Figure 19 An example schematic of a Jenike shear cell tester; A is the base; B is the ring and C is the lid. Taken from [100] | 35 |
| Figure 20 Schematic showing the three stages of compaction, where (a) shows the rearrangement of particles, (b) shows the flattening and densification, and (c) shows neighbour contacts impinging the deformation. Taken from [101] | 36 |
| Figure 21 Diagram demonstrating the uses of metal wires and the quality required from them. | 39 |
| Figure 22 Schematic of a wire-fed deposition process taken from [125]. | 42 |
| Figure 23 Photograph (bottom) and corresponding simulation (top) of an Angle of Repose with CP-Ti Gr2 HDH..... | 47 |
| Figure 24 Photograph of the tools in the Arbitrary Strain Path (ASP) test machine | 50 |
| Figure 25 Schematic of the top and bottom tools used during a powder shear test..... | 51 |
| Figure 26 Light micrographs showing the morphologies of the powders used in this work. (Left) irregular morphology shown in the CP Ti HDH Gr 2 and Ti-6Al-4V HDH Gr 5 feedstocks, (Centre) spherical Ti-6Al-4V GA feedstock, and (Right) Ti-6Al-4V swarf..... | 55 |
| Figure 27 Photograph showing the ASP tooling (a) immediately after a test, demonstrating a thin foil film across the surface of the feedstock. (b) shows the unconsolidated feedstock underneath the film. | 61 |
| Figure 28 A schematic showing the change in the density of the powder (a) at the start of the test and (b) after testing, where the load and rotation has resulted in a drop in the displacement of the top tool into the bottom tool. | 61 |
| Figure 29 The change in density of the different feedstocks during ASP trials at different speeds. | 62 |
| Figure 30 The change in density of the different feedstocks during ASP trials at different loads. | 63 |
| Figure 31 Graphs showing the displacement against the angle for each test completed on the ASP. The results are separated by feedstock. | 64 |
| Figure 32 Graph of the displacement against the angle for the tests conducted with Ti-6Al-4V GA..... | 65 |
| Figure 33 Tooling set-up for the Conform TM process as designed in CAD for this project. .. | 70 |
| Figure 34 CAD drawing of the wheel. | 71 |
| Figure 35 CAD drawing of the abutment. | 72 |
| Figure 36 CAD drawing of the die chamber. | 72 |

| | |
|---|-----|
| Figure 37 CAD drawing of the die..... | 73 |
| Figure 38 CAD drawings of the entry block (left) and entry block extension (right) | 74 |
| Figure 39 CP Ti HDH particle designed in EDEM for use in the EDEM simulations..... | 77 |
| Figure 40 (a) Simulated Angle of Repose for CP Ti HDH Gr 2 irregular particles; (b) Experimental Angle of Repose for CP Ti HDH Gr 2 irregular particles. | 78 |
| Figure 41 Spherical Ti-6Al-4V GA generated for use in EDEM simulations. | 80 |
| Figure 42 (a) Simulated Angle of Repose for Ti-6Al-4V GA particles; (b) Experimental Angle of Repose for Ti-6Al-4V GA particles..... | 80 |
| Figure 43 Ti-6Al-4V swarf particle designed in EDEM for use in the EDEM simulations ... | 82 |
| Figure 44 (a) Simulated Angle of Repose for Ti-6Al-4V swarf particles; (b) Experimental Angle of Repose for Ti-6Al-4V swarf. | 82 |
| Figure 45 Left: Small toolset designed for the Conform trials complete in this work. showing the top of the simulation, the toolset from the side of the shoe and the front face of the simulation; Right: Large toolset designed for the Conform trials completed during this work | 85 |
| Figure 46 5s EDEM simulation for CP Ti HDH Grade 2 in the small toolset. | 88 |
| Figure 47 Data obtained from the EDEM simulation of CP Ti HDH Grade 2 in the small toolset. | 89 |
| Figure 48 EDEM simulation for CP Ti HDH Grade 2 in the large toolset. | 91 |
| Figure 49 Data obtained from the EDEM simulation of CP Ti HDH Grade 2 in the large toolset. | 92 |
| Figure 50 EDEM simulation of Ti-6Al-4V GA in the small toolset. | 95 |
| Figure 51 Data obtained from the EDEM simulation of Ti-6Al-4V GA in the small toolset. | 96 |
| Figure 52 EDEM simulation of Ti-6Al-4V GA in the large toolset..... | 98 |
| Figure 53 Data obtained from the EDEM simulation of Ti-6Al-4V GA in the large toolset.. | 99 |
| Figure 54 EDEM simulation of Ti-6Al-4V swarf in the small toolset. | 102 |
| Figure 55 Data obtained from the EDEM simulation of Ti-6Al-4V swarf in the small toolset. | 103 |
| Figure 56 EDEM simulation of Ti-6Al-4V swarf in the large toolset. | 105 |
| Figure 57 Data obtained from the EDEM simulation of Ti-6Al-4V swarf in the large toolset. | 106 |
| Figure 58 EDEM simulations demonstrating the difference between CP Ti HDH Gr 2. in the differently sizes toolsets. | 108 |

Figure 59 Data obtained in trial 1 with CP-Ti Gr 2 HDH feedstock including the calculated abutment stress; b) The average and standard deviation of the abutment stress with the coefficient of variation; c) Change in the grip length over the course of the trial..... 114

Figure 60 a) Data obtained in trial 2 with CP-Ti Gr 2 HDH feedstock including the calculated abutment stress; b) The average and standard deviation of the abutment stress and the coefficient of variation; c) Change in the grip length over the course of the trial..... 115

Figure 61 Photograph showing an example of abutment wear during a Conform™ trial.... 117

Figure 62 a) Data obtained in trial 3 with CP-Ti Gr 2 HDH feedstock including the calculated abutment stress; b) The average and standard deviation of the abutment stress and the coefficient of variation; c) Change in the grip length over the course of the trial..... 119

Figure 63 a) Data obtained in trial 4 with CP-Ti Gr 2 HDH feedstock including the calculated abutment stress; b) The average and standard deviation of the abutment stress and the coefficient of variation; c) Change in the grip length over the course of the trial..... 119

Figure 64 a) Data obtained in trial 5 with CP-Ti Gr 2 HDH feedstock including the calculated abutment stress; b) The average and standard deviation of the abutment stress and the coefficient of variation; c) Change in the grip length over the course of the trial..... 121

Figure 65 a) Data obtained in trial 7 with CP-Ti Gr 2 HDH and Ti-6Al-4V GA feedstock including the calculated abutment stress; b) The average and standard deviation of the abutment stress and the coefficient of variation; c) Change in the grip length over the course of the trial 122

Figure 66 a) Data obtained in trial 8 with CP-Ti Gr 2 HDH and Ti-6Al-4V GA feedstocks including the calculated abutment stress; b) The average and standard deviation of the abutment stress and the coefficient of variation; c) Change in the grip length over the course of the trial 123

Figure 67 a) Data obtained in trial 9 with CP-Ti Gr 2 HDH and feedstock including the calculated abutment stress; b) The average and standard deviation of the abutment stress and the coefficient of variation; c) Change in the grip length over the course of the trial 125

Figure 68 a) Data obtained in trial 10 with CP-Ti Gr 2 HDH and Ti-6Al-4V swarf feedstocks including the calculated abutment stress; b) The average and standard deviation of the abutment stress and the coefficient of variation; c) Change in the grip length over the course of the trial 126

Figure 69 Graph showing the average, maximum and minimum temperatures and stresses for each individual trial. (Top left) Wheel Temperature, (Top Right) Abutment Temperature, (Bottom Left) Abutment Stress and (Bottom Right) Grip Length..... 129

Figure 70 Graph showing the average, maximum and minimum temperatures and stresses for each set of trials containing the parameters listed on the x-axis. (Top left) Wheel Temperature, (Top Right) Abutment Temperature, (Bottom Left) Abutment Stress and (Bottom Right) Grip Length..... 130

Figure 71 Photographs of CP Ti HDH Gr 2 rod extruded through the die during the Conform process (a) from trial 2; (b) from trial 3 132

Figure 72 Photograph of CP Ti HDH Gr 2 rod extruded through the die during the Conform process from trial 7 133

Figure 73 Photograph demonstrating the length of the wire extruded during Trial 8. 134

Figure 74 CP Ti HDH Gr 2 and Ti-6Al-4V swarf derived wire produced during Trial 10. . 134

Figure 75 Polarised light micrograph of as-extruded wire from CP-Ti Gr2 HDH powder in the swarf tooling. The indents are result of microhardness testing. 135

Figure 76 Polarised light micrograph of as extruded wire from Ti-6Al-4V GA powder. (a) Shows the distinct layered structure around the outside of the wire. b) A more uniform microstructure in the inner core of the wire). The arrow denotes an example of the porosity. 135

Figure 77 Cross polarised light micrograph of a transverse section of as-extruded Ti-6Al-4V GA wire. The flow direction, as indicated by the arrow is evident based on the flow lines across the material. 136

Figure 78 Light micrographs showing the cross-section and transverse sections of the rod produced in Trial 2..... 137

Figure 79 Light micrographs taken along the length of the CP Ti HDH Gr 2 and Ti-6Al-4V GA rod extruded during Trial 8..... 138

Figure 80 Light micrographs of CP Ti HDH Gr 2 and Ti-6Al-4V swarf derived rod extruded during Trial 10. 140

Figure 81 BSE micrograph and EDX of the Ti-6Al-4V GA extruded during Trial 8. 141

Figure 82 BSE micrograph of Sample 8 extruded during Trial 10. The sample contains both CP Ti HDH Gr 2 and Ti-6Al-4V swarf..... 142

Figure 83 EDX of Sample 8, CP Ti HDH Gr 2 and Ti-6Al-4V swarf derived rod extruded during Trial 10. 143

| | |
|---|-----|
| Figure 84 Sub-size tensile specimen prepared from as-Conformed titanium rod with a gauge length of 15 mm and gauge diameter of 2.5 mm | 144 |
| Figure 85 Collets for sub-size tensile specimens produced for this project..... | 144 |
| Figure 86 Light micrographs of the tensile sample fracture surfaces from the Trial 10 tensile samples. | 149 |
| Figure 87 Microhardness results for samples taken of the CP Ti HDH Gr 2 and Ti-6Al-4V GA rod extruded during Trial 8..... | 152 |
| Figure 88 Microhardness results for samples taken of the CP Ti HDH Gr 2 and Ti-6Al-4V GA rod extruded during Trial 8..... | 154 |
| Figure 89 Diagram showing the workflow for the work carried out during this project. | 156 |
| Figure 90 Examples of powder size ranges in powder metallurgy processes. Reproduced from [29], [129], [130]..... | 176 |
| Figure 91 Schematic of a Conform TM machine used to consolidate powder directly into wire. | 179 |
| Figure 92 Schematic demonstrating the various wire production routes commonly used and the potential feedstocks identified for investigation into low-cost wire production using the disruptive technology of Conform TM | 180 |
| Figure 93 Summary of particle characteristics for titanium alloy feedstocks used in this study. No particle size distribution was recorded for the swarf owing to a lack of valid techniques for determining this. | 182 |
| Figure 94 Photograph of the titanium alloy wire being extruded from the Conform TM machine. The wire glows white/red as it emerges from the back of the extrusion die in the centre of the photograph. | 183 |
| Figure 95 Photograph of as-Conformed CP-Ti Gr 2 wire with blue oxide film (top) and ϕ 3.00 mm cold-wire drawn wire with bright surface (bottom) from the same extruded product. .. | 185 |
| Figure 96 Photographs (at the same magnification) of as-extruded Ti-6Al-4V wire derived from GA powder with multi-coloured oxide film (top) and a sub-size tensile specimen with 15.00 mm gauge length (bottom) tested according to ASTM E8/E8M-15a. | 186 |
| Figure 97 Polarised light micrograph of as-extruded wire from CP-Ti Gr2 HDH powder in the swarf tooling. The indents are result of microhardness testing (and correlates with the data for sample 2a in Fig 15). | 186 |
| Figure 98 Polarised light micrograph of as extruded wire from Ti-6Al-4V GA powder. (a) Shows the distinct layered structure around the outside of the wire. b) A more uniform | |

| | |
|--|-----|
| microstructure in the inner core of the wire). The arrow denotes an example of the porosity. | 187 |
| Figure 99 Cross polarised light micrograph of a transverse section of as-extruded Ti-6Al-4V GA wire. The flow direction, as indicated by the arrow is evident based on the flow lines across the material. | 188 |
| Figure 100 Polarised light micrographs of the extruded wire for both trials. The micrographs are ordered as they exited the Conform™ die, where sample 1 was extruded first and sample 5 last. All micrographs were taken at the same magnification. | 190 |
| Figure 101 a) Graph showing the change in the average grain size as the trial progresses. b) Graph showing the change in the porosity in the material as the trial progresses. | 191 |
| Figure 102 Backscattered electron micrographs of the swarf wire (a) before and (b) after heat treatment of wire containing extruded Ti-6Al-4V swarf..... | 191 |
| Figure 103 Room temperature tensile mechanical properties for the as-extruded wire produced from the gas atomised and swarf titanium alloy feedstocks. | 192 |
| Figure 104 The microhardness of the cross-section material. 1a/b are recorded from the cross- section of the Ti-6Al-4V GA wire and 2a/b are taken from the Ti-6Al-4V swarf wire. a is from the initial extrusion; b is the last material to be extruded during a trial. | 192 |
| Figure 105 Polarised light micrographs of the cold drawn CP-Ti Gr 2 wire cross section after each pass, before and after heat treatment. The first pass reduction from 5.00 mm to 4.09 mm, second pass 4.09 mm to 3.50 mm and the third pass from 3.50 mm to 3.00 mm. | 194 |
| Figure 106 Graph showing the change in the grain size of the cold drawn CP-Ti Gr 2 wire through each of the three drawing passes with intermediate annealing heat treatments (HT).4. | 194 |

Table of Tables

| | |
|---|-----|
| Table 1 Titanium particulate feedstocks used for Conform trials. | 45 |
| Table 2 The geometries of the key components of the toolsets used during the Conform trials | 57 |
| Table 3 Data provided for the ASP trials, including the mass of the feedstock added to the tools. *Swarf tests used a larger toolset to accommodate particulate size | 59 |
| Table 4 Simulated angle of repose results using the particle shown in Figure 39 | 79 |
| Table 5 Results of the Ti-6Al-4V GA powder angle of repose simulations for 27 variations of coefficient values. | 81 |
| Table 6 Results of the Ti-6Al-4V swarf angle of repose simulations for 27 variations of coefficient values. | 83 |
| Table 7 Tooling geometries and materials for the trials conducted in this work | 111 |
| Table 8 Raw tensile data for the sub-specimen tensile samples from trial 8 | 145 |
| Table 9 Tensile data for trial 8 after the correction factor has been applied | 145 |
| Table 10 Raw tensile test data from the tensile samples taken from the Ti rod extruded during Trial 10. | 147 |
| Table 11 Corrected tensile test data from the tensile samples taken from the Ti rod extruded during Trial 10. | 147 |
| Table 12 Geometries of the tooling used in the trials and the abutment materials used. | 183 |

List of Abbreviations

| | |
|-------|--|
| AM | Additive Manufacturing |
| ASP | Annular Strain Path |
| BCC | Body-Centred Cubic |
| BE | Blended Elemental |
| CAD | Computer-Aided Design |
| CP | Commercially Pure |
| DED | Direct Energy Deposition |
| DEM | Discrete Element Modelling/Method |
| DTI | Dial Test Indicator |
| ECAP | Equal Channel Angular Pressing |
| EDEM | Edinburgh Discrete Element Method |
| FEM | Finite Element Modelling/Method |
| FFC | Fray-Farthing-Chen |
| GA | Gas Atomised |
| HCP | Hexagonal Close Packed |
| HDH | Hydride Dehydride |
| HE | Hydrostatic Extrusion |
| HIP | Hot Isostatic Pressing |
| HPT | High Pressure Torsion |
| NNS | Near-Net Shape |
| PA | Pre-Alloyed |
| PBF | Powder Bed Fusion |
| PSD | Particle Size Distribution |
| SEM | Scanning Electron Microscopy |
| SPD | Severe Plastic Deformation |
| UKAEA | United Kingdom Atomic Energy Authority |
| WAAM | Wire+Arc Additive Manufacturing |

Chapter 1 : Introduction

Developed in Preston, Lancashire in the 1970s, ConformTM, a continuous forming process is a severe plastic deformation method originally used for the production of metal rod/wire from rod feedstock [1]. From its outset, the ConformTM process was designed and used to convert copper and aluminium waste feedstock into lengths of rod with a different cross-sectional profile. Being somewhat continuous, the process allows for large volumes of material to be produced relatively quickly, to serve the purpose of reducing waste material and creating products of use to industry, such as for the United Kingdom Atomic Energy Authority (UKAEA) in the 1970s. An early patent for the ConformTM process is shown in Figure 1.

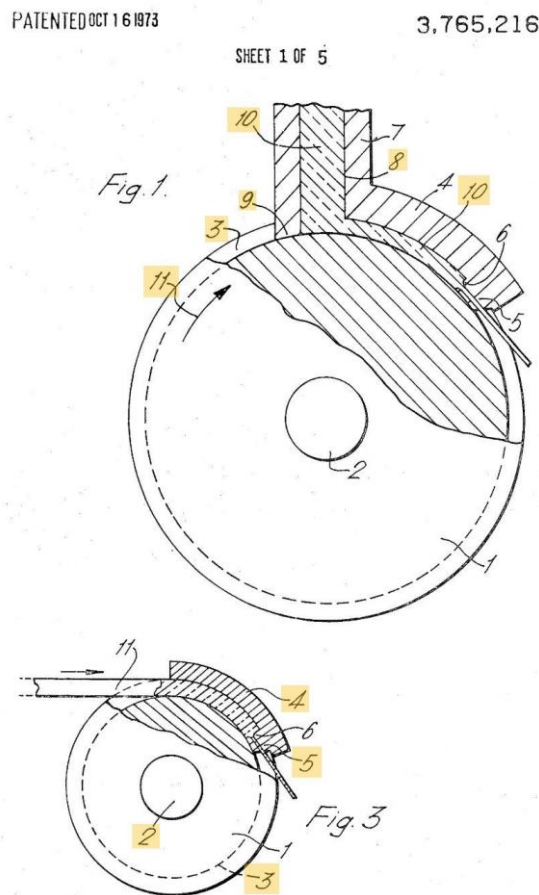


Figure 1 Schematic from the original 1973 ConformTM patent [1]

In more recent years, the process is still in use by various companies and research groups across the world [2], [3], although there have been a few significant updates. Firstly, the use of alternative forms of feedstock, such as powder [4] have been developed. Secondly, there has been a change in the metals being processed, with research being carried out in the use of titanium feedstocks [4] as opposed to aluminium or copper.

The investigation into the alternative forms of feedstock and the use of titanium has been heavily guided by trends in the aerospace industry. In recent years, additive manufacturing (AM) processes have become a front runner in aerospace research, owing to the ability to produce high quality components with a low buy-to-fly ratio. The use of AM has reduced the amount of machining waste, as near-net shape components can be produced, however, there is still waste. Additionally, there is a new waste source from the use of AM, as the powders have specific requirements to meet. Any powders which do not meet the requirements or have already been used in the process go to waste.

Titanium has different mechanical properties to metals like copper or aluminium. It exhibits high strength, low weight and corrosion resistance, but consequently is notoriously difficult to process due to titanium's enthalpy of formation of its oxide. This difficulty exists throughout its production - from extraction from rutile, through to the manufacturing of parts for industry. Therefore, titanium is currently an expensive material which restricts its use in a range of non-aerospace industry sectors.

There are various steps that could be taken to make titanium production more commercially viable. There are now alternative extraction routes for titanium, which focus on using

electrolysis to produce titanium sponge, such as the Fray-Farthing-Chen (FFC) process [5]. Alternatively, there is a significant volume of waste titanium, which is commonly in the form of machining turnings or swarf. Such material has the potential to be recycled as a Conform™ feedstock.

The reason that much of the titanium waste is in the form of swarf is due to the intensive machining of titanium alloy parts for the aerospace industry. Critical aerospace parts tend to be machined from large forged billets, where up to 95 percent [6] of the material is turned into swarf. Most of the titanium swarf is compacted and melted into ferrotitanium ingots as steelmaking additions. It is important, however, to note that not all this waste can be recycled, and some is even substandard for melting down for non-critical parts. However, in theory, much of the waste could be used in the Conform™ process.

Ultimately, the titanium alloy wire produced could be used in a number of applications, such as those seen in Figure 2. Metal wires are used in various ways, for example, steel wires being used to support bridges, titanium wires being used in dental applications and copper wire being used in electronics. These wires all require different mechanical properties, depending on the quality of the wire required and how demanding the application is. Wires used in titanium springs require high ductility to allow them to be coiled, but often they are used in automotive engines, so they cannot afford to have defects or low fatigue life. This means that they require much greater mechanical properties but also a high-quality material is required. This is in great contrast to wires used for welding processes, where the ductility and strength must be high enough to coil and feed into the process, but the quality is much less strict.

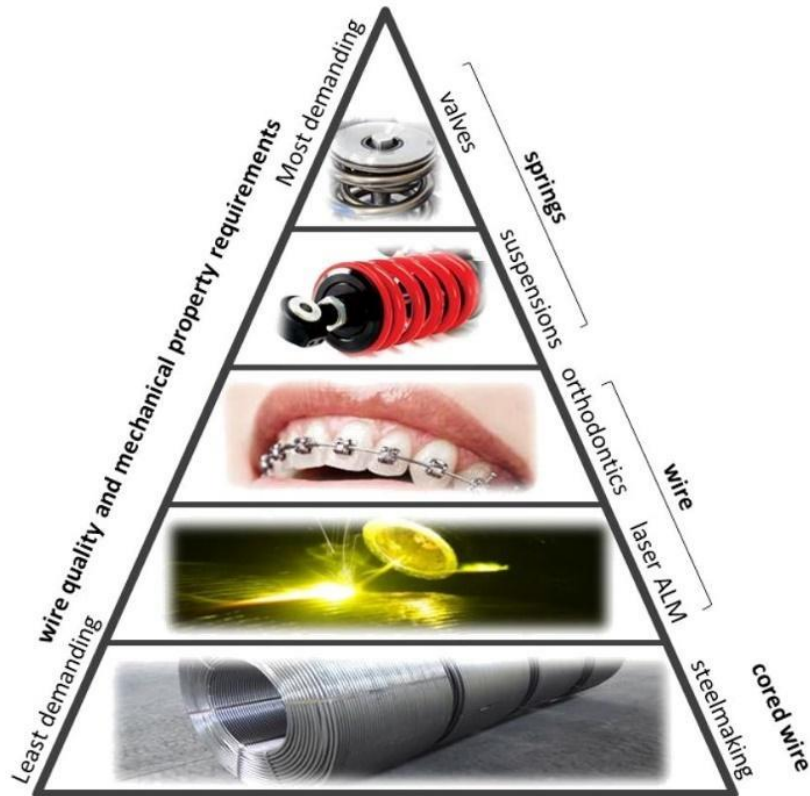


Figure 2 The various applications for wire produced with different mechanical property requirements.

1.1 Aims & Objectives

This work seeks to further develop the ConformTM process, produce titanium wire from waste materials, including both swarf and powder feedstocks, which can then be used in the aerospace industry. The primary aim of the wire is to demonstrate that it could be used as feedstock for additive manufacturing, where wire feedstock is becoming an ever more present feature.

Key objectives include:

1. Based on past research, to design tools and trialling methods to optimise the production of wire during the ConformTM process

2. Develop further understanding of the thermomechanical processes and powder behaviour occurring during Conform™ trials
3. Produce wire from alternative, waste feedstocks and consequently, characterise the produced material (assessing the microstructure and mechanical properties)
4. Develop an alternative small-scale powder characterisation method, which could, ultimately, allow predictions to be made on the feedstocks capable of Conform™ extrusion

1.2 Thesis Structure

This thesis is made up of twelve chapters (including the introduction) and brief descriptions are described below.

Chapter 2 presents a detailed background, which aims to discuss the key literature and research completed on titanium and the Conform™ process. Additionally, it demonstrates the motivations for this work based on previous challenges.

Chapter 3 outlines the materials and methods required during this work including an introduction to the Conform™ process, the Arbitrary Strain Path testing and Discrete Element modelling.

Chapter 4 investigates a novel powder characterisation process, which aims to inform the choice of powder used within the Conform™ process. Results are provided for the tests

performed and the outcomes, with a particular highlight on the changing densities under load and shear.

Chapter 5 provides an introduction to the Conform™ process and an extended discussion about the tools used and how variations in the design can impact the results of a Conform™ trial.

Chapter 6 highlights the use of the discrete element method for the simulation of powder within the Conform™ process. This chapter aims to demonstrate how the tool design impacts on the extrusion and discusses the motivations for the tools used.

Chapter 7 introduces the data obtained from the Conform™ trials and aims to develop the understanding of the Conform™ process and allow for predictions to be made based on the raw data.

Chapter 8 discusses the resulting mechanical properties and microstructure of the material produced in the Conform™ trials.

Chapter 9 provides the conclusions to this research.

Chapter 10 discusses the future challenges and further research that could be done on the Conform™ process and the ASP.

Chapter 2 : Literature Review

2.1 Titanium

Renowned for its high specific strength, corrosion resistance and biocompatible properties [8]–[10] titanium (Ti) is one of the most desirable metals available. Although, it is one of the most abundant elements on Earth (ninth in the Earth's crust [11]), it is expensive. This cost is heavily related to its structure and behaviour, which can make it difficult to extract (high affinity for oxygen and nitrogen) and mechanically deform. The issues with titanium machining and extraction result in a significantly high cost, often 20 times more expensive than carbon steel and 4 - 5 times the price of stainless steel [12]. This is amplified further when the buy-to-fly ratio is considered, which is often 12:1 for aerospace components, as there can be up to 95% waste [13], [14].

2.1.1 Structure

The behaviour of titanium is influenced by its structure. Ti has two dominant allotropic phases: alpha (α) and beta (β). Pure titanium exists in α ; however, it is possible for both phases to exist simultaneously in an alloy, resulting in a multi-phase material. This is often the case with alloys, as the interstitial and substitutional elements may favour a different crystal structure to the bulk. Additionally, it is noteworthy that in pure titanium, an allotropic phase transformation occurs at $\sim 882^\circ\text{C}$, changing from β at high temperatures, to α at low temperatures. This is also the case in alloys; however, the phase transformation temperature can vary.

The two phases are distinct from each other, stemming from a different crystal structure. This variation in the crystal structure has a significant impact on the materials properties and behaviour.

The α phase adopts the hexagonal close-packed (HCP) crystal structure [15]. This is a prismatic crystal structure with 7 atoms at each basal plane and, between the two basal planes lie, three atoms in a triangular structure. This is best described in Figure 3. The HCP crystal structure is commonly found in titanium but is also present in elements such as zirconium and magnesium.

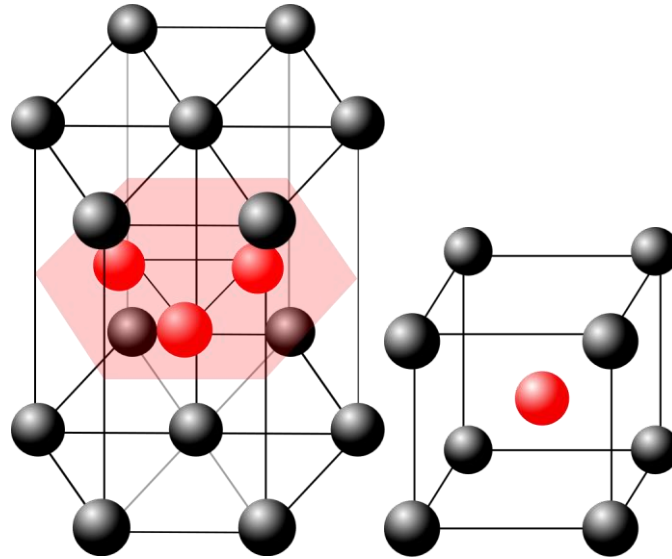


Figure 3 Hexagonal Close-Packed (HCP) crystal structure and Body-Centred Cubic (BCC) crystal structure.

In contrast to the α phase, the β phase adopts the body-centred cubic (BCC) crystal structure [16]. This crystal structure consists of eight atoms, which denote each of the corners, with a single atom within the centre of the cube (shown in Figure 3).

In order to maintain any given crystal structure, α/β -stabilisers can be added as alloying elements [17]. These elements help to stabilise the crystal structure, typically as either α or β , depending on the required properties of the alloy. In addition to this, it is possible to convert between the different phases by temperature alone [18]. Figure 4 shows the pseudo titanium phase diagram, which demonstrates the transformation of the crystal structure at a given temperature or through the use of a β stabiliser. By heating a titanium alloy above the β -transus temperature, the α grains can be transformed into β . This is particularly advantageous when it comes to forming processes, as it means that the previously unattainable deformation modes are now possible. It is important to note, however, that this temperature is relatively high and upon cooling, the phases may revert to α . Further to this, there are clear combinations of crystal structure, which fall between the α and β regions. It is possible to have a near α or near β crystal structure, which is often a result of the alloying elements within the alloy. Prior to reaching the β state, with the exception of through a pure titanium route, there is also the possibility of obtaining a metastable β , where the structure is a combination of α and β structures.

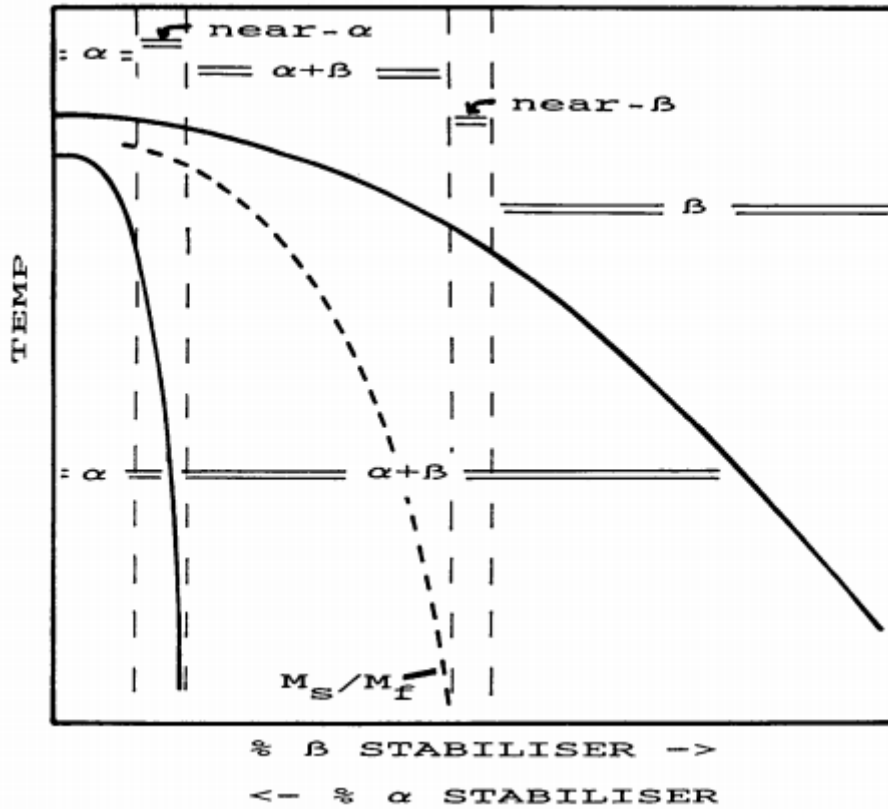


Figure 4 Pseudo phase diagram of titanium taken from [19]

Once the alloy is defined, any further changes to the microstructure are dominated by thermomechanical processing [20]. Thermomechanical processes are methods where there is both temperature and working involved, which is often the case in hot-forming or similar methods.

α alloy compositions are not able to retain a β phase once at room temperature, even in a metastable form and are typically equiaxed α grains [19]. Near- α alloys may contain β at room temperature; however, this is in relatively small quantities and is in a metastable form. The microstructure will typically be made up of large β grains or small amounts of β at the α grain boundaries. The resulting mechanical properties from these alloys include high tensile strength and high creep resistance [16], [21].

In alloys that fall within $\alpha + \beta$, there is a much wider range of achievable microstructures than seen in pure α . When slow cooling from β , large prior β grains form, which grow α during cooling. This results in finer grain sizes as the α limits β growth. The most popular of the

titanium alloys, Ti-6Al-4V, is an α - β alloy and is well-used as it has a higher strength than CP Ti, good formability and can be heat-treated [22].

In the near- β case, metastable- β can be retained at the lower temperatures, rather than being forced out through the growth of α grains. Further to this, there is a point in which the β -phase is stable at room temperature, which is typically when the β -stabilising elements are present in a significant volume to avoid cooling through the martensite start line (M_s) [16]. Where this is the case, transformation into α does not happen, and the resulting alloy is cold workable and can be recrystallised at lower temperatures. β and near- β alloys are heat-treatable and offer good strength-to-weight ratios and ductility, owing to their BCC structure [16].

As stated, upon cooling β can be transformed into α , because it becomes unstable as the temperature drops below the β -transus. In the case of slow cooling, α can form along prior β grain boundaries, resulting a lamellar structure. With fast cooling, lamellar α colonies can be formed with β grains. This results in basketweave α . At the faster cooling rates, precipitation can become finer and this results in a Widmännstätten α structure.

2.1.2 Extraction

Titanium was first isolated from ore in 1910 via the Hunter process [23], which was the first industrial process to extract pure titanium from its ore. Prior to the Hunter process, many attempts to isolate titanium were hampered by the affinity of the element to nitrogen, as often titanium nitrides were formed. The Hunter process was adapted into the Kroll process in the 1940s, as the use of sodium for reduction was expensive and magnesium offered a more cost-effective route.

The Kroll process (see Figure 5) has been used for the extraction of titanium from TiO_2 . First proposed by Kroll in 1940, the Kroll process uses several chemical steps to convert TiO_2 to pure Ti sponge. There are three key steps involved, which are relatively energy and chemically expensive.

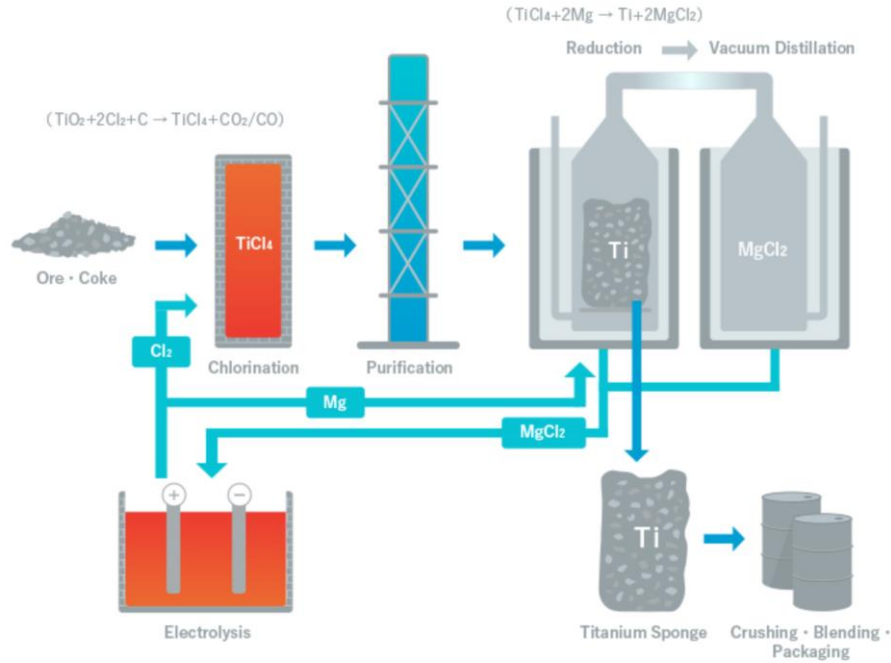
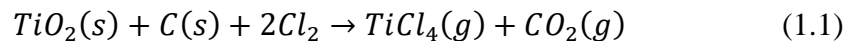
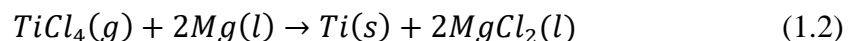


Figure 5 Schematic of the Kroll process. Taken from [24]

The first step is to take the ore with coke (a form of pure carbon) and react this with chlorine gas in a chlorination step. This is an electrolytic process and requires the oxygen to be separated from the titanium via electrolysis. Chlorine gas is then passed through, which takes the place of O_2 . The chemical equation for this process is shown below.



In the second step, the products of this reaction are left to cool and are then distilled. In the final step, the titanium(IV)chloride is then heated with magnesium (or sodium, in the case of the Hunter process) under an argon atmosphere. This leads to the reduction from Ti(IV) to Ti(0), which leaves pure titanium in a solid sponge form.



The resultant titanium sponge contains the magnesium salt, which can be separated via acid leaching or high temperature vacuum distillation. The final product can then be melted to form billets.

Since the Kroll process was first used, many different methods of titanium extraction have been introduced. The aim for many of these products was to create a lower cost source of titanium, as, currently, a large proportion of the cost comes from titanium extraction. Additionally, the rise in demand for powder products has led to new methods, which allow for specific alloys to be prepared in powder form.

One such method is the Fray-Farthing-Chen (FFC) process (shown in Figure 6). Although there are a number of steps required, they are significantly quicker and much less energy intensive. The process allows for multiple metal oxide powders to be used at once, meaning that alloys can be prepared *in situ*. Because materials can be prepared from their constituent metal powders with minimal remelting to achieve a homogeneous alloy, exotic alloys are becoming more viable.

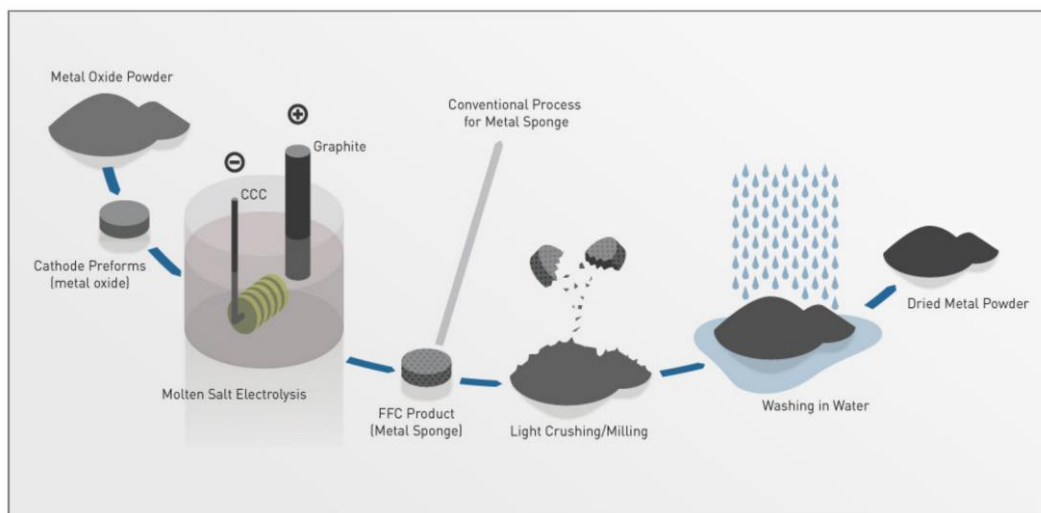
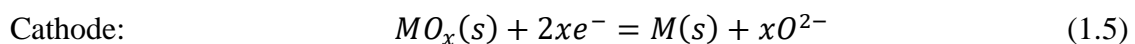
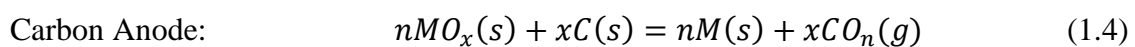
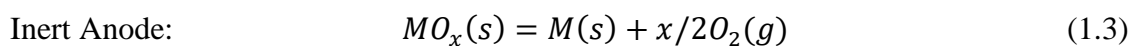


Figure 6 Schematic of the FFC process. Taken from [25]

The process forms molten salts from the metal oxides, which are then electrochemically reduced. This can be seen in equations [1.3 – 1.5].



The FFC process does have some cost implications, however, with cathode production being rather expensive. Yet it still remains cheaper than the Kroll process [26]. There are other processes, which also follow a similar pattern to the FFC process, such as TiRO, ITP/Armstrong and CSIRO [27].

Each of these steps is much more cost effective than the Kroll process and the benefits of the process also allow for metal powder production, of which there is a growing trend. With the rise in the use of additive manufacturing processes and an aim to reduce waste, powder-based processes are fuelling the research. It should be noted that despite the cost reduction and improved processing routes, there are still issues with impurities, which lead to higher costs. In future development, there is a clear potential for producing low cost, high quality powder.

2.1.3 Powder Metallurgy

The cost of powder for many processes is high, especially in processes where the mechanical, chemical and microstructural requirements are high. There are various methods of forming titanium powders, some formed directly from the extraction phase as demonstrated in section 2.1.2, however, others are direct from scrap.

When it comes to powder production, there are two main approaches: blended elemental (BE) and pre-alloyed (PA) powders [28]. Out of both methods, PA powders typically have greater mechanical properties, but this can come at a significant cost. BE powders are much more popular due to their lower cost, but this comes at a reduction of mechanical properties.

Gas atomised powders are a particularly costly powder to make as they are commonly used for additive manufacture. GA powders are prepared as pre-alloyed powders and result in spherical powder particles. Typical production routes include air atomisation, where compressed air breaks up the molten metal; inert gas atomisation, where the melt is broken up by gases such as oxygen or nitrogen; and plasma atomisation, which uses plasma torches to melt and atomise the material and is most commonly used for titanium [29].

HDH powders are cheaper than their GA counterparts and are also produced as pre-alloyed powders. The titanium feedstock is heated in a hydrogen atmosphere, leading to embrittlement.

Once this occurs, the material is easily broken down and can then be dehydrided by heating under vacuum. Unlike GA production the resulting morphology is irregular and can result in contaminants [30].

Although slightly larger than the typical powder particles, particulate swarf is a viable alternative for use in powder processes. Swarf is the by-product of the machining of metal billets and is high source of waste in industries such as aerospace. The swarf can be of various morphology but is often around 1 – 10 mm at its maximum length and could potentially be a higher quality than commercially available titanium alloy powders, owing to the previous processing of the material [31]. This feedstock has been used in various processes, which are discussed later in the chapter, with success. The use of swarf serves as an important cost-effective recycling process, as swarf is often sold at a low cost to the steel-making industry. This could result in a circular economy of waste by-product through to a welding wire that could be used in aerospace.

2.1.4 Uses

Titanium is a very desirable metal within many industries, owing to its mechanical and chemical properties. However, its price leaves it as a luxury in industries such as the automotive industry – where, although these properties fit the specifications, some compromise has to be made. There are, however, industries where this compromise cannot be made, such as the aerospace industry, where striving for lightweight, corrosion resistance and high strength is important. There are a number of parts in an aero engine that could conceivably be made from titanium, however, the current cost means that cheaper alternatives are used, such as steel or nickel [31].

The properties required by aerospace manufacturers are now being replicated by automotive manufacturers. Traditionally made with steel and aluminium alloys, new innovation is always required to improve the current engines [32]. Recent developments in low-cost titanium, such as the alternate extraction methods and the additive manufacturing of components, are driving the cost of this once niche material, into a more accessible choice for less-critical components. Additionally, the drive for faster and more powerful engines has made the use of titanium ideal to reduce the fuel consumption and increase the efficiency [33].

There are now examples of titanium being used in the form of suspension springs and connecting rods in vehicles. These parts are also often prioritised in the research of alternative manufacturing methods for titanium parts, with work at the University of Sheffield developing new powder methods for producing solid, forged engine parts [34].

Aside from the aerospace and automotive industries, due to the excellent biocompatibility of titanium, it and its alloys are often used in medical applications. There have been many studies highlighting the viability of titanium wire for dental implants [35], [36] but also the use of titanium in joint replacement [37], [38]. The biocompatibility of titanium increases the likelihood that a replacement bone structure will be accepted in the body and therefore a reduced chance of further ailment. The components typically cause little to no damage to the surrounding bone, where often components can increase the brittleness of bone [39].

Ultimately, the aim with titanium is to reduce the costs to make it more accessible for components that otherwise would seek cheaper alternatives. Additionally, if this can be coupled with a reduction in the waste of titanium (typically from machining), this would make a viable, low-cost alternative than that currently available.

2.2 Severe Plastic Deformation

Severe plastic deformation (or SPD) is when a large plastic strain is applied to a material, leading to grain size refinement, often resulting in ultra-fine grain sizes [40]. Typically, traditional processes such as extrusion, forging and rolling cannot achieve the ultra-fine-grained microstructure and consequently the mechanical properties of SPD processed materials.

SPD processes also involved the retention of the cross-sectional area of the material, which is not seen traditional forming methods. By retaining the cross-sectional area, the strain applied to the material results in the accumulation of a deformation energy. This energy is a result of a high density of dislocations in the material, which ultimately results in grain boundary changes, and grain refinement.

Grain refinement mechanisms have been proposed and typically fall in one of two categories: grain fragmentation mechanisms and dislocation density-based mechanisms [41]. The first involves the breaking up of grains due to the formation of dislocation walls [42]. The second category covers a much wider range of possible mechanisms, including (but not limited to) the continual decrease of grain size through the accumulation of misorientations between dislocation cells [43], [44], with various alternatives on the behaviour of the dislocation cells such as the formation of high angled grain boundaries [41].

Methods of SPD are commonly used for the production of wire [45], where grain-size refinement is required to improve the strength of the material. However, it should be noted that when wire drawing, there is a drop in the cross-sectional area, which is not a requirement of SPD processes [46], [47].

2.2.1 Methods

Plastic deformation methods are typically rolling, forging or extrusion processes. These lead to the plastic (permanent) deformation of a material into a given shape. Once a material has been plastically deformed it will retain the shape. Unfortunately, some negatives are attached to traditional plastic deformation methods. Despite leading to microstructural refinement, the ductility of the material is often compromised [48]. The reduction in ductility could ultimately lead to brittle components which may prematurely fail.

Because of this, severe plastic deformation methods were developed, which, unlike the cold-rolling, forging and extrusion methods previously used, lead to both microstructural refinement and the retention (or even improvement) of the material's mechanical properties. This means that the ductility can be retained, whilst also increasing the strength and toughness of the material.

There are a number of different SPD processes currently used for grain-refinement including direct extrusion, hydrostatic extrusion, high pressure torsion and equal angle channel pressing [49] (Note, this is not an exhaustive list but these are some of the more frequently used methods).

2.2.1.1 Direct Extrusion

Direct extrusion processes are the most common methods of extrusion and have traditionally been used for the extrusion of rod products from billet. They are forming methods which produce products with a consistent cross-section, by forcing solid material into a profiled die. The material to be extruded has the key requirements that it must be plastically deformable, and that this deformation is irreversible. Conventional direct extrusion involves using a ram to force solid material through a die, in order to form a product with a defined cross-section, as shown in Figure 7.

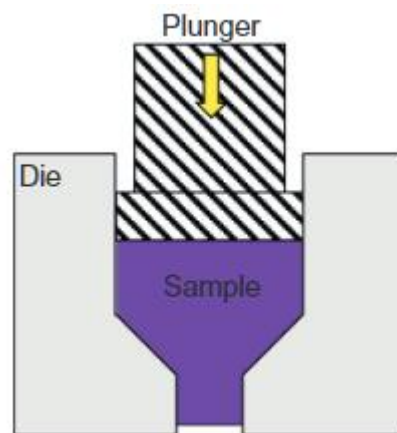


Figure 7 Schematic of conventional Direct Extrusion taken from [50]

There are clear advantages to direct extrusion, in that it is a relatively simple process that produces a severely plastically deformed product from a billet. However, as the ram forces a fixed volume of material into the die, the process is a batch process. Batch processes cannot run continuously and are limited by the volume of material that can fit into the machine. Although direct extrusion has been used as a fully commercialised process, the batch nature would be much more commercially viable if it were continuous.

Despite its flaws, direct extrusion is still used for further investigation into new processing methods. In recent years, direct extrusion processes have been used successfully with powder feedstocks and have shown that ultra-fine grained products can be produced as a result [51].

2.2.1.2 Indirect Extrusion

Unlike direct extrusion, indirect extrusion does not involve a ram or punch to push the billet towards the die, and rather, the die is moved towards the billet. One key benefit is that the force required to push the billet through the die is higher than if the die is being moved towards the product. This is because the billet material is met with frictional forces, which require more force to overcome and this is not the case if the die moves.

2.2.1.3 Hydrostatic Extrusion

Hydrostatic extrusion is focussed on elongation of a solid feedstock along the axis, rather than through shear [52]. It has been shown that excellent mechanical properties can be exhibited by products extruded in this way [53], however, the process requires high pressure and comes with a number of challenges with titanium feedstocks including issues with the surface finish of rod product. The issues with the surface finish have been addressed by the use of aluminium coatings, which helps to reduce frictional wear, decrease surface roughness and reduces the extrusion pressure so a greater rod diameter reduction is possible during a single pass [53]. A schematic of hydrostatic extrusion is shown in Figure 8.

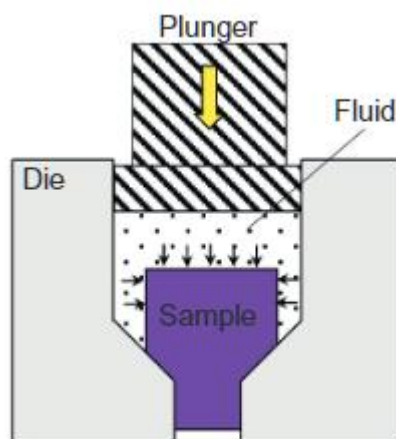


Figure 8 Schematic of Hydrostatic Extrusion taken from [50].

It has also been commonly reported that grain size reduction from around 50 μm to sub-nanometre [49]. Despite these improvements, however, it is still a relatively intensive and inefficient process, and similar results can be achieved through alternative, less expensive process routes. It also does not utilise powder-based feedstocks, which makes it infinitely

harder to achieve complex alloy systems, which exhibit the required mechanical properties. Within hydrostatic extrusion, an increase in the ductility is shown, which is not typically seen in processes such as direct or indirect extrusion. A low value for the mean normal stresses applied to the material, helps to retain, and even improve, the ductility of the material. Higher compressive stresses tend to push a material towards a more brittle state [54].

2.2.1.4 High Pressure Torsion

High pressure torsion (HPT), as the name suggests, requires a high pressure in order to severely plastically deform materials. Unlike the other methods discussed here, which either use rod or powder feedstocks, HPT uses a thin disk of material that is then subjected to torsional strain under a high hydrostatic pressure. The torsional strain is achieved by the rotation of an anvil, which is pressed onto the sample, as shown in Figure 9.

One of the greatest limitations of HPT is the inability to produce material on a large scale, as the equipment allows for a small disk of sample to be produced. This reduces the commercial viability, although some work has been done to attempt to rectify this issue with larger bulk samples being prepared [55].

Unlike HE, HPT can utilise powder feedstocks, however, these feedstocks must be pre-compacted to the shape of the die. This pre-form can then be extruded via hydrostatic extrusion.

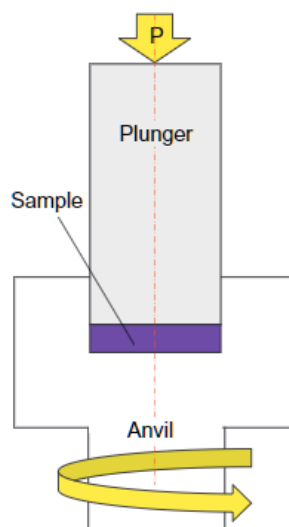


Figure 9 Schematic of High Pressure Torsion taken from [50]

2.2.1.5 Equal Channel Angular Pressing (ECAP)

Equal channel angular pressing (or ECAP) is a severe plastic deformation process that was developed to overcome some of the ductility issues found in traditional methods [40], [45]. Typically grain refinement results in a loss in the ductility, and whilst this is not seen in methods such as hydrostatic extrusion, ECAP often demonstrates this loss. The combination of limited strain rate hardening stemming from the small grains, which result in the movement of dislocations [56] and areas of deformation in the product, such as shear banding [57] can result in a reduced ductility as seen in ECAP.

This process takes a solid metal billet and forces it through a 90° or 120° channel in the ECAP die [58]. An example of the 120° channel is shown in the schematic in Figure 10. Through forcing the material through the angled channel and then into a smaller channel, the material is severely plastically deformed. This differs from traditional extrusion, where the material is forced straight through a die. There has been a significant amount of research done on the ECAP process, often highlighting the ultra-fine-grained product of the process [59], [60]. It should be noted that during ECAP, grain size refinement can be achieved without the reduction of the material diameter [61].

This process was of particular interest in the last few decades as it offered a way of achieving grain refinement in a material in a single step. The biggest downfall with ECAP was that it is not a continuous process, as the material is not continuously fed into the machine. Therefore, even though the process achieves improved mechanical properties through SPD, the resulting material is not on a large enough scale to make the process viable in industry, where large volumes of material need to be made continuously [62].

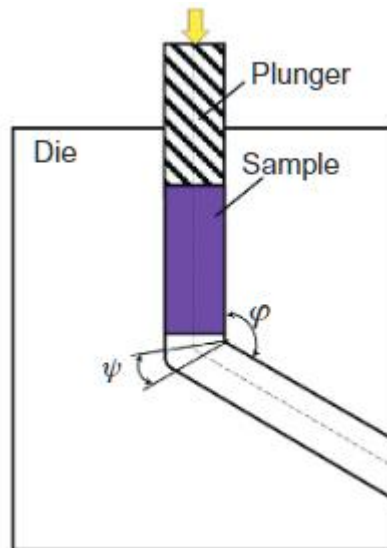


Figure 10 Schematic of ECAP for bulk samples. Taken from [50].

Further issues arise when the product requires coiling, such in the case of wire, as the Hall-Petch relationship would dictate the refined grain structure could result in improved strength but a decrease in ductility [63], [64]. In the case of ECAP with titanium, this reduced ductility is the result of microstructural changes such as an increase in the dislocation density [65]. It has been shown that following ECAP with a cold extrusion can result in a higher dislocation density and elongated grains. This step can further influence the mechanical properties of the resulting product, with higher yield and ultimate tensile strengths [66].

Work has been conducted comparing ECAP to HE, suggesting that each process undergoes different methods of microstructural refinement [67]. The work determined that HE provided the greater mechanical and microstructural properties owing to the highest fraction of ultra-fine grains. It was shown that for ECAP, the microstructure remains relatively coarse after 4 passes, with considerable refinement after 8 passes. This is shown in Figure 11. Ultimately, this shows that whilst ECAP often achieves ultra-fine grain structures, this does not always result in the greatest mechanical properties.

ECAP is often coupled with other processes to improve the overall microstructure and mechanical properties of the extruded material. Typically, methods such as cold rolling, cold extrusion or rotary swaging have been used [64], [65], [67] and the results show increases in the strengths of the resulting products. There is evident grain refinement, an increase in the

dislocation density and a more elongated grain structure, as demonstrated in the example in Figure 12.

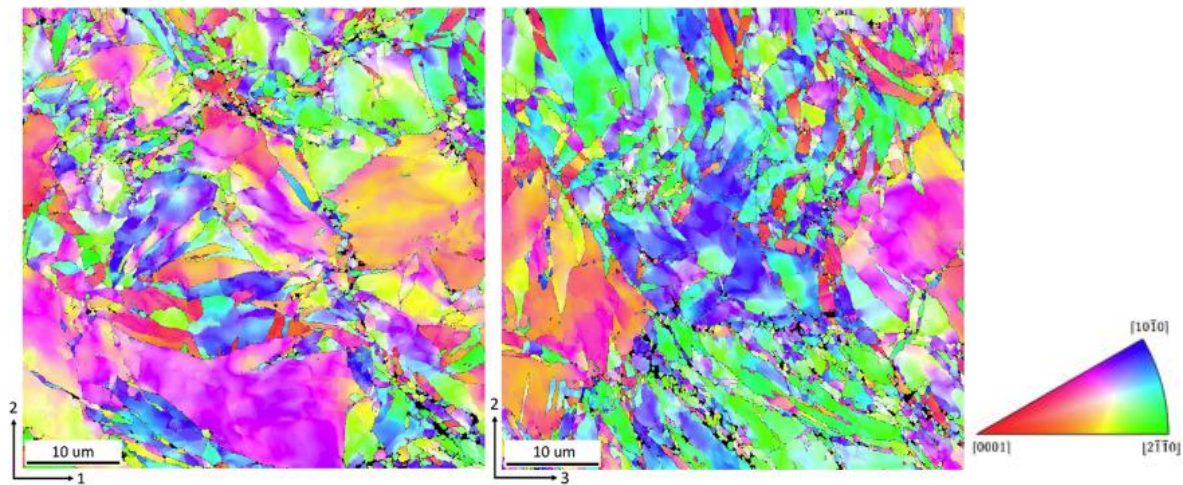


Figure 11 Orientation maps for ECAP, showing the appearance of fine grains along old grain boundaries and a relatively coarse microstructure, taken from [67].

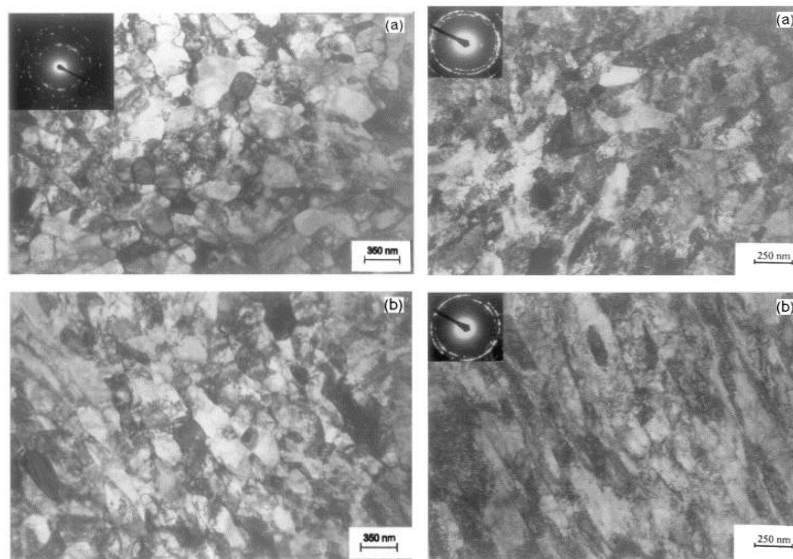


Figure 12 TEM of a Ti billet processed by ECAP for 8 passes (left) followed by cold rolling to a strain of 55%. (a) Cross-section and (b) longitudinal section. Taken from [68].

The process has often been coupled with the ConformTM process (outlined in Section 2.3), which allowed for a more continuous extrusion, whilst maintaining the ECAP method [69], [70]. The combination as Conform-ECAP can result in a higher strength material without a

substantial decrease in the elongation [65], however research suggests that this strengthening effect will no longer result in further improvement after a certain number of passes [71].

The ECAP process has utilised a wide range of metal feedstocks and despite it being common for solid, rod feedstocks to be used, the use of machining swarf has also been documented [72]. Compaction of the swarf under a single ECAP pass resulted in regions with voids and pores, however, further annealing treatments improved some of the porosity as seen in Figure 13 [72]. The work also resulted in a high theoretical density of around 99.3% and minimal porosity.

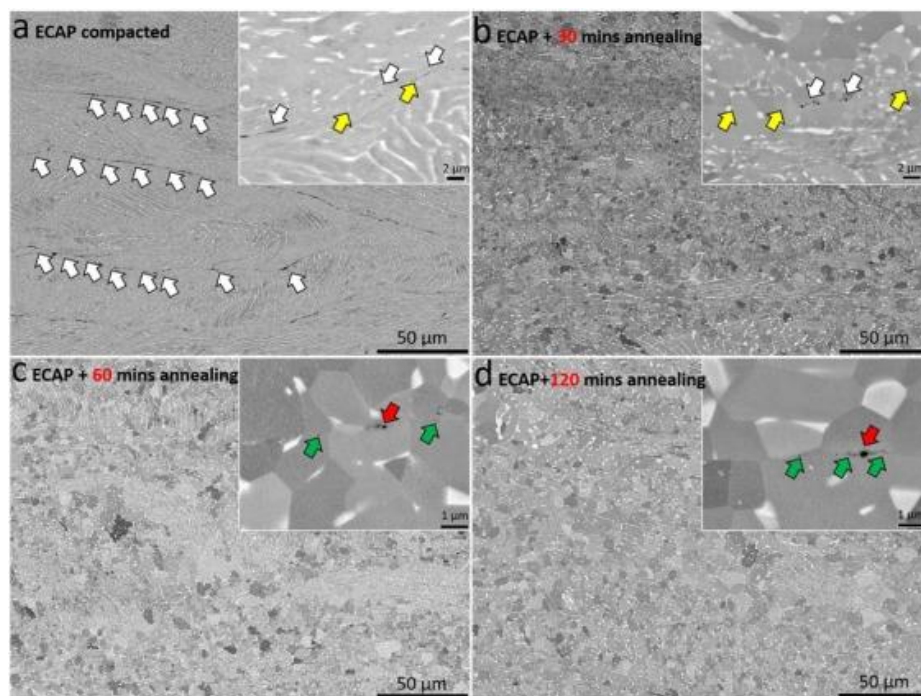


Figure 13 Back-scattered electron images of the microstructure after ECAP and consequent annealing at 120°C taken from [72] White arrows (a) indicate the interface between the chips, yellow arrows (b) show the boundary without pores when white arrows (b) indicate the pores, green arrows (c, d) show the nano-pores at interface, when red arrows (c, d) indicate the submicron pores at interface.

The combination with Conform™ is common in the literature, as it takes the batch process and makes it more continuous, and therefore, more industrially viable [70]. The processing deviates from both traditional ECAP and Conform™ by having a rotating wheel, as found in Conform™, to feed in the feedstock towards the 90° angle, found in ECAP, and use the friction between the groove wall and the material to severely plastically deform the material. The die

is often different to the shape of the groove in ConformTM, where in ECAP the die size tends to be the defining factor between the starting material and the product's cross-section. There have been successes using this process for the production of rod, however, the combination of the processes could be avoided by simply using the ConformTM process.

Results of CP Ti used in the ECAP-Conform process has often resulted in evident grain-refinement [73], as shown in Figure 14. The increasing grain size refinement, which ultimately results in a grain-size of around 200 nm, demonstrates a much higher yield and ultimate tensile strength than would be expected for a conventional rod of CP Ti.

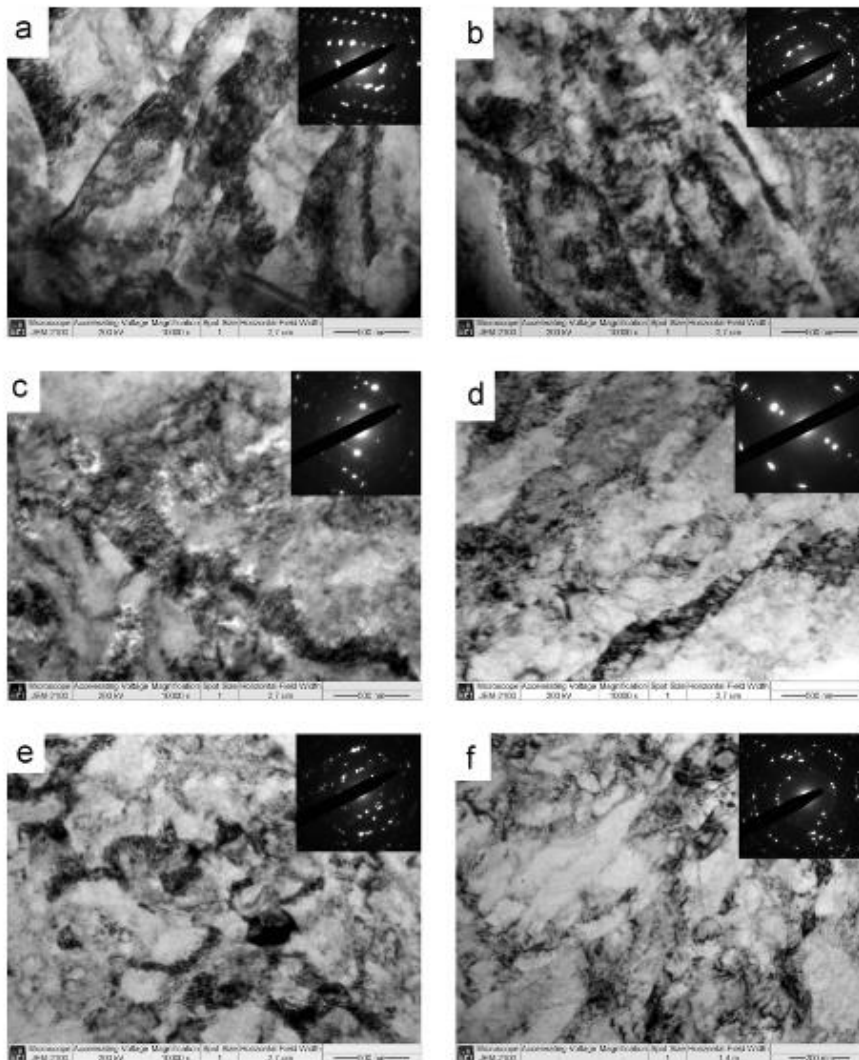


Figure 14 Bright-field TEM images of CP Ti after 1, 2, and 4 ECAP-C passes in cross and longitudinal sections. Cross section: (a) 1 pass, (c) 2 passes and (e) 4 passes; Longitudinal section: (b) 1 pass, (d) 2 passes and (f) 4 passes. Taken from [73].

Furthermore, whilst it is plausible for both ECAP and ConformTM to use particulate feedstocks, it is unusual in ECAP-Conform.

2.3 ConformTM

The ConformTM process was first developed in the 1970s by Derek Green, who was working for the UKAEA at Preston, Lancashire, UK [1]. The aim of the ConformTM process, at the time, was to recycle waste aluminium and copper components from the nuclear industry and deform these into new, usable parts [74]. The patent, simply titled ‘Extrusion.’, was published in 1973 and since then the process has been further developed [75]–[77]. Although, much of this research has occurred within the last 25 years, owing to a lack of understanding of the thermo-mechanical behaviour of the material during the process.



Figure 15 Photograph of a ConformTM machine produced by BWE Ltd., Ashford, UK. Taken from [78].

The ConformTM machine (shown in Figure 15) is a relatively simple machine to understand. There are multiple key components, which are the shoe (where the majority of the tooling is held), the wheel and the feedstock. A simple schematic of the machine is shown in Figure 16.

The shoe contains most of the tools used in the process, which include the abutment, the die, the die chamber and the entry block.

The feedstock is fed in using a powder hopper or some form of vibratory chute. This feeds into the apex of the wheel into the groove. As the wheel is rotated, the feedstock is forced around until it comes into contact with the abutment. The abutment protrudes into the groove of the wheel and is perhaps the most critical part of the process – without it, the material would not be led into the die, rather going completely around the wheel and into the waste.

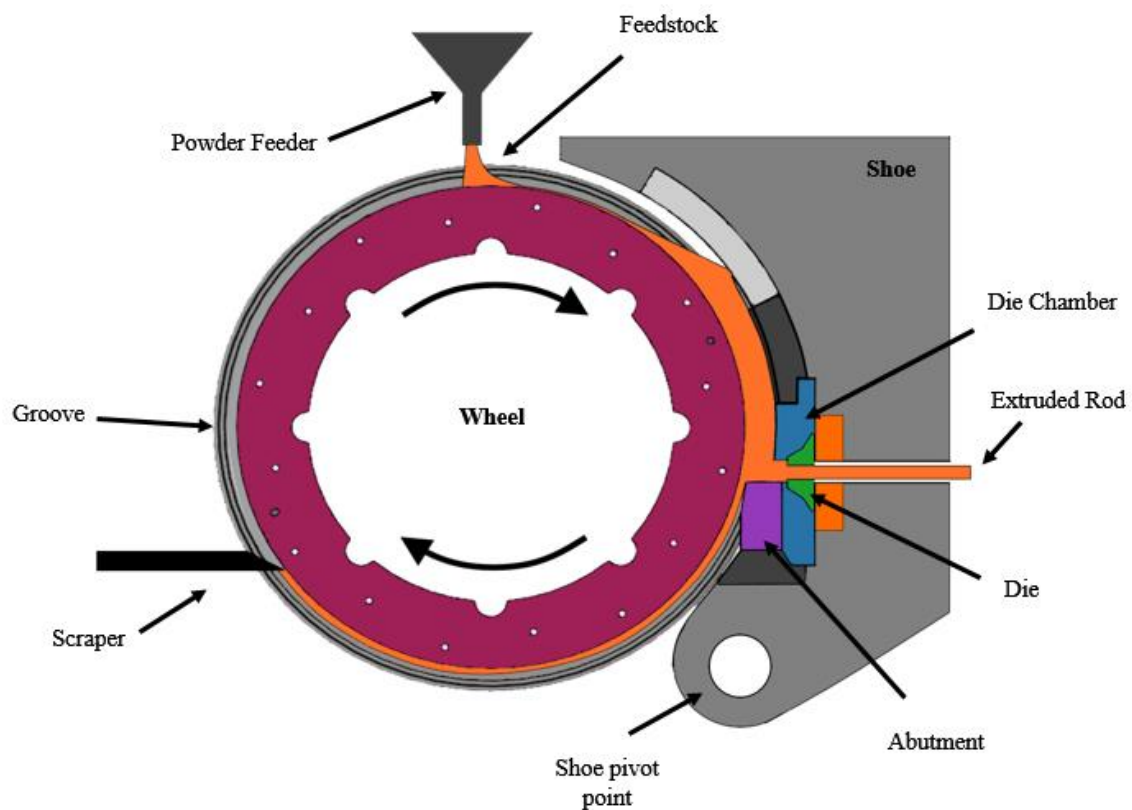


Figure 16 Schematic of a Conform™ continuous rotary extrusion machine.

Powder collects on top of the abutment; however, this will not yet be extruded. The process requires another key component – pressure. This pressure is generated from the temperature at the die, but most importantly, from friction. As the material is continuously rotated to the abutment, friction occurs between the material at the die and the material in the groove. This

leads to an increase in the pressure and ultimately causes the material to be forced through the die.

This process has some similarities with other SPD processes, especially with ECAP. The key link is found at the abutment, where the material is forced through a die which is perpendicular to the groove (which corresponds to the material flow).

2.3.1 Conform™ of rod feedstock

The initial use for the Conform™ process was to take a rod feedstock and deform this into a new rod feedstock. Since then, the process has primarily been used for the repurposing of aluminium and copper rod [79]–[81]. In recent years, however, there have been developments that have led to harder materials, such as titanium, being processed in this way [3], [82], [83].

In line with severe plastic deformation, the products of rod extrusion are often reported as having an ultra-fine grained microstructure [83], [84]. However, it is important to note that in many cases the rod has been processed multiple times, via processes such as rotary swaging [4]. Rotary swaging is where the cylindrical billet is formed using dies surrounding the workpiece and is, by definition, a forging process [85]. The processing will help to work-harden the material and consequently reduce the grain size further, leading to a higher strength material [86]. Typically a higher strength material will have a reduced ductility, but owing to the nature of severe plastic deformation, the ductility should be retained [87].

Whilst there are still significant gaps in the understanding of titanium rod feedstocks in the Conform™ process, such as trialling harder or alloyed materials, the focus of this research is particulate feedstocks.

2.3.2 Conform™ of particulate feedstocks

For the time that Conform™ has existed, the majority of the feedstocks have been in the form of rod. Recently, there has been an increase in the use of powder/particulate materials. One of the main reasons for this, is that the use of powder can reduce the cost from processing from ore to product.

The process has been trialling the use of particulate feedstocks since the 1978. In order to use particulate feedstocks, minor adaptations are made to the Conform™ machine by removing the coining roll for the feedstock and replacing this with a powder hopper or vibratory chute to feed the powder into the apex of the groove.

Changes to the Conform™ machine were first proposed in 1978 [75], when the use of machining chips was highlighted as a potential feedstock for the process. These changes are shown in Figure 17. However, these adaptations were not researched until later in the lifetime of the machine.

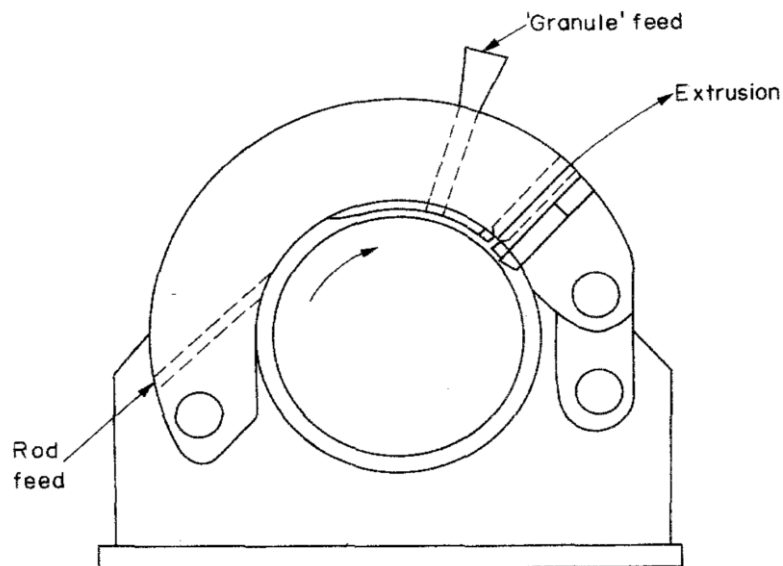


Figure 17 Schematic showing the adjustments made to the Conform™ process to allow for granular feedstocks. Taken from [75].

Typical feedstocks used in the process are particulate aluminium or copper. However, more recent developments have looked towards the use of titanium with results showing varying amounts of success, although this is improved when CP-Ti is used.

Results have also been shown with zinc [82] and magnesium [88] feedstocks, which have similar crystal structures to titanium. These have also been reported with success and help to pave the way for the Conform™ process to be used more commercially with feedstocks that are typically difficult to process.

However, the impact of particulate feedstocks, especially those which are traditionally harder to manufacture or process, is in much need of further investigation. With feedstocks such as titanium, higher processing temperatures and the higher strength of the feedstock can result in premature tooling failures, especially abutment wear. In some cases, brittle materials used for processing aluminium feedstocks can break away during titanium processing, resulting in highly contaminated products and trial failure.

Further to tooling faults, research by CSIRO has attempted to utilise inert gas shielding to prevent the encapsulation of interstitials, such as nitrogen, oxygen or carbon, as these elements can result in a more brittle product [89].

Currently, particulate ConformTM trials are hindered by the material of the abutment. In terms of tooling, previous work has shown the use of Stellite abutments [3], [90] which would demonstrate the brittle failure during a trial. This would mean that the end of the trial would be sudden. There has been little investigation into the impact of the tooling geometries and materials, with the exception of simulation-based work, where the feedstock was aluminium. Naturally, when trialling, the aim would be to produce tools which allow for significant volumes of material to be produced, and therefore the materials must be able to withstand high operating temperatures, extrusion pressure and the friction caused by the feedstock used.

Additionally, preliminary ConformTM research involving titanium has typically utilised commercially pure titanium, yet industries such as the aerospace industry, would be more likely to consider materials such as Ti-6Al-4V. There are various morphologies and powder size ranges to consider. Ultimately it would be ideal to collate a library of materials or even a reliable, inexpensive experimental testing method for powders prior to their use in the ConformTM process.

2.3.3 Simulating the ConformTM process

Despite being conceived in the 1970s, until recently, very little was understood about the thermomechanical processes occurring within the machine. In order to ascertain what it

happening, there have been a number of publications focussing on the simulation of the process, many of which are related to the use of an aluminium or copper feedstock [91]–[93].

Modelling and simulations are required to determine the optimal tools, feed rates and to help understand the process better. There are a number of different simulations and mathematical models proposed to develop the process and to investigate what exactly happens during the process. Both discrete element method (DEM) and finite element modelling (FEM) have been reported, as they are a more affordable method to investigate during an experiment without the need for expensive trials. They also allow predictions to be made on the outcome of the trials, which helps to maximise the process output.

The FEM is commonly used to investigate deformation of rod feedstocks and the stresses on the tooling. The key limitation is that it is not able to simulate particulate feedstocks, without significant processing or combination with DEM. DEM is ideal for particle modelling, which allows for investigation into how the particles are behaving during the process. Significantly less DEM has been performed for ConformTM in the literature, with common extrusion related to rod feedstocks rather than particulate.

Stadelmann [2] produced multiple simulations (see Figure 18), which aimed to investigate the change of various parameters on the outcome. For example, the study involved determining the impact of different alloy feedstocks, the impact of cooling at different points and the impact of various groove sizes. This was accomplished through the use of various mathematical models, particularly focussing on treating the material like a ‘thick fluid’ rather than a solid rod – as the material is expected to flow. For this reason, the use of fluid mechanics allows the material to be described in such a way. Key outcomes were that an increase in the wheel speed can lead to a reduction in the extrusion pressures and that by decreasing the cross-sectional area of the groove leads to an increase in the pressure gradient, suggesting that the higher pressure will help to increase the extrusion pressure.

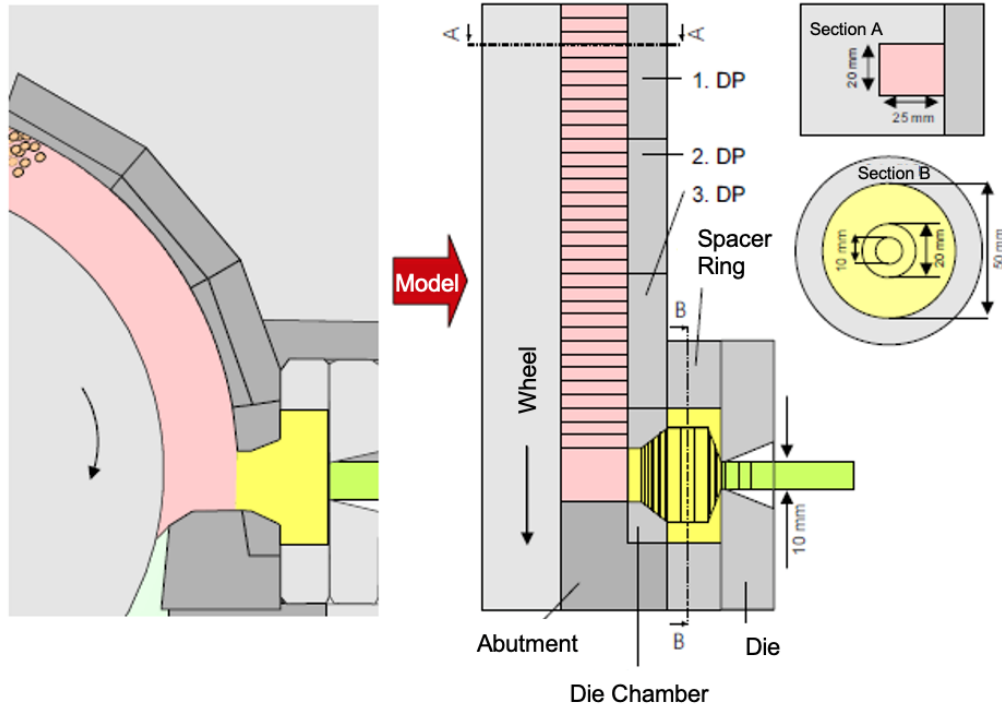


Figure 18 Tool and simulation schematic, showing the assumptions made for the wheel as a straight section.

Taken from the work of C Stadelmann [2].

However, this work was applied to rod aluminium feedstock, where the requirement of the groove is to grip the feedstock as it is pulled around to the abutment. This differs from particulate processing, where the groove helps to pull the material around to the abutment, but not by gripping, but purely through the material flowing through the groove and the rotation assisting that movement. The grip length in particulate corresponds to the height of the material held between the die chamber and the groove, which is material that has remained on top of the abutment, rather than falling through the flash gap. This is the point where friction between the tooling and the feedstock can result in consolidated material. There is little work investigating the impact of geometry variation for powder feedstock.

However, Thomas [90] created a mathematical model, which allows prediction of the extrusion pressures required for various material parameters and tooling geometries. This mathematical model was instrumental in the determination of the tool geometries within this work. It allows for changes in the geometries and consequent determination of the extrusion pressure. The experimental impact of these geometry changes has been little investigated, with this work looking to explore the variation in processing between two different tool sets. The

mathematical model takes the geometries of the proposed toolset, such as the port dimensions, flash gap width and wheel speed; the material data, including the flow stress, yield stress and powder size; and the extrusion parameters, such as temperature, powder feed rate and extrusion speed. With this information, the extrusion pressure, abutment pressure and wheel torque can be estimated for any given toolset or powder feedstock.

Despite recent work conducted to assess, via simulation, what is happening during the process, this is not often compared to data recorded during the trials. The work addressing the change in the grip length during the process and how the parameters can impact the resulting product, however, it does not conclude any similarities in the data between trials and allow predictions to be made for the point at which a material is extruding and whether the conditions are viable for the extrusion to continue. This data includes the changing temperature of the tooling and the consequently calculated stresses on the tooling.

2.3.4 Recycling

As with most materials, recycling and reducing waste material is a concept that has gained traction in recent years, despite being a key aim in many industries for centuries.

Even at its conception, the ConformTM process was outlined as a method of recycling waste components [94].

However, with waste typically arising from the machining of parts (particularly in aerospace and automotive industries), methods of recycling machining chips, or swarf, are equally necessary.

At this point, a note should be made to highlight that this was consideration made by Etherington in 1978 [75] suggesting that ConformTM could be adapted to make use of granular materials. In fact, the successful extrusion of aluminium scrap was reported in that very work.

Although ConformTM is the main focus of this thesis, there are other proposed (and used) methods for the recycling of swarf.

Possibly the most common method would be to remelt the material into a billet [95]. The resulting material would be viable for use in some non-safety critical components. The reason that it could not be reused for critical components is that the material would no longer reach the specifications outlined in the standards for aerospace components due to the possibility of minor contaminants and oxygen pick-up.

Despite some research on the recycling of waste titanium, there is still a significant amount of waste that cannot be reused, which naturally has a large cost impact on the use of titanium in industry. However, the use of Conform™ for recycling has been little investigated with potential benefits, especially considering the potentials of producing feedstocks for more recent process developments such as additive manufacturing. This would help to establish a circular economy, whereby industry could utilise their own waste to make feedstocks for processes they already use.

2.4 Powder Metallurgy

Powder metallurgy is a particularly important subset of metallurgy. It allows for the creation of novel alloys, which would not be feasible under traditional methods, and it has led to the use of novel and alternative manufacturing methods, such as additive manufacturing and extrusion.

In the context of this work, the use of powder metallurgy for use in novel processes is key. Previously, extrusion processes have been reserved for solid feedstocks, which are drawn down through numerous dies to form the desired profile. However, the introduction of powder to these processes allows for the creation of products, which may have otherwise been unattainable. Additionally, this extends into forging processes, where the product can be tailored to suit the purpose by using multiple alloy powders to produce a single billet.

Covered earlier in this chapter (see *Powder Metallurgy*), there are different ways to produce titanium powders. Those discussed, and consequently used in this work, are HDH and GA powders. The methods are distinct, and each have their own benefits. HDH powders are cheaper to manufacture, are irregular in morphology but have a higher chance of containing contaminants. GA powders, on the other hand, are much more expensive to produce, are often spherical in morphology and are unlikely to contain the contaminants seen in HDH powders.

2.4.1 Powder characterisation methods

Particulate materials have different behavioural properties to consider than the average rod feedstock. With rod feedstocks, the main considerations are how the bulk of the material responds to each of the conditions that will be applied. When starting to look at powders, it is important to consider that each individual particle can behave independently to the bulk.

There are a number of widely used methods for assessing powder behaviour, such as the flowability and density. Firstly, the angle of repose, which is a commonly used method for validating powder simulations (in discrete element modelling, DEM). Simply, the powder is poured into a pile and the angle of this pile is measured [96], [97]. This helps to determine how the particles stack. Secondly, there are the bulk and tap densities. When a powder is poured into any receptacle, it is classed as having its bulk density [98]. If this powder is then agitated, the arrangement of the particles can adjust, such that the density in the receptacle is reduced. When this happens, the tap density is achieved. Finally, there is often variation in the size of the particles in the feedstock. Following production, the powder is sieved to specific degrees of accuracy, leaving a powder size range. The size range of any powder can be assessed by taking a sample of the powder and using light to determine the average particle size, the range of the particle sizes and the mean particle size. Typically, powder processes (especially additive manufacturing processes) require specific particle size distributions, and this is a quick method for assessing this.

These are the three main methods used, however, advancements in characterisation equipment means that are more methods that can be used.

2.4.2 Shear Testing

Commonly used in the pharmaceutical industry to determine how well powders compress under shear, shear testing methods can also be applicable in powder metallurgy.

There are a few popular shear testing methods currently in use in the pharmaceutical industry, including the annular shear cell and the Jenike shear cell method. Both these methods operate in a similar manner [99]. A schematic of a Jenike shear cell tester is shown in Figure 19.

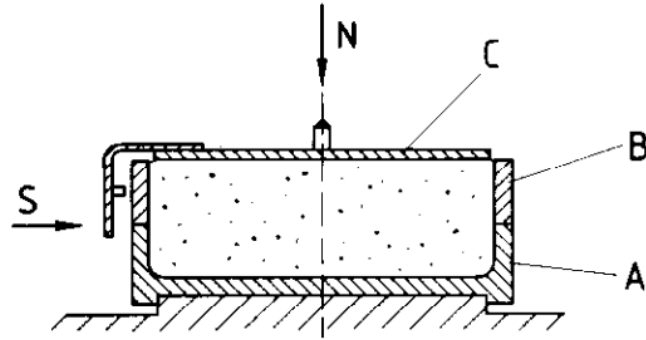


Figure 19 An example schematic of a Jenike shear cell tester; A is the base; B is the ring and C is the lid. Taken from [100]

However, these methods are not used for metal particles, with the focus being tablet compaction. The obvious step forward would be to investigate the consolidation and shear behaviour of metal powders, with particulate feedstocks becoming more popular in recent years.

For shear cell testing there are a few key components. Firstly, the material that is under the test must be placed into some sort of die or holder. This will both shape the powder but also hold it throughout the course of the test. Secondly, a ram is required to apply a downwards force on the material but also rotate, in order to generate shear.

These methods are typically attempting to produce consolidated preform. However, additional parameters can be assessed to optimise the consolidation process. When translating this method over to powder metallurgy, there are a few additional things to consider. The aim is not to produce a single tablet form, as this would have very little use. The interesting parameters are whether the material consolidates at all and what sort of pressures are required to do so. The aim of the test is to simulate the ConformTM process, where particles are under continuous shear led by wheel rotation and consequent friction between powder particles.

2.4.3 Powder behaviour under shear

It has been documented in the past [101], that in order to model the compaction of powder particles, there are three stages of compaction (also demonstrated in Figure 20) to consider:

- a) **Rearrangement of particles** - this relates directly to the coordination number of the particle. Particles which have formed additional contacts through rearrangement will deform plastically

- b) **Progressive flattening and densification** - particle neighbours are brought closer together and consequently form additional contacts

- c) **Neighbour contacts impinge deformation** - as the number of contacts increase, the more the deformation becomes impinged and therefore, harder to compress. This is last stage of compaction.

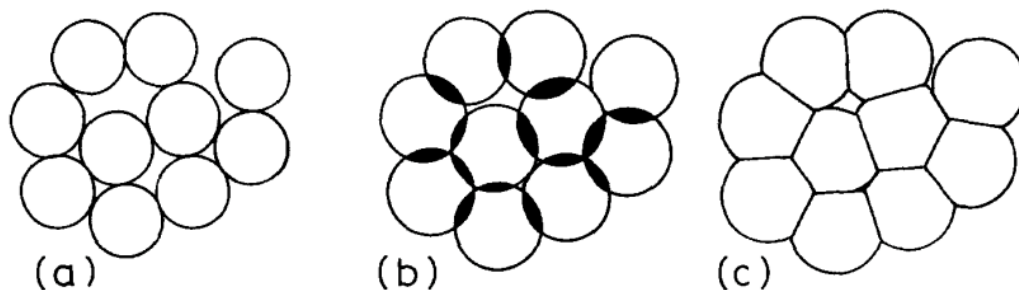


Figure 20 Schematic showing the three stages of compaction, where (a) shows the rearrangement of particles, (b) shows the flattening and densification, and (c) shows neighbour contacts impinging the deformation. Taken from [101]

Arguably, these three stages can be combined into two; (i) decrease in volume and (ii) particle fracture [102]. During the earlier stages, the forced reduction in volume results in strain on the particles from their contacts and ultimately, results in work-hardening of the particles [103]. The work-hardening coupled with growth of contact areas due to particle deformation results in an increased resistance to particle compaction. Particle fracture occurs during the last stage, as the oxide film is ruptured at the metal-metal contacts [104]. Further work [105] suggests that consolidation of powder particles can be explained by adhesion forces at the particle contacts, giving further evidence to the theory outlined above.

During compaction, the coordination number of each particle increases, and consequently, the forces on the contacts reduces as there are now more contacts to each particle. This happens slowly until a density of ~90% has been achieved, at which point contact impingement occurs

[106]. Whilst approaching the point of impingement, the densification reach a point of resistance, where further increases in the density are determined by the size and number of contacts to particles [101]. Finally, impingement leads to strain hardening, and as a result, the plastic properties of the particle influence the deformation and consequent joining of neighbouring particles.

In powder shear, there is more than the downwards compaction to consider, as uniaxial rotation further complicates matters. There are a number of powder shear methods currently available such as the FT4 powder rheometer, which can be used to determine powder flow properties alongside shear properties.

Work completed by Kondo *et al.* [107] has shown the densification of metal powders using uniaxial compression and rotation. The work investigated the impact of rotation on powder densification and showed a distinct increase in the density within the first 90° rotation.

However, this work did not investigate the impact of particle morphology or rotation speed on the densification of the material.

The University of Sheffield currently houses a novel testing machine, the Arbitrary Strain Path (ASP) test machine, often used for machining processes. The ASP is a servo-hydraulic machine, which is controlled via PID (positional, integral, derivative)-controllers. In past work, the PID-controllers have been tuned to hold the temperature more accurately during more complex processes [108] and can be used as part of the machine calibration, ensuring that the results achieved are accurate. During this work, the PID-controllers were not adjusted from their previous setting during the calibration. In future work, it would be advantageous to tune the PID-controllers to optimise the output from the tests.

The ASP has a number of imposed limits to ensure that operation of the machine is safe. Therefore, it is unable to exceed a displacement of 50 mm, the maximum number of rotations allowed is 7.2, the limit to the vertical load is 100 kN and the maximum torque is 500 Nm.

For this work, this machine has been adapted, by means of bespoke tooling, to allow for uniaxial compression and rotation. This would allow further investigation of the shear of powder particles, focussing on the influence of speed, load and particle morphology.

Ultimately, this may help further understand the behaviour of powder particles within the Conform™ process and therefore, provide a low cost, experimental method for assessing the ability of various feedstocks to consolidate during the Conform™ process.

2.5 Wire

2.5.1 Production

Wire is drawn down through various diameter dies in order to achieve the desired diameter. It is not possible to achieve a large reduction ($> 10\%$) in a single pass, and so multiple dies are used. It is often the case that heat treatments are conducted between passes to further improve and retain mechanical properties [109], [110].

Wire can be produced by different methods such as traditional wire drawing, rotary swaging, and, more recently, methods like accumulative angular drawing (AAD). These methods often lead to work hardening, which results in a higher tensile strength of the output wire, however, the ductility can be retained.

Traditional wire drawing takes the workpieces and draws it down through a die smaller than its cross-sectional diameter. This is then repeated, leading to a smaller diameter material, often with some grain refinement and resulting in a higher strength product. On the other side, there are forging processes such as rotary swaging (discussed previously), which can be used to forge wire through applying dies around the workpiece. This results in work hardening, grain refinement and a higher strength material.

Much like traditional wire drawing, AAD is a drawing, rather than forging techniques. Accumulative Angular Drawing (AAD) is a relatively recent technique, and the process works by drawing the material through a number of different dies, which can be set at linear, stepped or cranked positions; the latter introducing a more complex strain path for the material. It has been demonstrated in steels such as 304L stainless steel, aluminium and copper, and resulted in a wire with higher strengths as a result of grain refinement through severe plastic deformation and the application of high strain to the material [111], [112].

2.5.2 Uses

There are many different uses for metal wire, and the wire used depends entirely on the mechanical and chemical requirements. Figure 21 suggests various uses for titanium wire and each of these uses comes with its own set of requirements.

Starting at the least demanding properties, steelmaking utilises cored titanium wire. The cored wire is primarily used for reducing the oxygen, carbon and nitrogen content of the steel and owing to titanium's affinity for these elements, it is the prime choice for this role. Additionally, the quality required is low as the role does not require high mechanical properties.

Secondly, additive manufacturing, which is one of the more recent developments in titanium research. As more industries start to utilise this technology, the trend towards the use of wire (over powder) is increasing, as the feedstock is cheaper and ultimately less material is lost during the process [113]. The key properties required are mostly related to the oxygen content of the titanium wire used, as AM processes can pick up oxygen (unless completed in an inert atmosphere), and the ductility (the wire should be able to coil for ease of input into the system) [114].

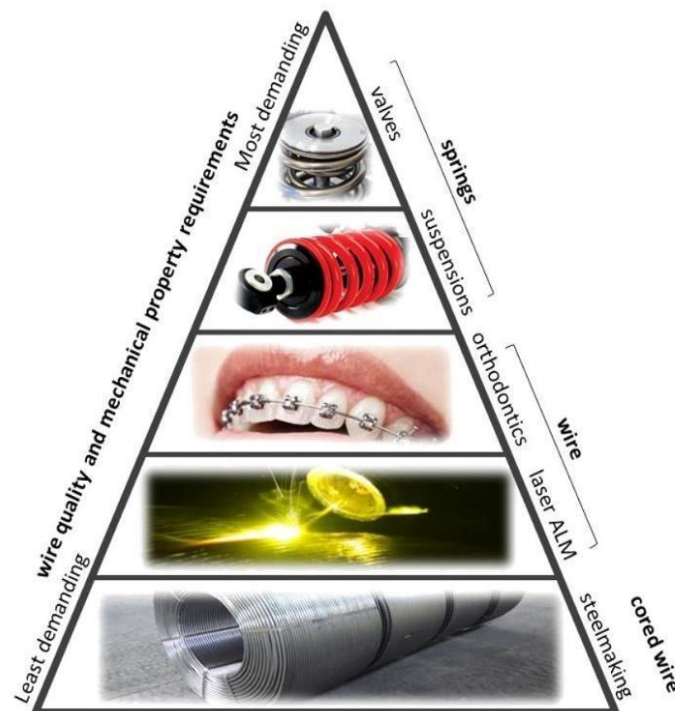


Figure 21 Diagram demonstrating the uses of metal wires and the quality required from them.

Titanium alloys, particularly Ti-6Al-4V, exhibit biocompatible properties, which mean that they can be used within the body. Control of the alloying additions can also reduce the likelihood of allergic reactions to the titanium, as elements such as nickel are common allergens. Coupling these properties with ductility, good strength and corrosion resistance makes titanium wire an ideal candidate for orthodontic devices, such as braces.

The automotive industry is trending towards lightweight engine components [115], [116], which although can be attained using some steels, the mechanical properties are not comparable to those of titanium. For components such as suspension and valves springs, titanium wire is a clear contender, with the high strength to weight ratio, good ductility and corrosion resistant properties. However, it is important to note that these properties can be difficult to attain, and failure to do so can be catastrophic for an engine.

As is clearly described above, there is a wide market for titanium wire and this is unlikely to decrease in the near future, with increased use of titanium in aerospace and automotive engines and medical devices. Additive manufacturing using titanium wire is an ever-growing area of research, with more benefits of wire (when compared to powder processes).

2.5.3 Additive manufacturing

Defined by the ASTM standard as the process of ‘joining materials to make objects from 3D model data, usually layer upon layer, as opposed to subtractive manufacturing methodologies’ [ASTM F2792-12a], additive manufacture has recently developed a surge of interest in its use for the manufacturing of non-critical aerospace components and medical implants. Conventional processing routes for components like this typically require large volumes of machining, with 80 – 90 % of the material being removed and this can have a direct impact on the cost of the component [117]. The buy-to-fly ratio is significantly impacted, as where forged material has a ratio of between 10 and 20 [118], with AM techniques, there is a potential for a value closer to 1 [119].

Using AM methods would generate a near-net shape (NNS) component, which would ultimately require less machining, thus reducing the cost and the volume of waste produced.

However, it is important to note, that at the time of writing, critical components will likely never be made from NNS powder processes.

Currently, titanium components are a luxury for many industries, owing to the high cost. Although, the mechanical and chemical properties of titanium would be ideal for these non-safety critical parts. There is a potential economic benefit from using NNS processes, as this could lead to a more viable price range for industries looking to expand their components into titanium – which offers an excellent strength to weight ratio, high corrosion resistance and biocompatibility.

There are a vast number of AM processes available at the moment but the majority fall under two key categories: powder bed fusion (PBF) and direct energy deposition (DED).

PBF processes, as the name suggests, consists of a powder bed, to which a power source is supplied. This power source is typically a laser or electron beam and is used to fuse the powder particles together to form a solid layer of the component. This is repeated as each layer is completed (based on the cross-sectional design of the component) [120].

DED processes differ from PBF as they do not require a powder bed. Instead, a melted material feedstock is deposited onto a surface. This melted material can consist of wire or powder and involves the formation of a melt pool, to which the wire or powder can be injected, forming each layer of the product [121].

The key considerations with products produced from AM processes are regarding the mechanical properties of the resultant component and how this is influence by the microstructure and defects present in the material.

Theoretically, AM processes could form a fully dense, 3D part with complex geometries [122], [123].

AM, whilst having slight reductions in the mechanical properties, combats the constraints of traditional subtractive and formative methods. With the increase in the ductility and the fatigue life, through the use of processes like HIPing and post-production heat treatments, the

reductions in the mechanical properties are greatly improved. The reduced component cost, reduction in waste and possibility of more complex builds places AM as a leader in the future of metals manufacturing.

Typically, additive manufacturing uses powder feedstocks, however, one alternative is wire deposition. Despite being a recent development, the method links back to a paper first published in 1920. The paper outlined the production of ‘decorative articles’ using wire, which had been welded layer by layer to form a finished product [124]. Since then, wire deposition processes have changed significantly, with the biggest update being that more critical aerospace components can be made, rather than just ‘decorative articles’.

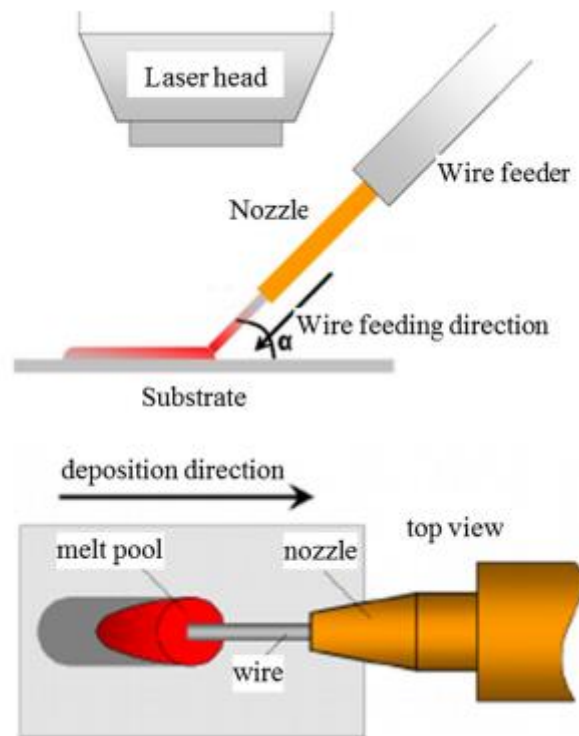


Figure 22 Schematic of a wire-fed deposition process taken from [125].

As shown in Figure 22, there are three key components required in wire additive manufacturing:

- a) **Feedstock** - a wire feedstock, which maintains enough ductility to be coiled prior to operation and a low enough oxygen content, that would not impact the resulting product performance (noting that oxygen is often picked up during AM processes)

- b) **Heat Source** - this source can be a laser or an electrode and is required to form a melt pool from the wire being added into the process. One such example is in WAAM, where an arc welding system is in place, where an electrode is used to melt the wire.

- c) **Movement** - the resulting product can be a complex shape, and so the heat source must be able to be moved according to the CAD file.

Simply put, wire deposition takes a CAD file of the product and wire is laid layer-by-layer, until the resulting product is achieved.

2.6 Summary

There is a lack of investigation into the use of alternative feedstock morphologies, where typical work utilises various titanium alloys as rod feedstocks or commercially pure titanium particulate feedstocks. The ability to extrude alternative feedstocks such as swarf, non-CP-Ti alloys and a discussion on the influence of particle morphology will allow a key step forward in the use of ConformTM with titanium. Additionally, with a rise in the use of titanium powders for AM, there is still significant waste and other than remelting, the current options for recycling are limited. The ConformTM process could provide a cost-effective, single-step alternative for the production of a potentially viable AM feedstock.

Further to this, the use of tooling is rarely discussed for particulate feedstocks, with work typically using one set up, rather than investigating alternatives. Examples of the investigation of the impact of changing the tooling geometries were simulations conducted by Stadelmann [2] and a mathematical model produced by Thomas [90], however, there is little experimental work using simulation and mathematical models to inform the tooling design.

Finally, whilst powder shear, including that for metallic powders, is growing in interest due to additive manufacturing, it is still relatively unexplored for titanium particulate of various

morphologies. The ASP gives a unique alternative, which would allow a link to be made between the densification and consolidation of powder particles, to how they behave in an environment such as that imposed during a ConformTM trial.

The work in this thesis looks to address the above points and open up a number of options for future.

Chapter 3 : Materials and Methodologies

3.1 Materials

A range of titanium alloy powders (listed below in Table 1) were used throughout the project and are shown in Table 1.

Table 1 Titanium particulate feedstocks used for Conform trials.

| Alloy | Grade | Size Range / μm | Chemical Composition / % | | | | | | | | Supplier |
|-----------------|-------|-------------------------------|--------------------------|------|------|-------|-------|--------|--------|------|----------|
| | | | Ti | Al | V | C | O | N | H | Fe | |
| CP Ti HDH | 1 | 45 – 105 | >99 | - | - | 0.1 | 0.18 | 0.03 | 0.015 | 0.2 | Phelly |
| CP Ti HDH | 2 | 45 – 150 | - | | | | | | | | Phelly |
| Ti-6Al-4V HDH | 5 | 75 – 150 | - | | | | | | | | Reading |
| Ti-6Al-4V GA | 5 | 67 - 750 | >89 | 6.01 | 3.73 | 0.025 | 0.137 | <0.005 | 0.0007 | 0.19 | Puris |
| Ti-6Al-4V Swarf | 5 | 1 – 10 mm | - | | | | | | | | Airbus |

The particulate feedstocks were selected based on (1) morphology and (2) alloy chemistry.

1) The particle **morphology** was typically ranged between spherical and irregular/angular. Under shear, both of these powders behave differently, with irregular powders being easier to consolidate as small fragments require less strength to break off from the powder particles. Selecting powders that fell under these categories allowed for a wider data set to be collected and helped to investigate the impact of powder morphology on consolidation during continuous extrusion. The swarf material was used in order to demonstrate that the recycling of titanium using the continuous extrusion approach was feasible.

2) The **alloy chemistry** ranged from the commercially pure (CP-Ti) to Ti-6Al-4V which is widely used in the aerospace industry. It is a widely used alloy due to its excellent mechanical properties and relatively lower cost compared to more exotic aerospace alloys. In terms of the

excellent mechanical properties of Ti-6Al-4V, it can be noted that the yield strength is typically almost double that of CP Ti HDH.

Ultimately, this gave a wide range of options with regards to particulate feedstocks and allowed for a data to be collected for various morphologies and chemistries.

3.2 Powder Characterisation

In order to evaluate and rank each of the particulate feedstocks, a number of methods needed to be employed. These are:

- 1) Angle of Repose
- 2) Bulk/Tap Density
- 3) Particle Size Distribution (PSD)
- 4) Powder imaging (SEM)

The methods used allowed for the determination of the powder size, the powder behaviour and the powder density. From this data, simulations can be developed for the starting powder characteristics to enable comparisons with experimental data.

3.2.1 Angle of Repose

The angle of repose (shown in Figure 23) was determined by the standard following on from Hall Flow measurements (ASTM B213). The powder was poured through a funnel to form a pile. The angle of the pile was then measured. This was repeated 3 times to ensure accurate results.

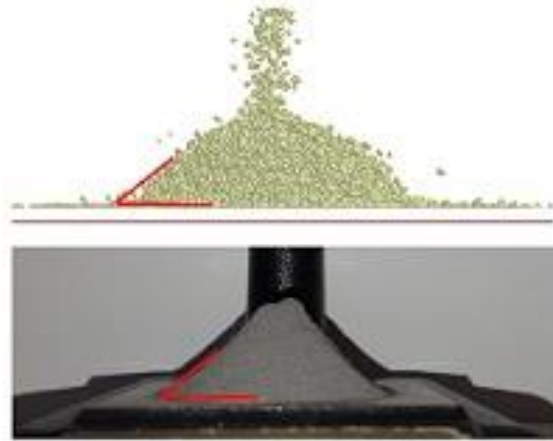


*Figure 23 Photograph (bottom) and corresponding simulation (top) of an Angle of Repose with CP-Ti Gr2
HDH*

The resulting angle can be compared against a simulated pile of powder (in discrete element modelling), which allows the simulation to be validated.

3.2.2 Bulk/Tap Density

The bulk density is the density of the material upon rest – where no agitation has been applied to the powder. This density is useful, particularly in shear testing, as it provided a base value for the powder and therefore, the density after shear can be compared after testing.

To determine the bulk density, a 250 cm³ measuring cylinder was weighed on a set of lab scales and then zeroed, to ensure that the scales were set at 0g before adding any powder. The powder was added by pouring slowly into a 250 cm³ graduated measuring cylinder, taking care not to disturb the powder once settled. The weight was recorded and the test repeated. The density was then calculated, and an average result was obtained.

The tap density is similar to the bulk density; however, the graduated cylinder is tapped on a flat surface for a fixed number of taps. The density is then calculated. Although not used in this work, the tap density often uses a fixed implement, which can provide consistent tapping of the graduated cylinder to ensure it can be standardised. The method, otherwise, is carried out in much the same way as the bulk density.

3.2.3 Particle Size Distribution

The particle size distribution was determined for each of the powders used. This was accomplished using a Malvern Mastersizer 3000. The data was processed after testing.

The particle size distribution (PSD) determines the number of particles at a given size fraction and can be used to inform computational simulations.

3.2.4 Powder Imaging

3.2.4.1 Light Microscopy

Powder was combined and mounted on an epoxy resin and then polished using a standard technique for titanium (see 3.3.1). The samples were imaged using a Nikon light microscope.

3.2.4.2 Scanning Electron Microscopy

Powder was mounted on a carbon dot on an SEM stub for high resolution electron microscopy using an Inspect F50 with a working distance of 10 mm, a spot size of 5 and an electron beam accelerating voltage of 20 kV.

3.3 Mechanical Testing

The results of the mechanical testing and microstructural analysis are given in *Chapter 8*.

3.3.1 Metallurgical Preparation

The powder was cold mounted in resin, after which the top layers were ground back using 400, 800 and finally 1200 grit papers for 30 s per paper, followed by polishing using a silica suspension (Colloidal Silica 9:1 30 percent H₂O₂ in water).

Solid titanium wire samples were prepared using a similar method. The sample was mounted in Bakelite and the top layers ground using 400, 800 and 1200 grit papers. Each grit was used

for 4 papers, at 30 s per paper. This was followed by 9 μm diamond suspension for 5 minutes and finally polished using a silica suspension (Colloidal Silica 9:1 30 percent H_2O_2 in water) for 15 minutes.

3.3.2 Light Microscopy

3.3.2.1 Wire Samples

Prepared samples were images using light microscopy. This was completed using a Nikon microscope. The images were taken at a magnification of 10x with cross-polarised light.

3.3.3 Tensile Testing

Tensile specimens were made to a variation of the ASTM E8/8M standard with 2.5 mm gauge diameter and 15 mm gauge length. These samples were to be used with 3 mm diameter collets. These were tested to failure on a Zwick/Roell Tensile tester.

3.3.4 Microhardness Indenting

The microhardness was recorded along the cross-section of the material and the longitudinal direction. This was completed using a Struers DuraScan 70 hardness tester with ecos Workflow software. The number of indents depended on the trial and length of the longitudinal samples. The number of indents for each sample is shown in the table below. The indents were made for HV1 with a dwell time of 10 - 15s (depending on the trial).

3.4 Arbitrary Strain Path Machine

The ASP is a bespoke piece of equipment (shown in Figure 24), which determines the torque and displacement during powder shear. The tooling, designed for the shearing of powder, is filled with powder at bulk density. This is then placed into the machine and a load is applied. The speed of rotation and the load are fixed. The test will run a single 360° rotation.

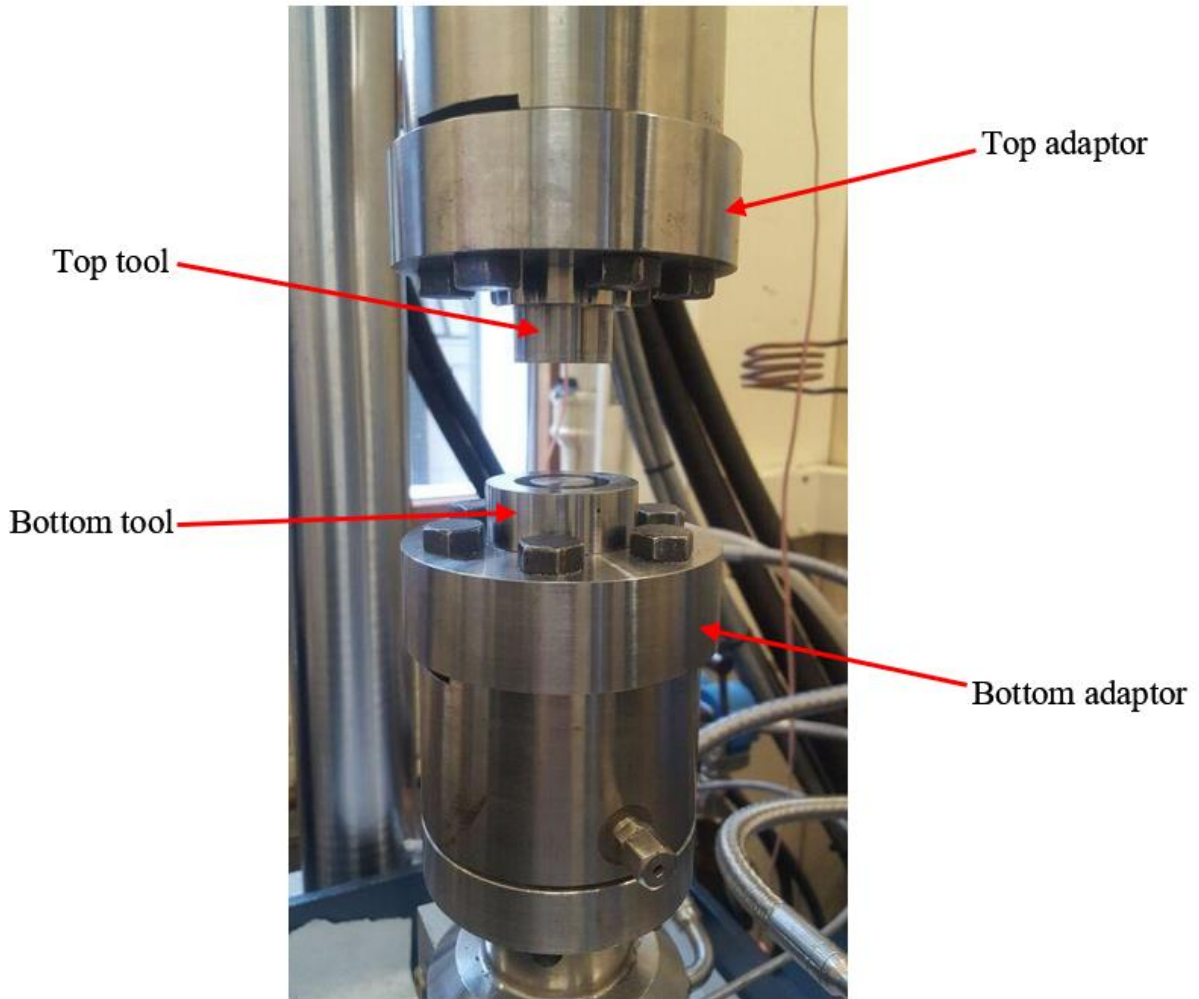


Figure 24 Photograph of the tools in the Arbitrary Strain Path (ASP) test machine

There are four components which make up the tooling for these trials. Two components are the holders, which hold the integral parts of the tooling. One is positioned on the upper portion of the machine, the second sits on the bottom half. The key tools however are distinctly different and are shown in Figure 25. The CAD drawings can be seen in *Appendix 2* and each piece was made from EN45 tool steel.

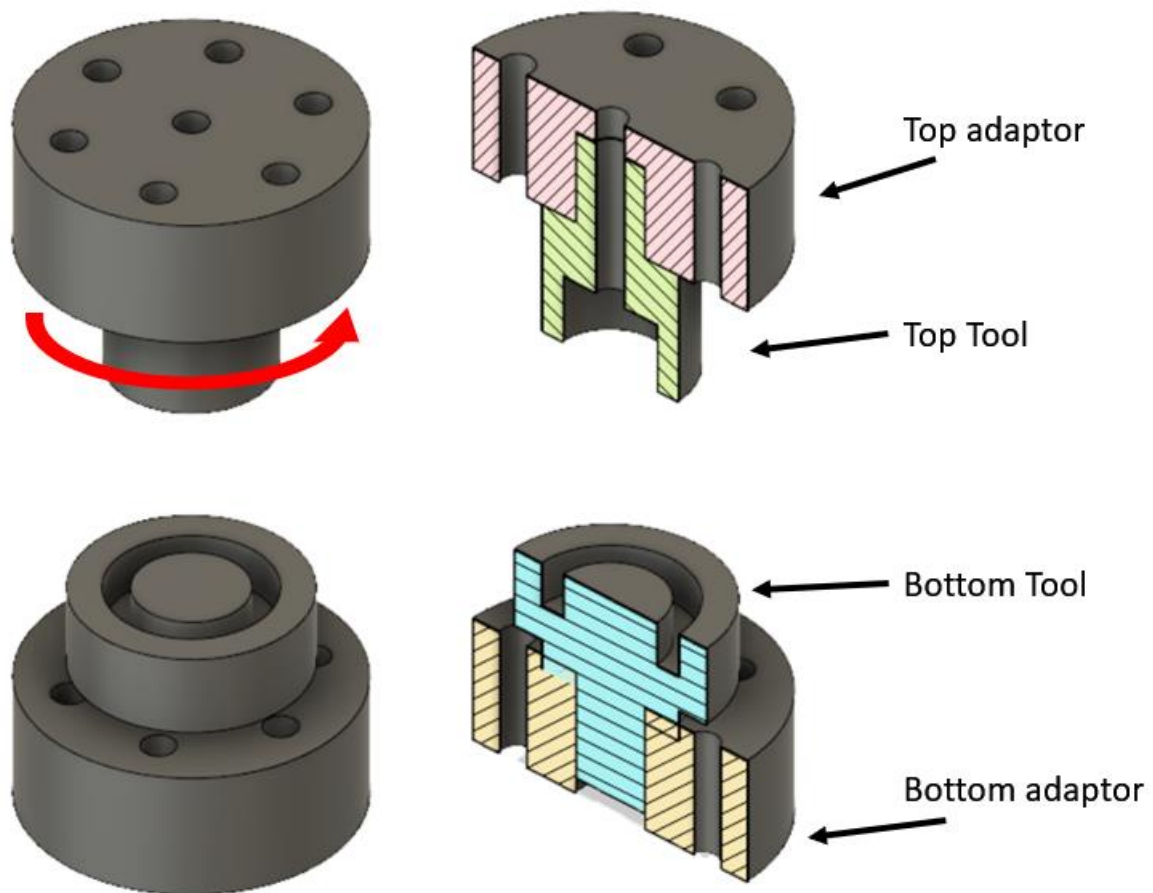


Figure 25 Schematic of the top and bottom tools used during a powder shear test.

3.4.1 Calibration

Prior to testing, the tooling must be calibrated in the machine, in order to prevent the tooling from being off-centre during the tests and to make sure that there is no interference between the top and bottom tools.

The process of calibration starts by installing the top tool to the machine. The tool should be installed loosely, as a dial test indicator (DTI) will be affixed to the side of the machine in order to make sure that the top tool is central before tightening. Once the DTI determines that the maximum and minimum are close in value (within 5 mm of each other), the top tool can be tightened in place.

Following this the bottom tool can be installed. The top tool should be dropped slowly into the

bottom tool to make sure that there is no catching or friction between the tools. This can be done by lowering the arm (adjusting the displacement) or the crosshead. Once this is done, the displacement can be set to zero by setting to zero when the tools are aligned (bottom of the top tool is in line with the top of the bottom tool).

Finally, the load and torque should be set to zero. The top tool is then lowered into the bottom tool (manually) and the test is started. Note: during this test, no fixed load is given, as this would lead to the tools crashing into one another.

3.4.2 Testing

After completing the calibration, powder can be added to the bottom tool. The powder should be added slowly in order to ensure that it compares more to the bulk density, rather than the much denser tap density of the powder used. The tooling is then weighed to ascertain the mass of the powder added, allowing for the density to be determined.

The bottom tool is placed into the machine, the top tool is lowered onto the bottom tool manually, with a slow descent of around 2 mm/s. Once the bottom tool starts to register a load of around 0.1 kN, the load can then be fixed. This means that the load settings are changed, so that an automatic load is applied directly to the material below. It is important that the registered load is monitored at this point, in case the tooling is catching. If this is the case, the calibration will have to be repeated to make sure that the tools are affixed correctly and are at the centre. However, should the tools be aligned, the test can begin.

There are a number of parameters, which must be adjusted in order to run the test. These parameters are:

- 1) Load (fixed)
- 2) Ramp rate (fixed)
- 3) Angle control (degrees per second and number of rotations)

The load is fixed for each test, in order to measure the displacement based on constant load and rotation speed. Typically, the tests only require one rotation – although a maximum of 7.2 are capable on this machine. The ramp rate is the speed at which the load is applied to the bottom

tool. This should be kept reasonably low to prevent powder spillage. Finally, the angle control is responsible for the rotation speed (fixed) and the number of rotations done. The rotation speed, like the load, is constant, in order to record the torque recorded.

3.4.3 Analysis Method

The result of each test is a file containing four sets of raw data. These sets are:

- 1) Load
- 2) Displacement
- 3) Torque
- 4) Angle

For each test, a single revolution is completed, therefore the angle is used instead of time.

The aim of this work is to investigate the density change (from the bulk density) for different loads and rotation speeds. This allows the determination of the required loads and speeds, which could be inferred to the extrusion pressures and wheel speeds required by Conform™ for different powders. Additionally, the consolidation of the material (other than the increased density) can be investigated based on the cover of material consolidated into a foil across the surface of the tooling. The different powders will also be compared to see how their morphologies and chemistries impact the results.

Fifteen tests were performed using the ASP under three key parameters:

- 1) Powder
- 2) Load
- 3) Rotation Speed

For each of the four powders, three tests will be performed at constant load but at three different speeds (120, 360 and 600°/s) and three tests at constant rotation speed (360°/s) but at three different loads (5, 10 and 15 kN). This gives a large enough data set to determine the impact of speed, load and powder morphology on the results.

CP Ti HDH Grade 1 was left out of the testing as the irregular powder and CP Ti HDH values were already accounted for through the CP Ti HDH grade 2. Additionally, the grade 1 powder was only used in one of the Conform™ trials.

3.4.4 Feedstocks

Four different feedstocks were used for the ASP tests, each with its own particle size distribution and morphology (shown in Figure 26). The materials used are:

1. **Commercially pure titanium hydride-dehydride (CP Ti HDH)** – this powder has an irregular morphology and is typically used to help initiate the extrusion of material during a Conform trial. The irregular morphology aids in generating friction, which leads to an increase in temperature and therefore, an increase in the extrusion pressure. The PSD is 45 – 150 μm .
2. **Ti-6Al-4V HDH** – similar to CP Ti, this powder also has an irregular morphology. However, it contains alloying elements, aluminium and vanadium, resulting in a higher strength and therefore, a slight reluctance to deform (compared to CP Ti HDH). The PSD is 75 – 150 μm .
3. **Ti-6Al-4V GA** – varies from previous materials as it is spherical in morphology, as opposed to the irregular structure of the previous materials. The PSD has a much larger size range of 65 – 750 μm .
4. **Ti-6Al-4V swarf** – resulting from the machining of titanium billet, the swarf has a much less regular structure and varies in both length and width significantly. The PSD could not be determined using the same method as the other materials and is expected to be 1 – 10 mm. The toolset used for the swarf is larger than for the other materials as the smaller set could not accommodate the particulate feedstock without overspill.

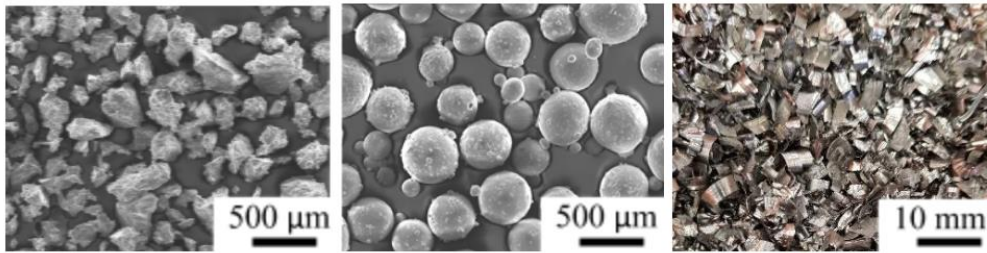


Figure 26 Light micrographs showing the morphologies of the powders used in this work. (Left) irregular morphology shown in the CP Ti HDH Gr 2 and Ti-6Al-4V HDH Gr 5 feedstocks, (Centre) spherical Ti-6Al-4V GA feedstock, and (Right) Ti-6Al-4V swarf

From these materials, tests were performed at various speeds and loads. Table 3 shows the mass of the powder used, with which the density can then be calculated, and the loads and speeds used for each test.

It should be noted that for Ti-6Al-4V GA the deformation of this material caused problems for four tests as the tooling became adhered. Consequently, the tests used variations on the previous tests with a higher maximum load and lower minimum rotation, which were determined through repeat assessment. Additionally, in the case of Ti-6Al-4V swarf, the tests greater than 5 kN did not reach the loads listed – as it would result in damage to the machine and tools. The maximum load achieved was 6.7 kN and this will be noted in the following discussion.

3.5 Conform™ Process

There is no standard operating procedure for processing titanium using the Conform™ process but there are some standard procedures for setting up the machine. Guidance was provided by the technical staff at BWE Ltd., Ashford, UK.

The shoe of the machine is withdrawn, to which the tooling can then be placed. The fitting of the tooling is adjusted by using shims, which are thin segments of copper/steel/aluminium, that can be fitted behind the tools to ensure a tight fit. The tools are then preheated via induction heating until the temperature of the shoe measures a consistent 520°C. It must be noted that whilst there are thermocouples present in the die chamber and shoe itself, the abutment does not have any. Because of this, the temperature may be slightly below 520 °C in all the tools.

The wheel is not preheated. Further to the setup, the setup does not use inert gas shielding or preheated powder feedstocks.

Once the temperature has been achieved (which can take up to an hour), the flash gap in the tooling must be determined. The flash gap is the gap between the tools in the shoe and the wheel and is where consolidated chips (henceforth referred to as flash) can be forced into the waste. This measurement is taken at two different points on the tooling, 1) across the port of the die chamber and 2) above the die chamber. A measurement is taken from each side to determine whether the tools are set in the shoe correctly. The shoe is raised with a piece of copper wire in the aforementioned locations, this is pushed up to the wheel and then withdrawn. The flattened sections of the copper wire can then be measured. The aim is to have a gap of between 0.4 and 0.8 mm, as this allows enough material through, whilst still allowing for friction to occur between the material on the abutment and in the groove.

During the trial, data from the process is recorded including the torque, abutment and wheel temperatures and the wheel speed. The analysis is performed in *Chapter 7*.

3.6 Discrete Element Modelling

Simulations were completed using EDEM, Edinburgh Discrete Element Method. The results of the simulations are given in *Chapter 6*.

The discrete element method (DEM) allows for the simulation of particulate material systems, where the focus is on the individual particle behaviour, rather than the bulk system.

In this work, EDEM (Edinburgh Discrete Element Method) software was used to simulate the behaviour of particulate feedstocks in various sets of ConformTM tooling. DEM was used as a method of justification for the design of the tools, which were designed solely for use in this work.

There are two distinct designs of tools for this process, which were designed with the particulate feedstock morphologies in mind (see *Chapter 5*). The designs were also influenced by a

mathematical model produced by Dr B. Thomas at the University of Sheffield [90]. The key differences are shown in **Error! Reference source not found.**

Table 2 The geometries of the key components of the toolsets used during the Conform trials

| Toolset | Groove | Abutment | Die |
|--------------|---------|----------|-----|
| | mm x mm | mm x mm | mm |
| Ti-6Al-4V GA | 11 x 13 | 10 x 12 | 6 |
| Swarf | 15 x 15 | 14 x 14 | 10 |

The most notable difference between the feedstocks is the morphology and size range. For this reason, the majority of the minor variations have been disregarded during the simulations.

The aim is to justify the different tools sets, by investigating the impact on the filling of the die, the grip length and material held within the wheel groove.

3.6.1 Particle Development

One of the predominant methods of validating the accuracy of a particle simulation is to use the Angle of Repose. Angle of repose is a common method of characterising a particulate material and is determined by the angle at which the powder settles after pouring.

For each material, the simulation requires different properties:

- **Poissons' ratio** – defined as the ratio between the change in width (per unit width), to the change in length (per unit length) as a result of strain on the material.
- **Solids density** – this is the bulk density of the material in kg/m³
- **Shear modulus** – defined as the ratio of shear stress to shear strain in Pa
- **Coefficient of restitution** – the ratio of final to initial relative velocity between two objects after collision. The value is between 0 and 1, where 1 defines a perfect elastic collision.
- **Coefficient of static friction** – indicates the extent of the rolling resistance, for a given force, between the wheel (in this case, the particle) and the surface it is rolling on. It is typically a value less than 1.

- **Coefficient of rolling friction** – defined as the friction force between two objects when neither object is moving. Typically, a value between 0 and 0.1, however can be higher in more complex conditions.

Additionally, a representative particle structure should be provided, along with a size distribution. Typically, the size distribution here has been determined using PSD results, although in the case of swarf, by trial and error – however, it is possible to make a mathematical determination for each material.

Chapter 4 : Arbitrary Strain Path Testing

As previously described, the arbitrary strain path (ASP) testing machine is a bespoke piece of equipment used for the investigation of strain paths during the machining of materials and other processes. However, in this project the ASP was used to perform shear cell style testing on titanium powders through the use of bespoke tooling, that allows for uniaxial compression and simultaneous rotation.

The powder is added to the tools at the bulk density and is then subjected to a fixed load and rotation speed. The result of this is a set of data corresponding to the change in the displacement and the torque.

The aim of this investigation is to determine the ‘Conform-ability’ of different powder morphologies based on a number of criteria:

- 1) **Ability to consolidate** - describing the formation of a consolidated, foil-layer across the sample under shear. The layer will form depending on a combination of load and speed. An example of this foil layer is shown in Figure 27.
- 2) **Density change** - investigating how the load and speed impact the reduction of the particle density over the course of a test. This is also a function of particle morphology, which will be discussed later.
- 3) **Impact on raw data** - The raw data generated includes the torque, the displacement, the load and the angle. Particle behaviour will influence a number of these parameters, in particular the torque.

*Table 3 Data provided for the ASP trials, including the mass of the feedstock added to the tools. *Swarf tests used a larger toolset to accommodate particulate size*

| Test | Powder | Mass g | Load kN | Rotation Speed | |
|------|-----------------|-----------|------------|----------------|-----|
| | | | | °/s | RPM |
| 1 | CP Ti HDH | 4.32 | 5 | 360 | 60 |
| 2 | CP Ti HDH | 4.41 | 10 | 120 | 20 |
| 3 | CP Ti HDH | 4.31 | 10 | 360 | 60 |
| 4 | CP Ti HDH | 4.35 | 10 | 600 | 100 |
| 5 | CP Ti HDH | 4.48 | 15 | 360 | 60 |
| 6 | Ti-6Al-4V HDH | 5.4 | 5 | 360 | 60 |
| 7 | Ti-6Al-4V HDH | 5.13 | 10 | 120 | 20 |
| 8 | Ti-6Al-4V HDH | 5.51 | 10 | 360 | 60 |
| 9 | Ti-6Al-4V HDH | 5.32 | 10 | 600 | 100 |
| 10 | Ti-6Al-4V HDH | 5.34 | 15 | 360 | 60 |
| 11 | Ti-6Al-4V GA | 8.00 | 2 | 30 | 5 |
| 12 | Ti-6Al-4V GA | 8.11 | 10 | 30 | 5 |
| 13 | Ti-6Al-4V GA | 8.44 | 20 | 30 | 5 |
| 14 | Ti-6Al-4V GA | 8.51 | 20 | 120 | 20 |
| 15 | Ti-6Al-4V GA | 8.39 | 20 | 360 | 60 |
| 16 | Ti-6Al-4V GA | 8.55 | 20 | 480 | 80 |
| 17 | Ti-6Al-4V GA | 8.06 | 20 | 600 | 100 |
| 18* | Ti-6Al-4V Swarf | 1.9 | 5 | 360 | 60 |
| 19* | Ti-6Al-4V Swarf | 2.2 | 10 | 30 | 20 |
| 20* | Ti-6Al-4V Swarf | 2.2 | 10 | 120 | 60 |
| 21* | Ti-6Al-4V Swarf | 1.8 | 10 | 600 | 100 |
| 22* | Ti-6Al-4V Swarf | 2.3 | 15 | 360 | 60 |

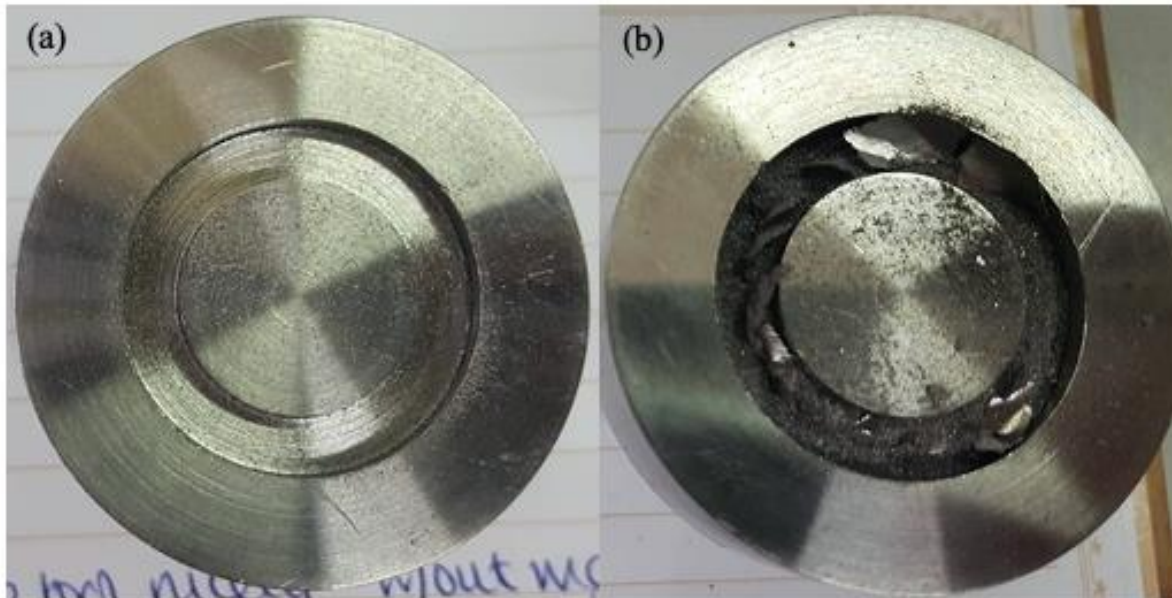


Figure 27 Photograph showing the ASP tooling (a) immediately after a test, demonstrating a thin foil film across the surface of the feedstock. (b) shows the unconsolidated feedstock underneath the film.

4.1 Density

The density of the particulate within the tooling increases during the test, as the load and rotation cause the particles to pack more densely.

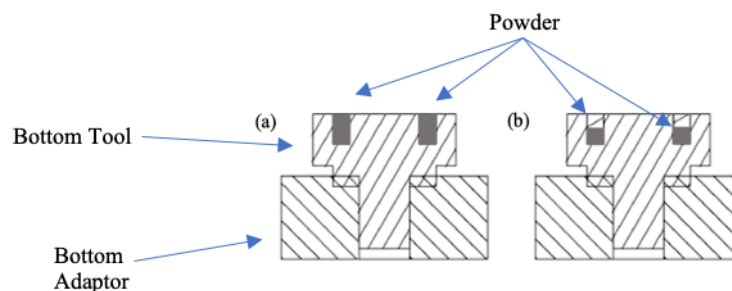


Figure 28 A schematic showing the change in the density of the powder (a) at the start of the test and (b) after testing, where the load and rotation has resulted in a drop in the displacement of the top tool into the bottom tool.

The initial density was calculated based on the mass of powder added to the tooling prior to testing and the volume of the tools (shown in Figure 28a). The final density was calculated based on the mass of powder, however the volume of space between the tooling has changed due to a reduction in the displacement (shown in Figure 28b). Therefore, the new volume was calculated for each test. The results are shown in Figure 29.

In Figure 29, the load is constant at 10 kN – however, it should be noted that the swarf material never reached 10 kN, as it would result in tool/machine damage (actual value is ~6.7 kN). The RPM of the top tool had a clear impact on the particulate density, with a clear increase in the density between the initial and final density values. From these results, it appears that the less spherical (more irregular) the material morphology, the lower the initial densities are. This is to be expected, as the irregular shapes would result in a much lower packing density. The GA powder has a density close to that expected for the bulk, solid density of Ti-6Al-4V, which is around 4.5 g/cm³. In addition to this, it appears that the more irregular structures also have the largest change in density across the course of the test. This should be expected for the swarf, as the structure of the chips affords them some flexibility and a higher chance of deformation.

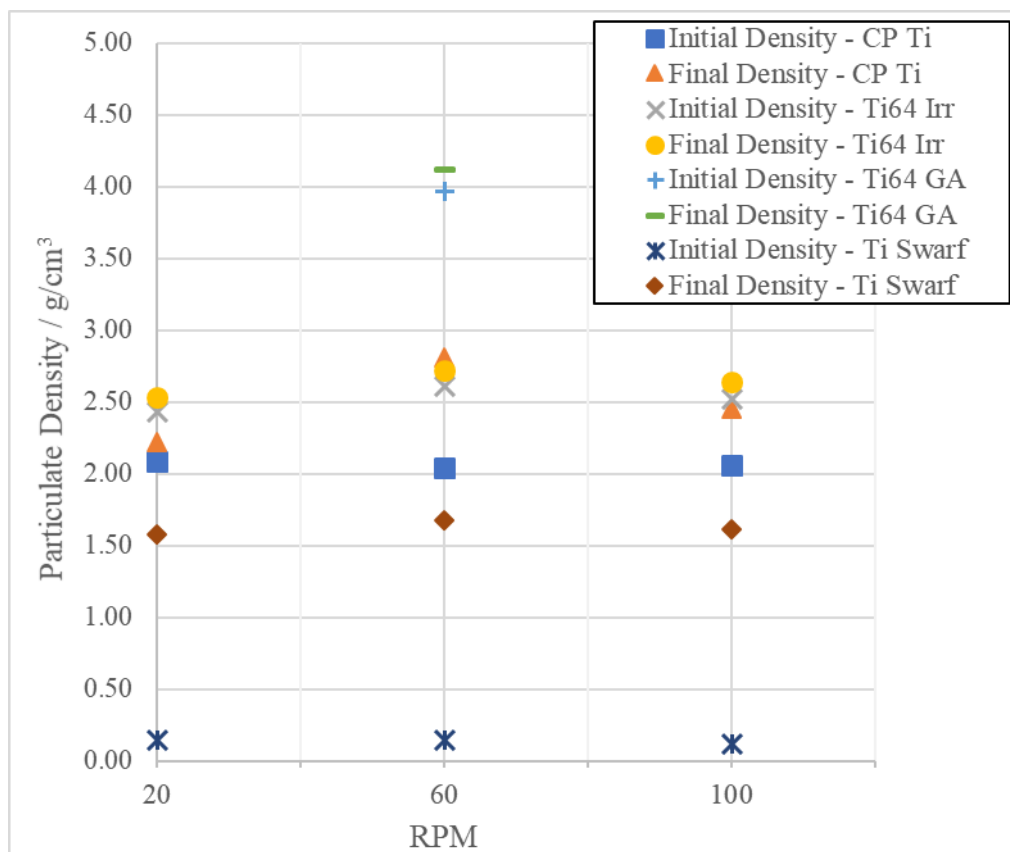


Figure 29 The change in density of the different feedstocks during ASP trials at different speeds.

In the case of Figure 30, the rotational speed is constant at 60 RPM. The results show similar trends in the density; however, it should be noted that there appears to be an increase in the resulting density as the load increases. This suggests that the load has a greater impact on the

consolidation of the particle feedstock. The results would benefit from additionally testing to determine a more rigid proof that this is the case.

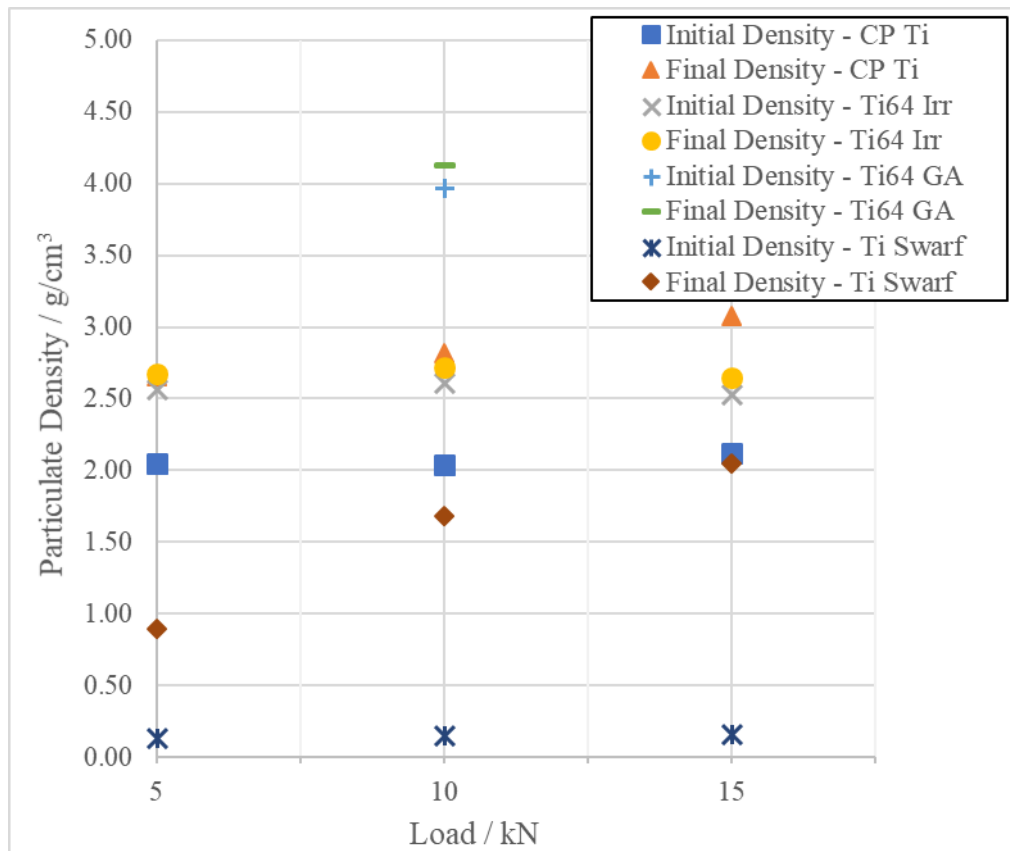


Figure 30 The change in density of the different feedstocks during ASP trials at different loads.

4.2 Displacement versus. Angle

The results of the tests, shown in Figure 31, show that each test demonstrates a drop in the displacement across the length of the test. There are clear variations based on each material, which relates to both the morphology and the material itself.

The Ti-6Al-4V GA tests were not conducted at the same loads and speeds as with the other materials, this is because the lower loads often resulted in powder particles becoming lodged between the walls of the tools. This resulted in the tools becoming adhered and the test data would be very noisy, especially for the torque. Therefore, the tests were, for the most part, conducted at 20 kN load.

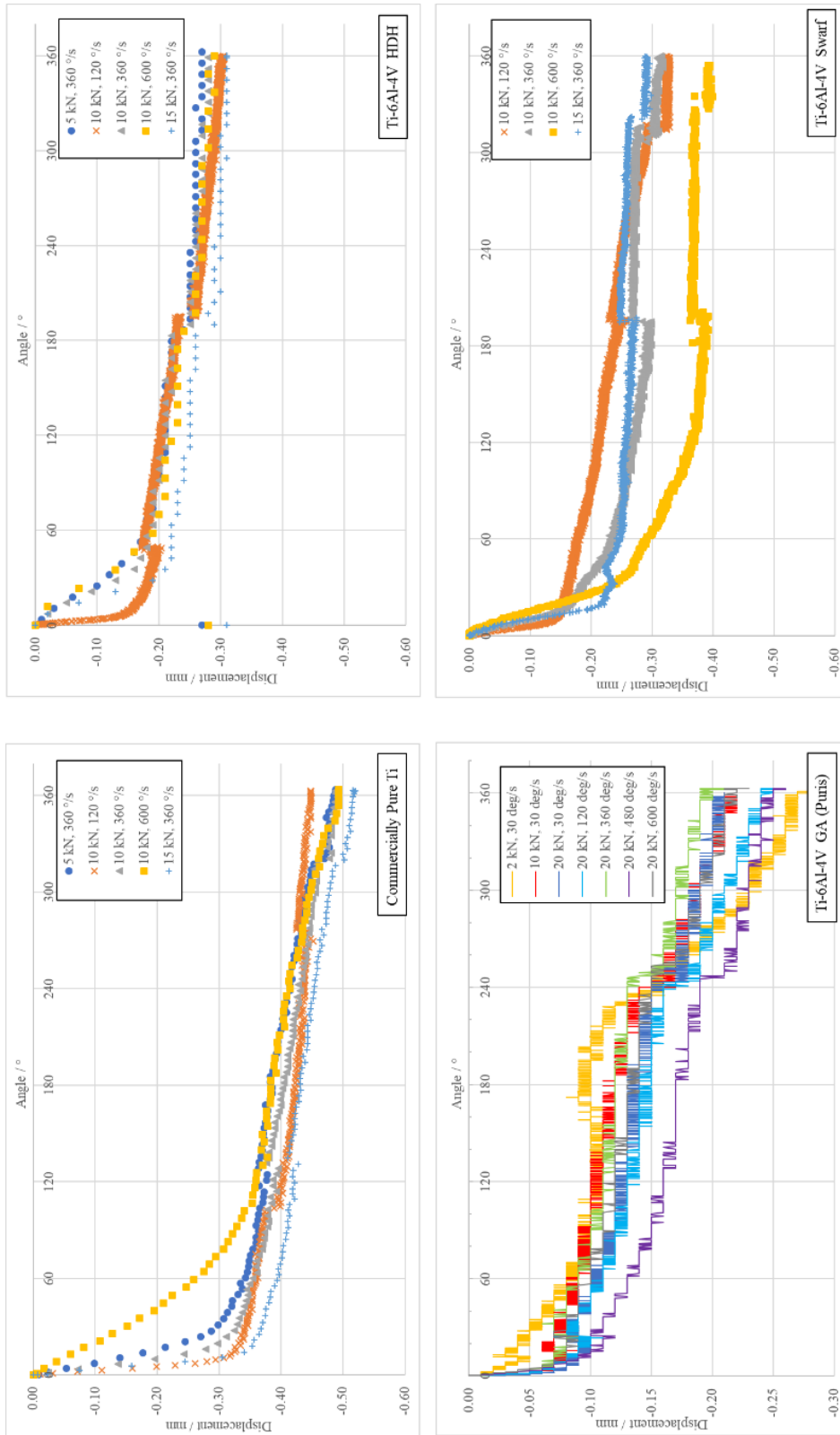


Figure 31 Graphs showing the displacement against the angle for each test completed on the ASP. The results are separated by feedstock.

Additionally, the tests were conducted without changing machine parameters, which has resulted in steps throughout the data. In order to mitigate this, a graph, in Figure 32, uses the rolling average (over each 7 data points) has been plotted and shows the data trends more clearly.

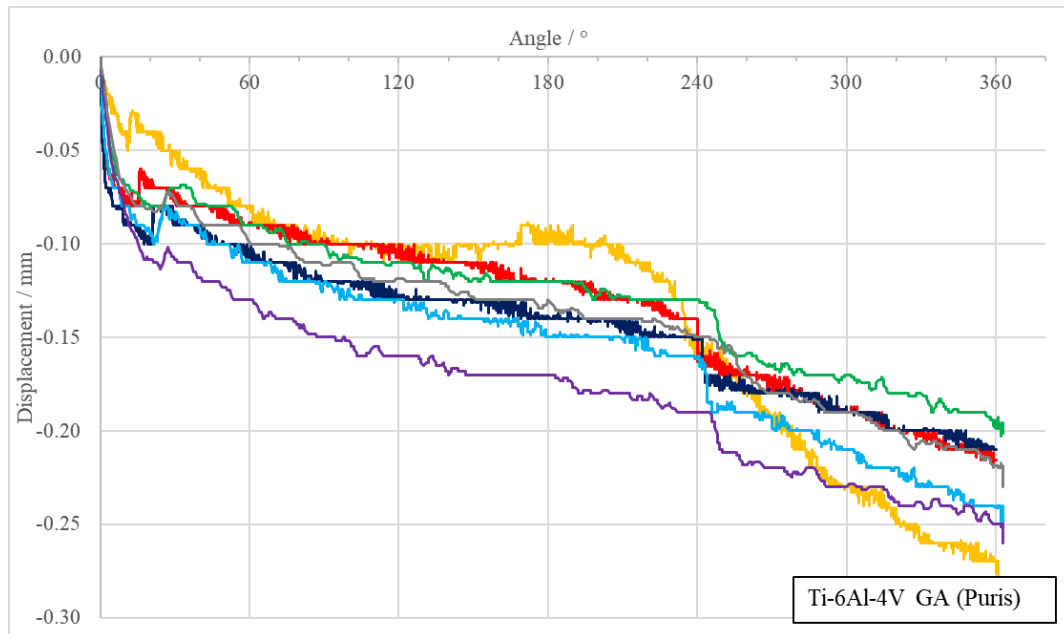


Figure 32 Graph of the displacement against the angle for the tests conducted with Ti-6Al-4V GA

There are clear similarities between the tests, which relate to the applied load and rotation speed. Firstly, in most cases, the 15 kN tests drop further in displacement during the first 20° than for the other loads. This is clear in both the CP Ti and Ti64 HDH results, where the 15 kN tests also result in the lowest displacement drop overall. This demonstrates that the load applied is integral in the consolidation of the material. The result for the swarf material differs slightly, however, it should be noted that the load was applied prior to the rotation and because of this, the swarf material was well compacted prior to testing. Additionally, the loads applied to the swarf material never exceeded 6.7 kN due to potential damage to the tools and machine.

In addition to the influence of the load, the faster rotations result in a decrease in the displacement over 120° rather than the <30° of the other speeds. This is most evident in the CP Ti HDH tests, however, there is some evidence in the Ti-64 HDH and swarf tests. This may be because the faster movement does not afford the displacement time to drop quickly, as the particles do not have time to adjust into position and are being pulled around further. This is

further emphasised by the slower tests, which appear to drop more quickly. This is most evident in Ti-6Al-4V HDH. In addition to dropping more quickly, the displacement drop is also often greater.

Further to this, in the case of the non-spherical materials, there is a distinct change in the displacement occurring at 60°, 120° or 180° depending on the test. This is accompanied by a reversal of this change around 90° later in the test. Although this change was not investigated further experimentally, however it is possible to make some predictions for the cause.

The ASP self-adjusts the parameters such as load, to make sure that they are consistent throughout the course of the test. For this reason, it may be that the load is being maintained through the adjustment of the displacement. This would also explain why the change can be either positive or negative.

The data for the Ti-6Al-4V GA spherical powders show a variation on the initial drop in the displacement followed by the plateauing of the displacement. Instead, there is not a significant initial drop in the displacement but rather a small drop followed by a steady decline in the displacement. In the case of all the spherical tests completed in this work, there is a second drop in the displacement around 240°. This drop may be similar to that found in the non-spherical particles, where the machine appears to regularly adjust, however, it occurs at a completely different point. It is more likely that the powder particles have yielded under the pressure and then undergo further rearrangement, as demonstrated by the further slow decline in the displacement. Interestingly, in the case of the 2 kN test, this drop is significantly larger than that shown for the other loads, with the second drop of ~0.15 mm. Without further testing, it is not possible to make robust assumptions or provide a detailed theory.

In the case of most of the tests, after the initial drop, there is a slight increase in the displacement. As the ASP is programmed to maintain a constant load, this increase must be an indicator that the load is appearing greater than the fixed value. This could be as the particles are shearing over one another, resulting in areas of greater load on to the bottom tool.

Based on the data in Figure 31, it is evident that the tests with the higher loads demonstrated a larger decline in the displacement prior to the second drop at the end of the test. The speed

appeared to have little impact; however, further testing would be required to confirm whether this is the case. It would be expected that the rotational shear should have impact on the results, however, the compaction of the material under load may reduce the impact of the speed.

In the case of the overall result, the largest decrease in the displacement is the 2 kN test. This is unexpected; however, the combination of the low load and slow speed may have resulted in a drop in the displacement later in the test. This would relate to an initial rearrangement of particles, which have taken longer to rearrange than in the case for the faster speeds, where the shear would pull the upper particles around with the top tool. This could then provide a drop in the displacement which is significantly greater than for the other tests. Overall, however, it appears that neither the load nor the speed has any impact on the end result of the tests. In order to ascertain for certain, it would be necessary to perform multiple repeats of each test and running the tests for multiple rotations. Furthermore, by completing multiple rotations, it would be possible to determine the absolute maximum powder density, which would be useful information for use in powder processing methods.

4.3 Summary

These tests have demonstrated preliminary work on an alternative bespoke testing method, which could be used to determine the ability to produce wire using the ConformTM process from a given material. The materials which do not produce consolidated layers are typically harder to deform and consequently, will require a higher extrusion pressure to ConformTM. As a relatively simple test, it is a cost-effective method to determine the ‘Conform-ability’ of the material. The ability to ascertain this Conform-ability could potentially result in costs of £100s for ASP tooling, rather than the £1000s for ConformTM toolsets, which would potentially not result in a product.

Highlighted by these results, is the differing behaviours of spherical and irregular morphology powders, and the impact of the alloying elements on the deformation of the particles. Further to this, the feedstock may be ranked by their Conform-ability, although further work would be needed to allow a higher degree of certainty. The HDH powders, both CP Ti HDH and Ti-6Al-4V were easily consolidated in the smaller toolsets, with a foil layer often being formed across the surface of the tooling. The smaller toolsets involve the same amount of force on a smaller

area of material, which suggests that there would be a higher pressure on the particles. When compared to the results of *Chapter 5 & 6*, the HDH feedstocks may find it possible to be consolidated in a larger toolset also, however, further work would be required to compare the behaviour in the different ASP tool geometries. The Ti-6Al-4V GA feedstock does not reach a plateau in the density, so further testing would be required to ascertain when it has dropped to its maximum final density. For this reason, it is clear to see that the GA feedstock needs a greater extrusion pressure, and therefore, it is not clear whether the feedstock is entirely Conform-able, but it is clear that a small ConformTM toolset would be needed. Finally, the swarf, whilst it does successfully reach a plateaued density, there was no foil produced on the surface. There is a possibility, with the swarf, that this is a result of the small volume of swarf used, which has resulted in gaps within the consolidated structure, and therefore no foil is produced. This highlights a key point of further work, where, again, the internal consolidation should be investigated further. Overall, the work completed here suggests that the HDH powders are most likely to consolidated under ConformTM, followed by the swarf and finally the GA powders. This is not an exhaustive list, but it agrees well with the data produced in *Chapter 5 & 6*.

As this work was mostly preliminary, future work should aim to investigate particle mixtures (i.e., quantities of swarf combined with powder) to determine how this improves the consolidation of the material. Additionally, it is not entirely evident how the particles are behaving during the test, as it is not possible to look inside the tools, so currently, particle rearrangement is presumed. One way that this may be achieved is to section the tooling after trialling - taking care not to deform the particles further and observing how the particle rearrangement differs from the bulk. This could be done at various stages.

Chapter 5 : The Conform™ Process

As outlined previously in Section 2.3, Conform™ is a continuous extrusion process for the processing of metals in rod and powder feedstocks. The machine used during this trial was a Conform™ 350i based at BWE Ltd, Ashford, Kent, UK. Despite being a process used in industry, the use of titanium in the process is not currently in a position for use in industry and because of this, there is no standard operating procedure for its use. Additionally, changes to the tooling are required, to accommodate the particulate feed and the parameters are often changed during the trial, depending on how the trial is going.

5.1 Feedstocks

A number of different feedstocks were used for the trials. With the exception of one trial, the trials start with CP Ti HDH Grade 2, as this is a relatively straightforward alloy to process and will allow the process to get going whilst causing minimal issues for the tooling. Additionally, as titanium powders are liable to ignite at high temperatures, this will help to prevent this. Once the initial extrusion has occurred, any new material added is extruded reasonably soon after entry.

5.2 Tool Design

In order to use the Conform™ machine for titanium powders and swarf, a number of alterations must be made to the tooling geometries. There is a mathematical approximation for tool design applied to the results, which will approximate the amount of extrusion pressure that could be generated and the grip length of the material. Tool design was completed using Autodesk Fusion 360 and then converted to drawings in Solidworks. With the exception of the die insert (carbide) and the abutment (various materials, see below), all other tools were made from H13 tool steel.

There were two distinct sets of tooling designed for use in the trials in this project. For each set (see Figure 33), the wheel, abutment, die, die chamber, entry block and entry block extension were redesigned.

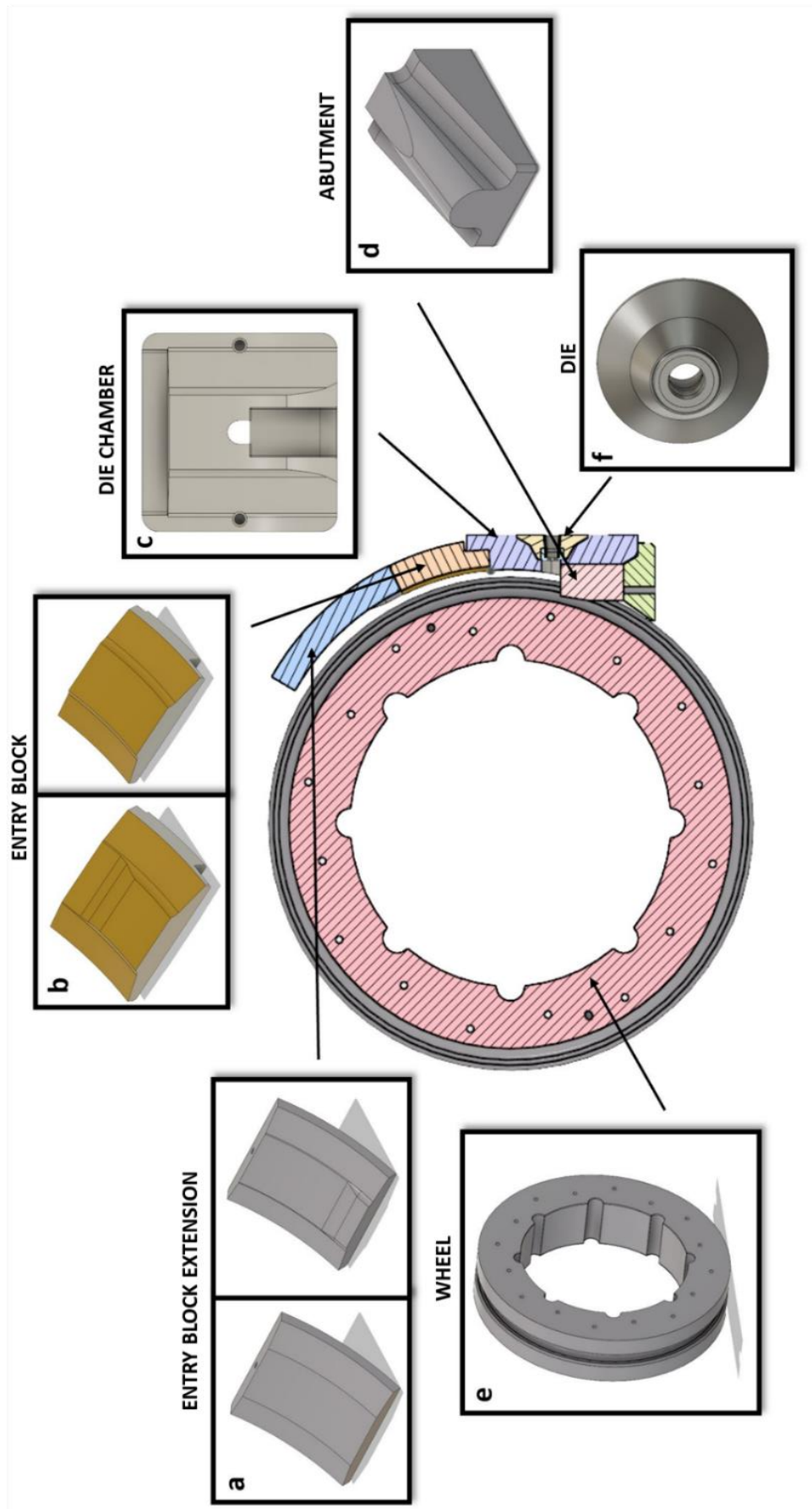


Figure 33 Tooling set-up for the Conform™ process as designed in CAD for this project.

5.2.1 Swarf Trials

Considerations must be made towards to morphology of the feedstock, with a particular focus on the size, as if the groove of the wheel is too small, then there is a risk that the material will not fall into the groove, nor coat the wheel. For this reason, the width and depth has been adjusted to accommodate the 1 - 10 mm size of the swarf, as shown in Figure 34. This means that when the material is poured into the groove, there will be little overspill and will maximise the volume that comes into contact with the abutment.



Figure 34 CAD drawing of the wheel.

If the groove size is increased, the abutment width and depth should increase also. The abutment (shown in Figure 35) must protrude into the groove, whilst leaving a sufficient gap (flash gap) between the two (to prevent the tooling coming into contact with each other and to aid with the shearing of the material). Therefore, the nose of the abutment was increased to be 13 x 13 mm. This was later revised as the flash gap was too large and meant that there was not sufficient pressure to extrude. The revised version had a 14 x 14 mm nose.

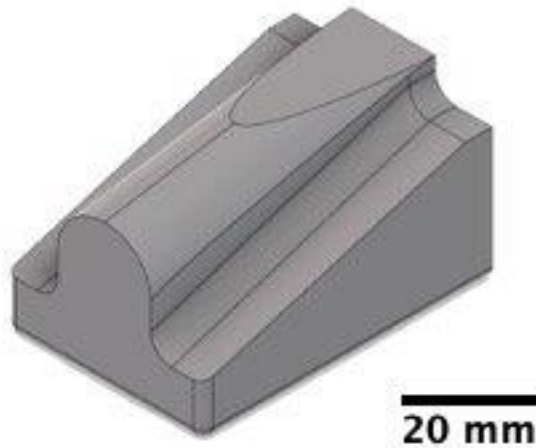


Figure 35 CAD drawing of the abutment.

In addition to the abutment, the port length also has been shown to have some impact on the extrusion, influencing the extrusion pressure. The longer the port length, the more pressure that would be required to force the material through the die. The port length is in part directed by the abutment but also the die chamber. The die chamber (see Figure 36), like the abutment, is situated in the shoe. It is attached to two plates (the entry block) and the die. The port diameter, for this work, was set to be 13 mm x 13 mm. The material for the abutment varied across the trials with materials including Inconel 718, RR1000 and a W-Re alloy (W-26 wt.% Re-2 wt.% HfC).



Figure 36 CAD drawing of the die chamber.

The width was set the same as the abutment to prevent material loss down the sides of the abutment, which would in turn, prevent high pressures along the abutment, which could lead

to premature abutment failure. The height was somewhat arbitrary. The length of the port was set to 20 mm, this was to allow sufficient space for material to fill, without impeding on the abutment, whilst generating enough force to force the material through the die. The die chamber size was revised alongside the abutment to a 14 x 14 mm port.

Inside the die chamber, there is a die. This die, shown in Figure 37, should aim to be filled by consolidated material during the extrusion and also takes most of the extrusion pressure. There are a few considerations to make here. Firstly, the die must be sufficiently wide enough that the material in the port can fill the die without further shearing too much on the edges of the die. Secondly, the die must be small enough to minimise the amount of empty space - to prevent pores and inconsistency in the produced wire. For this reason, a 10 mm die was produced. This die is smaller than the port, so for the full port, the amount of material should minimise the number of pores, but it is large enough that the material does not get stuck, back up or get sheared on the edges of the die - which could lead to a very rough surface finish.



Figure 37 CAD drawing of the die.

The final tooling to consider is the entry block and the entry block extension (see Figure 38). This is two pieces of tooling which follow each other and lead onto the die chamber. They sit above and have a protrusion that acts as a pressure relief point. This pressure relief should be above the grip length but near enough to the abutment, that the pressure is not lost. In the case of the tools for swarf, this was set on the entry block extension, which is the upper most plate in the shoe. The impact of the larger abutment and port size suggests that a larger grip length would be required. Should the die be decreased in size further, the grip length would further increase as the material that cannot fit through the die has nowhere else to go.

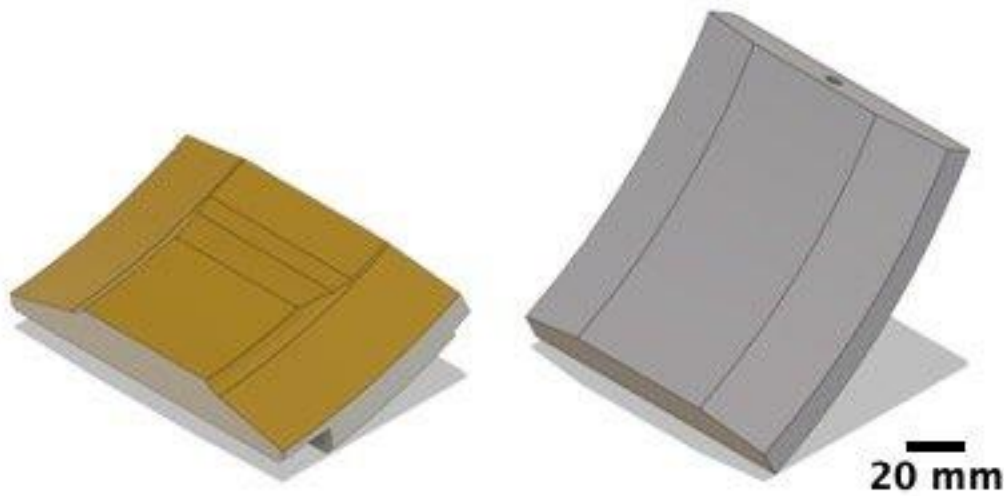


Figure 38 CAD drawings of the entry block (left) and entry block extension (right)

5.2.2 Spherical Powder Trials

Unlike with irregular powders, spherical powders are typically not used in Conform™. For this reason, the tooling has been designed to maximise the extrusion pressure for small morphologies. Despite being somewhat high for irregular powders, the extrusion pressure here will be required to consolidate the spherical powders. The groove for this tooling was designed to be 11 x 13 mm. Again, to aim for a flash gap of around 0.5 mm, the abutment was designed to be 10 x 12 mm. For the die chamber, the port was the same size as the abutment nose. The die was set at 6 mm. The entry block extension had two iterations. Firstly, the pressure relief was dropped to the die chamber, this was to increase the pressure for the spherical powder. However, this was revised to the feed plate after consideration.

5.3 Changes to the tooling

The changes to the stock tool designs were made based on a combination of trial and error, but also with some regard for the morphology of the powder feedstocks. It was, at first, important to consider the morphology of the feedstock, especially in the case of the swarf, where larger morphology particles would not fit well within the wheel groove on the initial toolsets. Second to this, there was some discussion regarding the ability to obtain the right extrusion pressure to

extrude any given material. In the case of the spherical Ti-6Al-4V GA powder, it was determined that a higher extrusion pressure may be required, and therefore a smaller wheel groove should allow for this to happen. There were issues during the trials, which have also led to the decisions made, with minor adjustments made following the initial set of trials. This was mostly directed at significant powder loss between the wheel groove and the abutment in the larger toolset, which would be rectified by increasing the size of the abutment.

Chapter 6 : Discrete Element Modelling

The discrete element method (DEM) allows for the simulation of particulate material systems, where the focus is on the individual particle behaviour, rather than the bulk system.

For each of the simulations, the Hertz-Mindlin (no slip) contact model was used. This model was used to minimise further complications to the data, when the main aim was to achieve a proof of concept for the tool designs. To heighten accuracy, alternative systems may be used, where there is a consideration for wear or particle velocity, for example. The interactions were between the particles, each other and the tools.

The particle size distribution ranges from 0.8 to 1 – from the designed particle – in the case of each material. Although it would have been more accurate to use particle size data, for simplicity, this was fixed at these parameters. Further to this, the material volume was set at 100000 particles per second of simulation, in the cases of both CP Ti HDH and Ti-6Al-4V GA. The swarf was set at a fixed rate of 10 g/s due to the larger morphology of the material.

Aside from any of the parameters discussed in this chapter, all remaining conditions were default to the software.

6.1 Particle Development

6.1.1 CP Ti HDH Gr 2

CP Ti HDH is used in each ConformTM trial; therefore, it was applied to both sets of tooling in the simulations. It will act as the control, allowing the other materials to be compared directly to it.

The parameters used for CP Ti were taken from the literature or adapted from previous work completed at the University of Sheffield. Poissons' ratio, solids density (kg/m^3) and shear modulus (Pa) were determined from the literature as 0.342, 4510 and $1\text{e}+08$, respectively. **The coefficient of restitution, static friction and rolling friction were determined based on previous work as 0.5, 0.5 and 0.01, respectively.**

The particle shape was also designed based on previous work, and consists of three spheres, arranged to make a shape that is representative of an irregular shaped particle (shown in Figure 39). It is important to note that the more detail added to the shape, the more computationally exhaustive the simulation will be, often with little benefit. For this reason, it was determined that, as long as the angle of repose result was in agreement with the experiment, the simplified design would be appropriate for the process simulations.

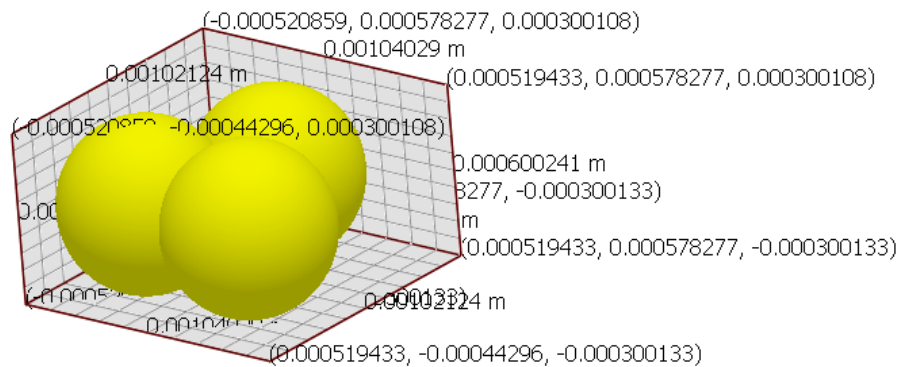


Figure 39 CP Ti HDH particle designed in EDEM for use in the EDEM simulations

From the powder particle, a simulation is run to form a pile of particles, which can then be compared to an actual angle of repose for CP Ti HDH Gr 2. In order to do this, various iterations of the coefficients used in the simulation were used to determine the most accurate powder particle properties. It is important to note that the particle will not be identical to real-life, with each particle sharing the same geometrical shape and the material is free from defects. There are no satellite particles, and the size range has been narrowed to ensure that the computational requirements for the simulation are achievable in a reasonable time period. For a more accurate simulation, the particles can be individually designed, and an accurate particle size distribution used. Based on Table 4, and a real-life angle of repose result, the coefficients used in the simulation would be 0.3, 0.75, 0.075, corresponding to AOR36 in the table.

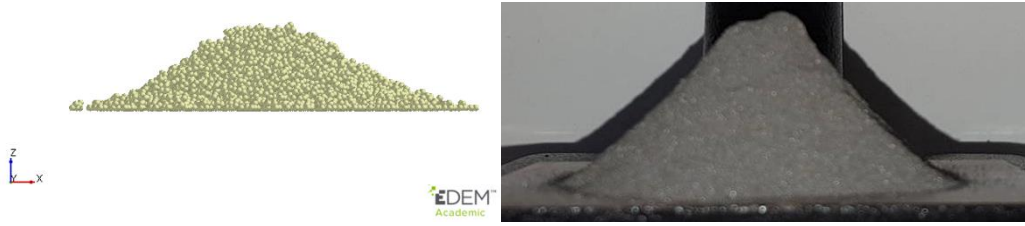


Figure 40 (a) Simulated Angle of Repose for CP Ti HDH Gr 2 irregular particles; (b) Experimental Angle of Repose for CP Ti HDH Gr 2 irregular particles.

Table 4 Simulated angle of repose results using the particle shown in Figure 39.

| Test Name | Coefficient | | | Angle of repose/° | | | | |
|-----------|-------------|-----------------|------------------|-------------------|-------|-------|---------|--------|
| | Restitution | Static Friction | Rolling Friction | 1.00 | 2.00 | 3.00 | Average | St Dev |
| AOR1 | 0.3 | 0.3 | 0.025 | 8.75 | 11.89 | 6.84 | 9.16 | 2.08 |
| AOR2 | 0.3 | 0.3 | 0.05 | 10.20 | 13.32 | 14.04 | 12.52 | 1.67 |
| AOR3 | 0.3 | 0.3 | 0.075 | 16.39 | 15.23 | 17.03 | 16.22 | 0.74 |
| AOR4 | 0.3 | 0.4 | 0.025 | 14.04 | 14.38 | 15.52 | 14.65 | 0.63 |
| AOR5 | 0.3 | 0.4 | 0.05 | 20.24 | 21.47 | 17.86 | 19.86 | 1.50 |
| AOR6 | 0.3 | 0.4 | 0.075 | 20.33 | 19.44 | 19.93 | 19.90 | 0.36 |
| AOR7 | 0.4 | 0.3 | 0.025 | 14.19 | 13.88 | 12.23 | 13.43 | 0.86 |
| AOR8 | 0.4 | 0.3 | 0.05 | 18.43 | 16.04 | 18.09 | 17.52 | 1.06 |
| AOR9 | 0.4 | 0.3 | 0.075 | 17.35 | 17.03 | 18.09 | 17.49 | 0.44 |
| AOR10 | 0.4 | 0.4 | 0.025 | 14.74 | 15.52 | 16.11 | 15.46 | 0.56 |
| AOR11 | 0.4 | 0.4 | 0.05 | 16.14 | 16.70 | 18.65 | 17.16 | 1.08 |
| AOR12 | 0.4 | 0.4 | 0.075 | 20.56 | 21.80 | 17.93 | 20.10 | 1.61 |
| AOR13 | 0.3 | 0.75 | 0.07 | - | - | - | - | - |
| AOR14 | 0.1 | 0.1 | 0.01 | 0.00 | 0.00 | 0.00 | 0.00 | 0.00 |
| AOR15 | 0.1 | 0.1 | 0.1 | 0.00 | 0.00 | 0.00 | 0.00 | 0.00 |
| AOR16 | 0.1 | 0.1 | 0.05 | 0.00 | 0.00 | 0.00 | 0.00 | 0.00 |
| AOR17 | 0.9 | 0.1 | 0.01 | 0.00 | 0.00 | 0.00 | 0.00 | 0.00 |
| AOR18 | 0.9 | 0.1 | 0.1 | 0.00 | 0.00 | 0.00 | 0.00 | 0.00 |
| AOR19 | 0.9 | 0.1 | 0.05 | 0.00 | 0.00 | 0.00 | 0.00 | 0.00 |
| AOR20 | 0.1 | 0.9 | 0.01 | 0.00 | 0.00 | 0.00 | 0.00 | 0.00 |
| AOR21 | 0.1 | 0.9 | 0.1 | 0.00 | 0.00 | 0.00 | 0.00 | 0.00 |
| AOR22 | 0.1 | 0.9 | 0.05 | 0.00 | 0.00 | 0.00 | 0.00 | 0.00 |
| AOR23 | 0.9 | 0.9 | 0.01 | 14.74 | 14.46 | 13.77 | 14.32 | 0.41 |
| AOR24 | 0.9 | 0.9 | 0.1 | 23.63 | 25.02 | 22.99 | 23.88 | 0.85 |
| AOR25 | 0.9 | 0.9 | 0.05 | 18.43 | 19.44 | 16.99 | 18.29 | 1.01 |
| AOR26 | 0.75 | 0.75 | 0.1 | 20.42 | 23.16 | 24.37 | 22.65 | 1.65 |
| AOR27 | 0.5 | 0.5 | 0.1 | 22.67 | 22.09 | 22.69 | 22.48 | 0.28 |
| AOR28 | 0.5 | 0.5 | 0.075 | 20.87 | 21.52 | 22.09 | 21.49 | 0.50 |
| AOR29 | 0.75 | 0.5 | 0.1 | 23.33 | 23.93 | 22.72 | 23.33 | 0.49 |
| AOR30 | 0.5 | 0.75 | 0.1 | 26.85 | 28.37 | 27.80 | 27.67 | 0.63 |
| AOR31 | 0.6 | 0.75 | 0.1 | 25.11 | 24.44 | 26.57 | 25.37 | 0.89 |
| AOR32 | 0.4 | 0.75 | 0.1 | 27.37 | 26.57 | 25.91 | 26.62 | 0.60 |
| AOR33 | 0.4 | 0.75 | 0.075 | 26.27 | 25.67 | 24.82 | 25.59 | 0.59 |
| AOR34 | 0.3 | 0.75 | 0.075 | 24.52 | 22.95 | 22.38 | 23.28 | 0.90 |
| AOR35 | 0.2 | 0.75 | 0.075 | 21.25 | 20.22 | 20.97 | 20.81 | 0.43 |
| AOR36 | 0.3 | 0.75 | 0.075 | 29.74 | 31.61 | 26.57 | 29.31 | 2.08 |
| AOR37 | 0.3 | 0.75 | 0.5 | 48.01 | 46.83 | 45.63 | 46.82 | 0.97 |
| AOR38 | 0.3 | 0.75 | 0.3 | 41.16 | 39.00 | 36.87 | 39.01 | 1.75 |
| AOR39 | 0.3 | 0.75 | 0.15 | - | - | - | - | - |

The simulated angle of repose is shown in Figure 40. The powder particle used was that shown in Figure 39 and will be used for the Conform simulations later in this chapter.

6.1.2 Ti-6Al-4V GA

Unlike in the case of CP Ti HDH, this material had no previous data, and so multiple angle of repose simulations were run to ascertain the best coefficient values. The results are shown in Table 5. Poissons' ratio, solids density (kg/m^3) and shear modulus (Pa) were determined from the literature, as 0.342, 4430 and $1\text{e}+08$, respectively. The particle was set up as a single sphere with a radius of 0.0003m and the simulated particle is shown in Figure 41. A lognormal size distribution was used with a mean of 1 and standard deviation of 0.2.

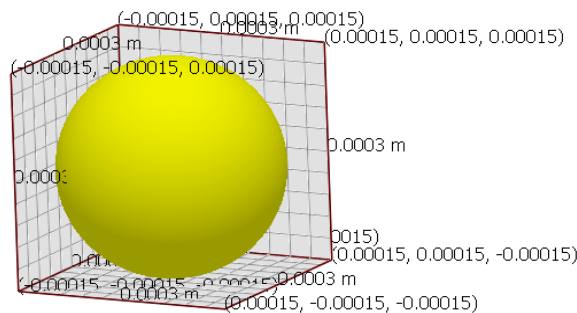


Figure 41 Spherical Ti-6Al-4V GA generated for use in EDEM simulations.



Figure 42 (a) Simulated Angle of Repose for Ti-6Al-4V GA particles; (b) Experimental Angle of Repose for Ti-6Al-4V GA particles.

As in the case of CP Ti, the simulated angle of repose (shown in Figure 42) is not completely identical to the experimental angle of repose. The simulation does not include satellite particles nor a completely accurate particle size distribution. Additionally, the simulation has been

completed at a much smaller scale than the experimental method, in order to save computational time.

Table 5 Results of the Ti-6Al-4V GA powder angle of repose simulations for 27 variations of coefficient values.

| Test Name | Coefficient | | | Angle of repose/° | | | | |
|-----------|-------------|-----------------|------------------|-------------------|-------|-------|---------|--------|
| | Restitution | Static Friction | Rolling Friction | 1.00 | 2.00 | 3.00 | Average | St Dev |
| AOR1 | 0.1 | 0.1 | 0.01 | 7.13 | 5.71 | 6.34 | 6.39 | 0.58 |
| AOR2 | 0.1 | 0.5 | 0.01 | 15.95 | 14.42 | 14.04 | 14.80 | 0.83 |
| AOR3 | 0.1 | 0.9 | 0.01 | 14.74 | 14.04 | 14.42 | 14.40 | 0.29 |
| AOR4 | 0.1 | 0.1 | 0.1 | 5.71 | 6.34 | 5.71 | 5.92 | 0.30 |
| AOR5 | 0.1 | 0.5 | 0.1 | 38.66 | 41.01 | 39.81 | 39.83 | 0.96 |
| AOR6 | 0.1 | 0.9 | 0.1 | 36.87 | 37.69 | 38.37 | 37.64 | 0.61 |
| AOR7 | 0.1 | 0.1 | 0.05 | 5.71 | 5.19 | 4.68 | 5.19 | 0.42 |
| AOR8 | 0.1 | 0.5 | 0.05 | 21.80 | 21.16 | 18.43 | 20.46 | 1.46 |
| AOR9 | 0.1 | 0.9 | 0.05 | 31.61 | 26.57 | 33.18 | 30.45 | 2.82 |
| AOR10 | 0.5 | 0.1 | 0.01 | 5.71 | 7.13 | 6.34 | 6.39 | 0.58 |
| AOR11 | 0.5 | 0.5 | 0.01 | 15.52 | 14.04 | 13.67 | 14.41 | 0.80 |
| AOR12 | 0.5 | 0.9 | 0.01 | 16.39 | 14.83 | 14.42 | 15.21 | 0.85 |
| AOR13 | 0.5 | 0.1 | 0.1 | 6.34 | 6.07 | 5.95 | 6.12 | 0.16 |
| AOR14 | 0.5 | 0.5 | 0.1 | 32.62 | 29.98 | 30.96 | 31.19 | 1.09 |
| AOR15 | 0.5 | 0.9 | 0.1 | 41.01 | 42.27 | 41.01 | 41.43 | 0.59 |
| AOR16 | 0.5 | 0.1 | 0.05 | 6.34 | 6.20 | 6.07 | 6.20 | 0.11 |
| AOR17 | 0.5 | 0.5 | 0.05 | 21.80 | 22.48 | 21.63 | 21.97 | 0.37 |
| AOR18 | 0.5 | 0.9 | 0.05 | 28.18 | 26.57 | 25.77 | 26.84 | 1.00 |
| AOR19 | 0.9 | 0.1 | 0.01 | 7.97 | 7.25 | 6.23 | 7.15 | 0.71 |
| AOR20 | 0.9 | 0.5 | 0.01 | 14.04 | 14.74 | 14.56 | 14.45 | 0.30 |
| AOR21 | 0.9 | 0.9 | 0.01 | 14.04 | 11.31 | 12.00 | 12.45 | 1.16 |
| AOR22 | 0.9 | 0.1 | 0.1 | 5.19 | 6.23 | 5.71 | 5.71 | 0.42 |
| AOR23 | 0.9 | 0.5 | 0.1 | 28.18 | 26.57 | 27.41 | 27.39 | 0.66 |
| AOR24 | 0.9 | 0.9 | 0.1 | 26.57 | 28.18 | 29.05 | 27.93 | 1.03 |
| AOR25 | 0.9 | 0.1 | 0.05 | 5.71 | 4.76 | 5.24 | 5.24 | 0.39 |
| AOR26 | 0.9 | 0.5 | 0.05 | 10.08 | 6.98 | 6.84 | 7.97 | 1.50 |
| AOR27 | 0.9 | 0.9 | 0.05 | 15.95 | 15.19 | 14.78 | 15.31 | 0.48 |
| AOR28 | 0.1 | 0.75 | 0.1 | 41.01 | 40.29 | 39.09 | 40.13 | 0.79 |
| AOR29 | 0.5 | 0.75 | 0.1 | 34.22 | 35.31 | 35.75 | 35.09 | 0.64 |
| AOR30 | 0.9 | 0.75 | 0.1 | 41.01 | 38.37 | 38.05 | 39.14 | 1.33 |
| AOR31 | 0.1 | 0.5 | 0.075 | 24.90 | 27.41 | 26.57 | 26.29 | 1.04 |
| AOR32 | 0.5 | 0.5 | 0.075 | 29.05 | 26.57 | 27.38 | 27.67 | 1.03 |
| AOR33 | 0.9 | 0.5 | 0.075 | 26.57 | 28.18 | 27.35 | 27.37 | 0.66 |
| AOR34 | 0.1 | 0.75 | 0.075 | 34.99 | 32.87 | 34.22 | 34.03 | 0.88 |
| AOR35 | 0.5 | 0.75 | 0.075 | 35.75 | 34.70 | 34.22 | 34.89 | 0.64 |
| AOR36 | 0.9 | 0.75 | 0.075 | 28.18 | 30.96 | 29.05 | 29.40 | 1.16 |

6.1.3 Ti-6Al-4V Swarf

Much like the previous case, there were no prior results to base the simulations on, so testing was completed as outlined in the previous section. The particle designed for this section, shown in Figure 43, was made up of four spheres and was to imitate the non-linear structure of the swarf material – which had significant impact on the packing of the material. Further to this, the angle of repose that has been simulated is different to the experimental.

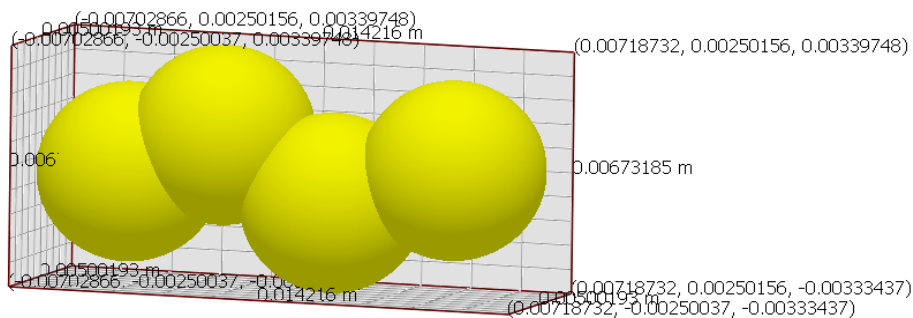


Figure 43 Ti-6Al-4V swarf particle designed in EDEM for use in the EDEM simulations



Figure 44 (a) Simulated Angle of Repose for Ti-6Al-4V swarf particles; (b) Experimental Angle of Repose for Ti-6Al-4V swarf.

Based on these results, shown in Table 6, the decision was made to use the values quoted in AOR10. Even though there are multiple options that show a similar angle of repose to the actual, some literature states a coefficient of restitution around 0.46 for titanium grade 2 – so it would be expected that the value does not differ by much. If the value for the coefficient of restitution is assumed to be around 0.5, it would be a choice of either AOR10 or AOR3, both of which are close to the angle of repose for swarf. Firstly, the standard deviation is less for AOR10 but also, the friction coefficients are more ‘average’, so this particle was selected for further simulations.

Table 6 Results of the Ti-6Al-4V swarf angle of repose simulations for 27 variations of coefficient values.

| Test Name | Coefficient | | | Angle of repose/° | | | | |
|-----------|-------------|-----------------|------------------|-------------------|-------|-------|---------|--------|
| | Restitution | Static Friction | Rolling Friction | 1 | 2 | 3 | Average | St Dev |
| AOR1 | 0.5 | 0.5 | 0.01 | 18.43 | 19.65 | 20.32 | 19.47 | 0.78 |
| AOR2 | 0.5 | 0.1 | 0.01 | 6.34 | 6.07 | 5.47 | 5.96 | 0.36 |
| AOR3 | 0.5 | 0.9 | 0.01 | 42.27 | 40.82 | 39.56 | 40.88 | 1.11 |
| AOR4 | 0.1 | 0.5 | 0.01 | 34.22 | 34.76 | 27.69 | 32.22 | 3.21 |
| AOR5 | 0.1 | 0.1 | 0.01 | 7.13 | 5.97 | 6.63 | 6.58 | 0.48 |
| AOR6 | 0.1 | 0.9 | 0.01 | 45.69 | 47.88 | 38.37 | 43.98 | 4.07 |
| AOR7 | 0.9 | 0.5 | 0.01 | 28.30 | 30.96 | 27.41 | 28.89 | 1.51 |
| AOR8 | 0.9 | 0.1 | 0.01 | 5.71 | 6.16 | 6.72 | 6.20 | 0.41 |
| AOR9 | 0.9 | 0.9 | 0.01 | 41.01 | 42.27 | 43.67 | 42.32 | 1.09 |
| AOR10 | 0.5 | 0.5 | 0.03 | 36.87 | 38.96 | 39.08 | 38.30 | 1.01 |
| AOR11 | 0.5 | 0.1 | 0.03 | 6.59 | 6.20 | 6.48 | 6.42 | 0.16 |
| AOR12 | 0.5 | 0.9 | 0.03 | 46.33 | 47.73 | 44.36 | 46.14 | 1.38 |
| AOR13 | 0.1 | 0.5 | 0.03 | 46.33 | 46.22 | 47.49 | 46.68 | 0.57 |
| AOR14 | 0.1 | 0.1 | 0.03 | 6.95 | 6.48 | 7.13 | 6.85 | 0.27 |
| AOR15 | 0.1 | 0.9 | 0.03 | 42.27 | 43.67 | 45.00 | 43.65 | 1.11 |
| AOR16 | 0.9 | 0.5 | 0.03 | 30.96 | 32.01 | 30.11 | 31.03 | 0.78 |
| AOR17 | 0.9 | 0.1 | 0.03 | 5.83 | 6.07 | 6.14 | 6.01 | 0.13 |
| AOR18 | 0.9 | 0.9 | 0.03 | 42.27 | 45.00 | 43.67 | 43.65 | 1.11 |
| AOR19 | 0.5 | 0.5 | 0.05 | 47.49 | 48.14 | 47.49 | 47.71 | 0.31 |
| AOR20 | 0.5 | 0.1 | 0.05 | 7.83 | 7.69 | 7.33 | 7.62 | 0.21 |
| AOR21 | 0.5 | 0.9 | 0.05 | 46.93 | 49.50 | 48.81 | 48.41 | 1.09 |
| AOR22 | 0.1 | 0.5 | 0.05 | 48.81 | 50.19 | 49.50 | 49.50 | 0.56 |
| AOR23 | 0.1 | 0.1 | 0.05 | 6.34 | 6.63 | 7.29 | 6.75 | 0.40 |
| AOR24 | 0.1 | 0.9 | 0.05 | 46.97 | 47.79 | 49.14 | 47.97 | 0.89 |
| AOR25 | 0.9 | 0.5 | 0.05 | 41.01 | 41.63 | 38.05 | 40.23 | 1.56 |
| AOR26 | 0.9 | 0.1 | 0.05 | 6.33 | 6.23 | 6.82 | 6.46 | 0.26 |
| AOR27 | 0.9 | 0.9 | 0.05 | 39.56 | 40.82 | 40.29 | 40.22 | 0.52 |
| AOR28 | 0.1 | 0.25 | 0.03 | 18.74 | 18.92 | 17.74 | 18.47 | 0.52 |
| AOR29 | 0.1 | 0.75 | 0.03 | 41.63 | 41.89 | 42.93 | 42.15 | 0.56 |
| AOR30 | 0.5 | 0.25 | 0.03 | 21.45 | 19.03 | 18.45 | 19.64 | 1.30 |
| AOR31 | 0.5 | 0.75 | 0.03 | 56.31 | 55.41 | 49.97 | 53.90 | 2.80 |
| AOR32 | 0.9 | 0.25 | 0.03 | 18.43 | 17.57 | 15.26 | 17.09 | 1.34 |
| AOR33 | 0.9 | 0.75 | 0.03 | 39.93 | 46.06 | 45.00 | 43.66 | 2.68 |
| AOR34 | 0.25 | 0.1 | 0.03 | 9.93 | 6.34 | 6.48 | 7.58 | 1.66 |
| AOR35 | 0.25 | 0.5 | 0.03 | 41.01 | 42.27 | 40.40 | 41.23 | 0.78 |
| AOR36 | 0.25 | 0.9 | 0.03 | 50.19 | 51.34 | 50.77 | 50.77 | 0.47 |
| AOR37 | 0.75 | 0.1 | 0.03 | 7.23 | 6.95 | 6.20 | 6.79 | 0.43 |
| AOR38 | 0.75 | 0.5 | 0.03 | 26.57 | 28.30 | 41.01 | 31.96 | 6.44 |
| AOR39 | 0.75 | 0.9 | 0.03 | 41.01 | 42.27 | 43.60 | 42.29 | 1.06 |
| AOR40 | 0.25 | 0.25 | 0.03 | 20.14 | 19.03 | 20.32 | 19.83 | 0.57 |
| AOR41 | 0.75 | 0.75 | 0.03 | 42.27 | 41.55 | 42.88 | 42.23 | 0.54 |
| AOR42 | 0.25 | 0.75 | 0.03 | 43.67 | 40.82 | 39.56 | 41.35 | 1.72 |
| AOR43 | 0.75 | 0.25 | 0.03 | 16.70 | 14.04 | 17.04 | 15.93 | 1.34 |
| AOR44 | 0.3 | 0.25 | 0.03 | 20.14 | 18.43 | 19.03 | 19.20 | 0.71 |
| AOR45 | 0.4 | 0.25 | 0.03 | 18.14 | 17.57 | 17.40 | 17.70 | 0.32 |

6.2 ConformTM Tooling Simulation

Once the particles had been simulated, it was possible to apply the particles to the tool sets. There were two sets of tooling designed for this work. The smaller set was designed for the GA powder, as it has a much more varied morphology, and the spherical shape requires a higher extrusion pressure to be generated than for CP Ti. The swarf tools are much larger, which would be expected as the particulates can be up to 1 cm long. Therefore, it would be better that they fit into the groove, rather than causing damage to the tools, from friction against the side of the wheel and the shoe.

In order to obtain a baseline, the CP Ti was used in both sets of tools. This would reduce the number of simulations required, as the CP Ti will respond to each set of tooling differently. The tools have previously been discussed in *Chapter 5*, however, for clarity the smaller toolset is shown in Figure 45 and the larger toolset in Figure 59. The light pink region corresponds to the factory in the simulation. This is where all the particles are generated and it was positioned to ensure that all feedstock entered the groove, rather than bouncing off the wheel or filling over the die chamber (as the top portion of the shoe was removed). The light blue region is the abutment, which has been highlighted to make it clear where the feedstock is heading in the toolset.

The work carried out for the simulations is based on a number of assumptions and simplifications. Firstly, this is to ensure that the model is not too computational heavy, that the time it would take to get any information out of it is kept to a minimum. Secondly, if the simulation were as accurate as reality, it would be difficult to make predictions if the reality changed. It is not possible to answer every single question using a simulation, but it must be possible to use it as a foundation for predictions.

For this reason, the following assumptions were made:

- (1) The temperature is not included in the simulation
- (2) Simplification of particle design – no satellite particles, consistent size distribution, all particles within a simulation are the same morphology
- (3) No mixed feedstock – the same feedstock is used for the duration of the simulation

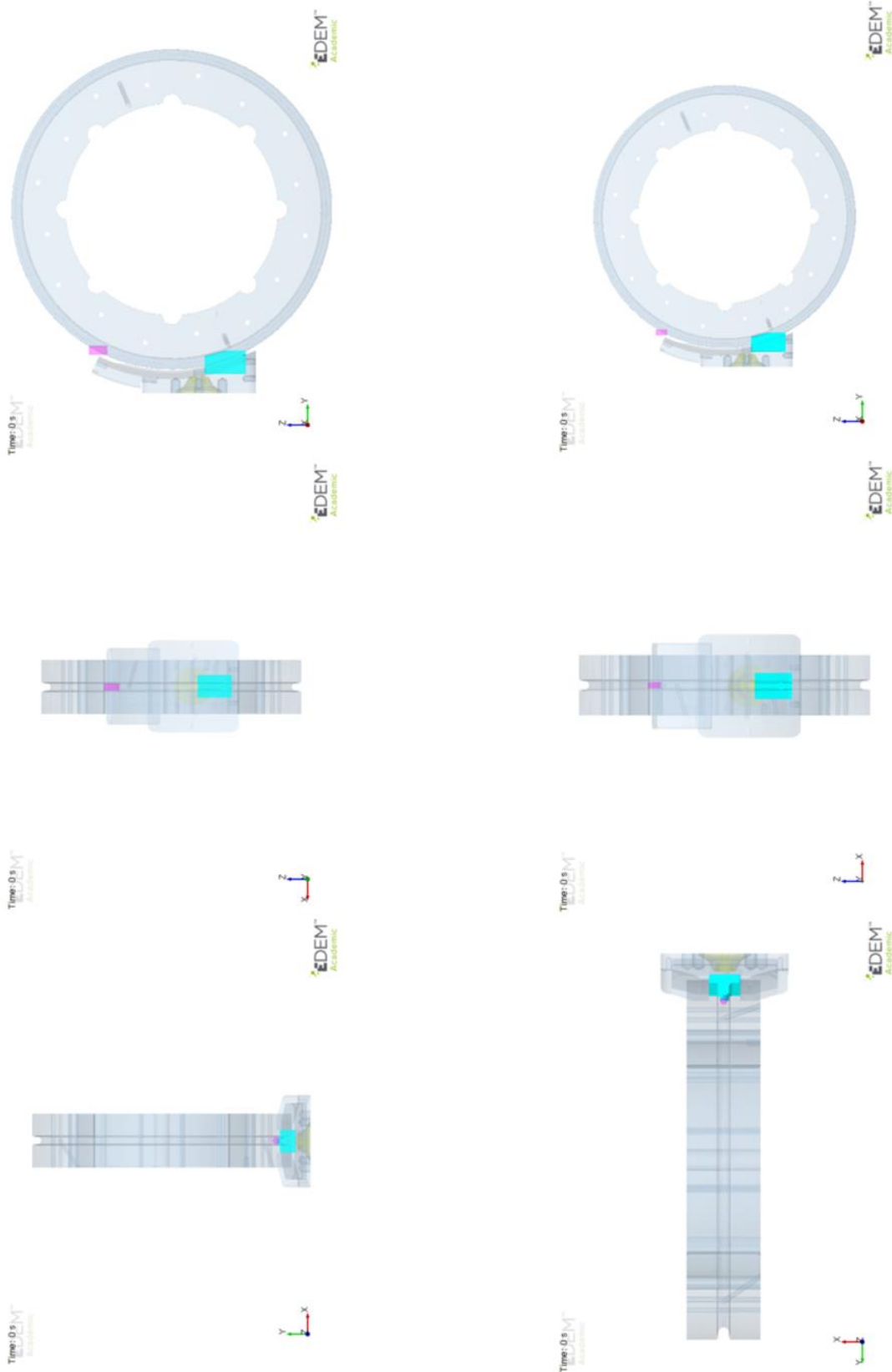


Figure 45 Left: Small toolset designed for the Conform trials complete in this work, showing the top of the simulation, the toolset from the side of the shoe and the front face of the simulation; Right: Large toolset designed for the Conform trials completed during this work

As previously discussed, for each toolset, 3 different particulate feedstocks are used. The simulations have been divided into feedstocks, to allow for a discussion about the behaviour of the feedstocks in differently sized toolsets.

6.2.1 CP Ti HDH Gr 2 simulations

6.2.1.1 Small Toolset

The CP Ti HDH Gr 2 Conform™ simulation was run to a simulation time of 5s. The results of the simulation are shown in Figure 60. From the Figure, it is clear that the particles fill the available space with relative ease and very quickly, and at 2s, the port is almost completely filled. The reason for this is that the smaller geometry can accommodate less feedstock, which means that it will fill faster. However, this does not mean that it will achieve the extrusion pressure required to consolidate the material. The compressive force is a guide for how the particles are compacting in the tooling and as is clear from 2s, there is a clear region of higher force on the particles. This is commonly seen in both DEM and FEM simulations of Conform™, where there is a clear increase in stress at the 90° corner.

The graphs shown in Figure 47 help to reinforce the results of the simulation and how they clearly mimic the process. There is an increase in both the pressure and compressive force on the abutment, much like that seen in the Conform™ trial data (see *Chapter 7: Experimental Trials*). Unfortunately, unlike experimental trials, there is no wear on the abutment during these simulations. This means that it is not possible to determine the point of trial failure. However, unlike during the process, it is possible to estimate how the particles will behave in the different geometry toolsets and this will be discussed further with the alternative feedstocks and tooling. Based on the mass flow rate graph shown in Figure 47, it is clear that as the trial progresses, particles are lost at an increasing rate from the bottom of the abutment. This means that the particles are not being extruded out of the die, but rather being forced between the abutment and groove and are lost. This results from a combination of the flash gap (which is around 0.5 mm) and the particle morphology. It should be noted that this simulation does not reach a point of steady state, and therefore, extrusion out of the die is not significant. Further to this, the material does not consolidate, which results in gaps between the particles still existing and therefore, the pressure will be lower than that achieved in the process. However, as is clear

from both the simulation images and the mass flow graph, there is some particle extrusion with particles leaving the die during the process.

Finally, the wheel torque graph in Figure 47 demonstrates the increasing torque as the process continues, which is what is expected from the process. As the particles become more compacted, the energy required to rotate the wheel increases, owing to the role of the wheel in the friction generated during the trial. The particles will become lodged in the flash gap and in any open space between the groove and the die chamber.

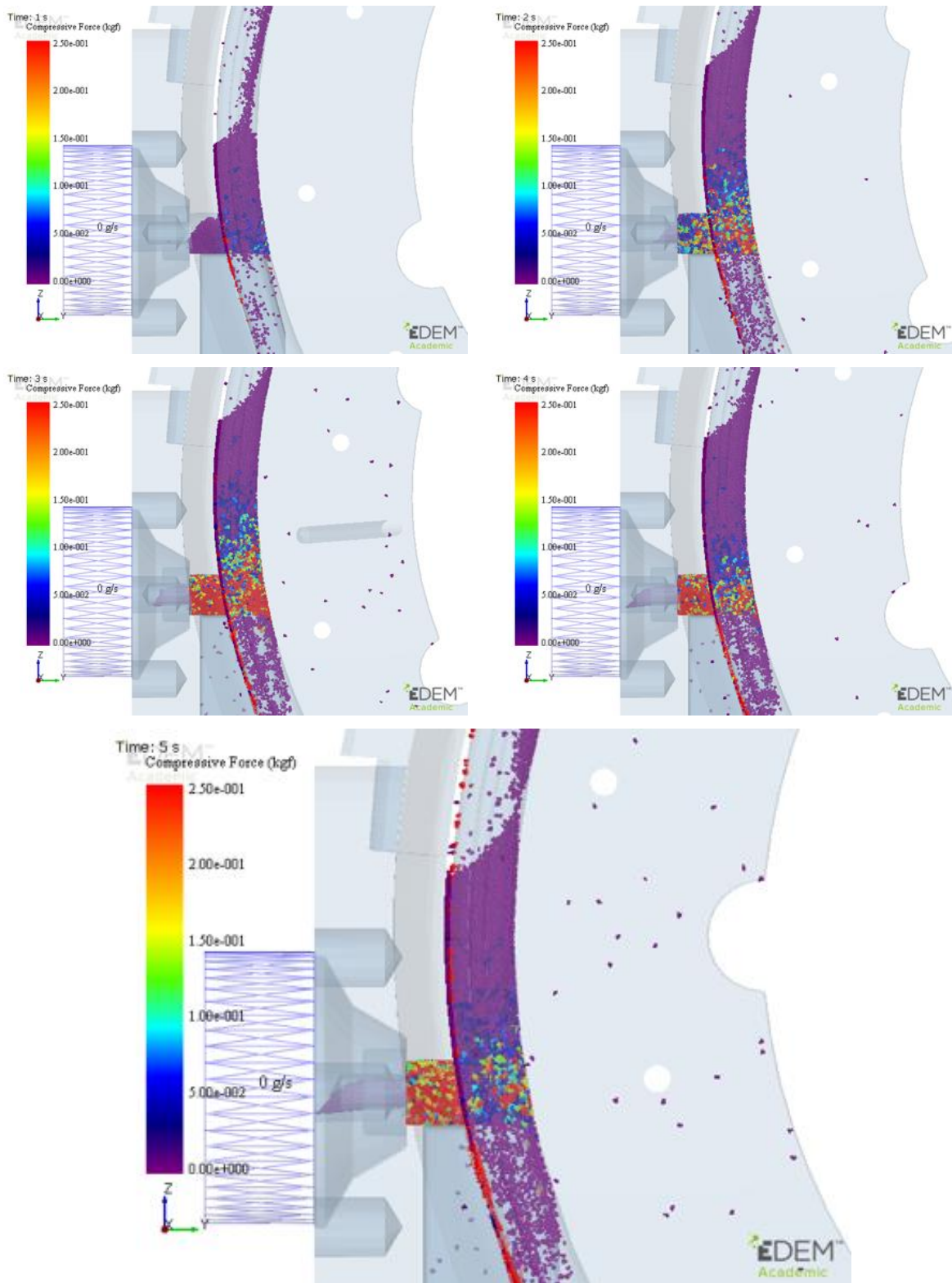


Figure 46 5s EDEM simulation for CP Ti HDH Grade 2 in the small toolset.

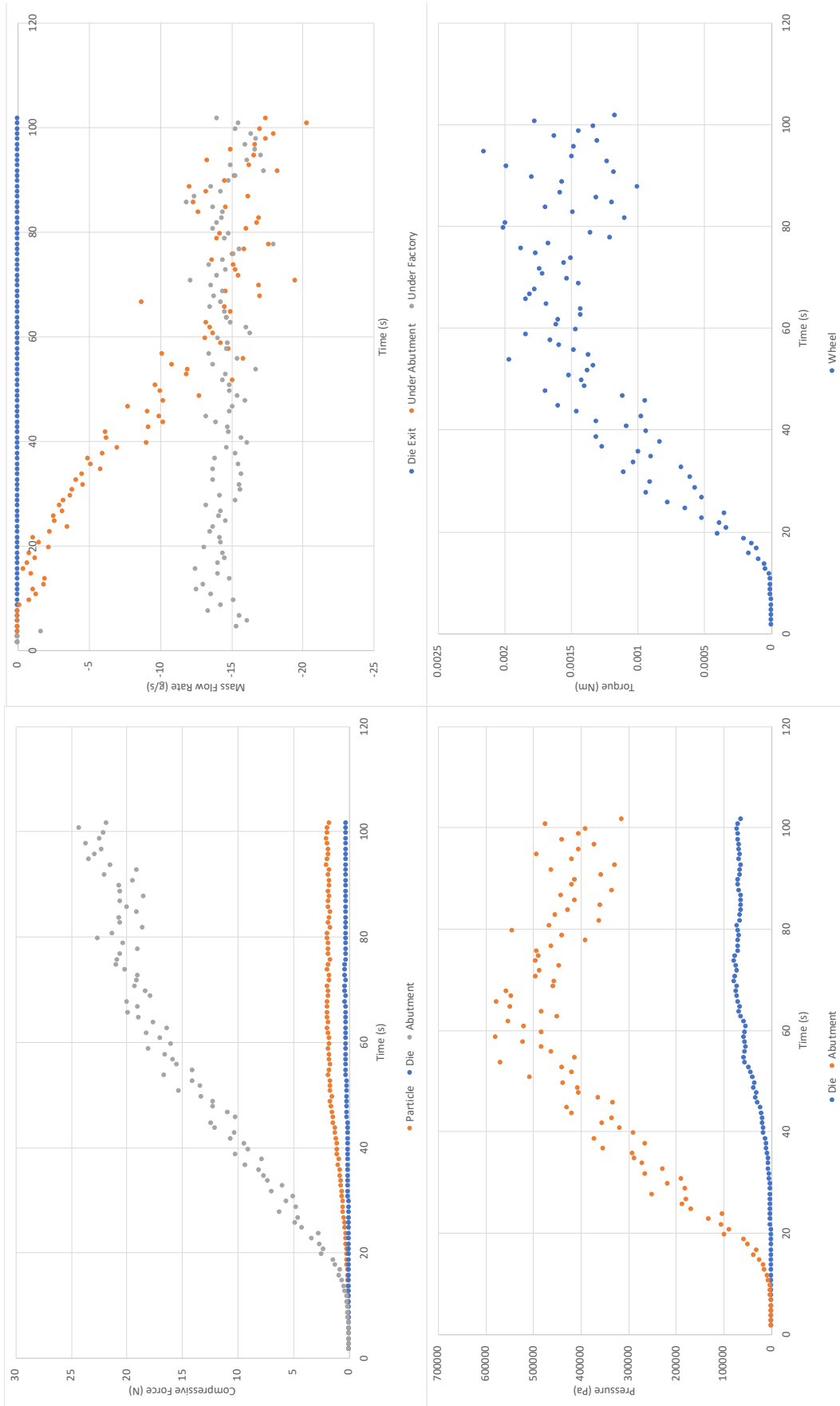


Figure 47 Data obtained from the EDEM simulation of CP Ti HDH Grade 2 in the small toolset.

6.2.1.2 Large Toolset

As shown in the simulations in Figure 48, this toolset, as expected, fills much more slowly than the smaller toolset. There is successful filling of the port and consequently the die. Unlike with the small toolset, the compressive force on the particles is lower, which would be expected. This is because more particles are required to fill the available space and therefore, there are more gaps between the particles. In theory, the compressive force will continue to increase as the volume of particles added to the system increases.

The graphs shown in Figure 49, particularly those corresponding to the compressive force and wheel torque, are similar to those seen in the experimental trials (see *Chapter 7: Experimental Trials*). As the simulation progresses, the pressure on the tooling reduces, which is similar to what occurs when not enough feedstock is added during the experimental trials.

Finally, it is clear that the mass flow loss from the system under the abutment increases as the trial progresses. This is as particles are becoming compressed and consequently are forced into any available space. This includes into the flash gap. As the particles are forced into the flash gap between the abutment nose and the groove, the particles are lost as waste.

Unfortunately, there is little to no extrusion during the simulation, however, if the powder mass flow was increased, as it would be during a trial, the pressure on the particles would increase. This would ultimately result in a higher compressive force between the particles, a higher torque as the particles are sheared past each other and finally, the extrusion pressure would build, allowing particles to be forced through the die.

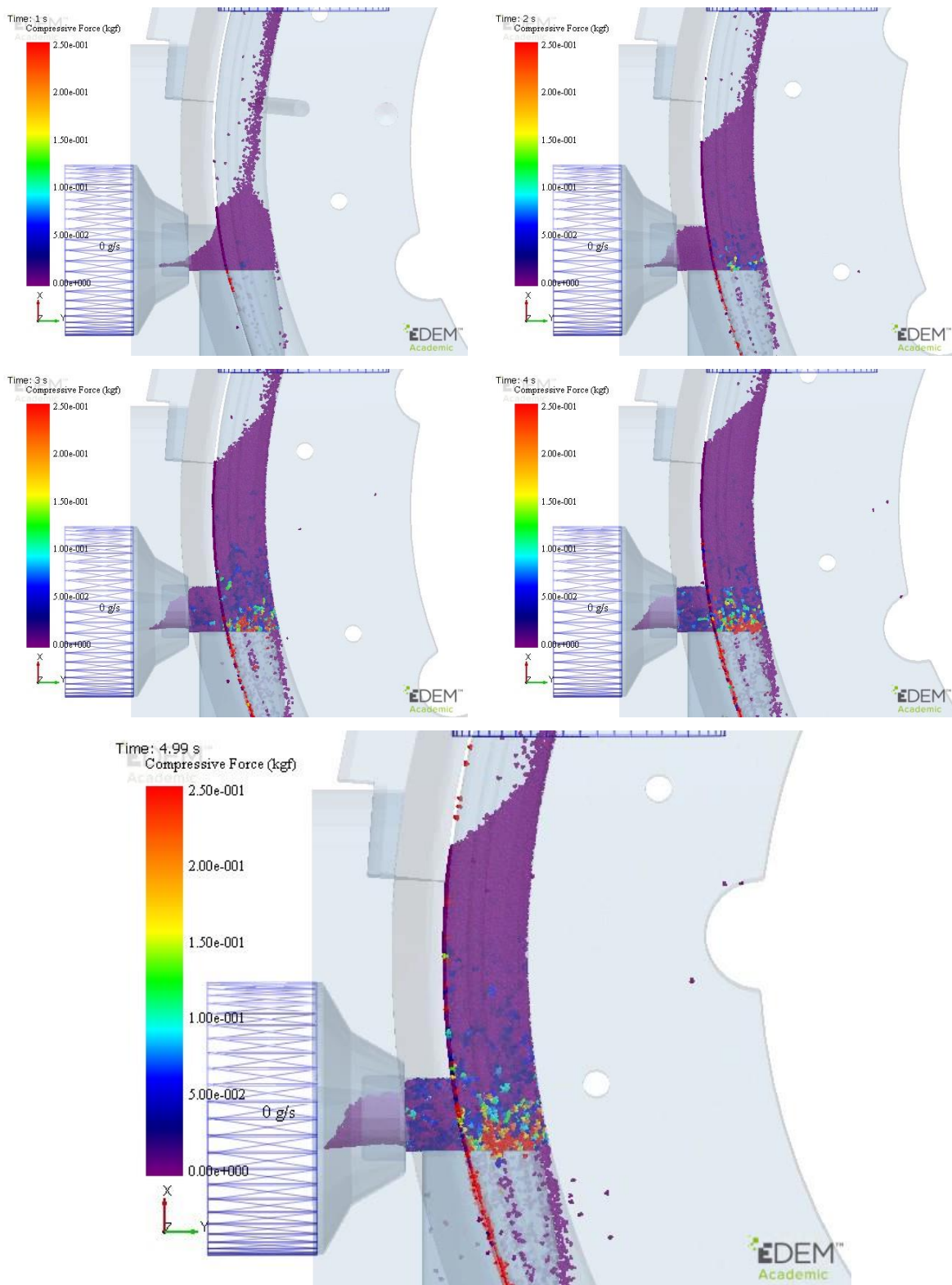


Figure 48 EDEM simulation for CP Ti HDH Grade 2 in the large toolset.

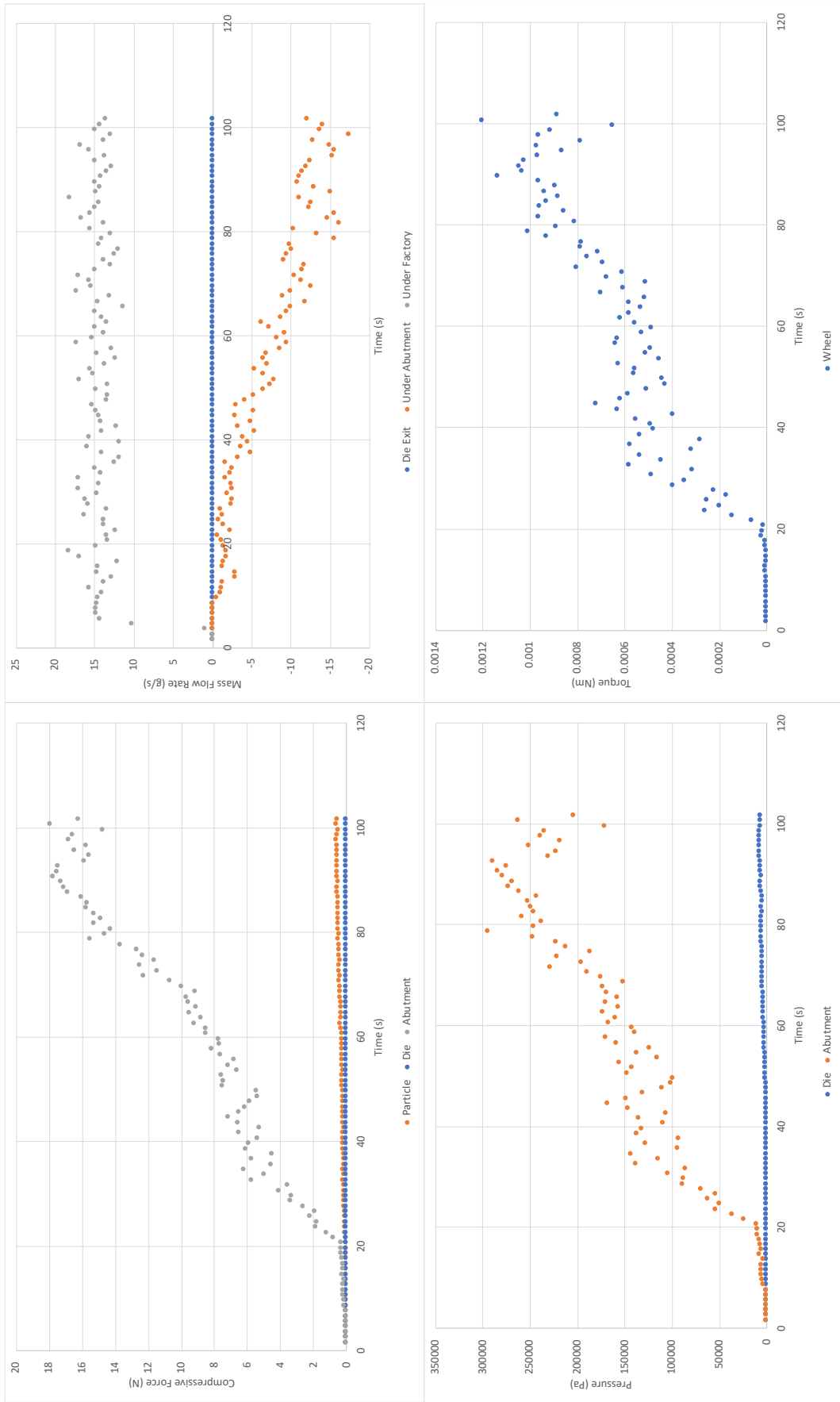


Figure 49 Data obtained from the EDEM simulation of CP Ti HDH Grade 2 in the large toolset.

6.2.1.3 Summary

Although both toolsets gave similar outcomes, it is clear that the smaller toolset lends better to higher compressive forces between the particles, more efficient port filling and a much higher chance of extrusion. The larger toolset clearly has its place, and should a larger feedstock be used, it would allow for accommodation of the larger particles morphologies and generate extrusion pressures that would likely extrude these materials.

In the case of both sets, the graphs produced in Figure 48, are similar. The pressure and torque graphs have some clear replication of the graphs produced from the experimental trial data (see *Chapter 7: Experimental Trials*) and suggest that trial conditions can be determined from the results. For example, the higher torque results in a higher compressive force between the particles, as the particles are pulled together from the friction between the groove and the feedstock particles. Therefore, it is clear that in the case of the larger toolset, that for CP Ti HDH Gr 2, it may be advantageous to employ a higher wheel speed to increase the friction and the torque.

Finally, the mass flow rates can be predicted based on the results, as it is more evident here that the loss of particles is often a result of the friction, forcing particles into the gap between the wheel groove and the abutment nose. This suggests, that as the trial continues, particle loss may increase, and that when this is the case, the mass flow of particles into the process should increase to mitigate any loss.

6.2.2 Ti-6Al-4V GA simulations

6.2.2.1 Small Toolset

Unlike the CP Ti HDH Gr 2 in small tools shown earlier (see Figure 46), the simulation of Ti-6Al-4V GA powder, as seen in Figure 50, in the smaller geometry toolset clearer demonstrates that a much higher mass flow is required to maintain the tool fill, however it should also be noted that this simulation ran for 10s rather than 5s. Initially, the tooling fills well with a reasonable length of feedstock held between the groove and the die chamber, however, there is

very little compressive force between the particles. This suggests that the extrusion pressure would not be high enough to extrude a significant amount of material. This is contrary to the case during the trials, where the Ti-6Al-4V GA has been successfully extruded (see *Chapter 9: Paper*).

There is some reason behind this, however, as during a trial there is a warm-up period where CP Ti HDH Gr 2 is used as a feedstock to start extrusion (as discussed in *Chapter 9: Paper*). The Ti-6Al-4V GA is then added once this has begun to extrude, which would help to prevent feedstock loss as it is combined with the material on the abutment. As is shown in *Chapter 9*, Ti-6Al-4V GA was never extruded as a pure rod and was entirely in combination with CP Ti. Additionally, during a trial the flow of the feedstock into the tooling can be constantly monitored, in order to ensure that there the material lost is not the total amount of feedstock going in. Whilst this is possible during a simulation, in order to obtain a direct comparison between the toolsets, it was decided that the flow should be constant, so that the behaviour of the particles within the different geometries could be monitored. Further work should be done to investigate the behaviour under different mass flow of particles, in order to be able to accurately estimate the volumes required during a ConformTM trial. However, this work gives a reasonable bottom estimate for this. As is shown in the mass flow graph in Figure 51 and from 4s of simulation, there is some extrusion of Ti-6Al-4V from the tools and as the simulation progresses, further material is forced through the die.

The wheel torque and compressive force graphs both demonstrate that the loss of powder can cause a significant drop in the extrusion pressure, which ultimately reduces the amount of material that can be extruded. This is similar to the drop found in the experimental trial data (see *Chapter 7: Experimental Trials*), where evident feedstock changes can result in a loss of extrusion pressure. The die compressive force does not increase like that in the CP Ti HDH Gr 2 in this toolset, which is a result of the low compressive force between the particles and ultimately, suggests that much more feedstock is required and potentially higher wheel speeds, to increase the friction and produce a fully consolidated rod product.

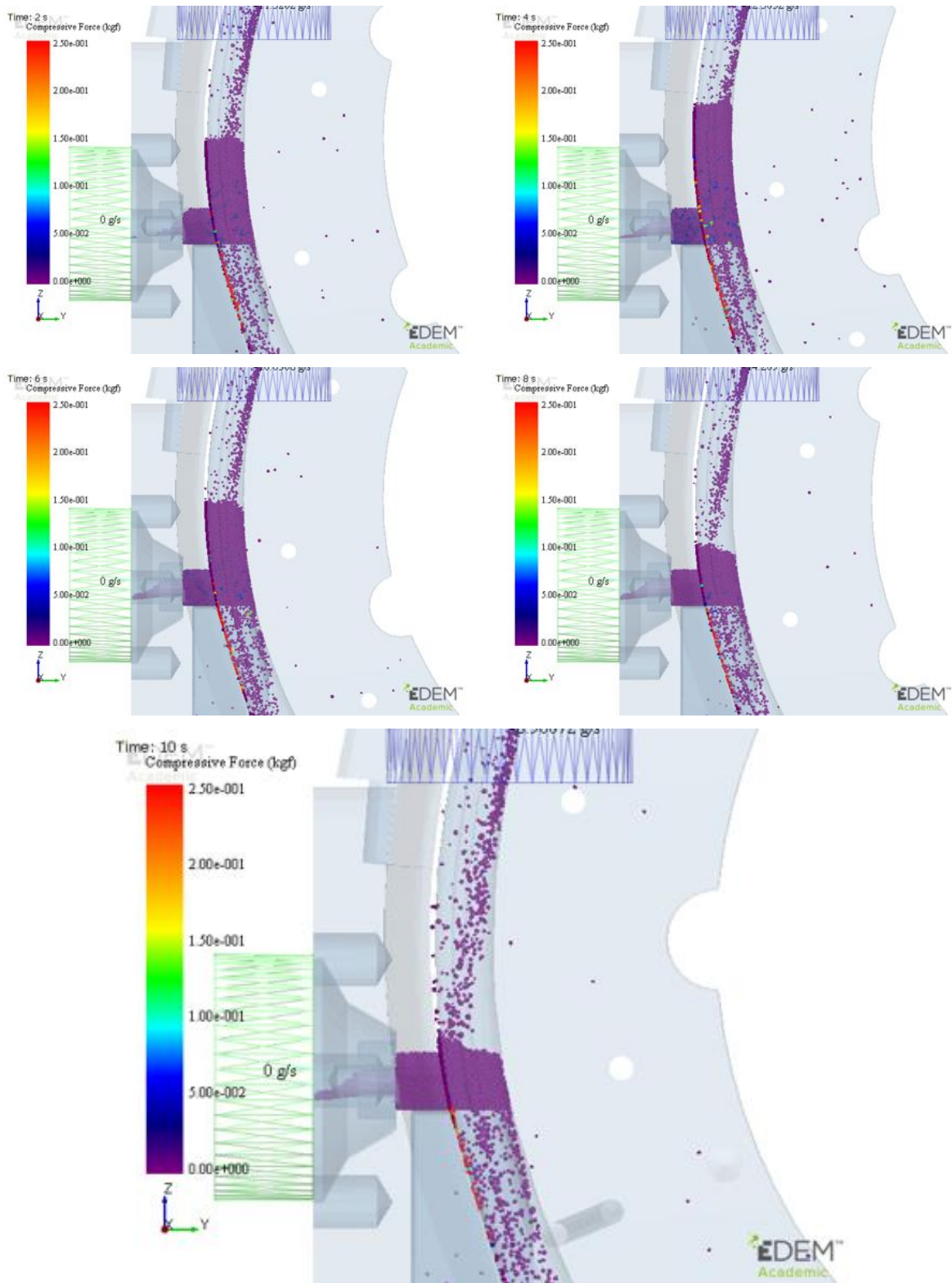


Figure 50 EDEM simulation of Ti-6Al-4V GA in the small toolset.

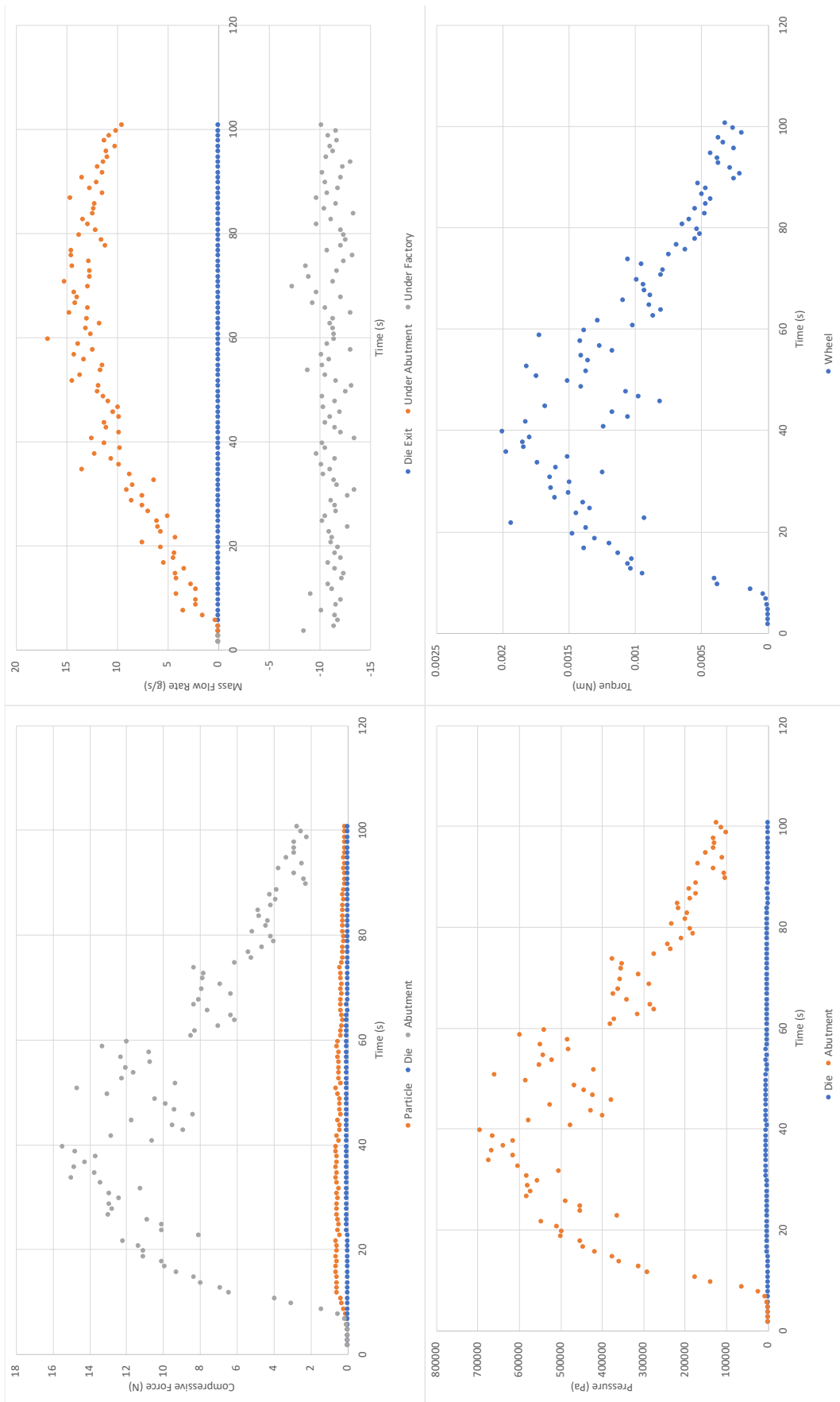


Figure 51 Data obtained from the EDEM simulation of Ti-6Al-4V GA in the small toolset.

6.2.2.2 Large Toolset

The smaller geometry toolset had previously demonstrated that a significantly higher volume of feedstock would be required to successfully extrude the Ti-6Al-4V GA powder used in these trials. The larger geometry toolset is no different and would require an even higher mass flow of feedstock. There is some filling of the toolset shown in the simulations in Figure 52, however, a grip length greater than the height of the port is never obtained. Significant volumes of feedstock are lost to the flash gap and the material that is lost to the die is mostly coincidental and has no sway from extrusion pressure.

There is some clear compressive force between the particles and the wheel, as the particles become lodged between the wheel and the die chamber, however, there is very little compressive force between the particles. This is because the lack of particles means that there is not enough material interacting between the wheel groove and the front face of the die chamber. Ultimately, this means that there would not be enough friction between the particles and the groove to consolidate the material and increase the extrusion pressure. If there is not enough extrusion pressure, consolidated material will not be forced through the die and the resulting product, if any, would not be well consolidated and there is a high chance of porosity and poor-quality material.

From the graphs shown in Figure 53, there is very little pressure at the abutment or the die, as a result of a much lower volume of feedstock, which has not filled the port. This is echoed in the wheel torque, which is more than 5x lower than that seen in the smaller toolset.

It is possible that with a significant increase in the feedstock volume, that the compressive force between particles, wheel torque and pressure on both the die and abutment would increase. However, with the increase in the feedstock volume comes a significant material cost and it would be more beneficial from both a processing and economic standpoint that using the smaller geometry tooling would be of more interest and would result in the successful extrusion of Ti-6Al-4V rod product.

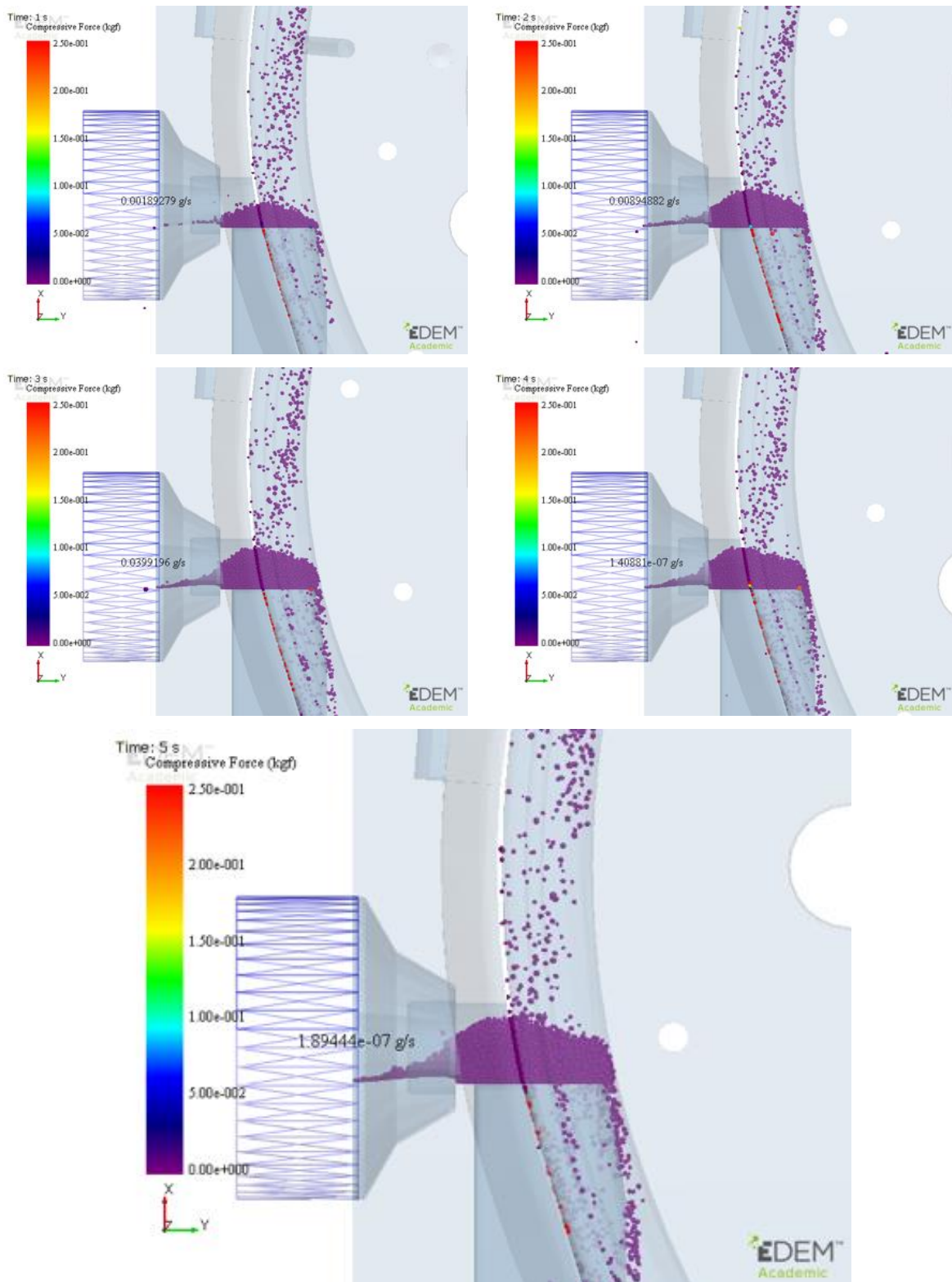


Figure 52 EDEM simulation of Ti-6Al-4V GA in the large toolset.

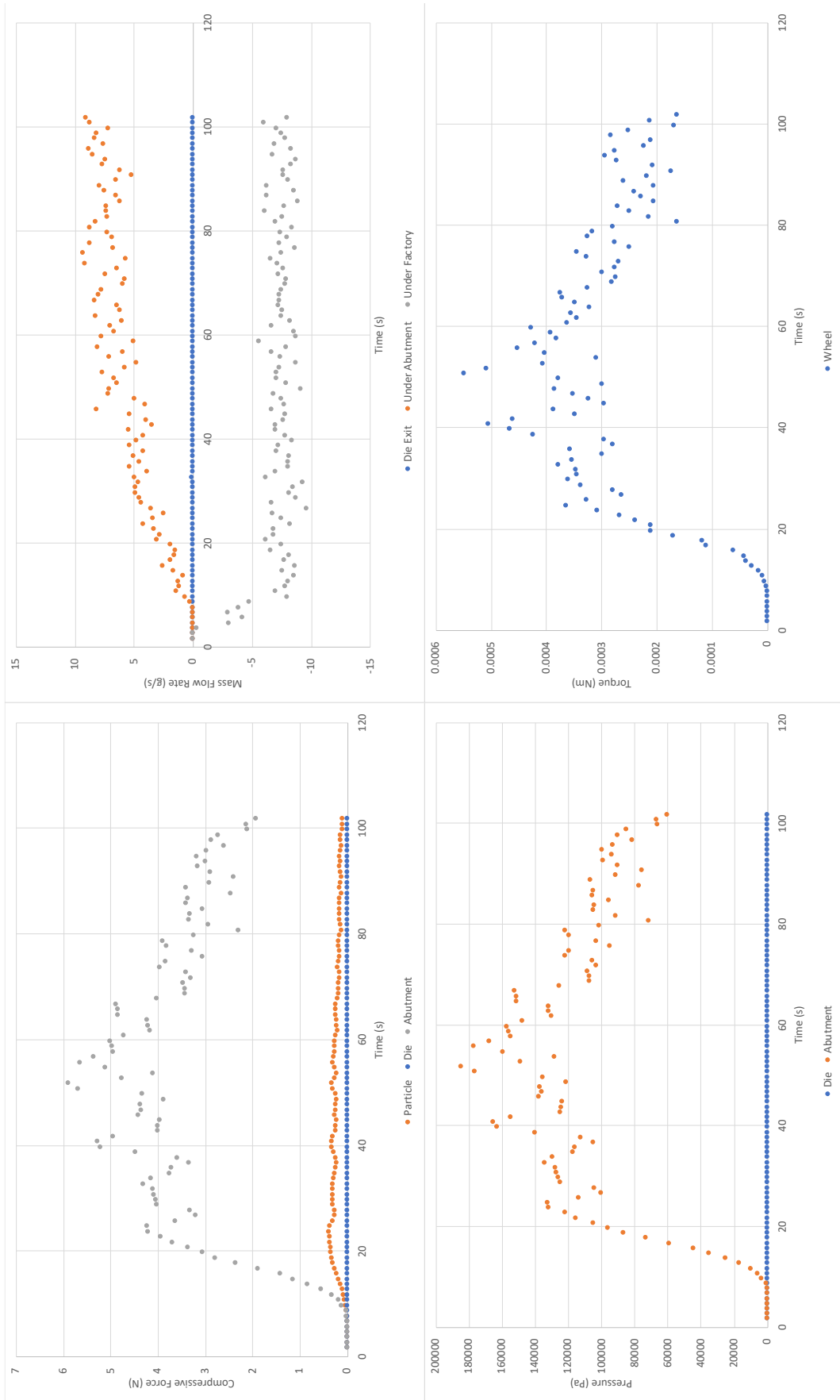


Figure 53 Data obtained from the EDEM simulation of Ti-6Al-4V GA in the large toolset.

6.2.2.3 Summary

From the data, it is clear that the Ti-6Al-4V GA is much more suited to the smaller toolset. There is a much better fill between the die chamber and the groove and ultimately, this has resulted in a filled port and some extrusion of the particles. Despite this, there is a clear issue with the particle mass flow, as there is not enough feedstock to produce a steady state simulation, especially when compared to the CP Ti HDH Gr 2 simulation in the smaller toolset. In an experimental trial, CP Ti HDH Gr 2 is used as a warm-up feedstock and this may mean that the increase in the mass flow of the second feedstock, Ti-6Al-4V GA, is not entirely necessary as there will already be a build-up of material on top of the abutment.

Naturally, this is echoed in the larger toolset, however, a significant volume of feedstock would be required to extrude a consolidated product. This would result in much higher costs and therefore, would not be industrially or commercially viable.

The data shows that the smaller toolset is an ideal choice for the smaller morphology particles, as the material does result in a filled port, clear extrusion pressure across the particles and a dense stack of particles on top of the abutment. The particle loss is a little high, however, with CP Ti HDH Gr 2 starting in the trial, there should be less gap for particles to be lost.

In order to obtain a more robust simulation, it would be worthwhile to investigate the impact of higher mass flow on the simulation, including a further investigation into the particles lost. The geometry of the Ti-6Al-4V GA particle could be further analysed, and satellite particles may be included for a more accurate result.

6.2.3 Ti-6Al-4V Swarf

6.2.3.1 Small Toolset

The swarf feedstock is much larger morphology than the other feedstocks used in this work, therefore the mass flow rate was reduced to 5 g/s from the factory added to the tooling.

From Figure 54, it is clear to see that the particles of the feedstock fill the space between the groove and the die chamber quickly, however, there is some clear issue with the 90deg change in direction as the feedstock is forced into the port. Early on in the simulation, there is little material in the port and most of the compressive force of the tooling relates to the friction between the particles and the groove. This compressive force builds throughout the simulation, however, there is no extrusion. The port is not filled, however, the force begins to build on the die, as the particles are forced into the port.

The graphs in Figure 55 show that there is a similar increase in pressure and compressive force on the tooling, as shown in both the earlier simulations but also in the experimental trial data in *Chapter 7: Experimental Trials*. The compressive force between the particles is much higher than that seen in the previous simulations, as the volume of the particles and the limited space between the groove and the die chamber have led to an increase in the friction on these tools. Unfortunately, the 90° bend into the port is much tighter than in the larger toolsets, that there is a clear issue with the feedstock filling the port and then the die.

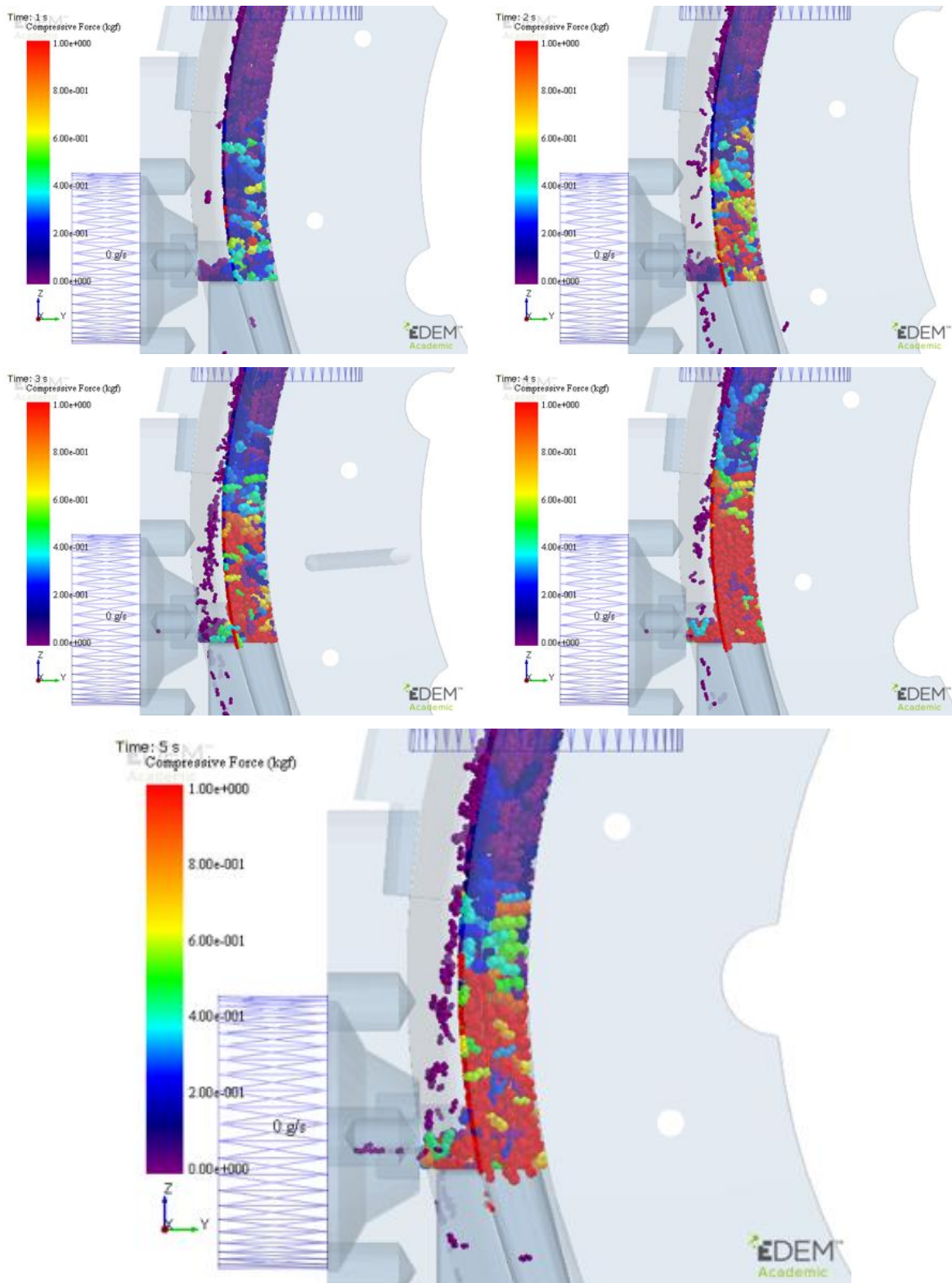


Figure 54 EDEM simulation of Ti-6Al-4V swarf in the small toolset.

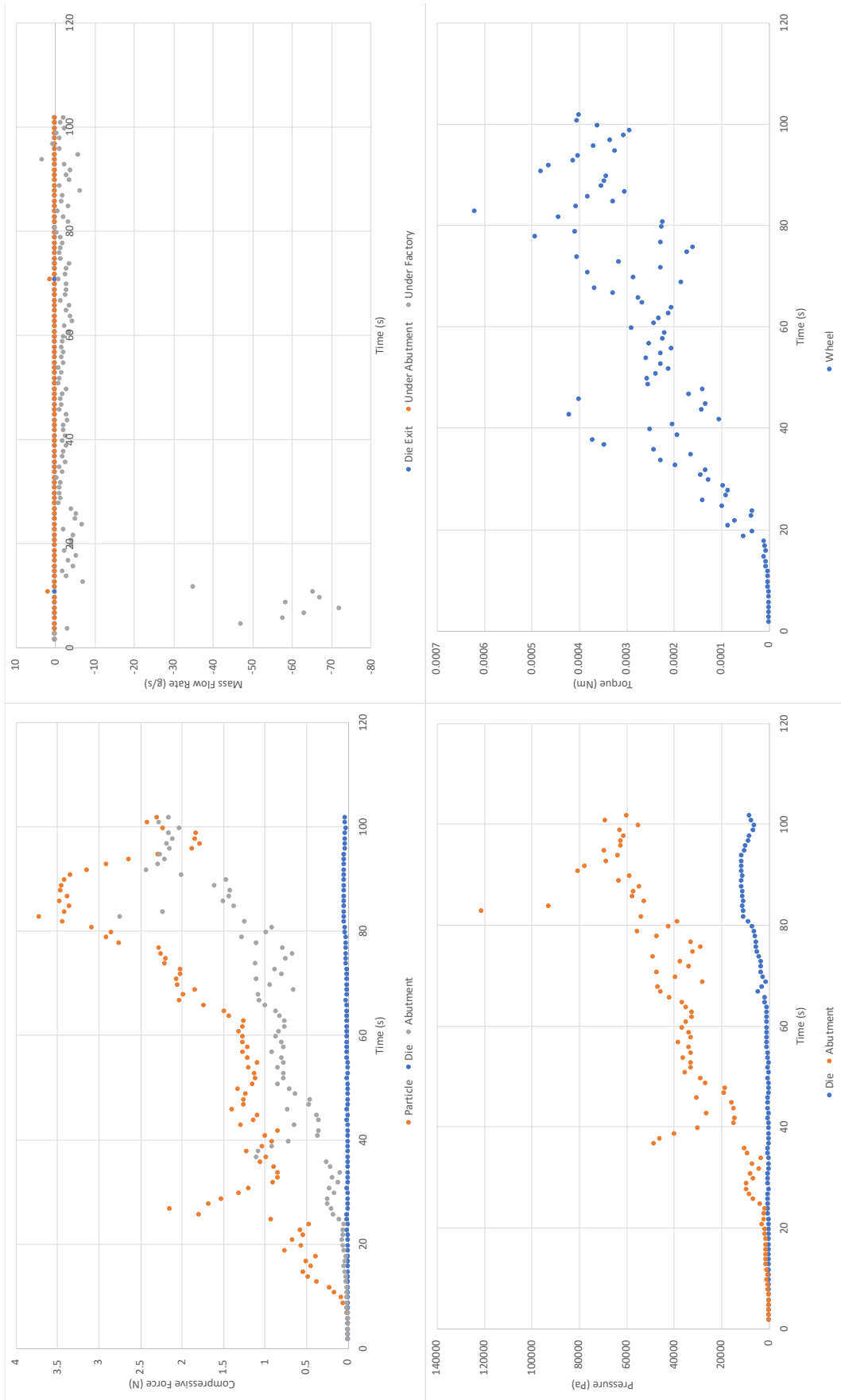


Figure 55 Data obtained from the EDEM simulation of Ti-6Al-4V swarf in the small toolset.

6.2.3.2 Large Toolset

The larger toolset lends well to the larger particulate morphology, and although there is no extrusion demonstrated in the simulation in Figure 56, there is much more port filling and there are less particles being forced between the flash gap, with very little being lost underneath the abutment. The simulation itself is over 10s, and the compressive force scale is higher than it was for the previous simulations. Much like the Ti-6Al-4V GA and CP Ti HDH Gr 2 in the smaller toolset, there is clear evidence of stress at the 90° abutment nose. The compressive force in the particles is high, with many of the gaps seen in the early simulation (2s – 6s) becoming filled in as the particles become denser. This is a replication of the process, where the packing of particles is improved with the friction from the wheel forcing the particles together and consequently forcing them into the port.

Although the port is not filled during this trial, the force on the particles in the port is not as high as the compressive force on the particles in the groove. If the simulation were to run for longer, it is likely that the compressive force would increase further and push particles into the port.

Unlike previous simulations, the compressive force and pressure on the abutment and the wheel torque, shown in the graphs in Figure 57, do not decrease towards the 10s point. This is a sign that the trial could run for longer, and that the feedstock is not being lost in the flash gap.

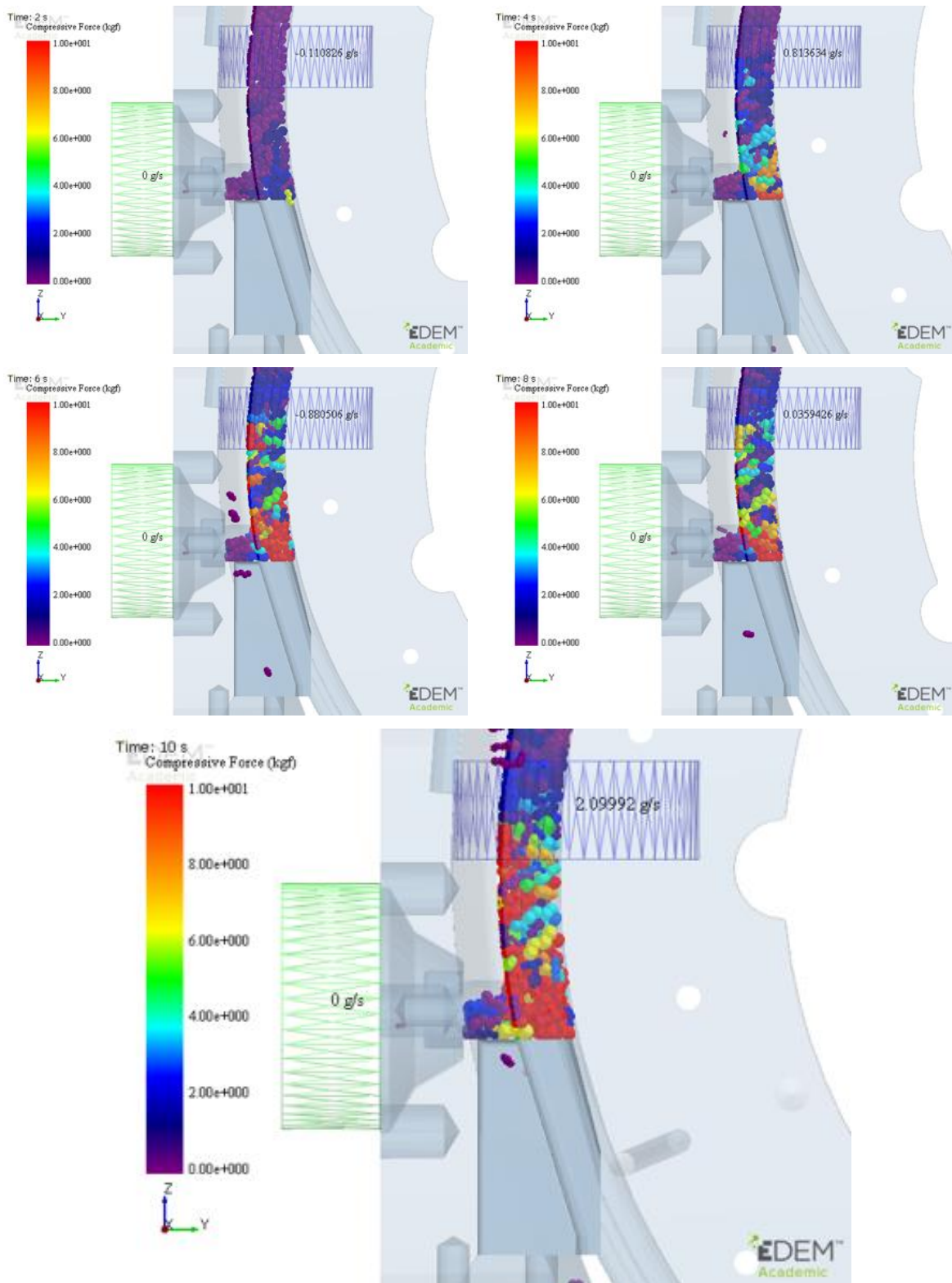


Figure 56 EDEM simulation of Ti-6Al-4V swarf in the large toolset.

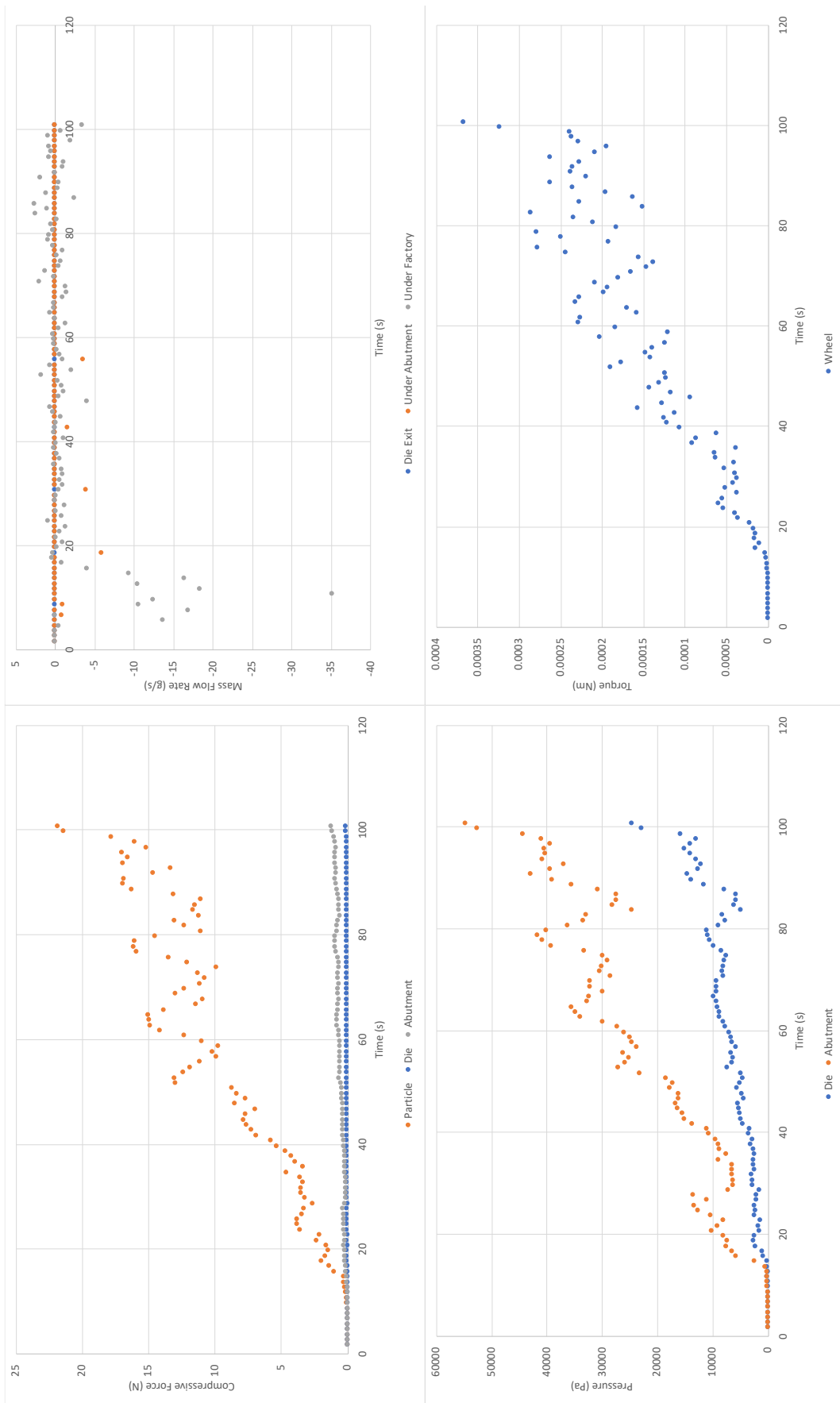


Figure 57 Data obtained from the EDEM simulation of Ti-6Al-4V swarf in the large toolset.

6.2.3.3 Summary

As with the Ti-6Al-4V GA, there is a clear toolset which has a much more useful outcome than the other. In the case of the swarf, this is the larger geometry toolset. Although it was initially designed to accommodate the length of the particles within the groove (see *Chapter 5*), further confirmation of the ability of the toolset to consolidate swarf was shown here. There is a high compressive force between the particles, and a visible reduction in the free space between each particle, suggesting consolidation of the feedstock. The wheel torque is slightly lower for the larger tools than the smaller tools, however, this is because the particles in the smaller toolset are filling a much smaller space. This results in force against the wheel and therefore an increase in the torque. Visually, it is evident that the wheel is pulling the particles around and increasing the consolidation of the particles.

The compressive force on the abutment and the die are much lower than for the other toolsets, however, it should be noted that the particles do not quite reach the die. This is a flaw in the simulation, which could be addressed by adjusting the size distribution of the swarf particles. Much like for the GA particles, the initial feedstock will be CP Ti HDH Gr 2, which would mean that the port should already be filled before the swarf is added. This would mean that the insufficient filling with pure swarf will be mitigated.

6.2.4 Summary

There are evident flaws in the simulations completed in this work, however, they do still assist in the justification of the tooling design and allow for predictions of how different particle geometries will behave in the various toolsets.

In terms of flaws, there are a number of changes that would be required to vastly improve the simulations. Firstly, the conditions during the trial do differ from those shown in the simulations, as the shoe is typically preheated to $\sim 500^{\circ}\text{C}$. This is not the case here and because of this, there is no way of determining how the particles will behave under the shear in the process at temperature.

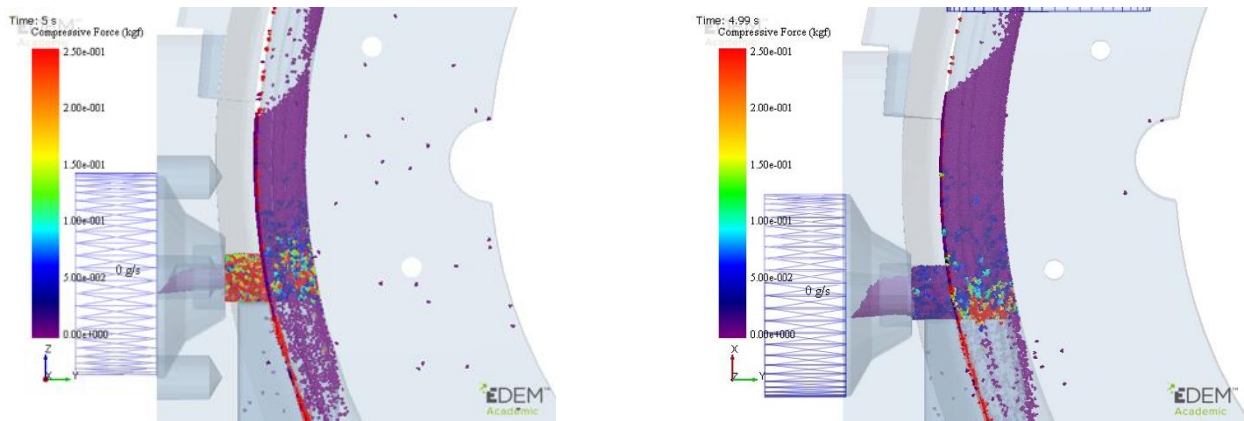


Figure 58 EDEM simulations demonstrating the difference between CP Ti HDH Gr 2. in the differently sizes toolsets.

Secondly, the initial feedstock in each trial is CP Ti HDH Gr 2, and although there was a simulation using this feedstock, there was no investigation into how the following feedstock would behave in the process. It would be important to know how the tooling responds with the addition of an alternative feedstock, following on from the CP Ti HDH Gr 2. It would also make the simulation more accurate to the conditions in the Conform process.

Thirdly, there are fundamental flaws in the particle design. The particles were overly simplified, and the coefficients were determined to generate a similar angle of repose to the experimental particles. There are obviously some issues in doing it this way, as the assumption that there are no satellite particles, no particles of different geometry and a relatively consistent size distribution. In reality, this isn't the case, but in creating a more complex set of particles, the computational power required to run the simulation is significantly increased.

Additionally, the particle mass flow was consistent for each of the toolsets and further to this, they were not the same for all particles. This means comparison can be relatively difficult, but it should be noted, that due to the sizes of the particles, having the same mass flow for each feedstock would also not be advised. It should also be considered that during an experimental trial, the mass flow can be adjusted according to what is coming out of the machine at the waste or extrusion points. Further study should include an investigation into how the processing of the particles behave during changing mass flow during a trial.

Finally, in terms of the method of DEM itself. There are some obvious questions to be asked about the validity of using DEM for a process that results in a fully consolidated product. DEM allows a detailed look at how the individual particles are behaving during the process, which is important when deciding what tool geometries are needed for a trial. However, since starting work on this project, alternative methods have become more known, where DEM and finite element modelling (FEM) are combined. The result of this is that the particles can be investigated individually, however, it is possible to also investigate how the bulk material is behaving. This allows for further investigation into bulk stresses and strains and would allow even more informed decisions to be made on the tooling and the processing parameters.

Aside from the flaws, there are clear uses for the work completed in this project. The cross-comparison between the various powder particles and their behaviour in the tooling gives a clear justification for the design of the toolset. It also directs the user to an idea of the expected particle mass flow, which although it is not completely accurate, gives a clear indication of how much would be required. The swarf feedstock in the swarf tooling gives a clear insight into how the larger morphologies behave in the process, with very little material lost as waste, but also there is a clear reduction in the density, which is both visible in the simulation but also in the compressive force on the particles graph.

Much of the graphed data in the section appears to be similar to that in the experimental trials, with the abutment pressure demonstrating similar trends. This is particularly interesting in the case of the GA powder in the smaller toolset. The loss of the particles shows a clear drop in the pressure on the abutment and the wheel torque, and whilst this could be assumed, it is useful to understand that this is the case, and it helps to explain the drops in abutment pressure within the experimental trial data shown in *Chapter 7: Experimental Trials*.

Chapter 7 : Experimental Trials

As the ConformTM process does not have a standard operating procedure, this work has involved further development of the process and understanding the optimum parameters required to obtain a consolidated wire product.

Ten trials were completed, with variations across each of the trials, in terms of parameters, materials and outcomes. Each trial has key requirements such as a titanium-based particulate feedstock, one of two tool sets and similar starting procedures.

In all cases, the trials were started by applying rotation to the wheel of 2 RPM, prior to the addition of powder. This slow speed was to allow for any interference between the tooling to be detected and to determine if there were any machine-based issues, such as electrical or mechanical issues, which would need to be rectified prior to trialling.

Other than the product of the trial, data is also recorded. This data gives information on the wheel speeds, tooling temperatures and motor torque, from which the stress on the abutment and the grip length can be determined. In addition to this, the data also yields information on the extrusion itself. After a number of trials, it became evident that certain criteria must be met in order to extrude and there are trends in the data, which clearly show the point at which the extrusion has failed. Because of this, parameters such as the wheel speed or the feed rate could be adjusted according to the real time data on display during the trial.

7.1 Tooling

As discussed previously (see *Chapter 5* and *Chapter 6*), the tooling geometries used in trials varies between trials, as they were designed for the processing of particles of different morphologies. The smaller toolset was designed for processing both smaller morphology materials but also to generate an extrusion pressure high enough to consolidate and extrude the material. The larger set was designed for the processing of swarf, to ensure that the material would fit within the groove, to minimise particle loss, but also to allow sufficient material to build and generate friction with the wheel. The toolsets used for each of the trials is shown in Table 7, along with the flash gap, which is determined at the start of each trial.

Table 7 Tooling geometries and materials for the trials conducted in this work

| Trial # | Powders | Tooling | | | | | Wheel Speed RPM | Product length mm | Product diameter mm | Tensile | Fractography | Hardness | Light Microscopy | Extruded Rod | Data Analysis |
|---------|----------------------------|-----------|-------------------|---------------------|---------------------------|---------------------------|--------------------|----------------------|------------------------|---------|--------------|----------|---------------------|--------------|---------------|
| | | Die mm | Groove mm x mm | Abutment mm x mm | Die Chamber mm x mm | Abutment Material | | | | | | | | | |
| 1 | CP Ti HDH Grade 2 (Phelly) | 10 | 15 x 15 | 13 x 13 | 13 x 13 | Inconel 718 Ionbond 25 | 8 | - | x | x | x | x | x | 7.3.1 | |
| | Ti-6Al-4V HDH (Reading) | 10 | 15 x 15 | 13 x 13 | 13 x 13 | Inconel 718 Ionbond 25 | 8 | 200 | x | x | x | 8.2.1 | 8.1.1 | 7.3.2 | |
| 2 | CP Ti HDH Grade 2 (Phelly) | 10 | 15 x 15 | 13 x 13 | 13 x 13 | Inconel 718 Ionbond 25 | 6 | 400 | x | x | x | x | 8.1.1 | 7.3.3 | |
| | Ti-6Al-4V HDH (Reading) | 10 | 15 x 15 | 13 x 13 | 13 x 13 | Inconel 718 Ionbond 25 | 6 | 400 | x | x | x | x | 8.1.1 | 7.3.3 | |
| 3 | CP Ti HDH Grade 2 (Phelly) | 6 | 10 x 12 | 10 x 12.2 | 10 x 12 | Tungsten-Rhenium | 8 | 1000 | x | x | x | x | x | 7.3.4 | |
| | Ti-6Al-4V (Puris) | 6 | 10 x 12 | 8.75 x 11.5 | 10 x 12 | RR1000 Ionbond 25 | 8 | - | x | x | x | x | x | 7.3.5 | |
| 4 | CP Ti HDH Grade 2 (Phelly) | 10 | 15 x 15 | 14 x 14 | 14 x 14 | RR1000 Ionbond 25 | 8 | - | x | x | x | x | x | 7.3.6 | |
| | Ti-6Al-4V (Puris) | 10 | 15 x 15 | 14 x 14 | 14 x 14 | RR1000 Ionbond 25 | 8 | - | x | x | x | x | x | 7.3.6 | |
| 5 | CP Ti HDH Grade 2 (Phelly) | 10 | 15 x 15 | 14 x 14 | 14 x 14 | Inconel 718 Ionbond 25 | 6 | 800 | x | x | x | x | 8.1.2 | 7.3.7 | |
| | Ti-6Al-4V (Puris) | 10 | 15 x 15 | 14 x 14 | 14 x 14 | Inconel 718 Ionbond 25 | 6 | 800 | x | x | x | x | 8.1.2 | 7.3.7 | |
| 6 | CP Ti HDH Grade 2 (Phelly) | 6 | 10 x 12 | 8.75 x 11.5 | 10 x 12 | RR1000 Ionbond 25 | 6 | 6000 | 8.4.1 | x | 8.6.1 | 8.2.2 | 8.1.3 | 7.3.8 | |
| | Ti-6Al-4V (Puris) | 6 | 10 x 12 | 8.75 x 11.5 | 10 x 12 | RR1000 Ionbond 25 | 6 | 6000 | 8.4.1 | x | 8.6.1 | 8.2.2 | 8.1.3 | 7.3.8 | |
| 7 | CP Ti HDH Grade 1 (Phelly) | 10 | 15 x 15 | 14 x 14 | 14 x 14 | Inconel 718 Ionbond 25 | 6 | 1500 | x | x | x | x | x | 7.3.9 | |
| | Ti-3Al-2.5V HDH | 10 | 15 x 15 | 14 x 14 | 14 x 14 | Inconel 718 Ionbond 25 | 6 | 1500 | x | x | x | x | x | 7.3.9 | |
| 8 | CP Ti HDH Grade 1 (Phelly) | 8 | 15 x 15 | 14 x 14 | 14 x 14 | Inconel 718 Ionbond 25 | 6 | 2000 | 8.4.2 | 8.5 | 8.6.2 | 8.2.3 | 8.1.4 | 7.3.10 | |
| | Ti-6Al-4V Swarf (Airbus) | 8 | 15 x 15 | 14 x 14 | 14 x 14 | Inconel 718 Ionbond 25 | 6 | 2000 | 8.4.2 | 8.5 | 8.6.2 | 8.2.3 | 8.1.4 | 7.3.10 | |

7.2 Calculations

In order to calculate the abutment stress, the wheel speed must be converted into radians from RPM.

The wheel speed, along with the motor voltage, the motor efficiency and the motor current, can be used to determine the wheel torque. Torque is a result of the friction generated due to the interaction between the wheel and the material, which has built up on the abutment.

Finally, as the torque is a result of the increased current, due to the increased friction, the abutment stress can be calculated.

$$\text{wheel torque} = \frac{\text{motor voltage} * \text{motor efficiency} * \text{motor current}}{\text{wheel speed}}$$

The values for the wheel speed and motor current vary across the length of a trial and are given in units amps and radians, respectively. The motor voltage = 415.0 V and the motor efficiency = 0.8.

$$\text{abutment stress} = \frac{\text{wheel torque}}{\text{wheel radius} * \text{abutment area}}$$

The grip length is a function of the abutment stress, as the grip length is directly related to the stress on the abutment, as the material builds up on top of the abutment. The material is exposed to the same conditions as the abutment.

The grip length can be calculated using a power law. In this instance, $a = 5.8078$ and $n = 1.1692$. The reason that the grip length can be determined in this way, is because the grip length is directly proportional to the abutment stress.

In this chapter all trial data has been analysed, including trials that did not result in a product. Whilst it may not provide new information about the extrusion parameters, it sheds some light on trial and abutment failure.

In the graphs produced for each of the trials, there is often a wide scatter in the abutment stress. As the abutment stress is calculated using the wheel current and the motor torque, the scatter relates back to these. The reason for the scatter is that the data records the fluctuations in the torque and current, resulting in a wide scatter of peaks. For this reason, the average abutment stress was determined, so that the trends would be more visible across the recorded data.

7.3 Trials

7.3.1 Trial 1

Trial 1 took commercially pure titanium HDH grade 2 and utilised tools designed for larger feedstocks. The flash gap, which is the gap between the wheel and the tools in the shoe, was at an average of 0.73 mm across the die chamber. There was no material extruded during this trial, owing to an inconsistent powder flow and powder fire below the wheel, caused by the high temperature of the flash being produced, which can ignite powder underneath the machine. In addition to this, a machine electrical fault meant that the clamp for the machine was not working and so the tooling was able to move, which ultimately reduced the extrusion pressure by increasing the flash gap. It also meant that material could fall away from the abutment much more easily.

Although the trial did not lead to extrusion, the data is supplied in Figure 59, to give an example of the information obtained in these trials. Note that the coefficient of variation is determined, which is a measure of variability and determines how much the standard deviation lies from the mean. It means that comparisons can be made more easily between data sets, where the values may differ - owing to the fact it is a unitless figure. The coefficient of variation is particularly useful within the trial data because the data points often fluctuate, leading to a wider range of values, making it hard to differentiate the points.

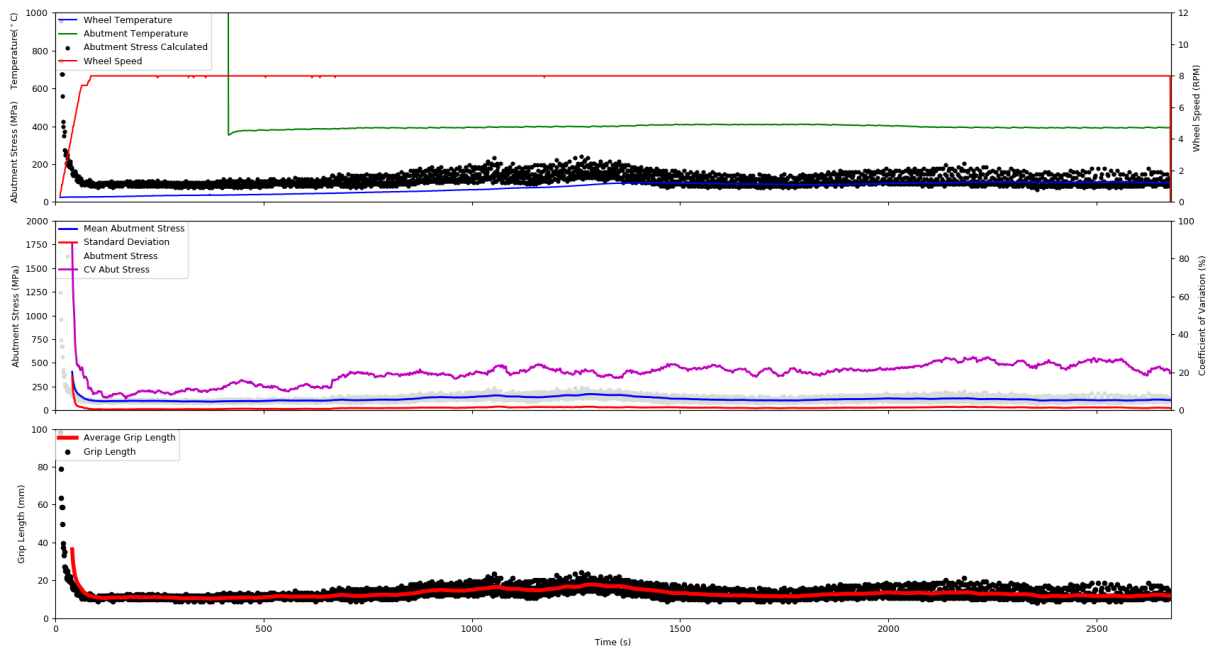


Figure 59 Data obtained in trial 1 with CP-Ti Gr 2 HDH feedstock including the calculated abutment stress; b) The average and standard deviation of the abutment stress with the coefficient of variation; c) Change in the grip length over the course of the trial

7.3.2 Trial 2

This trial followed directly from trial 1 and therefore, the electrical fault with the clamp was still present, however, this was managed and so the pressure would hold throughout the trials. Both trial 2 and trial 3 resulted in the production of roughly 50 cm of titanium wire (shown in Chapter 8) and gave further information about the parameters required for extrusion. Unlike the previous trial, more information can be yielded from the data. The data from trial 2 is shown in Figure 2.

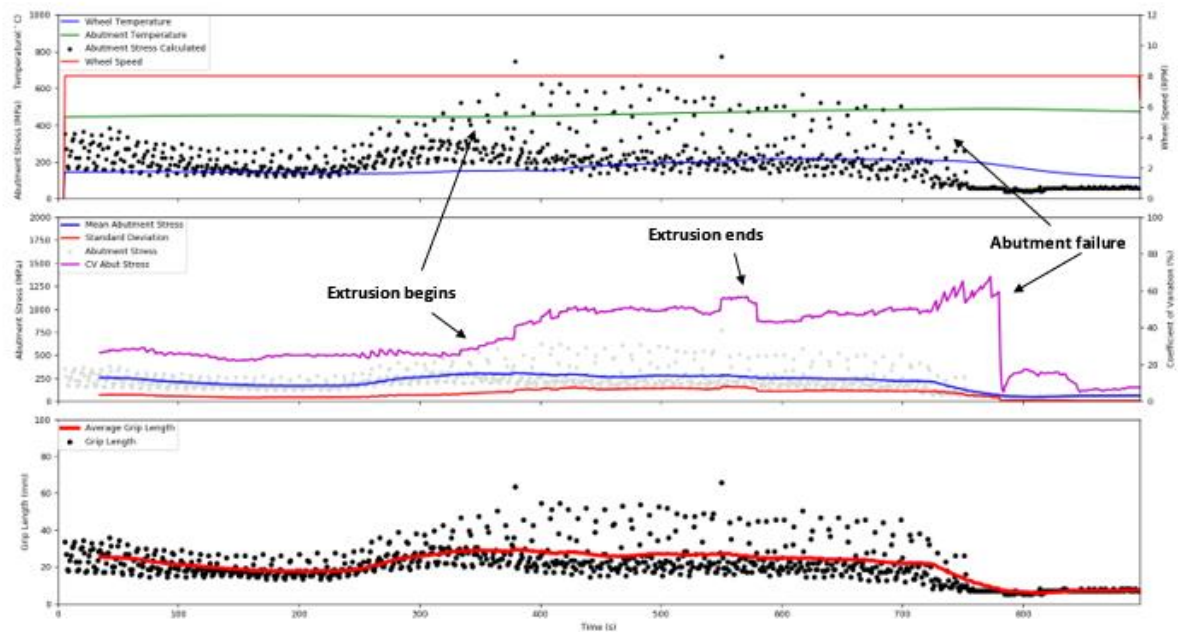


Figure 60 a) Data obtained in trial 2 with CP-Ti Gr 2 HDH feedstock including the calculated abutment stress; b) The average and standard deviation of the abutment stress and the coefficient of variation; c) Change in the grip length over the course of the trial

Starting with Figure 60a, it is possible to determine the start and end points of extrusion, based on the increase in the wheel temperature and the fluctuation in the abutment stress. Firstly, the steeper rise in the wheel temperature is an indication that the wheel is making more contact with the material on the abutment than previously. This heat is generated due to the friction between the coated wheel groove (coated from the feedstock that has adhered to its surface) and the material on top of the abutment. This friction is, in part, responsible for the increase in the extrusion pressure and consequently, this means that the feedstock in the port of the die chamber will be forced through the die.

The rise in the wheel temperature is not particularly steep, but this is still important when it comes to determining the point of extrusion.

Figure 60b shows (i) the abutment stress throughout the course of the trial, in addition to the (ii) average abutment stress at any given time, (iii) the standard deviation of the abutment stress at any given time and (iv) the coefficient of variation, which shows the variation around the average. The coefficient of variation highlights the increase in the abutment stress at around 420 s. This is indicative of the contact between the wheel and the material on the abutment,

and when this is the case, extrusion is typically occurring. The reason extrusion occurs at this point is because the increased pressure from the contact between the wheel and the feedstock leads to an increase in the temperature and the pressure, which forces the consolidated material through the die, extruding a wire product (see *Chapter 2, Chapter 3 and Chapter 5* for further information). The increase in the abutment stress can also be seen in the average of the stress. It is important to note that the fluctuations in the abutment stress are constant throughout the trial and are related to the machine itself and because of this, the standard deviation, whilst showing increases as the stress gets higher, does not help to explain the outcome of the results.

The final graph, Figure 60c shows the grip length calculations performed on the data. The grip length is the height at which the powder on the abutment has reached, whilst still remaining adhered to the die chamber. A large grip length is required for material to be extruded, as this is material which is consolidated and will be extruded through the die chamber in the process. As shown in the graph, there is an increase in the grip length prior to the extrusion, which highlights that friction between the wheel and the powder is leading to consolidated material above the abutment. During the extrusion, this continues, whilst the material is extruded out.

Not only does the information gained from Figure 60 show the start of the extrusion, but also the end of extrusion and, therefore, the failure of the trial. Extrusion ends when no more material is being forced through the die, often led by a reduction in the pressure within the process. Following this reduction in the pressure, the temperature of the wheel also reduces, as it is no longer making contact with the shoe. From the data, it is possible to denote the point of the extrusion end because there is a sharp decrease in the abutment stress but also a decrease in the grip length. This is because there is less friction being generated, which is further demonstrated by a reduction in the wheel temperature, although here, this appears to not be as clear as expected.

The trials end when it is no longer possible to extrude any more material and is dependent on a number of factors. The ultimate cause is the loss of extrusion pressure, without which the wire will no longer be extruded through the die and will, instead, remain in the port of the die chamber indefinitely. The key parameters maintaining this pressure are the grip length, the friction between the wheel and the shoe, and the temperature of the shoe. Each of these parameters can be governed further, as each relates to the interaction between the particulate

feedstock and the tooling. Firstly, the feedstock must be fed in continuously, although this can fluctuate in feed rate. The particulate feedstock builds up at the abutment and then friction between that material and the coated wheel is, in part, responsible for the build-up of the extrusion pressure. Secondly, machine faults can lead to trial failure, such as that in trial 1, where, in this case, the electrical clamp failure meant that there was no interaction between the wheel and the shoe. Finally, and most importantly, damage to the tooling within the shoe can lead to the failure of a trial. Typically, this failure is related to the abutment. As the abutment is made from a high temperature resistant material, which has a wear resistant coating, it should be able to withstand the conditions within the process. However, damage to the coating or even too high pressure, can lead to premature failure of the abutment, which in the case of more ductile materials is demonstrated in Figure 61.



Figure 61 Photograph showing an example of abutment wear during a Conform™ trial.

It is evident by the distinct reduction in the abutment stress around 780 s, that abutment failure has occurred. This is coupled with a significant drop in the grip length and a reduction in the wheel temperature, which is no longer in contact with the hot shoe.

7.3.3 Trial 3

Trial 3 produced similar results to trial 2, with the extrusion of ~ 1 m of titanium rod (seen in Chapter 8). The graphs shown in Figure 62 demonstrate similar trends to the data provided in

Figure 60. The initial rise in the abutment stress is coupled with the distinct increase in the wheel temperature, that often results in the extrusion of the material. In the case of trial 3, this initial extrusion was responded to by an increase in the wheel speed, however, this led to a reduction in the overall temperatures around the abutment and the wheel. The extrusion then started a second time around 3400s, where the increase in the wheel temperature was accompanied by a rise in the abutment stress and resulted in an increase in the abutment temperature. The abutment temperature increase was maintained for the rest of the trial, however, the ability for the material to cool during the process is hindered by the friction occurring by the wheel on the titanium powder and the abutment nose.

Shortly after the second burst of extrudate, the powder feedstock was changed to Ti-6Al-4V HDH Gr 5, which resulted in a drop in the abutment pressure and the wheel temperature, possibly due to the non-preheated powder on the wheel. Despite the increase in the abutment stress at ~5000s, the wheel temperature did not increase, and the increase soon levelled off. It is at this point, that abutment failure was confirmed. The abutment failure was evident from the inability for the wheel temperature to increase during the abutment stress peak. The contact between the wheel and the material on the abutment nose should result in friction and ultimately an increase in the wheel temperature – with the abutment temperature being significantly higher than the temperature at the wheel. In order to assess whether the issue related to the abutment failure, the wheel speed was increased, however, this did not result in an increase in the wheel temperature and the abutment stress started to drop off. It is quite evident that the wheel temperature can be used as an indicator for both extrusion and trial failure, with higher temperatures suggesting contact between the wheel and the abutment and lower temperatures suggesting a lack of contact between the two. This could be easily applied in later trials, where an increase in the wheel speed is often used to establish the increased friction and hopefully, extrusion.

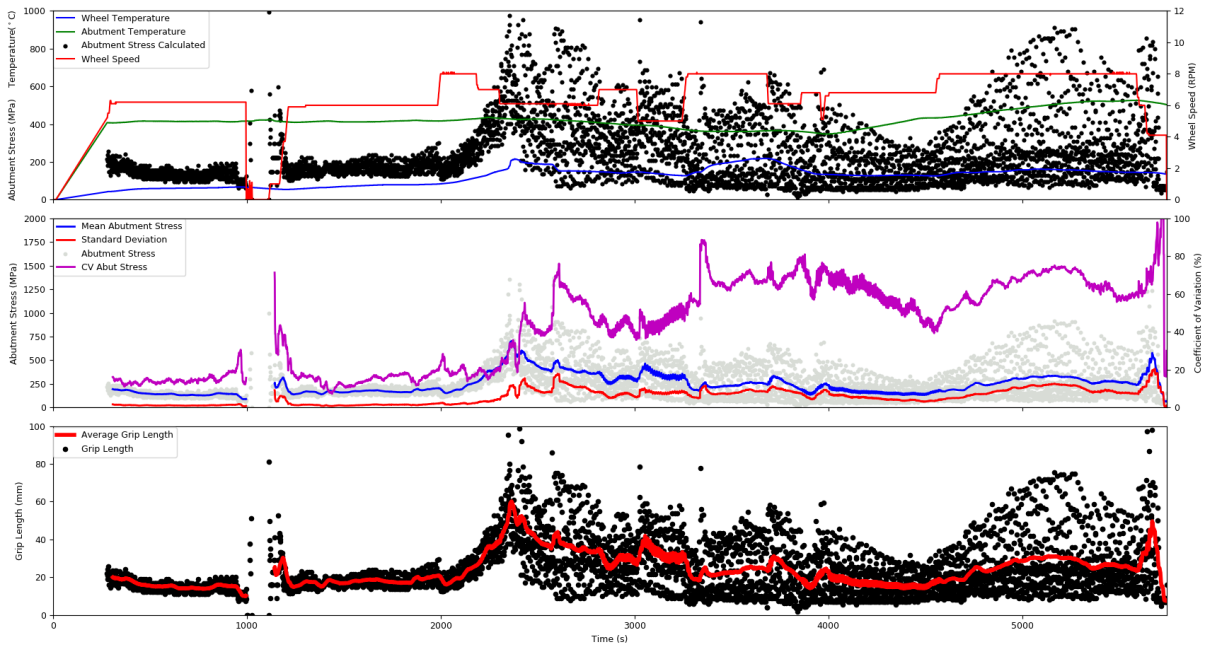


Figure 62 a) Data obtained in trial 3 with CP-Ti Gr 2 HDH feedstock including the calculated abutment stress; b) The average and standard deviation of the abutment stress and the coefficient of variation; c) Change in the grip length over the course of the trial

7.3.4 Trial 4

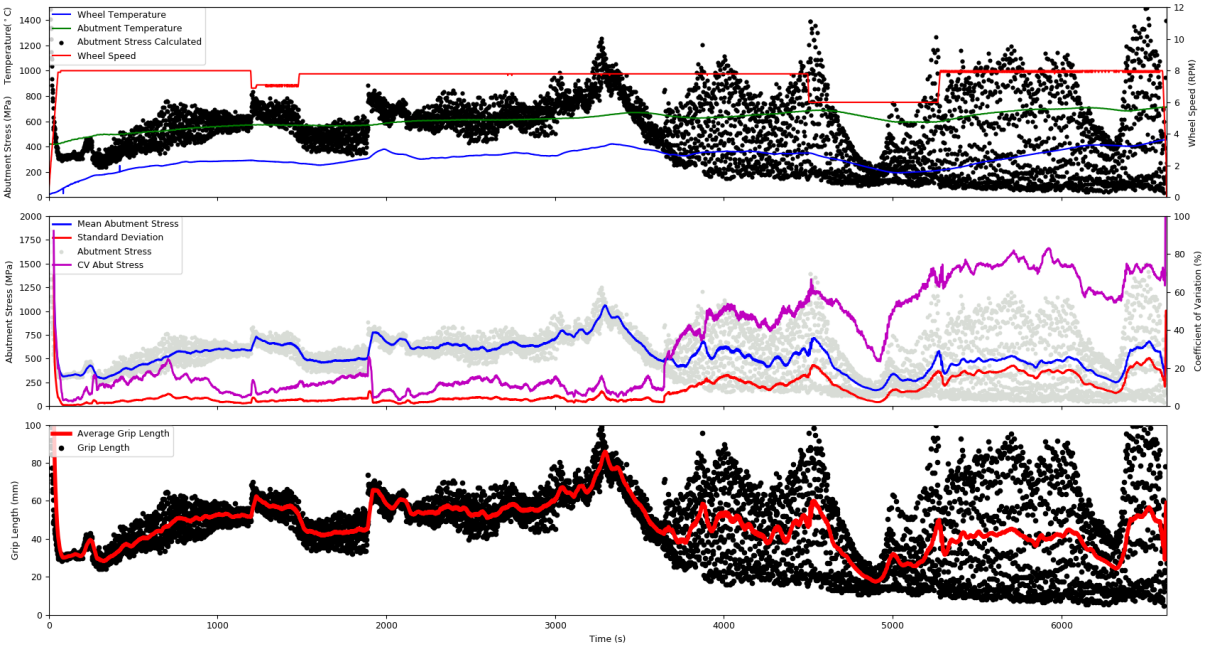


Figure 63 a) Data obtained in trial 4 with CP-Ti Gr 2 HDH feedstock including the calculated abutment stress; b) The average and standard deviation of the abutment stress and the coefficient of variation; c) Change in the grip length over the course of the trial

Trial 4 used a much stronger abutment material (see Figure 63) than in the earlier trials, which meant that the abutment should last in the process for a longer amount of time. At ~3800 s, some extrusion of CP-Ti Gr2 HDH, however, this remained within the die and therefore, further microstructural and mechanical property analysis was not possible.

From the data produced in this trial, it is not as straightforward to understand as previous trials. There were further complications which significantly impact the trial including the stresses and temperatures.

Despite the high strength abutment and changing feedstock, the trial ended prematurely. The clamp pressure was lost relatively early on, as with the previous trials, which meant that the even though some extrusion occurred, it did not continue for long. The lack of pressure resulted in the movement of the shoe, leading to an increased flash gap and therefore a significant loss of powder feedstock. Further to this, the gap between the die chamber and the groove widened, and, therefore, powder could be consolidated onto the wheel, rather than in the port of the die chamber. A tyre of titanium formed around the wheel, potentially pushing the shoe further away from the wheel.

Although the trial ended prematurely, the abutment had very little damage by the end of the trial. The data in Figure 63 shows that the abutment stress was still relatively close to that of the successful trials, and even though the material was not forced through the die, there was evidently still some pressure on the abutment. The material used for the abutment was a lot stronger and more wear resistant than the Inconel 718 used in the previous trials, but this comes at a significant cost.

7.3.5 Trial 5

Despite some success in trials 2 - 4, trial 5 and 6 were less successful. The data shown for trial 5 (in Figure 64b) clearly shows that the abutment stress is relatively low throughout the process. The wheel thermocouple was not correctly installed during the trial; therefore, the data has been removed from Figure 64a. This also meant it was difficult to determine if wheel cooling or wheel speed reductions were required.

Secondly, there was some contact between the tools within the shoe and the wheel. This related to the manufacturing of the tooling, where the dimensions of the die chamber did not allow the abutment to sit correctly, resulting in damage to the die chamber and the abutment, which meant that the trial had to be aborted.

Overall, there was no extrusion due to tooling damage prior to the addition of the feedstock to the trial. The damage was directly related to a poor tool fit and therefore, it was possible to rectify for future trials (Trial 7 - 10).

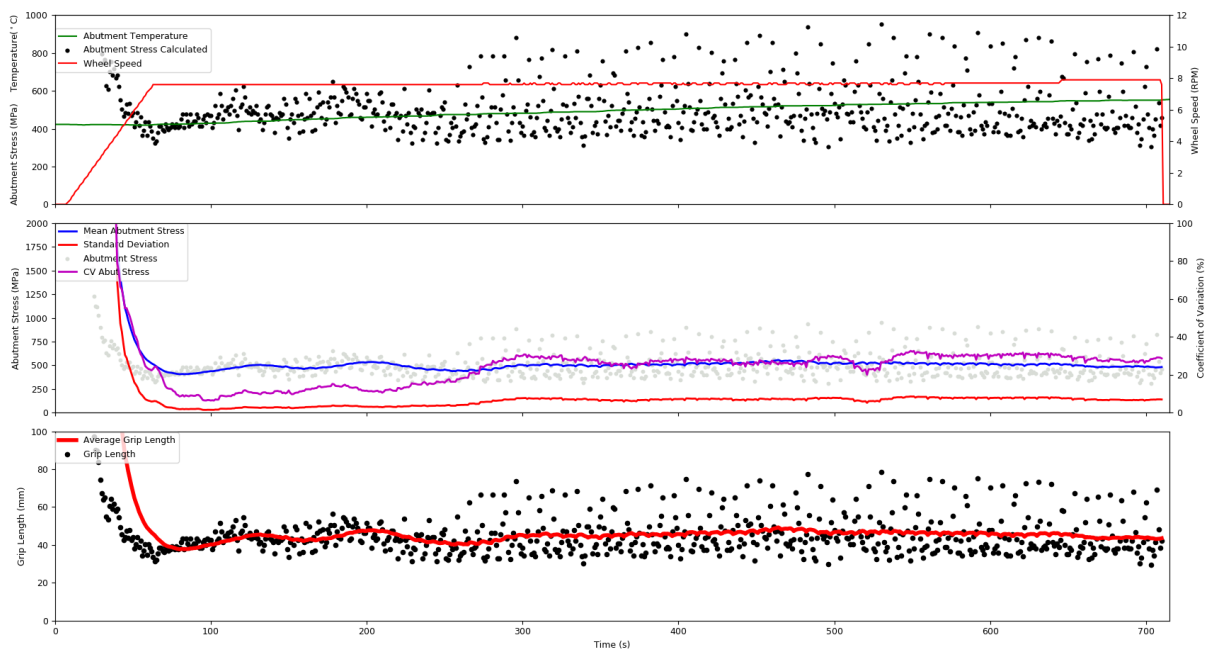


Figure 64 a) Data obtained in trial 5 with CP-Ti Gr 2 HDH feedstock including the calculated abutment stress; b) The average and standard deviation of the abutment stress and the coefficient of variation; c) Change in the grip length over the course of the trial

7.3.6 Trial 6

Completed within the same time frame as trial 5, trial 6 also resulted in tool failure prior to adding the feedstock for the trial. Although attempts to rectify the issues with the tool fit, it would involve machining too much material from the abutment, which would result in additional damage. Unfortunately, there is no data available for this trial.

7.3.7 Trial 7

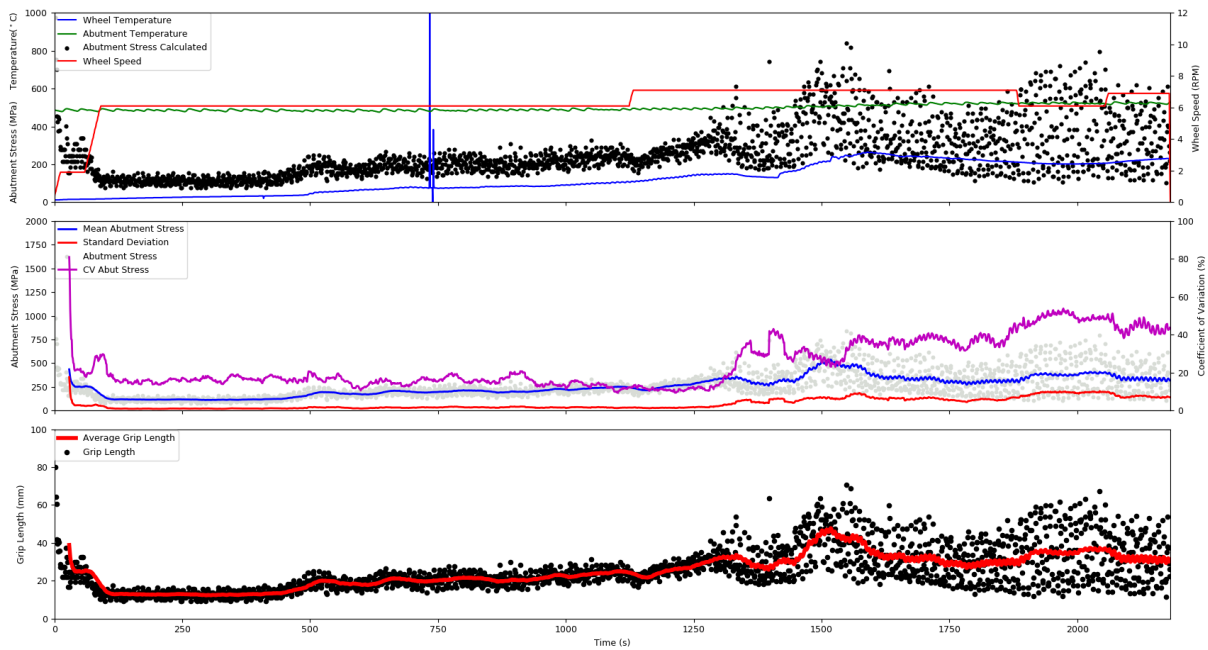


Figure 65 a) Data obtained in trial 7 with CP-Ti Gr 2 HDH and Ti-6Al-4V GA feedstock including the calculated abutment stress; b) The average and standard deviation of the abutment stress and the coefficient of variation; c) Change in the grip length over the course of the trial

The data in trial 7, shown in Figure 65, has a longer period of low abutment stress. Early in the trial, there was some evidence of the tooling within the shoe catching on the wheel, however this stopped relatively soon into the trial ~200 s. The abutment stress then starts to rise, as the CP-Ti Gr2 HDH is added to the machine, and the wheel temperature slowly creeps to around 200°C. This increase is expected as the friction between the wheel and the powder atop the abutment will lead to some heat being generated, alongside the extrusion pressure increase. Extrusion begins to occur around ~1400 s, where the wheel temperature begins to reach 200°C and the abutment stress starts to spike.

The wheel temperature continues to increase; however, this is not entirely due to the friction between wheel and powder, but rather related to the ignition of powder underneath the wheel. This temperature increase was steadied out by utilising the wheel cooling available. At ~1600 s the feedstock was changed to synthetic rutile, and extrusion continued. This was quickly replaced, with Ti-6Al-4V GA, as there was not enough synthetic rutile available to continue. Around ~2000 s, there is another spike in the abutment stress, but it is not accompanied by any temperature increase. The stress starts to drop, and it is assumed that the abutment has been destroyed.

Inspection of the abutment after the trial indicated that there was some wear to the sides, which may have occurred at the start of the trial, as there was clearly interaction between the wheel and the tooling in the shoe. This may have reduced the abutment lifespan. Damage to the tooling and multiple powder feedstock changes have meant that the optimum extrusion parameters were not met, and consequently only 50 cm of material was extruded.

7.3.8 Trial 8

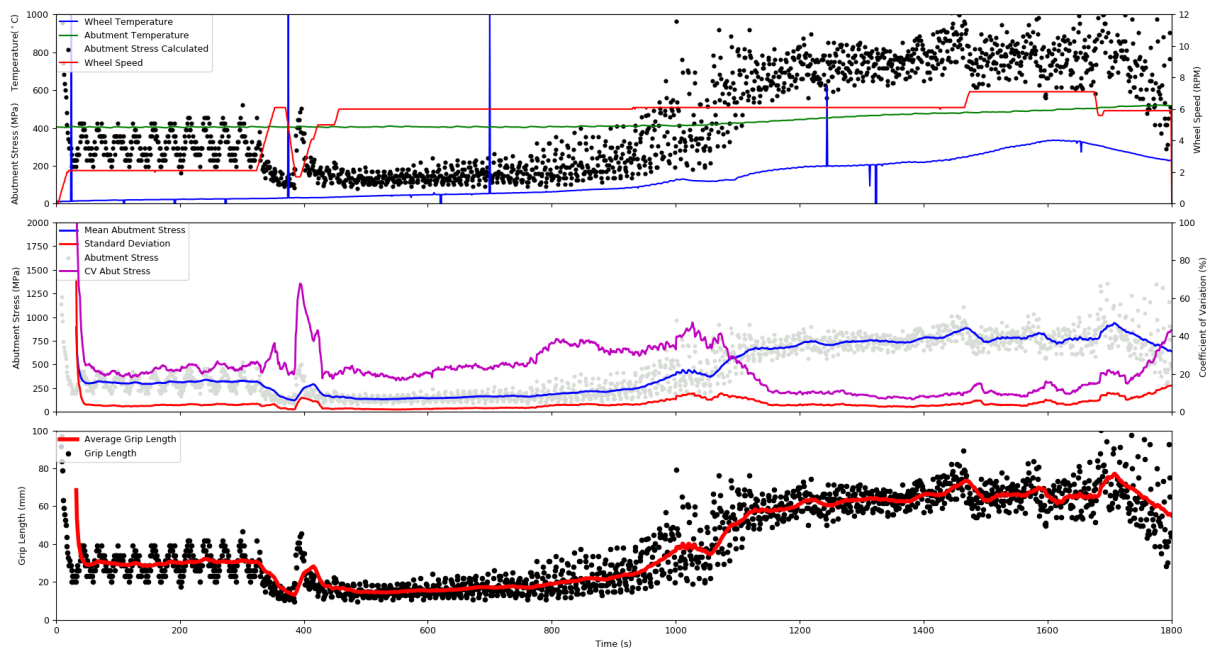


Figure 66 a) Data obtained in trial 8 with CP-Ti Gr 2 HDH and Ti-6Al-4V GA feedstocks including the calculated abutment stress; b) The average and standard deviation of the abutment stress and the coefficient of variation; c) Change in the grip length over the course of the trial

The data from this trial differs from that of the other trials, in that the start of the trial has a false start. The slow wheel speed highlighted some interaction between the wheel and the die chamber, however, after increasing the speed and then reducing back to 2 RPM to check, it appeared that the damage was minor and so the trial was able to continue. There are some fluctuations in the wheel temperature, which are the result of a loose thermocouple and occurs randomly throughout the trial. For this reason, the fluctuations in the wheel temperature can be ignored for the purpose of trial data analysis. Unfortunately, this means it will not be possible to predict the point of extrusion based on the wheel speed.

Around 1070 s, there is a peak in the abutment stress, which is more evident in the coefficient of variation as the standard deviation is very small (see Figure 66). This peak may be due to the reduction in the wheel speed and coming into contact with the die chamber. This was not detrimental to the trial, and much like the false start, has little importance here.

The key information yielded from this data is a definite start and end of extrusion. From the data it is clear to see the start at around 1300 s, which is the point at which there is an increase in the wheel temperature that is steeper than previously. Additionally, there is an increase in the grip length and the abutment stress.

In trial 8, the extrusion occurred continuously, however, the wheel speed is increased at ~1470 s. Prior to this point, the extrusion of material had reduced significantly, and in order to maintain the pressure, the wheel speed was increased. The reduction in material extrusion would typically relate to a loss in extrusion pressure, which may occur due to loss of abutment, reduction in temperature or lack of feedstock. The increased wheel speed should result in higher torque, followed by higher abutment stress and ultimately, a higher extrusion pressure. As the higher wheel speed did not result in an increase in the abutment stress, it was clear that abutment failure had occurred.

The material resulting from this trial has been further analysed in *Chapter 8*.

7.3.9 Trial 9

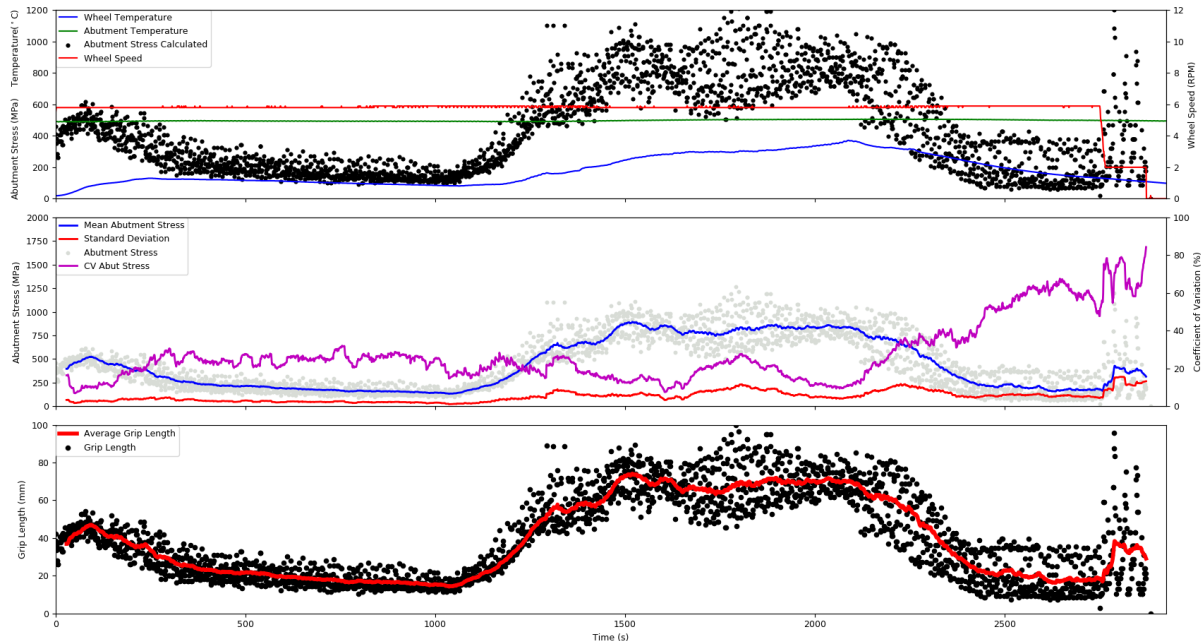


Figure 67 a) Data obtained in trial 9 with CP-Ti Gr 2 HDH and feedstock including the calculated abutment stress; b) The average and standard deviation of the abutment stress and the coefficient of variation; c) Change in the grip length over the course of the trial

It is clear in the trial 9 data in Figure 67 shows that extrusion would be expected around ~1100 s, with a distinct increase in the abutment stress and the wheel temperature. From the data previously discussed in this chapter, it is becoming clearer that extrusion is typically signified by (i) an increase in the abutment stress and (ii) an increase in the wheel temperature.

In a contrast to many of the other trials, there is a clear drop in the abutment stress, which is a key indicator of abutment failure. Likewise, the wheel temperature and abutment temperatures begin to drop, which would suggest less friction is occurring and therefore, there must be an increase in the flash gap.

7.3.10 Trial 10

The final trial, which differs from the others in that titanium swarf was processed for the first time. The extrusion of swarf has been discussed further in *Chapter 8*. The tools used were designed specifically for swarf, and despite being used in non-swarf trials, this was their main design aim. Unlike the other trials, this trial did not start with an initial 2 RPM run to determine if there were any issues related to the set-up. The data for trial 10 is shown in Figure 68.

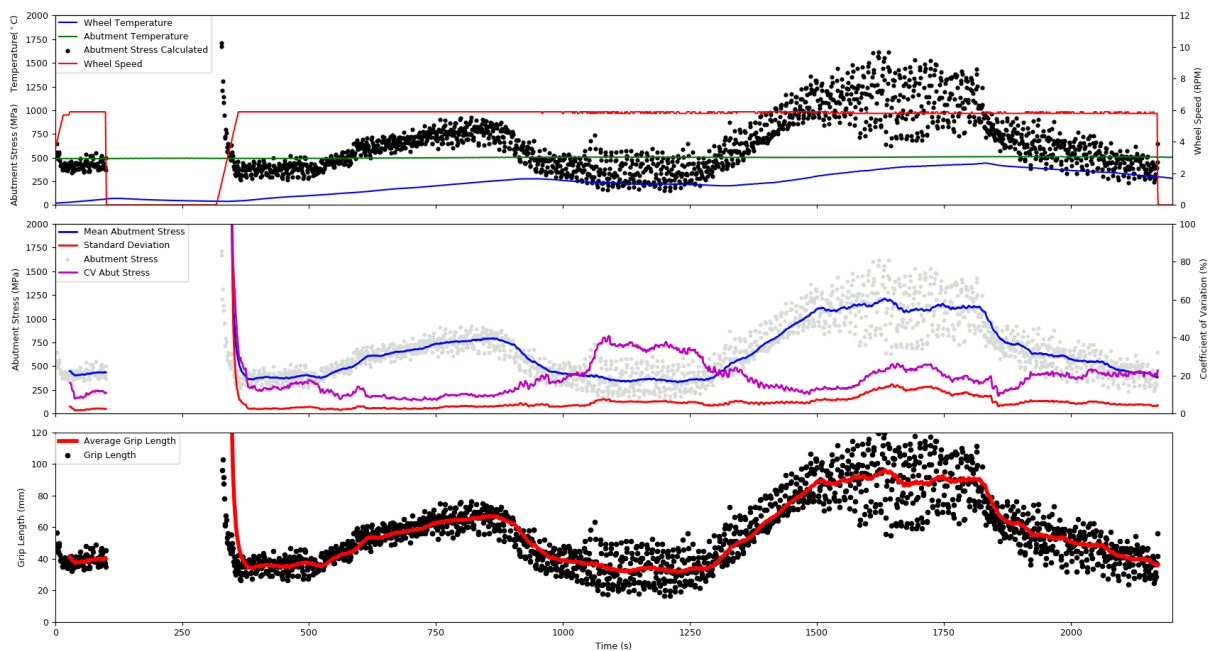


Figure 68 a) Data obtained in trial 10 with CP-Ti Gr 2 HDH and Ti-6Al-4V swarf feedstocks including the calculated abutment stress; b) The average and standard deviation of the abutment stress and the coefficient of variation; c) Change in the grip length over the course of the trial

During this trial, there are two distinct peaks in the data, the first starting around 200 s and ending at 320 s and the second at around 1000 s and ending at 1310 s. Extrusion occurred later in the trial than the first set of peaks would suggest, highlighting that the initial increase in the abutment stress and tooling temperature is related to the interaction between the wheel and the die chamber. In this case, the tools did come into contact with each other at the start, although the trial was continued. The interaction reduced, which would explain the consequent drop in the abutment stress and grip length. There is also the possibility of the generation of flash, which has led to a decrease in the material and stress on the abutment. It can be noted that the coefficient of variation is not relevant in this data set as the abutment stress is more consistent - thus has a lower standard deviation, so the coefficient of variation will be higher.

The extrusion during the trial can be demonstrated following an increase in the abutment stress, coupled by an increase in the wheel temperature, which had previously plateaued around 1000 s. The trial is relatively consistent throughout, with minimal drops in the abutment pressure. However, the definite end of the trial is particularly obvious. There is a sudden drop in the

abutment stress, as can be seen in Figure 68b. Naturally, this is coupled with a decrease in the wheel temperature and grip length.

7.4 Comparison

The results of each trial can be compared based on a number of factors:

- 1) Rod/Wire produced
- 2) Abutment stress
- 3) Grip length

The wire is discussed in later chapters, with the mechanical properties and micrographs for trials 8 and 10. The abutment stress is an important criterion during these trials, as if it is too high, it can result in the failure of the abutment. Monitoring the health of the process and measuring/managing the stress on the abutment will be important for scaling up the process.

The abutment stress can be affected by the pressure, temperature, and the geometry of the tooling. The pressure that is required to extrude material is generated in relation to the friction of the wheel on the powder above the abutment stress. As the feedstock is being severely plastically deformed perpendicular to the wheel, the abutment is under high stress at a high temperature. The material of the abutment is temperature dependent, as with any material, as the temperature increases, there is the possibility of softening the material. Fortunately, in the case of these trials, the abutment was made of Inconel 718, which can withstand high temperatures, although abutment temperature has exceeded 750 °C in some cases.

The tooling geometry can have a significant impact on the pressure within the system, with a smaller groove leading to higher pressures. This was investigated in the work of Ben Thomas [3] at the University of Sheffield, where calculations for the pressures in the system were determined.

Additionally, the grip length can be used to compare the trials, with the system requiring a grip length, which can aid the increase in the pressure but also lead to extrusion. This is a parameter which can also be determined based on the tooling geometries and powder morphology alone. The tools have a pressure relief, which helps to prevent premature tool failure, but also control the grip length.

In order to compare the various trials and the impact of changes between feedstocks, materials and wheel speeds, the graphs shown in Figure 69 and Figure 70 have been created. This breaks down the trial data into key parameters, wheel temperature, abutment temperature, abutment stress and grip length. For Figure 70, the maximum and minimum are individual figures from each trial, whereas the average was across all data points in a given trial. For Figure 69, the average values were determined by averaging the values from each trial and then taking the average of these values across the trials included in that data set. The maximum and minimum values were the average maximum and minimum for that parameter also.

It should be noted that the values corresponding to the swarf feedstocks and the tungsten-rhenium abutment material do not have error bars, as they were only used in one trial and therefore, the error between trials is unknown.

Although the data in Figure 69 allows for comparison between trials, the influence of parameters on the results of a trial are more evident in Figure 70. The W-Re, swarf feedstock and smaller toolset trials appeared to result in higher overall temperatures and stresses than their alternatives. The wheel speed appeared to have very little influence on the temperature or stress, however, as each trial changed a number of parameters simultaneously, it may be that another factor influenced a change in the temperature or stress, thus making it difficult to be entirely accurate. These graphs, however, do allow for some comparison and make it easier to understand what influence any given parameter may have on the result of a trial.



Figure 69 Graph showing the average, maximum and minimum temperatures and stresses for each individual trial. (Top left) Wheel Temperature, (Top Right) Abutment Temperature, (Bottom Left) Abutment Stress and (Bottom Right) Grip Length.

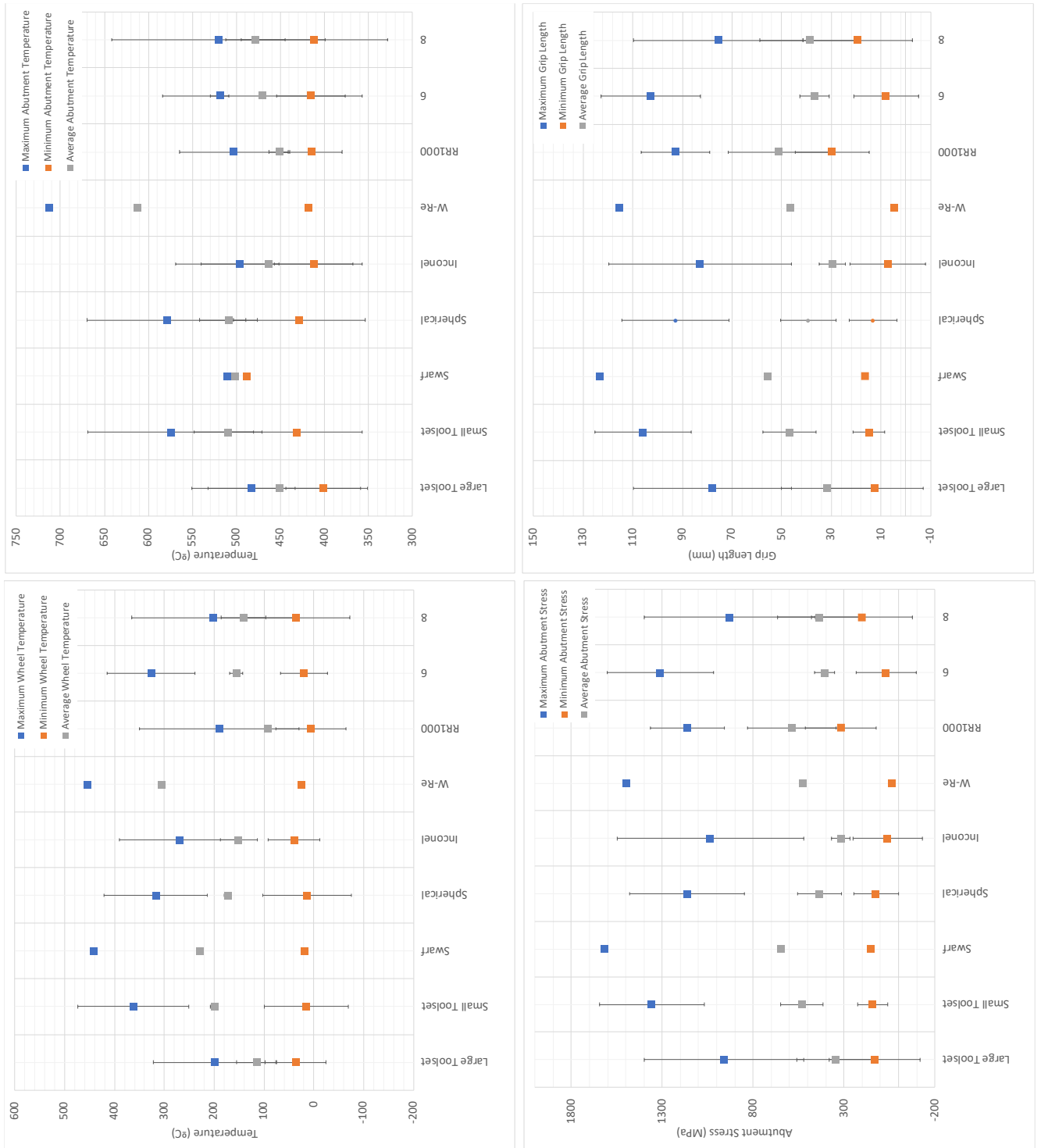


Figure 70 Graph showing the average, maximum and minimum temperatures and stresses for each set of trials containing the parameters listed on the x-axis. (Top left) Wheel Temperature, (Top Right) Abutment Temperature, (Bottom Left) Abutment Stress and (Bottom Right) Grip Length.

7.5 Optimum Parameters

The parameters required for a successful extrusion are almost wholly dictated by the feedstock used, as this has implications on the feed, the extrusion pressure required and the tooling geometries. However, there are considerations that can be made, coupled with some estimations, which can allow for a successful trial. Additionally, during the trial, it is possible to make decisions based on the raw data, in particular the wheel temperature, which upon reaching temperatures of 200 °C or above, extrusion should be occurring. If that temperature can be maintained, damage to the abutment can be reduced and consequently more material can be extruded. This, however, would benefit from further investigations, in order to confirm and to develop a more precise mechanism of determining what makes a trial last longer.

In addition to being able to predict the point at which extrusion will occur, it is also possible to determine the point of failure based on the data provided. The abutment stress is key to extrusion and when this does not increase, despite the application of higher wheel speeds, increase powder flow or decreased temperature (from wheel cooling), then it can be determined that the trial has concluded due to abutment failure. The wheel temperature has also been demonstrated here to be a key indicator of trial failure, with a loss in wheel temperature suggesting a lack of contact between the wheel and abutment nose. This would only occur if the wheel had moved, which was a possible case in the early trials owing to electrical failures which allowed the shoe to move backwards as pressure increased, or as a result of loss of the abutment nose, to a point where material would no longer sit on the nose, or that the nose would no longer make contact within the groove of the wheel. This can sometimes be complicated as the application of wheel coolant, which occurred in the later trials, can mimic the reduction in temperature from the abutment loss. However, if the abutment stress is not increasing, material is not being extruded and powder loss is higher, there is a high chance that the abutment has failed.

Chapter 8 : Microstructure and Mechanical Properties

8.1 Extruded Rod

8.1.1 Trial 2 and Trial 3

Trial 2 was the first successful trial completed during this project, although an electrical fault may have reduced the efficacy of the trial. The result was a short, ~ 10 cm, length of material (shown in Figure 71a) encompassing CP Ti HDH Gr 2 and, to a minor extent, Ti-6Al-4V HDH Gr 5. The diameter of the material was 10 mm.

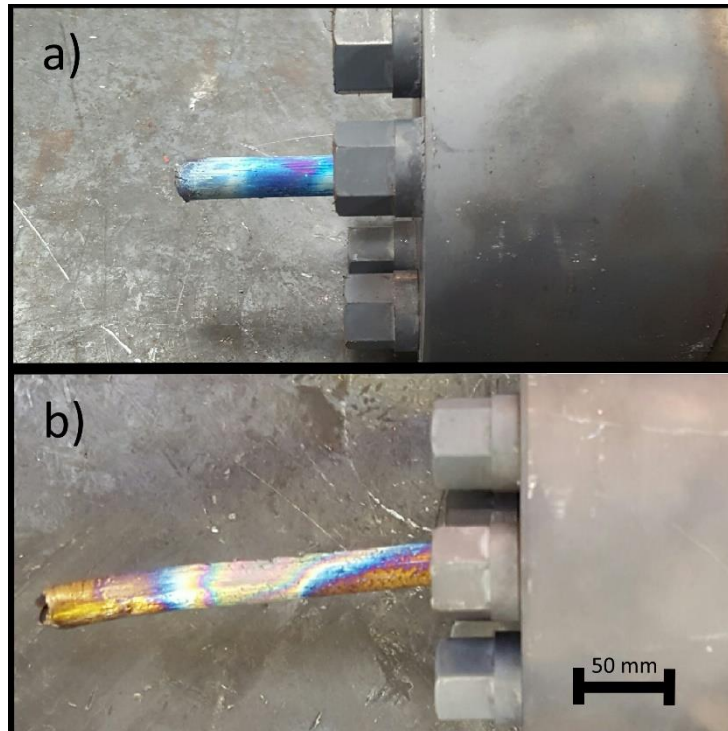


Figure 71 Photographs of CP Ti HDH Gr 2 rod extruded through the die during the Conform process (a) from trial 2; (b) from trial 3

In trial 3, the extrudate was ~20 cm in length with a 10 mm diameter (shown in Figure 71b). This meant that there was not sufficient material for multiple sample testing or mechanical property determination. The main reason for the lack of material relates directly to the electrical clamping fault, which led to the shoe being pushed away as the extrusion pressure built.

8.1.2 Trial 7

Trial 7 was significantly more successful than the preceding trials, with ~50 cm of extruded titanium rod (as shown in Figure 72). The feedstocks used during the trial were CP Ti HDH Gr 2, Ti-6Al-4V HDH Gr 5 and Synthetic Rutile (Metalysis).



Figure 72 Photograph of CP Ti HDH Gr 2 rod extruded through the die during the Conform process from trial

7

The improved length of material that was extruded, may relate to the change in the tooling used. Additionally, unlike the previous trials, there were no machine faults, which hindered previous results. Despite the length of material extruded, no analysis was conducted on the material. The cost of preparing tensile specimens for this material was too high, and owing to time, micrograph specimens were not produced.

8.1.3 Trial 8

During Trial 8, ~ 6m of titanium rod was extruded with a 6 mm diameter.



Figure 73 Photograph demonstrating the length of the wire extruded during Trial 8.

8.1.4 Trial 10

During the trial, ~ 2 m of CP Ti HDH and Ti-6Al-4V rod was extruded through an 8 mm die. The resulting rod did not achieve a uniform die filling and therefore, the diameter of the rod varies between 6 – 8 mm.



Figure 74 CP Ti HDH Gr 2 and Ti-6Al-4V swarf derived wire produced during Trial 10.

8.2 Microstructural Analysis

In all cases, the as-extruded material shows a distinctive macrostructure in its cross-section. This macrostructure is shown in Figure 75. A further cross-section is shown in Figure 76 and demonstrates two distinct areas of flow structure.

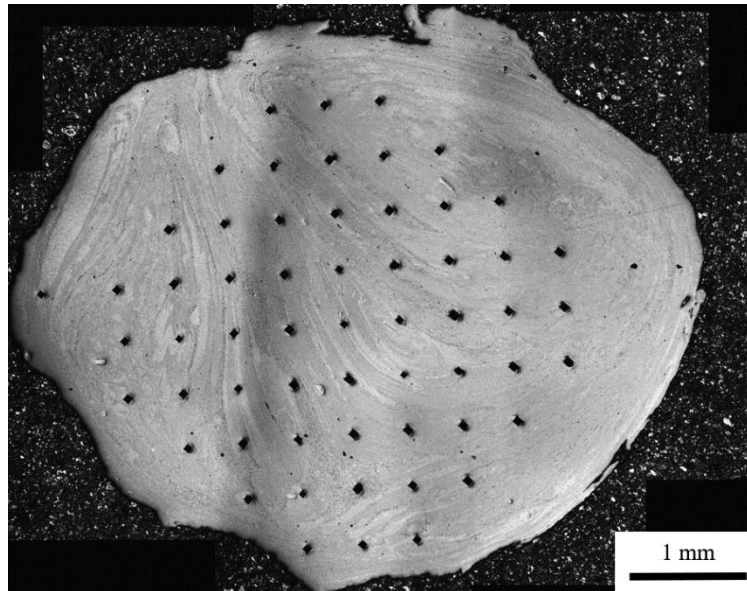


Figure 75 Polarised light micrograph of as-extruded wire from CP-Ti Gr2 HDH powder in the swarf tooling. The indents are result of microhardness testing.

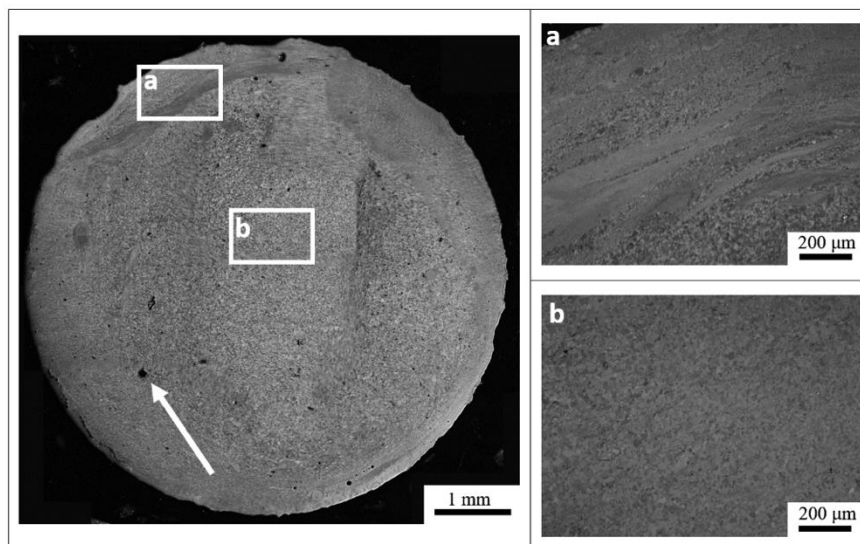


Figure 76 Polarised light micrograph of as-extruded wire from Ti-6Al-4V GA powder. (a) Shows the distinct layered structure around the outside of the wire. (b) A more uniform microstructure in the inner core of the wire). The arrow denotes an example of the porosity.

It has been demonstrated in other work that the material can exhibit flow behaviour like that seen in the flow of liquid in a pipe [2], [126]. This is as a result of material moving faster through the centre of the die. This has mostly been shown in aluminium but there is further evidence demonstrated in work by Etherington in 1978 [75], where a transverse-section of the rod produced from the extrusion of OFHC (oxygen-free high conductivity copper) demonstrated similar flow lines. This suggests that material is not necessarily extruded in the same order it entered the process. A transverse section of the titanium produced in this work shows a similar flow system, with clear banding across the sample, as shown in Figure 77.

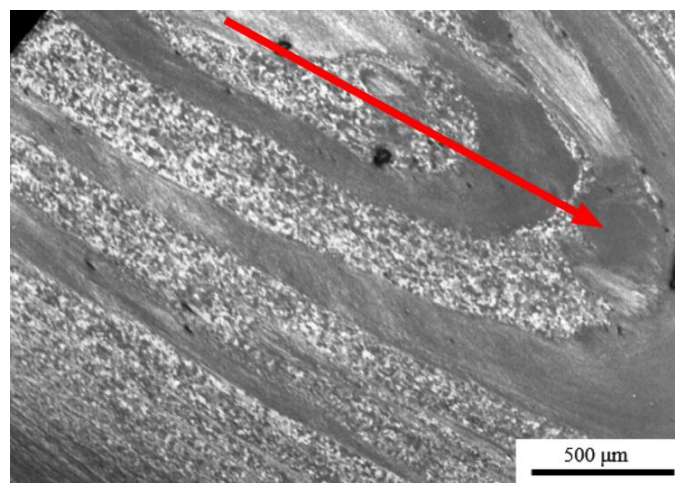


Figure 77 Cross polarised light micrograph of a transverse section of as-extruded Ti-6Al-4V GA wire. The flow direction, as indicated by the arrow is evident based on the flow lines across the material.

8.2.1 Trial 2

Owing to the length of the material, a single sample was taken of the material, upon which light microscopy was conducted. The short length of extrudate was not viable for mechanical testing as it would leave no samples for future study. As shown in

Figure 78, there is a clear equiaxed grain structure in the cross-section. This is an indicator of a consistent single-phase material, which would be expected for CP Ti HDH. In the transverse direction, there is a clear direction of material flow, with striations across the sample indicating the flow, and there is still a relatively equiaxed structure shown. Unfortunately, for this sample, it is not possible to investigate the change in microstructure across the length of the trial.

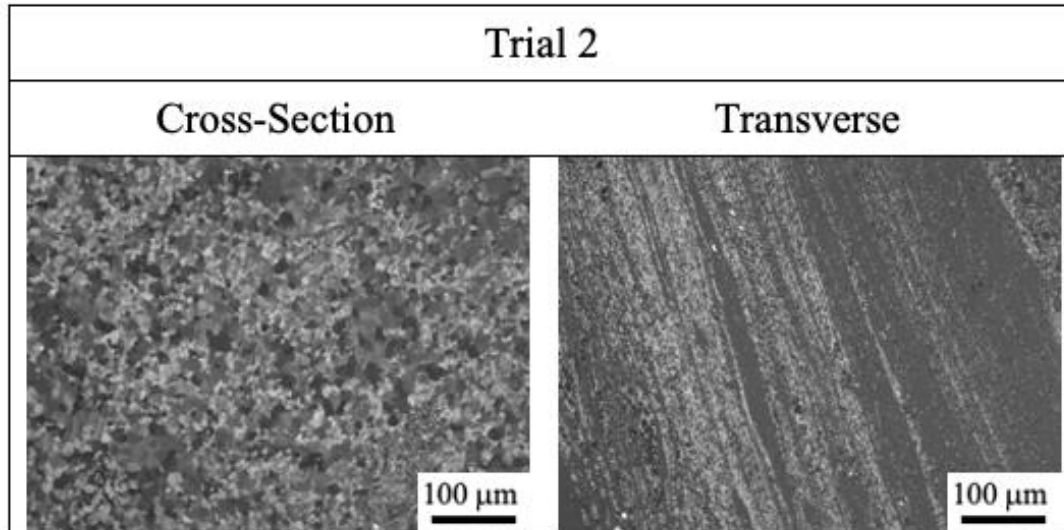


Figure 78 Light micrographs showing the cross-section and transverse sections of the rod produced in Trial 2.

8.2.2 Trial 8

In the case of the micrographs (shown in Figure 79), images were taken at various locations along the extruded rod. The initial microstructure of the rod was moderately fine-grained; however, this was an average of the grain size shown in the micrographs. There were mixed grain sizes across the sample, varying from very-fine grains at 2-5 μm to much larger grains at 30 – 50 μm . This is seen most clearly in the transverse sample, where the larger grains surround the smaller grains in the direction of the material flow. During Conform, it is common to see a macrostructure flow pattern, where there are two defined rings structures; an outer flow structure, where grain growth has occurred, whilst the material has been held during the process; and an inner flow structure, where the newest feedstock into the process has been forced through the die, which results in a smaller grain size.

In the early extrusion, there is evidence of prior particle grain boundaries in the microstructure. This is a result of inconsistent particle consolidation, which was caused by the reduced temperature and pressure after the initial extrusion. This same reduction in the pressure also accounts for the small amount of porosity found in the microstructure of the rod.

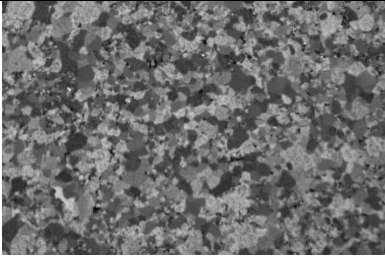
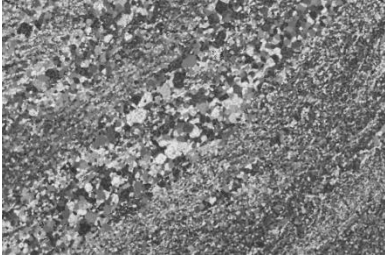
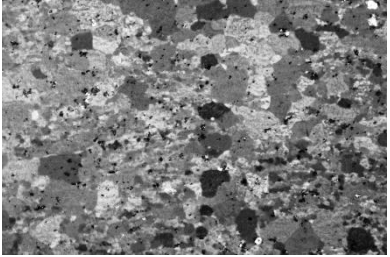
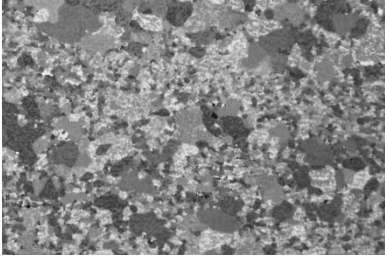
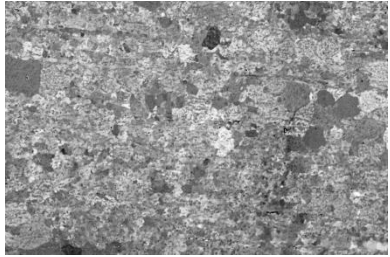
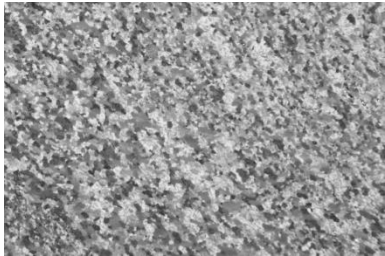
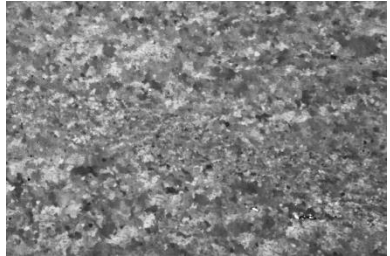
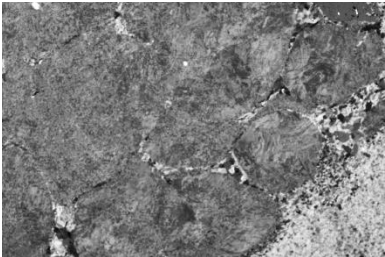
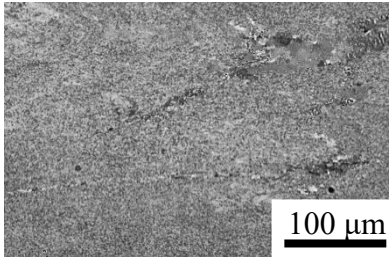
| | Trial 8 | |
|--------|---|--|
| Sample | Cross-Section | Transverse |
| 2 |  |  |
| 4 |  |  |
| 8 |  |  |
| 11 |  |  |
| 15 |  |  |

Figure 79 Light micrographs taken along the length of the CP Ti HDH Gr 2 and Ti-6Al-4V GA rod extruded during Trial 8.

As the process continues, there is a slight increase in the grain size. This may be a result of staggered extrusion pressure, such that as the pressure is lost from the early extrusion, this must be kept at a constant rate to guarantee further extrusion. Because of this, material in the die and

on top of the abutment will have been sat in the process for a significant time, resulting in grain growth from the high temperature at the shoe.

Near to the end of the extruded material, there is a further drop in the grain size, which is a key factor in severe plastic deformation methods. This grain size drop may be emphasised further by the initial fine microstructure of the Ti-6Al-4V GA particles. In addition to this drop in overall grain size, the cross-section of Sample 15 shows evidence of particle inclusion, with distinct spherical particles in the microstructure. There is some evidence of the particles becoming consolidated together, however, there is a very definite distinction between the Ti-6Al-4V particles and the CP Ti HDH microstructure around the particles.

8.2.3 Trial 10

The microstructural evolution of the rod produced in Trial 10 is shown in Figure 80. In the early stages of extrusion, there are clear equiaxed grains in both directions, which is more uniform than in the Trial 8 microstructures. The main difference between these two trials is the tooling geometries, which would lead to the suggestion that the tooling has a major impact on the severe plastic deformation of the material. The larger die requires more feedstock to fill and therefore it takes longer to fill. In addition to it taking longer to fill the die, the pressure needs to build in order to extrude. If the die is not full, the pressure will be lower than if it was. The longer time means that, under the high temperature of the shoe, grain growth can occur, which results in a denser material with lower porosity and a slightly larger grain size when compared to Trial 8. This is also reiterated in the tensile results, which are much higher than those shown in Trial 8. Further investigation would be required to understand the extent of impact of the tooling geometries on the product, although there is a pre-existing mathematical model [90], which can estimate the required extrusion pressure from the geometry and feedstock flow properties.

As the trial progresses, it is evident that the tools have abraded, resulting in small fragments of tool becoming embedded in the rod. This occurs during the early trial and, due to the way Conform works, the material abraded is not necessarily first out of the process. The grain size between Sample 1 and 4 drops, resulting in a very-fine microstructure.

In the late extrusion, there is a further increase in the grain size, likely as a result of fluctuating pressure and temperature as material leaves the die. Despite this increase, the grain size is more uniform, with wide regions of equiaxed grains. Outside of these regions, there is evidence of non-equiaxed grains in the structure, which would suggest the presence of a different titanium alloy. In this trial, Ti-6Al-4V swarf was fed in, which has been consolidated in the material. In order to understand to what extent, the material has been encapsulated in the material, SEM is used.

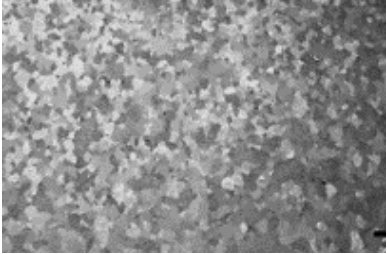
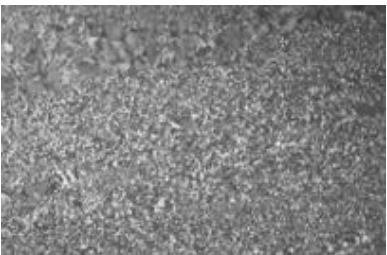
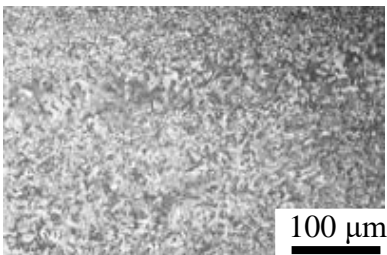
| | Trial 10 | |
|--------|---|--|
| Sample | Cross-Section | Transverse |
| 1 |  |  |
| 4 |  |  |
| 8 |  |  |

Figure 80 Light micrographs of CP Ti HDH Gr 2 and Ti-6Al-4V swarf derived rod extruded during Trial 10.

8.3 SEM and EDX

8.3.1 Trial 8 – Ti-6Al-4V GA

SEM and EDX were conducted on Sample 15 of the Ti-6Al-4V GA material, in order to determine whether the feedstock particles were successfully integrated into the consolidated material. As is shown in the Figure 81, the bulk of the image shows an equiaxed grain structure with some lighter areas of equiaxed grains. Using EDX it was possible to confirm that the lighter areas are likely CP Ti HDH Grade 2 material, whereas the much larger, darker region belongs to that of the Ti-6Al-4V feedstock. The Ti-6Al-4V particle still exhibits some of the spherical structure shown in the optical micrographs of Sample 15. The material has been encompassed well into the material; however, further study should be conducted to determine to what extent the feedstock has integrated and to calculate the percentage of Ti-6Al-4V in the sample.

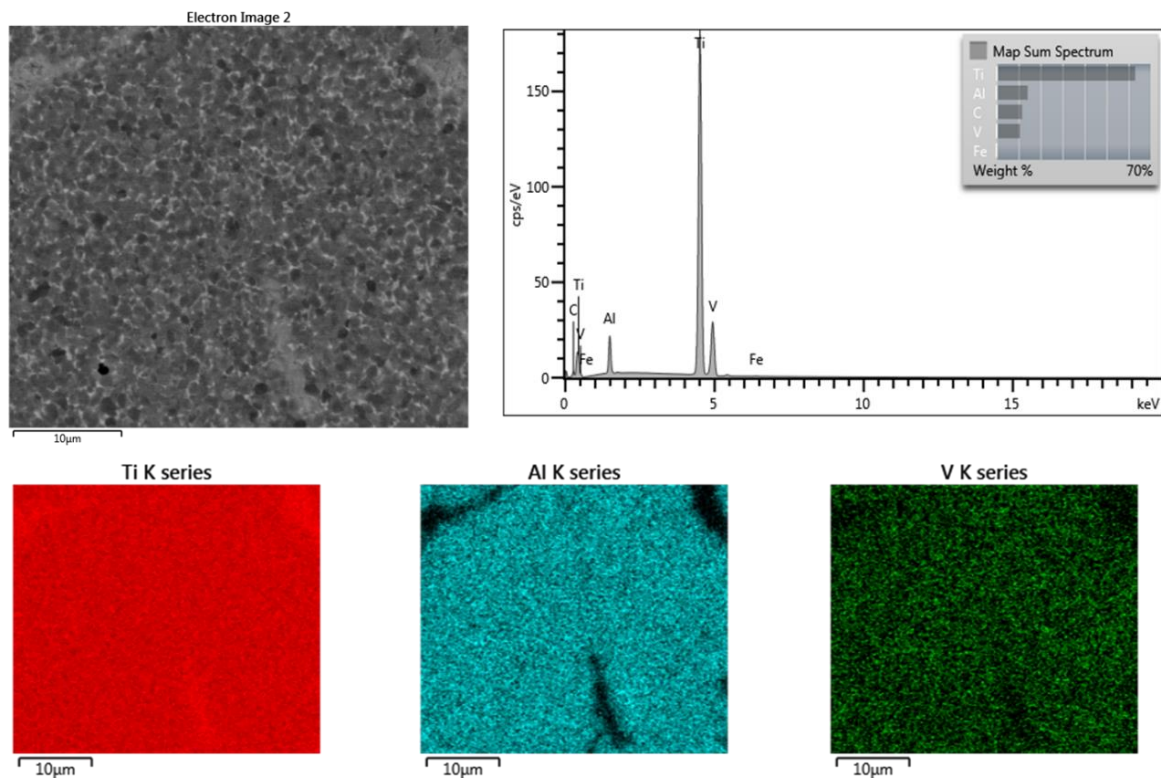


Figure 81 BSE micrograph and EDX of the Ti-6Al-4V GA extruded during Trial 8.

8.3.2 Trial 10 – Heat Treatment of Ti-6Al-4V swarf derived rod

SEM was conducted on material taken from the die chamber at the end of the trial and the micrographs are shown in Figure 82. Within the microstructure, there are two distinct grain structures. There are clearly some equiaxed grains, which accounts for the majority of the grains in the structure, and additionally some more elongated grains. In order to ascertain the reason for the variation, EDX was used to estimate the elements within those areas and consequently, determine whether the Ti-6Al-4V was consolidated within the material.

The EDX results, shown in Figure 83, clearly demonstrate that there is a region containing both Al and V alongside the Ti expected in the structure. This region contains mostly elongated grains, with areas with some equiaxed grains. The elongated grains are a result of the cooling of the β -grains produced from the Ti-6Al-4V, suggesting that the material did not exceed the β -transus temperature, which would have led to the production of α grains in the swarf material. The surrounding equiaxed grains are mostly pure titanium.

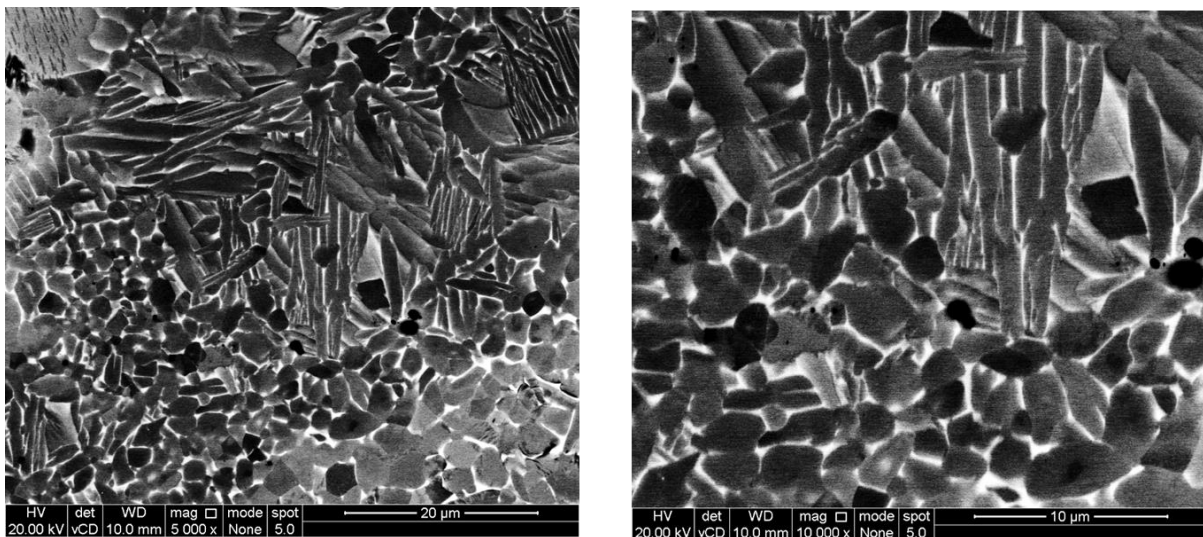


Figure 82 BSE micrograph of Sample 8 extruded during Trial 10. The sample contains both CP Ti HDH Gr 2 and Ti-6Al-4V swarf.

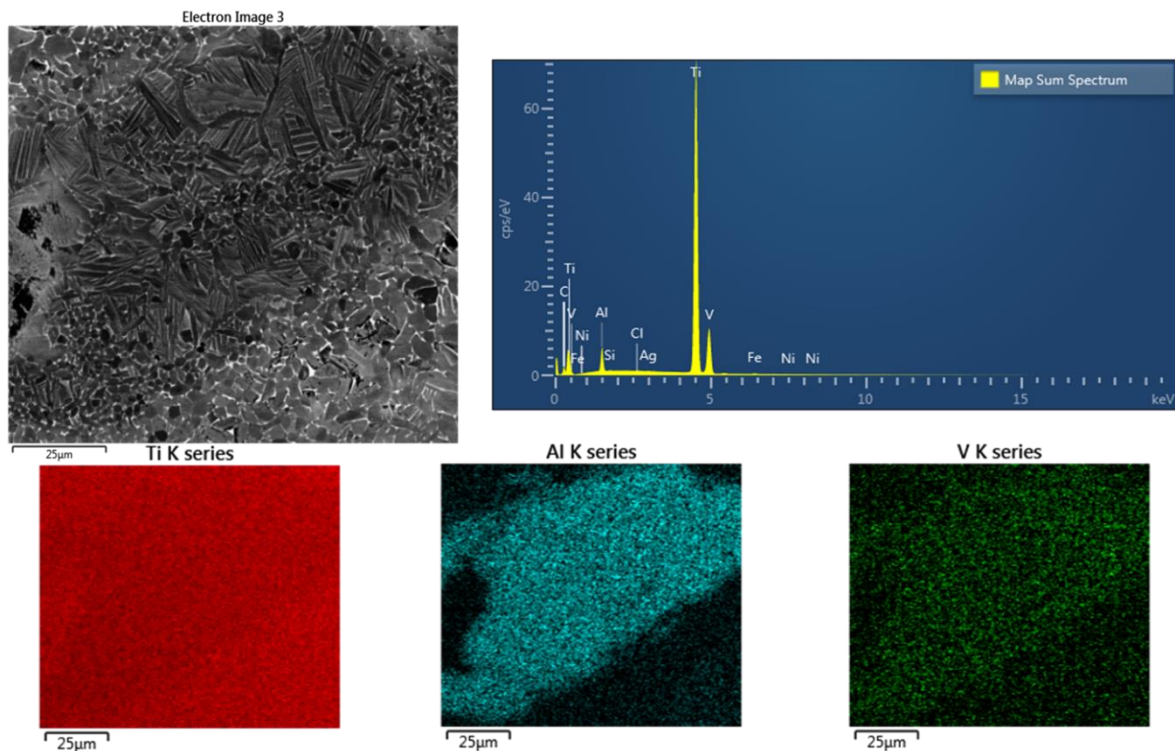


Figure 83 EDX of Sample 8, CP Ti HDH Gr 2 and Ti-6Al-4V swarf derived rod extruded during Trial 10.

From the micrographs, it is clear that the swarf has been successfully extruded alongside the CP Ti. However, it would be useful to know to what extent and to determine the presence of dynamic recrystallisation. In order to achieve this, a small sample was taken from next to the previous sample and heat treated for 3 h at 1010°C, slightly higher than the β -transus temperature for Ti-6Al-4V. After the heat treatment, the sample was imaged under SEM to obtain a close-up look of the microstructure. As is shown in Figure 15, there is a significant reduction in the volume of elongated grains. This is because the sample was heated above the β -transus, resulting in transformation of all β -grains to α grains. Upon cooling there are some grains that are still elongated, however, there is also clear dynamic recrystallisation.

8.4 Tensile Testing Results

From the as-Conformed material, sub-size tensile specimens were prepared with a 2.5 mm gauge diameter, as shown in Figure 84. Additionally, collets were prepared for the sub-size specimens, as the unusually small gauge diameter required smaller collets than are available commercially. The collets are shown in Figure 85.

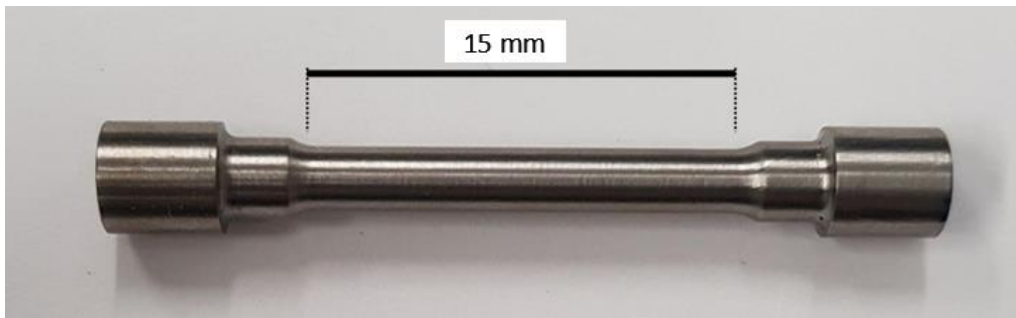


Figure 84 Sub-size tensile specimen prepared from as-Conformed titanium rod with a gauge length of 15 mm and gauge diameter of 2.5 mm



Figure 85 Collets for sub-size tensile specimens produced for this project

The disparity between the expected results for this material against the actual results relate to a few possibilities. Firstly, the largest impact on the results is the compliance of the tensile tester itself. The tester used in this work had no defined compliance, which would allow the results to be adjusted accordingly. Secondly, the test was monitored via grip-to-grip separation and an extensometer, rather than using a camera to improve the accuracy. This was not known before starting the work, and consequently has led to results which require significant adjustment; these will be discussed shortly. Finally, further discrepancies may occur based on the porosity of the material and the possibility of impurities from the tooling or the atmosphere.

In order to address the impact of the compliance and grip issues on the results, the Young's modulus has to be adjusted manually for a known sample. This adjustment can then be used to adjust the displacement of the unknown samples, thus correcting the data obtained from the

tensile tests. The adjustment made is the generation of a linear correction factor, which is an estimation of mm/N.

The displacement is adjusted by multiplying the force by the linear correction factor and subtracting the result. Through trial and error, it was determined that the linear correction factor was ~0.00014. The displacement was then adjusted for each value by $0.00014 \times \text{Force}$, providing a more realistic Young's Modulus.

8.4.1 Trial 8

From the post-correction results shown in Table 8, it is clear that there is significant variation across the trial samples.

Table 8 Raw tensile data for the sub-specimen tensile samples from trial 8

| Sample | Gauge Diameter | Gauge Length | Area | UTS | Yield Stress | | | | | Youngs Modulus | | | | | Elongation |
|--------|----------------|--------------|------|--------|--------------|--------|--------|---------|-------|----------------|-------|-------|---------|------|------------|
| | | | | | 1.00 | 2.00 | 3.00 | Average | SD | 1.00 | 2.00 | 3.00 | Average | SD | |
| 1.00 | 2.49 | 14.92 | 3.91 | 585.90 | 473.80 | 469.80 | 481.00 | 474.87 | 4.63 | 17.60 | 12.10 | 13.00 | 14.23 | 2.41 | 7.70 |
| 2.00 | 2.50 | 14.99 | 3.93 | 536.20 | 438.50 | 399.29 | 452.16 | 429.98 | 22.41 | 13.10 | 13.80 | 13.00 | 13.30 | 0.36 | 18.70 |
| 3.00 | 2.50 | 14.97 | 3.93 | 658.20 | 555.39 | 581.25 | 563.38 | 566.67 | 10.81 | 15.40 | 16.50 | 15.20 | 15.70 | 0.57 | 18.00 |
| 4.00 | 2.48 | 14.95 | 3.90 | 507.80 | 399.80 | 422.80 | 411.25 | 411.28 | 9.39 | 12.80 | 17.20 | 13.00 | 14.33 | 2.03 | 19.70 |
| 5.00 | 2.49 | 14.97 | 3.91 | 547.10 | 430.67 | 441.96 | 409.53 | 427.39 | 13.44 | 15.90 | 16.80 | 13.60 | 15.43 | 1.35 | 19.60 |
| 6.00 | 2.52 | 14.98 | 3.96 | 595.20 | 493.70 | 509.63 | 461.87 | 488.40 | 19.85 | 16.50 | 17.20 | 13.20 | 15.63 | 1.74 | 18.90 |
| 7.00 | 2.49 | 15.04 | 3.91 | 560.00 | 481.83 | 498.21 | 488.00 | 489.35 | 6.75 | 10.40 | 11.70 | 10.80 | 10.97 | 0.54 | 17.90 |
| 8.00 | 2.50 | 14.99 | 3.93 | 532.40 | 441.94 | 402.73 | 412.95 | 419.21 | 16.61 | 13.00 | 13.40 | 12.60 | 13.00 | 0.33 | 14.80 |
| 9.00 | 2.46 | 14.98 | 3.86 | 567.60 | 494.80 | 469.25 | 496.50 | 486.85 | 12.46 | 15.40 | 17.40 | 15.60 | 16.13 | 0.90 | 15.20 |
| 10.00 | 2.49 | 15.02 | 3.91 | 504.10 | 432.50 | 435.12 | 414.65 | 427.42 | 9.10 | 14.20 | 14.30 | 15.40 | 14.63 | 0.54 | 18.20 |
| 11.00 | 2.47 | 15.03 | 3.88 | 638.40 | 549.42 | 565.35 | 542.75 | 552.51 | 9.48 | 18.60 | 18.80 | 18.20 | 18.53 | 0.25 | 18.50 |
| 12.00 | 2.49 | 15.01 | 3.91 | 536.10 | 416.30 | 453.90 | 412.40 | 427.53 | 18.71 | 14.10 | 16.00 | 13.30 | 14.47 | 1.13 | 10.80 |

Table 9 Tensile data for trial 8 after the correction factor has been applied

| Sample | Gauge Diameter | Gauge Length | Area | UTS | Yield Stress | | | | | Youngs Modulus | | | | | Elongation |
|--------|----------------|--------------|------|--------|--------------|--------|--------|---------|-------|----------------|--------|--------|---------|-------|------------|
| | | | | | 1.00 | 2.00 | 3.00 | Average | SD | 1.00 | 2.00 | 3.00 | Average | SD | |
| 1.00 | 2.49 | 14.92 | 3.91 | 586.70 | 468.30 | 500.38 | 460.90 | 476.53 | 17.14 | 33.90 | 28.00 | 34.80 | 32.23 | 3.02 | 5.20 |
| 2.00 | 2.50 | 14.99 | 3.93 | 536.10 | 424.90 | 438.90 | 451.86 | 438.55 | 11.01 | 42.00 | 49.10 | 32.90 | 41.33 | 6.63 | 16.80 |
| 3.00 | 2.50 | 14.97 | 3.93 | 658.20 | 541.90 | 564.40 | 578.10 | 561.47 | 14.92 | 53.90 | 59.80 | 64.30 | 59.33 | 4.26 | 15.60 |
| 4.00 | 2.48 | 14.95 | 3.90 | 507.00 | 389.10 | 406.90 | 422.30 | 406.10 | 13.57 | 35.90 | 56.20 | | 46.05 | 10.15 | 17.10 |
| 5.00 | 2.49 | 14.97 | 3.91 | 547.10 | 390.35 | 438.90 | 406.90 | 412.05 | 20.15 | 64.20 | 96.30 | 75.30 | 78.60 | 13.31 | 17.60 |
| 6.00 | 2.52 | 14.98 | 3.96 | 595.20 | 479.20 | 461.30 | 489.71 | 476.74 | 11.73 | 58.50 | 65.90 | 84.80 | 69.73 | 11.07 | 16.60 |
| 7.00 | 2.49 | 15.04 | 3.91 | 560.00 | 483.70 | 488.80 | 463.26 | 478.59 | 11.04 | 19.20 | 24.00 | 20.10 | 21.10 | 2.08 | 16.14 |
| 8.00 | 2.50 | 14.99 | 3.93 | 532.30 | 412.20 | 422.29 | 438.95 | 424.48 | 11.03 | 34.60 | 31.60 | 36.50 | 34.23 | 2.02 | 13.70 |
| 9.00 | 2.46 | 14.98 | 3.86 | 567.60 | 480.95 | 463.24 | 472.20 | 472.13 | 7.23 | 45.60 | 46.90 | 46.40 | 46.30 | 0.54 | 13.10 |
| 10.00 | 2.49 | 15.02 | 3.91 | 504.10 | 419.74 | 422.28 | 408.23 | 416.75 | 6.11 | 38.30 | 34.70 | 45.70 | 39.57 | 4.58 | 16.70 |
| 11.00 | 2.47 | 15.03 | 3.88 | 638.00 | 546.40 | 538.98 | 547.92 | 544.43 | 3.91 | 104.10 | 108.70 | 108.60 | 107.13 | 2.15 | 16.29 |
| 12.00 | 2.49 | 15.01 | 3.91 | 536.20 | 428.50 | 383.10 | 344.20 | 385.27 | 34.45 | 37.40 | 41.80 | 37.80 | 39.00 | 1.99 | 9.00 |

The Young's Modulus for all tests is often below the expected value for this material, which highlights that repeat tests need to be conducted to ensure the accuracy of the results. The value for Sample 11 is the closest to the value expected for CP Ti HDH Grade 2 or Ti-6Al-4V. The correction factor used made a significant improvement to these results, however, it appears that further work is required. The UTS, elongation and yield stress results are only slightly affected by the correction factor, and these results will be discussed in order to establish the trends across the sample.

Across all 12 tests, there is some consistency in the ultimate tensile strength, with the value never dropping below 500 MPa. This is a higher-than-expected value for the UTS of CP Ti HDH Grade 2 and is closer to that expected from CP Ti HDH Grade 4. This is improved further when the process begins to reach steady state, where the UTS may exceed 600 MPa. Unfortunately, during these trials, the feedstocks and processing parameters are adapted to minimise damage to the abutment. This can be done through the change of the wheel speed, reduction of the temperature through wheel cooling and changing the feedstock. Because of this, the material properties vary across the length of the trial. For example, there is a significant drop of 151.2 MPa between the UTS of Sample 3 and Sample 4. Whilst it is not possible to be entirely accurate about the position of the sample in relation to the recorded experimental data (see *Chapter 7*), it can be estimated that this drop relates to the levelling off of the wheel temperature after the initial extrusion at ~1000 s. The drop in the wheel temperature is linked to a reduction in the friction and therefore, the material is not as plastically deformed as other material within the die. Alternatively, the material may have been in the die for a much shorter period of time than the material extruded before it, as the extrusion pressure will have been built-up prior to this.

The yield stress results very closely mimic the trends found for the UTS, with relatively consistent results across the course of the extruded product. Unlike for the UTS, multiple readings for the yield stress were taken and highlighted that in the early stages of the trial, there is much more variation in the potential result as shown by the standard deviation. As the trial progresses, the yield strength results become more accurate with a much smaller variation. It is at this point that it would be expected that the process has achieved a steady state and consequently, this has resulted in a more consistent tensile result. This is also exhibited in the microstructure, with the presence of a more equiaxed grain structure across the entire sample.

8.4.2 Trial 10

In the case of the tensile samples, the poor surface finish, varied diameter and curvature of the product meant that the subsize samples were prepared as for Trial 8. Further to this, there are also only 8 tensile specimens with no repeats. These were taken equidistantly across the rod with Sample 1 equating to within the first 10 cm of rod to be extruded and Sample 8 within the final 10 cm outside of the die. As with Trial 8 the tensile results were corrected with a correction factor of 0.00014, and the raw data is shown in Table 10. The corrected results are shown in Table 11.

Table 10 Raw tensile test data from the tensile samples taken from the Ti rod extruded during Trial 10.

| Sample | Gauge Diameter | Gauge Length | Area | UTS | Yield Stress | | | | | Youngs Modulus | | | | | Elongation |
|--------|----------------|--------------|------|--------|--------------|--------|--------|---------|-------|----------------|-------|-------|---------|------|------------|
| | | | | | 1.00 | 2.00 | 3.00 | Average | SD | 1.00 | 2.00 | 3.00 | Average | SD | |
| 1.00 | 2.40 | 15.15 | 4.52 | 762.20 | 702.90 | 710.30 | 704.80 | 706.00 | 3.14 | 20.60 | 19.40 | 20.10 | 20.03 | 0.49 | 9.10 |
| 2.00 | 2.39 | 14.80 | 4.49 | 839.60 | 837.47 | 842.60 | 835.10 | 838.39 | 3.13 | 22.20 | 22.00 | 20.80 | 21.67 | 0.62 | 4.10 |
| 3.00 | 2.40 | 15.11 | 4.52 | 689.70 | 585.90 | 596.90 | 606.80 | 596.53 | 8.54 | 17.70 | 15.20 | 18.40 | 17.10 | 1.37 | 7.70 |
| 4.00 | 2.37 | 15.00 | 4.41 | 782.40 | 693.70 | 682.60 | 679.70 | 685.33 | 6.03 | 15.00 | 14.90 | 14.30 | 14.73 | 0.31 | 10.40 |
| 5.00 | 2.44 | 15.07 | 4.68 | 690.00 | 687.20 | 647.00 | 646.20 | 660.13 | 19.14 | 18.60 | 18.00 | 17.60 | 18.07 | 0.41 | 3.90 |
| 6.00 | 2.44 | 14.97 | 4.68 | 640.90 | 556.80 | 582.70 | 576.90 | 572.13 | 11.10 | 13.60 | 16.30 | 14.70 | 14.87 | 1.11 | 9.20 |
| 7.00 | 2.43 | 15.06 | 4.64 | 604.60 | 605.50 | 585.00 | 594.10 | 594.87 | 8.39 | 14.80 | 17.00 | 14.70 | 15.50 | 1.06 | 4.00 |
| 8.00 | 2.42 | 14.95 | 4.60 | 807.30 | 702.90 | 714.00 | 699.30 | 705.40 | 6.26 | 17.40 | 18.70 | 18.30 | 18.13 | 0.54 | 8.80 |

Table 11 Corrected tensile test data from the tensile samples taken from the Ti rod extruded during Trial 10.

| Sample | Gauge Diameter | Gauge Length | Area | UTS | Yield Stress | | | | | Youngs Modulus | | | | | Elongation |
|--------|----------------|--------------|------|--------|--------------|--------|--------|---------|-------|----------------|--------|--------|---------|-------|------------|
| | | | | | 1.00 | 2.00 | 3.00 | Average | SD | 1.00 | 2.00 | 3.00 | Average | SD | |
| 1.00 | 2.40 | 15.15 | 4.52 | 761.60 | 706.27 | 705.39 | 710.69 | 707.45 | 2.32 | 146.70 | 135.20 | 126.30 | 136.07 | 8.35 | 6.40 |
| 2.00 | 2.39 | 14.80 | 4.49 | 842.60 | 839.90 | 831.30 | 839.00 | 836.73 | 3.86 | 596.00 | 536.00 | 429.00 | 520.33 | 69.07 | 0.80 |
| 3.00 | 2.40 | 15.11 | 4.52 | 690.30 | 588.40 | 593.40 | 609.10 | 596.97 | 8.82 | 68.50 | 77.30 | 65.50 | 70.43 | 5.01 | 5.70 |
| 4.00 | 2.37 | 15.00 | 4.41 | 782.40 | 683.90 | 699.67 | 691.73 | 691.77 | 6.44 | 40.20 | 43.70 | 41.90 | 41.93 | 1.43 | 7.80 |
| 5.00 | 2.44 | 15.07 | 4.68 | 694.50 | 640.27 | 643.27 | 656.40 | 646.65 | 7.00 | 96.10 | 132.30 | 97.20 | 108.53 | 16.81 | 1.30 |
| 6.00 | 2.44 | 14.97 | 4.68 | 638.20 | 575.38 | 574.10 | 580.04 | 576.51 | 2.55 | 56.20 | 47.80 | 153.00 | 85.67 | 47.74 | 6.30 |
| 7.00 | 2.43 | 15.06 | 4.64 | 605.49 | 573.04 | 605.50 | 604.22 | 594.25 | 15.01 | 46.60 | 62.50 | 31.30 | 46.80 | 12.74 | 2.20 |
| 8.00 | 2.42 | 14.95 | 4.60 | 807.30 | 696.59 | 715.59 | 707.64 | 706.61 | 7.79 | 92.30 | 82.20 | 83.80 | 86.10 | 4.43 | 5.30 |

The tensile results show more variation than in the case of Trial 8. This is particularly clear in the UTS where the range is ~605 MPa - ~842 MPa, which is much larger than in the case of Trial 8. It is possible that there is improved processing of the particulate feedstock due to the altered tooling, which was not a consideration made when the tools were designed (see *Chapter 5*).

The elongation is generally poor, with values < 1% elongation, which may be a result of grain refinement, as suggested by the Hall-Petch relationship. This would suggest that with an

annealing heat treatment, which would allow for grain growth, the elongation could improve with a slight drop in the already high, tensile strength. Much like in Trial 8, the yield strength exhibits a similar trend to the UTS, equally with higher values.

The Young's Modulus results for these samples appear to be more in-line with what would be expected from similar material, however, there are some issues. Firstly, they are typically much lower than the value for CP Ti HDH Grade 2, which was shown in the Trial 8 results. Secondly, Sample 2 resulted in an extremely high value, which is potentially an issue within the data file. However, it should be noted that the correction factor used is not a perfect solution for calibrating the results, and the only way to accurately determine the tensile strength of this material would be to repeat the tests. Unfortunately, as previously stated, this was not an option as there was insufficient material to produce samples and they were all tested before the error was determined. The UTS and elongation results do work as a clear guide and obvious trend for the material and are relatively close to what would be expected for this material.

8.5 Fractography

In order to better assess the failure of the tensile samples, some fractography of the tensile surfaces was conducted on the material from Trial 10.

The fracture surfaces were imaged using light microscopy for all eight tensile specimens and are shown in Figure 86. Based on the samples obtained, the failures appear to be ductile in nature, with some evidence of a cup-and-cone structure. This is what would be expected from the material, as the alloys are not brittle in nature and have exhibited reasonable elongation in their tensile results.

With a closer look across the sample surfaces, there are various distinguishing features. Sample 1 has a fracture across the sample, suggesting that the fracture propagated from both sides and their connection led to failure. Sample 1 has two indents, on opposite sides of the tensile specimen, which may have been points of crack propagation leading to the tensile failure. There is some mild porosity, however, without further investigation this may also be attributed to particle drop out during the testing. Sample 2 contains darker regions in the fracture surface, which may result from the inclusion of tooling materials in the extruded rod.

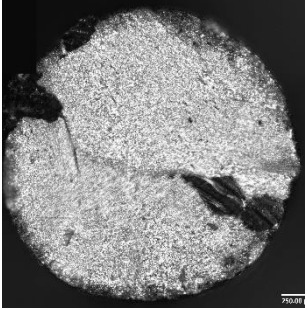
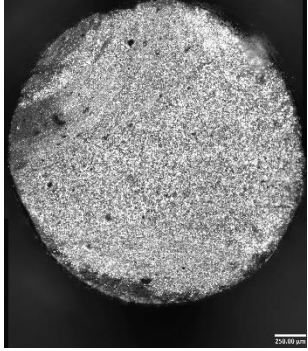
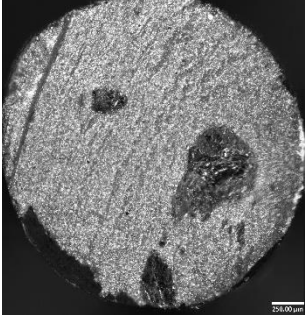
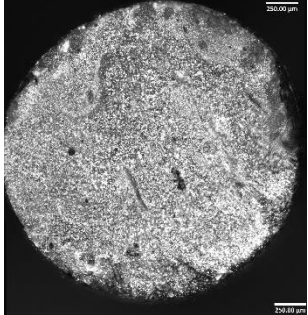
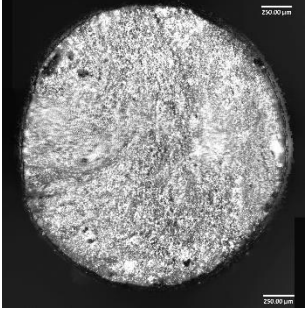
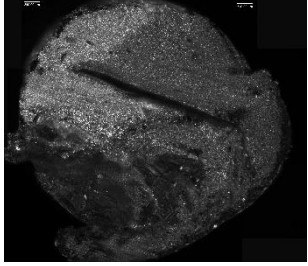
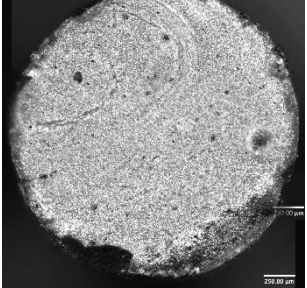
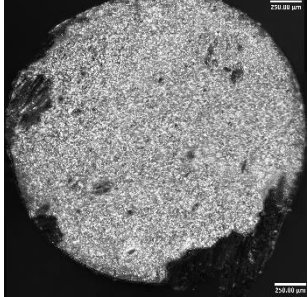
| Trial 10 | | | |
|----------|---|--------|---|
| Sample | Fracture Surface | Sample | Fracture Surface |
| 1 |  | 5 |  |
| 2 |  | 6 |  |
| 3 |  | 7 |  |
| 4 |  | 8 |  |

Figure 86 Light micrographs of the tensile sample fracture surfaces from the Trial 10 tensile samples.

The fracture surfaces were imaged using light microscopy for all eight tensile specimens and are shown in Figure 86. Across the sample surfaces, there are various distinguishing features. Sample 1 has a fracture across the sample, suggesting that the fracture propagated from both

sides and their connection led to failure. Sample 1 has two indents, on opposite sides of the tensile specimen, which may have been points of crack propagation leading to the tensile failure. There is some mild porosity, however, without further investigation this may also be attributed to particle drop out during the testing. Sample 2 contains darker regions in the fracture surface, which may result from the inclusion of tooling materials in the extruded rod.

During the early stages of the trials, wear on the wheel and die chamber can result in small fragments of tooling material becoming encapsulated in the product. Unlike the previous samples, Samples 3, 4 and 5 show the clear flow structure of Conformed material, where there is a circular flow pattern, much like the flow found in pipes. There are some small areas of porosity or holes, but again, these may be a result of the tensile testing. Sample 6 is much less uniform than Samples 3 – 5, with some darker regions, which may correspond to the swarf feedstock added to the process. At this stage, it would not be expected that the swarf has fully consolidated.

There is further evidence of this in Sample 7, where there is a clear line in the fracture surface. This may be an un-deformed fragment of swarf, however, without elemental analysis it is not possible to give a precise answer. There are also darker areas, not unlike those found in Sample 2, which may be abutment material, as it will have started to wear at this point. Sample 8 is much more uniform than Sample 7, with no evidence of inclusions. There is some slight porosity, however, the extrusion pressure will have started to drop as a result of abutment deformation. Overall, much like with Trial 8, these fracture surfaces give some indication of whether there are particle inclusions and information about the sample failure, however, there is not enough information to be completely accurate in the assessment without further analysis such as elemental analysis or SEM.

8.6 Microhardness Results

8.6.1 Trial 8

Microhardness was conducted at three points across the extruded product and the results are shown in Figure 87. The indents were made directly onto the samples used for the micrographs, in order to provide an accurate representation of that stage of the extruded material. The results were recorded at Sample 5, where the initial CP Ti HDH Grade 2 had a higher chance of reaching steady state; Sample 9, this is prior to the change in feedstock so gives an idea of the end of the pure CP Ti HDH Grade 2 section; and Sample 13, which starts to include Ti-6Al-4V GA, however it should be noted that this is not 100% Ti-6Al-4V but rather an unknown blend of both feedstocks.

Sample 5 exhibits a cross-sectional average of 180.6 ± 20.2 HV1 and an average of 191.5 ± 15.3 HV1 in the extrusion direction. Sample 9 had an average of 198.7 ± 21.5 HV1 in the cross-section and 214.0 ± 17.3 HV1 in the transverse direction. Sample 13 showed a cross-section average of 176.7 ± 12.3 HV1 and a transverse average of 200.3 ± 14.6 HV1.

From the results, there is a clear increase in the average hardness between Sample 5 and Sample 9, with an increase in both the cross-section and transverse samples. This improvement is due to work hardening and grain refinement through severe plastic deformation, which is led by a combination of the increase in the grip length and the extrusion pressure. There is a drop in the case of Sample 13, however, this material was extruded after the change in powder feedstock to the spherical Ti-6Al-4V GA feedstock. Further to this, it was extruded close to the end of the trial and therefore, it is likely that the damage to the abutment will have resulted in a reduced extrusion pressure. The cross-section of Sample 13 demonstrates the lowest HV1, however, when the standard deviation is taken into consideration, it is not statistically that different from the other results, with clear overlap.

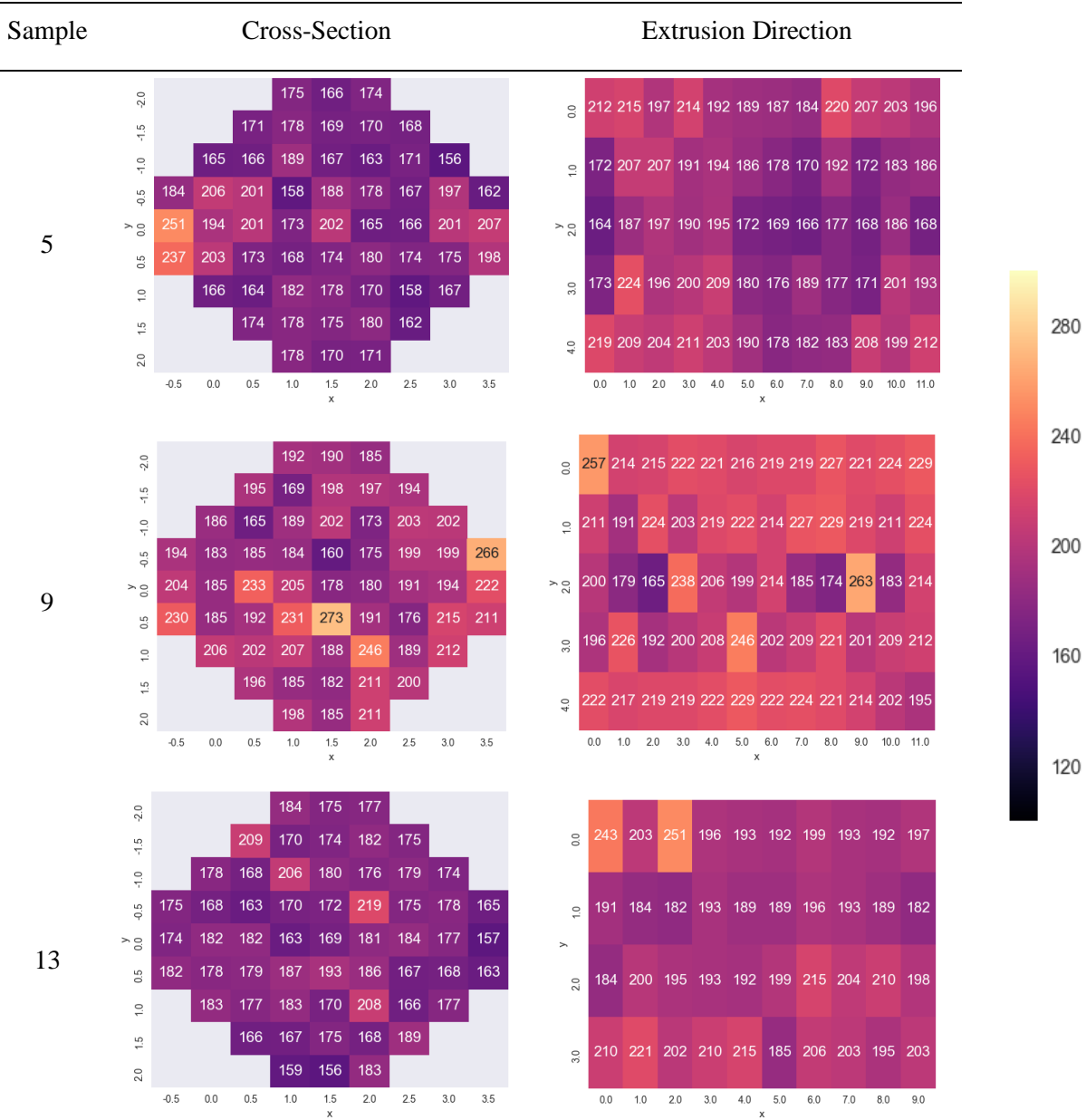


Figure 87 Microhardness results for samples taken of the CP Ti HDH Gr 2 and Ti-6Al-4V GA rod extruded during Trial 8.

In the early samples, there is a possibility of the inclusion of tooling material as the tools are abraded by the titanium feedstocks in the early stages of trialling. This can lead to areas of higher hardness and consequently sway the average result. Without clear micrographs of the entire sample, it is not possible to ascertain, for certain, that the higher HV1 values are from inclusions of tooling material.

8.6.2 Trial 10

The microhardness was performed on two samples for Trial 10 and the results are shown in Figure 88. The first sample was taken near to the start of the trial (within 50 cm) and was performed on Sample 3. The second sample was performed on Sample 8 and was positioned next to the die at the end of the trial.

The results show that the overall hardness has improved between Sample 3 and Sample 8. This may be a result of reaching a more steady-state extrusion, however, it should also be considered that by this point in the trial, Ti-6Al-4V swarf has been processed. Therefore, this higher hardness may also be attributed to the different titanium alloy in the rod.

In Sample 3, there are some regions with higher hardness than in other areas, which can be attributed to undeformed particles or impurities in the microstructure. As discussed with relation to the tensile results, the tooling material, particularly in the early stages of the trial, can break away from the tools resulting in being encompassed in the extruded rod, if it is not lost as flash.

Sample 8 does not exhibit the same peaks in the microhardness, however, there are some regions of lower hardness. This may be a result of a reduction in the extrusion pressure leading to some porosity in the microstructure or the loss of particles during polishing. The average hardness is higher than expected for CP Ti HDH Grade 2 and Ti-6Al-4V, thus showing the improvement in hardness during the severe plastic deformation.

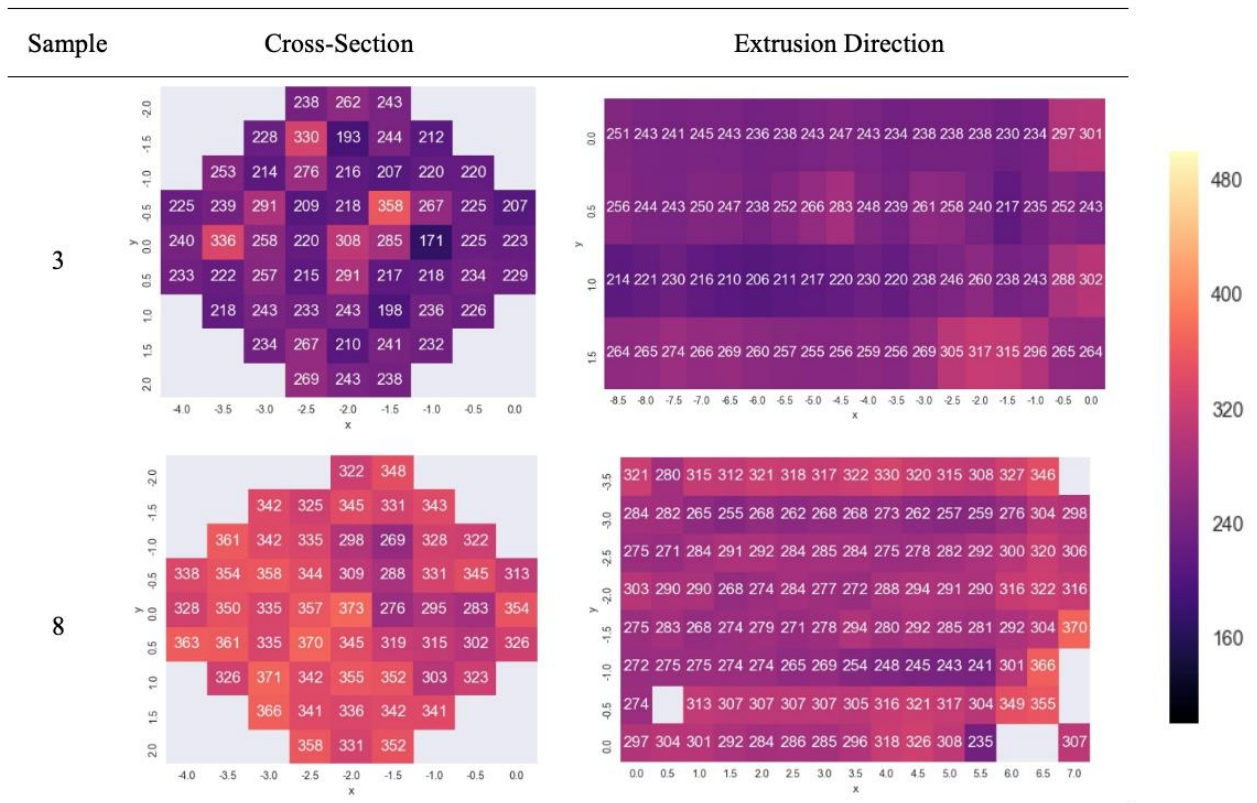


Figure 88 Microhardness results for samples taken of the CP Ti HDH Gr 2 and Ti-6Al-4V GA rod extruded during Trial 8.

8.7 Summary

Both the mechanical properties and microstructural analysis shown in this chapter, have clearly demonstrated that the material produced via the Conform process is of a reasonable quality. It has been demonstrated it is possible to extrude waste titanium via the Conform process and achieve a high-density material with a fine-grained structure. The mechanical properties, in the case of Trial 8 and 10 material, are good, with values exceeding those expected for CP-Ti HDH Gr 2.

The results for the microhardness show clear increases as the trial progresses, suggesting both a more steady state process as time has progressed, but also the inclusion of the harder alloy in the later trial stages. This is echoed in the tensile tests, with the improved UTS results as the material is changed, and in the microstructural analysis, with a reduction in the material grain size and inclusion of less equiaxed grain structures, which can be attributed to the Ti-6Al-4V.

It should be noted that although a small number of tensile samples were taken across the length of the rod, it may be possible to relate the tensile samples with the parameters occurring during their extrusion. However, there was no fixed extrusion rate, as this often happened sporadically, owing to the way the material was fed, the ability of the Conform machine to generate enough pressure and damage to the tooling within the shoe. This would mean that, although there could be some guess as to where the material came from, without further investigation it would be difficult to ensure any high degree of accuracy.

There is potential for the samples tested here to be cross-referenced with their positions in their trials, however, within this work, the powder flow was not consistent and nor was the extrusion rate. Therefore, currently it would be possible to make assumptions, but further information would be required to ensure the accuracy.

There are, however, clear issues within the results, which should be addressed in further work. The tensile samples were tested on a machine that was not correctly calibrated prior to use. This resulted in a much lower Young's modulus than what would typically be seen in titanium alloys, and as such, a correction factor was generated to adjust the data to a more consistent figure. The correction factor was generated as a result of trial and error, with comparison with the expected result for a Ti-6Al-4V HDH sample. This is not an ideal situation, and it would be advantageous to repeat the testing on a calibrated machine, but the low volume of material and cost of tensile specimens made this an impossibility in the timeline of the project.

Additionally, the material from trial 7 was not analysed owing to time constraints.

Overall, the material produced in the trials shows that there are good mechanical properties, and a clear microstructural development occurring across the course of a trial, resulting in a fine-grained product. The products have a potential downstream use in additive manufacturing, but it would be advantageous to demonstrate the oxygen content of the material, especially from the perspective of the additive manufacturing community. This would provide a better understanding of the oxygen pick-up during the process.

Chapter 9 : Conclusions

The main aims of this thesis were to further investigate the use of the Conform™ process for the consolidation of particulate titanium feedstocks, utilising titanium from various waste streams, including additive manufacturing out-of-specification powders and swarf from the machining of titanium billet.

Figure 89 breaks down all the work carried out during this project and separates it into two clear sections. The first section highlights the work carried out in the development stages of the project, where the focus was on assessing the ability of the feedstock to consolidate, the design of the tooling used during the trials and the creation of simulations which could be used to reduce the cost of the process. The second section covers the process of trialling in a Conform machine and the analysis of the resulting data and material produced during the trial.

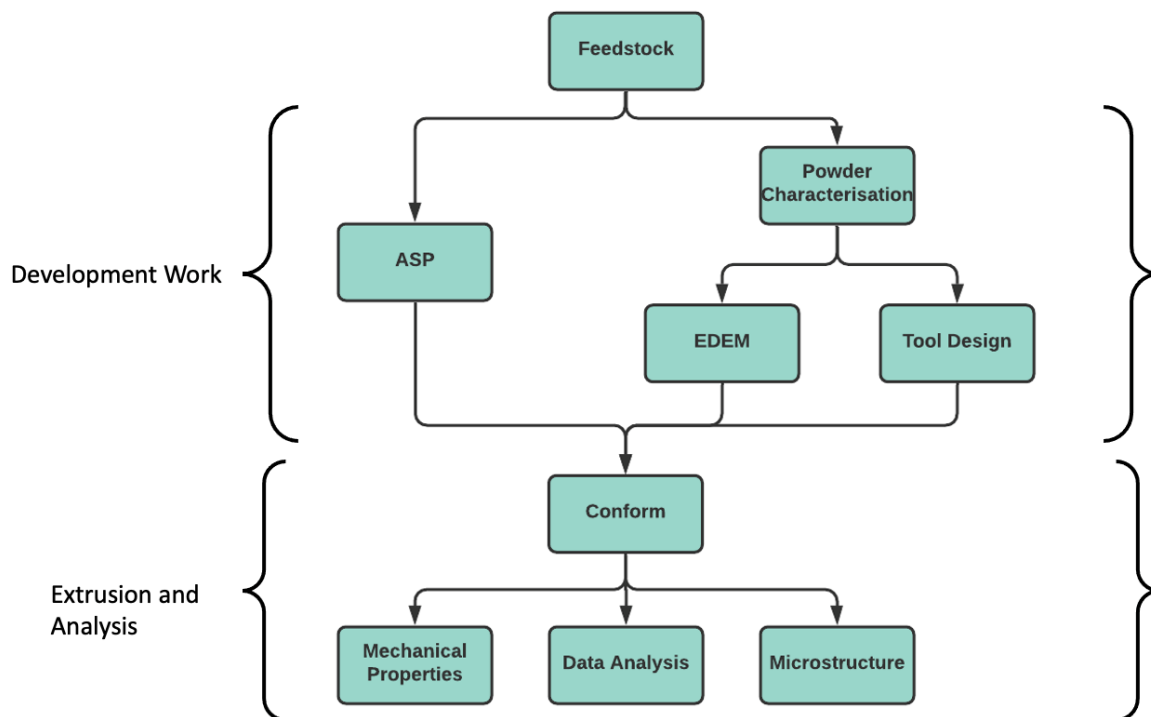


Figure 89 Diagram showing the workflow for the work carried out during this project.

Despite being demonstrated in previous work, the extrusion of titanium feedstocks, particularly particulate, has been limited and typically isolated to commercially pure titanium feedstocks with a relatively small size range. For the first time, the extrusion of Ti-6Al-4V swarf and spherical Ti-6Al-4V has been reported (see *Chapter 8*). This is a significant step towards

making the production of titanium wire, through the Conform™ process, a viable option for industrial purposes.

The mechanical and microstructural properties were ascertained for much of the material produced during the trials and gives an insight into what is happening at each stage in the process. There is a clear investigation into the ramp up of the trial into the steady state and ultimately the change in powder throughout this. The variation in the grain size across the samples (see Section 11.5) is a key example of the severe plastic deformation occurring throughout the process, with an improvement in the strength with small grain sizes, demonstrating some conformation to Hall-Petch. The resulting material, in all cases, typically had an average grain size of less than 3 µm. Once steady state has been reached, it was evident that mechanical properties also started to improve, however, it should be noted that as feedstocks were typically changed at the point of extrusion, some of the improvement may be down to the change in material.

Additionally, wire produced via the Conform™ process has been cold drawn with a 40% reduction to a diameter of 3.00 mm, which would make it a potential source for wire+arc additive manufacturing (see Section 11.5.1). This, however, is only the first step and further mechanical property testing and oxygen analysis should be performed on material produced in this manner.

In addition to reporting the first attempts at the recycling of titanium feedstocks in this manner, this work has also provided further guidance on the Conform™ process, highlighting the influence of tool design and different material morphologies. Starting with the design of tooling, where development work completed, demonstrated that for larger morphology materials, the tools require a much larger groove and abutment nose. For smaller morphology materials, the larger tools do not fill as quickly, nor is the extrusion pressure high enough to extrude the material.

This is most clearly represented by EDEM simulations (see *Chapter 6*), which were completed with a variety of tooling geometries and particulate feedstocks. The larger toolsets worked best for the larger particles, with the swarf generating a much larger compressive force on the

particles, leading to a well consolidated area of particles. There are some obvious flaws in the work, and these should be further investigated in future work.

As an aside from the ConformTM process, work was also completed on the characterisation of the powders used in the process and consequently, development on a bespoke powder testing method was performed. This testing rig, the ASP (shown in *Chapter 4*), allowed for powders to be uniaxially compressed and then sheared. The resulting data allowed for the determination of the change in the density of the material over time, the visual confirmation of the consolidation of the material and also some determination of the pressure required to consolidate the material. These parameters ultimately align with the requirements of the ConformTM process, where the consolidation of particulate feedstocks into a single, solid material is performed. It has also been shown that the ASP can be used to obtain information about the Conform-ability of a given feedstock and the current work goes some way to determining the toolset required to successfully consolidate and extruded the feedstocks used.

From the aims and objectives outlined in the *Chapter 1*, it can be said that this work successfully utilised previous research to influence the design of the tools used for trialling. This was clear from the use of alternative abutment materials, which did not result in brittle failure and could withstand the temperatures and pressures required during a trial. The tools designed in this work successfully extruded the desired feedstocks as a solid product with good mechanical properties and a fine-grained microstructure.

Some further understanding of the thermomechanical processes and the powder behaviour during a trial has been developed, with the use of the of the trial data to ascertain the points at which extrusion occurs with relation to the other parameters of the machine. There is potential for further development of this understanding, with a closer investigation of the trial parameters and making smaller changes between trials to understand the implication of these changes, such as the wheel speed, abutment material or feedstock.

As a highlight of the work, wire was produced via the ConformTM process from waste feedstocks including Ti-6Al-4V GA powder and Ti-6Al-4V swarf. This demonstrates the potential of the process for recycling of waste materials into usable downstream materials. The produced material also had good mechanical properties and microstructure, that lends to being

a good candidate for wire-based additive manufacturing. However, it would have been useful to understand the oxygen content of the material, to further assess the viability for AM processes.

Finally, development work using the ASP as an alternative small-scale powder characterisation method showed promise. There was some correlation between the ability of the material to consolidate in the Conform™ process and the shear of the powder in the ASP. This will be further discussed in *Chapter 10* owing to the potential for future work.

Overall, the aims and objectives of this work were met to some extent, however, there is clear scope for future research in this area.

Chapter 10 : Future Work

10.1 ConformTM

The ConformTM process has successfully been used to produce titanium wire from various particulate feedstocks, however, there is additional work that needs to be done to optimise and further improve the process. The key research that would aid the future development of the abutment can be broken down into a few important sections:

- a. Optimisation of the tooling design
- b. Investigation into the materials used in the tooling
- c. Powder feeding

The tools designed so far have been based on equations previously used for tool design for ConformTM and computational simulations, however, there are still parameters which could be further investigated. For example, it is important to understand how changing certain parameters has an impact on the result and more quantitatively than is discussed in this work. The influence of varying the die size, the groove size and the positioning of the pressure relief has been, in part, developed in this work, however, further research would trial the change more rigorously and determine the outcome on the product.

The largest failing of the tooling during a trial is the loss of the abutment, which was the main cause of the loss of pressure. The current materials are coated nickel superalloys, which operate well at high temperatures and have a wear resistant coating, however, damage to the surface from the high pressures can lead to loss of the coating and ultimately, the shearing of the abutment – which is what is shown to happen here. For this reason, it is clear that the abutment material is a key requirement for extending the life of a trial. There are a number of material options, which could be investigated, although there are a number of parameters which need to be met. The abutment material must a) **tolerate high temperature environments**, b) **have a lower wear rate than the currently used material**, c) **exhibit ductile failure**, and d) **be cost-effective**.

Finally, the powder feed during this project was manual owing to a significant problem with the vibratory feeder – which would not operate correctly during a trial. There are various different feeding systems, which currently be purchased, however, these are mostly used in the pharmaceutical industry or, in some instances, are used with rock products, which make them significantly larger than required. Of the options available, the aim would be to have a consistent flow rate and have the capacity to change this during a trial (increasing/decreasing the rate).

There are a number of directions this work could go in, however, most critically is the improvement of the tooling materials as these play the most important role in the trial and are often responsible for the failing of the trial.

10.2 Simulations

As outlined in *Chapter 6*, there are evident shortcomings in the simulations, which should be addressed in order to achieve a more accurate and more useful set of simulations for ConformTM. These are discussed in *Chapter 6*, however, in summary:

- 1) **Temperature** – during a ConformTM trial, the shoe is preheated to ~500°C, which has implications on the particle consolidation and the pressure within the extrusion zone. There is no temperature provided in the simulation and therefore, this deformation or pressure increase can be accounted for.
- 2) **Feedstock Morphology** – the particles were simplified to minimise the computation time for the simulations. There are a number of steps that can be taken to adjust this and improve the accuracy of the simulation, such as adding satellite particles, generating multiple particle shapes to match those of the feedstock and use the particle size distribution data to generate an exact replica of the distribution seen in the feedstock.
- 3) **Mass Flow** – the mass flow of particles being generated within the simulation varies based on the size of the particle, however, this is not completely accurate to the

experimental trials. During a trial, the mass flow of powder is constantly monitored to ensure that there is enough feedstock to fill the port.

Further to this, it would also be advantageous to investigate alternative methods of simulating the process, such as a combination of DEM and FEM. This would allow for both investigation of the particle behaviour but also the bulk feedstock and extruded product.

10.3 Annular Shear Testing

The ASP was used to determine the ability of the feedstocks to consolidated in the Conform process. Whilst it has demonstrated itself to be a useful tool, it would be worthwhile to investigate alternative feedstocks to understand how a wider range of sizes and morphologies behave in the process. It would also be advantageous to understand the implication of alternative speeds and loads on the particles, which would allow for the estimation of required wheel speeds for good consolidation. Finally, much like the simulations, there is no temperature consideration for the shear. As Conform operates with a shoe temperature of $\sim 500^{\circ}\text{C}$, it would be helpful to understand the impact of the temperature on the shear and consolidation of the particles.

Further to additional ASP testing, there is another route that should be explored. The ASP is controlled through PID, as discussed in *Chapter 4*. In order to achieve more accurate results, the parameters can be adjusted. The improved accuracy may work to investigate the drops in displacement regularly across the testing, as well as allowing for a more detailed look at the behaviour of the particles. Additionally, the tool design could be amended further to minimise calibration centring, suggestions would be to form the tools as part of the adaptors attached to the machine, or to remove the use of bolts and find a more secure method of loading the tools onto the machine.

Chapter 11 : Bibliography

- [1] D. Green, "Extrusion," 3765216, 1973.
- [2] C. Stadelmann, "Extrusion von Metallpulven durch kontinuierliches Pulverstrangpressen," 2009.
- [3] B. M. Thomas, F. Derguti, and M. Jackson, "Continuous extrusion of a commercially pure titanium powder via the Conform process," *Mater. Sci. Technol. (United Kingdom)*, vol. 33, no. 7, pp. 899–903, 2017, doi: 10.1080/02670836.2016.1245256.
- [4] J. Palan, J. V Taboada, T. Kubina, L. Malecek, and J. Hodek, "Continuous extrusion of commercially pure titanium GRADE . 4," vol. 69, no. 1, pp. 33–37, 2015.
- [5] D. Fray, T. Farthing, and G. Chen, "Removal of oxygen from metal oxides and solid solutions by electrolysis in a fused salt," 1999.
- [6] B. Denkena, M.-A. Dittrich, and S. Jacob, "Energy Efficiency in Machining of Aircraft Components," *Procedia CIRP*, vol. 48, pp. 479–482, 2016, doi: 10.1016/j.procir.2016.03.155.
- [7] S. A. Smythe, B. M. Thomas, and M. Jackson, "Recycling of Titanium Alloy Powders and Swarf through Continuous Extrusion (Conform™) into Affordable Wire for Additive Manufacturing," *Metals (Basel)*, vol. 10, no. 6, p. 843, Jun. 2020, doi: 10.3390/met10060843.
- [8] R. R. Boyer, "An overview on the use of titanium in the aerospace industry," *Mater. Sci. Eng. A*, vol. 213, no. 1–2, pp. 103–114, 1996.
- [9] M. Niinomi, "Recent research and development in titanium alloys for biomedical applications and healthcare goods," *Science and Technology of Advanced Materials*, vol. 4, no. 5, pp. 445–454, 2003, doi: 10.1016/j.stam.2003.09.002.
- [10] H. Friedrich, J. Kiese, H. Haldenwanger, and A. Stich, "Titanium in Automotive Applications - Nightmare, Vision or Reality," in *Proceedings of 10th World Conference on Titanium, Ti-2003, Hamburg.*, 2003, pp. 3393–3402.
- [11] F. Farges, "Titanium: Element and geochemistry," in *Geochemistry*, Dordrecht: Kluwer Academic Publishers, pp. 636–637.
- [12] Z. Z. Fang *et al.*, "Powder metallurgy of titanium – past, present, and future," *Int. Mater. Rev.*, vol. 63, no. 7, pp. 407–459, Oct. 2018, doi: 10.1080/09506608.2017.1366003.
- [13] E. H. Kraft, "Summary of Emerging Titanium Cost Reduction Technologies," Washington, 2004. [Online]. Available:

- <http://scholar.google.com/scholar?hl=en&btnG=Search&q=intitle:Summary+of+Emerging+Titanium+Cost+Reduction+Technologies#0>.
- [14] S. Seong, O. Younossi, B. Goldsmith, T. Lang, and M. Neumann, *Titanium: Industrial Base, Price Trends, and Technology Initiatives*. 2018.
- [15] I. Weiss and S. . Semiatin, “Thermomechanical processing of alpha titanium alloys—an overview,” *Mater. Sci. Eng. A*, vol. 263, no. 2, pp. 243–256, May 1999, doi: 10.1016/S0921-5093(98)01155-1.
- [16] I. Weiss and S. L. Semiatin, “Thermomechanical processing of beta titanium alloys—an overview,” *Mater. Sci. Eng. A*, vol. 243, no. 1–2, pp. 46–65, Mar. 1998, doi: 10.1016/S0921-5093(97)00783-1.
- [17] J. Donachie, *Titanium - A Technical Guide*, 2nd Edition., vol. 55. ASM International, 2000.
- [18] M. Monhaga, *A Quantum Approach to Alloy Design*. 2019.
- [19] H. M. Flower, “Microstructural development in relation to hot working of titanium alloys,” *Mater. Sci. Technol.*, vol. 6, no. 11, pp. 1082–1092, Nov. 1990, doi: 10.1179/mst.1990.6.11.1082.
- [20] F. H. Froes, “Titanium Alloys: Thermal Treatment and Thermomechanical Processing,” in *Encyclopedia of Materials: Science and Technology*, Elsevier, 2001, pp. 9369–9373.
- [21] I. Polmear, D. St. John, J. F. Nie, and M. Qian, *Light Alloys: Metallurgy of the Light Metals: Fifth Ed*. 2017.
- [22] T. R. Bieler, R. M. Trevino, and L. Zeng, “Alloys: Titanium,” in *Encyclopedia of Condensed Matter Physics*, Michigan State: Elsevier, 2005, pp. 65–76.
- [23] M. A. Hunter, “Metallic titanium,” *J. Am. Chem. Soc.*, vol. 32, no. 3, pp. 330–336, 1910, doi: 10.1021/ja01921a006.
- [24] T. T. C. Ltd., “Titanium Metals - Titanium Sponge.” <https://www.toho-titanium.co.jp/en/products/sponge.html> (accessed Jul. 26, 2019).
- [25] M. Bertolini, L. Shaw, L. England, K. Rao, J. Deane, and J. Collins, “The FFC Cambridge Process for Production of Low Cost Titanium and Titanium Powders,” *Key Eng. Mater.*, vol. 436, pp. 75–83, May 2010, doi: 10.4028/www.scientific.net/KEM.436.75.
- [26] T. Ebel, “Metal injection molding (MIM) of titanium and titanium alloys,” in *Handbook of Metal Injection Molding*, Elsevier, 2012, pp. 415–445.
- [27] P. W. Sutcliffe and P. G. Mardon, *Titanium Powder Metallurgy.*, no. 627. 2015.

- [28] V. Moxson, O. N. Senkov, and F. H. Froes, “Innovations in titanium powder processing,” *JOM*, vol. 52, no. 5, pp. 24–26, May 2000, doi: 10.1007/s11837-000-0027-y.
- [29] J. J. Dunkley, “Metal Powder Atomisation Methods for Modern Manufacturing,” *Johnson Matthey Technol. Rev.*, vol. 63, no. 3, pp. 226–232, Jul. 2019, doi: 10.1595/205651319X15583434137356.
- [30] J. Donachie and J. M., *Titanium – A Technical Guide*, vol. 55, no. 11. 2000.
- [31] N. S. Weston and M. Jackson, “FAST-forge of Titanium Alloy Swarf: A Solid-State Closed-Loop Recycling Approach for Aerospace Machining Waste,” *Metals (Basel)*, vol. 10, no. 2, p. 296, Feb. 2020, doi: 10.3390/met10020296.
- [32] A. M. Sherman, C. J. Sommer, and F. H. Froes, “The use of titanium in production automobiles: Potential and challenges,” *JOM*, vol. 49, no. 5, pp. 38–41, May 1997, doi: 10.1007/BF02914682.
- [33] A. D. Hartman, S. J. Gerdemann, and J. S. Hansen, “Producing lower-cost titanium for automotive applications,” *JOM*, vol. 50, no. 9, pp. 16–19, Sep. 1998, doi: 10.1007/s11837-998-0408-1.
- [34] N. S. Weston and M. Jackson, “FAST-forge – A new cost-effective hybrid processing route for consolidating titanium powder into near net shape forged components,” *J. Mater. Process. Technol.*, vol. 243, pp. 335–346, May 2017, doi: 10.1016/j.jmatprotec.2016.12.013.
- [35] J. R. P. Jorge, V. A. Barão, J. A. Delben, L. P. Faverani, T. P. Queiroz, and W. G. Assunção, “Titanium in Dentistry: Historical Development, State of the Art and Future Perspectives,” *J. Indian Prosthodont. Soc.*, vol. 13, no. 2, pp. 71–77, Jun. 2013, doi: 10.1007/s13191-012-0190-1.
- [36] K. T. Kim, M. Y. Eo, T. T. H. Nguyen, and S. M. Kim, “General review of titanium toxicity,” *Int. J. Implant Dent.*, vol. 5, no. 1, p. 10, Dec. 2019, doi: 10.1186/s40729-019-0162-x.
- [37] C. Y. Hu and T.-R. Yoon, “Recent updates for biomaterials used in total hip arthroplasty,” *Biomater. Res.*, vol. 22, no. 1, p. 33, Dec. 2018, doi: 10.1186/s40824-018-0144-8.
- [38] A. Sidambe, “Biocompatibility of Advanced Manufactured Titanium Implants—A Review,” *Materials (Basel)*, vol. 7, no. 12, pp. 8168–8188, Dec. 2014, doi: 10.3390/ma7128168.

- [39] D. D. Bosshardt, V. Chappuis, and D. Buser, “Osseointegration of titanium, titanium alloy and zirconia dental implants: current knowledge and open questions,” *Periodontol. 2000*, vol. 73, no. 1, pp. 22–40, Feb. 2017, doi: 10.1111/prd.12179.
- [40] A. Azushima *et al.*, “Severe plastic deformation (SPD) processes for metals,” *CIRP Ann. - Manuf. Technol.*, vol. 57, no. 2, pp. 716–735, 2008, doi: 10.1016/j.cirp.2008.09.005.
- [41] Y. Estrin and A. Vinogradov, “Extreme grain refinement by severe plastic deformation: A wealth of challenging science,” *Acta Mater.*, vol. 61, no. 3, pp. 782–817, Feb. 2013, doi: 10.1016/j.actamat.2012.10.038.
- [42] F. Nabarro and J. Hirth, Eds., “Dislocations in Solids,” in *Dislocations in Solids, Volume 12*, 1st Editio., 2010, p. iii.
- [43] U. F. Kocks, “Laws for Work-Hardening and Low-Temperature Creep,” *J. Eng. Mater. Technol.*, vol. 98, no. 1, pp. 76–85, Jan. 1976, doi: 10.1115/1.3443340.
- [44] Y. Estrin, L. S. Tóth, A. Molinari, and Y. Bréchet, “A dislocation-based model for all hardening stages in large strain deformation,” *Acta Mater.*, vol. 46, no. 15, pp. 5509–5522, Sep. 1998, doi: 10.1016/S1359-6454(98)00196-7.
- [45] L. Li and J. Virta, “Ultrahigh strength steel wires processed by severe plastic deformation for ultrafine grained microstructure,” *Mater. Sci. Technol.*, vol. 27, no. 5, pp. 845–862, May 2011, doi: 10.1179/026708310X12677993662087.
- [46] V. V. Stolyarov, V. V. Latysh, R. Z. Valiev, Y. T. Zhu, and T. C. Lowe, “The Development of Ultrafine-Grained Ti for Medical Applications,” in *Investigations and Applications of Severe Plastic Deformation*, Dordrecht: Springer Netherlands, 2000, pp. 367–372.
- [47] M. R. Shankar, B. C. Rao, S. Lee, S. Chandrasekar, A. H. King, and W. D. Compton, “Severe plastic deformation (SPD) of titanium at near-ambient temperature,” *Acta Mater.*, vol. 54, no. 14, pp. 3691–3700, Aug. 2006, doi: 10.1016/j.actamat.2006.03.056.
- [48] R. Z. Valiev, I. V Alexandrov, Y. T. Zhu, and T. C. Lowe, “Paradox of strength and ductility in metals processed by severe plastic deformation,” *J. Mater. Res.*, vol. 17, no. 1, pp. 5–8, 2002, doi: 10.1557/JMR.2002.0002.
- [49] W. Pachla, M. Kulczyk, M. Sus-Ryszkowska, A. Mazur, and K. J. Kurzydowski, “Nanocrystalline titanium produced by hydrostatic extrusion,” *J. Mater. Process. Technol.*, vol. 205, no. 1–3, pp. 173–182, 2008, doi: 10.1016/j.jmatprotec.2007.11.103.
- [50] G. Faraji, H. S. Kim, and H. T. Kashi, “Severe Plastic Deformation Methods for Bulk Samples,” in *Severe Plastic Deformation*, Elsevier, 2018, pp. 37–112.

- [51] M. Balog, F. Simancik, O. Bajana, and G. Requena, “ECAP vs. direct extrusion—Techniques for consolidation of ultra-fine Al particles,” *Mater. Sci. Eng. A*, vol. 504, no. 1–2, pp. 1–7, Mar. 2009, doi: 10.1016/j.msea.2008.12.014.
- [52] W. H. Sillekens and J. Bohlen, “Hydrostatic extrusion of magnesium alloys,” in *Advances in Wrought Magnesium Alloys*, Elsevier, 2012, pp. 323–345.
- [53] K. Topolski, W. Pachla, and H. Garbacz, “Progress in hydrostatic extrusion of titanium,” in *Journal of Materials Science*, 2013, vol. 48, no. 13, pp. 4543–4548, doi: 10.1007/s10853-012-7086-7.
- [54] J. J. Lewandowski and A. Awadallah, *Hydrostatic Extrusion of Metals and Alloys*. 2018.
- [55] G. Sakai, K. Nakamura, Z. Horita, and T. G. Langdon, “Developing high-pressure torsion for use with bulk samples,” *Mater. Sci. Eng. A*, vol. 406, no. 1–2, pp. 268–273, Oct. 2005, doi: 10.1016/j.msea.2005.06.049.
- [56] M. Y. Alawadhi, S. Sabbaghianrad, Y. Huang, and T. G. Langdon, “Evaluating the paradox of strength and ductility in ultrafine-grained oxygen-free copper processed by ECAP at room temperature,” *Mater. Sci. Eng. A*, vol. 802, p. 140546, Jan. 2021, doi: 10.1016/j.msea.2020.140546.
- [57] Y. M. Wang and E. Ma, “Strain hardening, strain rate sensitivity, and ductility of nanostructured metals,” *Mater. Sci. Eng. A*, vol. 375–377, pp. 46–52, Jul. 2004, doi: 10.1016/j.msea.2003.10.214.
- [58] P. Kumar, M. Kawasaki, and T. G. Langdon, “Review: Overcoming the paradox of strength and ductility in ultrafine-grained materials at low temperatures,” *J. Mater. Sci.*, vol. 51, no. 1, pp. 7–18, Jan. 2016, doi: 10.1007/s10853-015-9143-5.
- [59] P. Luo, D. T. McDonald, S. Palanisamy, M. S. Dargusch, and K. Xia, “Ultrafine-grained pure Ti recycled by equal channel angular pressing with high strength and good ductility,” *J. Mater. Process. Technol.*, vol. 213, no. 3, pp. 469–476, Mar. 2013, doi: 10.1016/j.jmatprotec.2012.10.016.
- [60] G. I. Raab, A. V. Polyakov, D. V. Gunderov, and R. Z. Valiev, “Formation of a nanostructure and properties of titanium rods during equal-channel angular pressing CONFORM followed by drawing,” *Russ. Metall.*, vol. 2009, no. 5, pp. 416–420, 2009, doi: 10.1134/S0036029509050097.
- [61] W. J. Kim and H. T. Jeong, “Grain-size strengthening in equal-channel-angular-pressing processed AZ31 Mg alloys with a constant texture,” *Mater. Trans.*, vol. 46, no. 2, pp. 251–258, 2005, doi: 10.2320/matertrans.46.251.

- [62] A. Rosochowski, M. Rosochowska, and L. Olejnik, “Severe plastic deformation by incremental angular splitting,” *J. Mater. Sci.*, vol. 48, no. 13, pp. 4557–4562, Jul. 2013, doi: 10.1007/s10853-012-7108-5.
- [63] S. H. Whang, “Introduction,” in *Nanostructured Metals and Alloys*, Elsevier, 2011, pp. xxi–xxxv.
- [64] P. Luo, D. T. McDonald, W. Xu, S. Palanisamy, M. S. Dargusch, and K. Xia, “A modified Hall-Petch relationship in ultrafine-grained titanium recycled from chips by equal channel angular pressing,” *Scr. Mater.*, vol. 66, no. 10, pp. 785–788, 2012, doi: 10.1016/j.scriptamat.2012.02.008.
- [65] J. Palán, T. Kubina, and P. Motyčka, “The effect of annealing on mechanical and structural properties of UFG titanium grade 2,” *IOP Conf. Ser. Mater. Sci. Eng.*, vol. 179, p. 012055, Feb. 2017, doi: 10.1088/1757-899X/179/1/012055.
- [66] V. V. Stolyarov, Y. T. Zhu, T. C. Lowe, and R. Z. Valiev, “Microstructure and properties of pure Ti processed by ECAP and cold extrusion,” *Mater. Sci. Eng. A*, vol. 303, no. 1–2, pp. 82–89, 2001, doi: 10.1016/S0921-5093(00)01884-0.
- [67] J. Kawalko *et al.*, “Microstructure of titanium on complex deformation paths: Comparison of ECAP, KOBO and HE techniques,” *Mater. Charact.*, vol. 141, pp. 19–31, Jul. 2018, doi: 10.1016/j.matchar.2018.04.037.
- [68] V. V. Stolyarov, I. V. Alexandrov, R. Z. Valiev, Y. T. Zhu, and T. C. Lowe, “Grain refinement and properties of pure Ti processed by warm ECAP and cold rolling,” *Mater. Sci. Eng. A*, vol. 343, no. 1–2, pp. 43–50, 2003, doi: 10.1016/S0921-5093(02)00366-0.
- [69] C. Xu, S. Schroeder, P. B. Berbon, and T. G. Langdon, “Principles of ECAP-Conform as a continuous process for achieving grain refinement: Application to an aluminum alloy,” *Acta Mater.*, vol. 58, no. 4, pp. 1379–1386, 2010, doi: 10.1016/j.actamat.2009.10.044.
- [70] G. J. Raab, R. Z. Valiev, T. C. Lowe, and Y. T. Zhu, “Continuous processing of ultrafine grained Al by ECAP-Conform,” *Mater. Sci. Eng. A*, vol. 382, no. 1–2, pp. 30–34, 2004, doi: 10.1016/j.msea.2004.04.021.
- [71] W. Cheng, L. Tian, S. Ma, Y. Bai, and H. Wang, “Influence of Equal Channel Angular Pressing Passes on the Microstructures and Tensile Properties of Mg-8Sn-6Zn-2Al Alloy,” *Materials (Basel)*, vol. 10, no. 7, p. 708, Jun. 2017, doi: 10.3390/ma10070708.
- [72] Y. Qi, I. B. Timokhina, A. Shekhter, K. Sharp, and R. Lapovok, “Optimization of upcycling of Ti-6Al-4V swarf,” *J. Mater. Process. Technol.*, vol. 255, pp. 853–864, May

- 2018, doi: 10.1016/j.jmatprotec.2018.01.036.
- [73] D. V. Gunderov *et al.*, “Evolution of microstructure, macrotexture and mechanical properties of commercially pure Ti during ECAP-conform processing and drawing,” *Mater. Sci. Eng. A*, vol. 562, pp. 128–136, 2013, doi: 10.1016/j.msea.2012.11.007.
- [74] C. Etherington, “Conform—A New Concept for the Continuous Extrusion Forming of Metals,” *J. Eng. Ind.*, pp. 893–900, 1974, doi: 10.1115/1.3438458.
- [75] C. Etherington, “Conform and the recycling of non-ferrous scrap metals,” *Conserv. Recycl.*, vol. 2, no. 1, pp. 19–29, 1978, doi: 10.1016/0361-3658(78)90025-5.
- [76] J. A. Pardoe, “‘ Conform ’ Continuous Extrusion of Metal Powders into Products for Electrical Industry : Development Experience,” *Powder Metall.*, no. October, pp. 22–28, 1979, doi: 10.1179/pom.1979.22.1.22.
- [77] J. A. Pardoe, “CONFORM continous extrusion process - its contribution to energy conservation,” *Met. Soc.*, vol. 11, no. 1, pp. 358–365, 1984, doi: 10.1179/030716984803275025.
- [78] B. Ltd., “Brochure.” <https://bwe.co.uk/brochure/>.
- [79] J. R. Dawson, “Conform technology for cost effective manufacture of copper strip,” 2006. [Online]. Available: papers3://publication/uuid/ABDF052C-9DAF-4233-8948-801223CD100D.
- [80] T. Tonogi, K. Okazato, and S. Tsukada, “Precise Extrusion Technology by Conform Process for Irregular Sectional Copper.,” *Hitachi Cable Rev*, vol. 21, no. 21, pp. 77–82, 2002, [Online]. Available: <http://sciencelinks.jp/j-east/article/200305/000020030503A0064744.php%5Cnpapers3://publication/uuid/4CFDF27B-712D-4E75-896A-62C154E3501B>.
- [81] D. J. Marsh, “Extrusion of Copper by the Conform Continuous Extrusion Process,” pp. 77–83, 1977, [Online]. Available: papers3://publication/uuid/F017C8E9-F8A6-4227-B81E-AC4B93C66F25.
- [82] M. Duchek, T. Kubina, J. Hodek, and J. Dlouhy, “Development of the production of ultrafine-grained titanium with the conform equipment,” *Mater. Tehnol.*, vol. 47, no. 4, pp. 515–518, 2013.
- [83] T. Kubina, J. Dlouhý, and M. Köver, “Preparation and thermal stability of ultra-fine and nano-grained commercially pure titanium wires using CONFORM equipment,” *Mater. Tehnol.*, vol. 49, no. 2, pp. 213–217, Apr. 2015, doi: 10.17222/mit.2013.226.
- [84] J. Palán, R. Procházka, and M. Zemko, “The microstructure and mechanical properties

- evaluation of UFG Titanium Grade 4 in relation to the technological aspects of the CONFORM SPD process,” *Procedia Eng.*, vol. 207, pp. 1439–1444, 2017, doi: 10.1016/j.proeng.2017.10.910.
- [85] R. L. Kegg, “Mechanics of the Rotary Swaging Process,” *J. Eng. Ind.*, vol. 86, no. 4, pp. 317–324, Nov. 1964, doi: 10.1115/1.3670548.
- [86] Y. Estrin, R. Lapovok, A. E. Medvedev, C. Kasper, E. Ivanova, and T. C. Lowe, “Mechanical performance and cell response of pure titanium with ultrafine-grained structure produced by severe plastic deformation,” in *Titanium in Medical and Dental Applications*, Elsevier, 2018, pp. 419–454.
- [87] R. Z. Valiev and T. G. Langdon, “The Art and Science of Tailoring Materials by Nanostructuring for Advanced Properties Using SPD Techniques,” *Adv. Eng. Mater.*, vol. 12, no. 8, pp. 677–691, Aug. 2010, doi: 10.1002/adem.201000019.
- [88] Y. He, F. Gao, B. Song, J. Li, R. Fu, and G. Wu, “Production of very fine grained Mg-3%Al-1%Zn alloy by continuous extrusion forming (CONFORM),” *Adv. Eng. Mater.*, vol. 12, no. 9, pp. 843–847, 2010, doi: 10.1002/adem.201000007.
- [89] R. Wilson, “Extrusion of high temperature formable non-ferrous metals,” WO 2012/119196 A1, 2012.
- [90] B. Thomas, “Continuous extrusion of commercially pure titanium powder,” University of Sheffield, 2015.
- [91] A. Barcellona, L. Cannizzaro, and R. Riccobono, “The Continuous Extrusion Process CONFORM: a full 3D Thermal and Mechanical Analysis,” in *Proceedings of the 33rd International MATADOR Conference*, London: Springer London, 2000, pp. 353–358.
- [92] G. Shimov, A. Bogatov, and D. Kovin, “Fem simulation of copper busbar pressing on the continuous extrusion line"conform",” *Solid State Phenom.*, vol. 284 SSP, pp. 547–551, 2018, doi: 10.4028/www.scientific.net/SSP.284.547.
- [93] T. Reinikainen, K. Andersson, S. Kivivuori, and A. S. Korhonen, “Finite-element analysis of copper extrusion processes,” *J. Mater. Process. Technol.*, vol. 34, no. 1–4, pp. 101–108, Sep. 1992, doi: 10.1016/0924-0136(92)90095-A.
- [94] S. Shamsudin, M. Lajis, and Z. W. Zhong, “Evolutionary in Solid State Recycling Techniques of Aluminium: A review,” *Procedia CIRP*, vol. 40, pp. 256–261, 2016, doi: 10.1016/j.procir.2016.01.117.
- [95] G. Lutjering and J. C. Williams, *Titanium*. .
- [96] H. M. Beakawi Al-Hashemi and O. S. Baghabra Al-Amoudi, “A review on the angle of

- repose of granular materials,” *Powder Technol.*, vol. 330, pp. 397–417, May 2018, doi: 10.1016/j.powtec.2018.02.003.
- [97] M. Krantz, H. Zhang, and J. Zhu, “Characterization of powder flow: Static and dynamic testing,” *Powder Technol.*, vol. 194, no. 3, pp. 239–245, 2009, doi: 10.1016/j.powtec.2009.05.001.
- [98] V. V. Artamonov, A. O. Bykov, P. O. Bykov, and V. P. Artamonov, “Measurement of the tap density of metal powders,” *Powder Metall. Met. Ceram.*, vol. 52, no. 3–4, pp. 237–239, Jul. 2013, doi: 10.1007/s11106-013-9518-6.
- [99] J. F. Carr and D. M. Walker, “An annular shear cell for granular materials,” *Powder Technol.*, vol. 1, no. 6, pp. 369–373, Apr. 1968, doi: 10.1016/0032-5910(68)80019-1.
- [100] J. Schwedes and D. Schulze, “Measurement of flow properties of bulk solids,” *Powder Technol.*, vol. 61, no. 1, pp. 59–68, Apr. 1990, doi: 10.1016/0032-5910(90)80066-8.
- [101] H. F. Fischmeister and E. Arzt, “Densification of Powders by Particle Deformation,” *Powder Metall.*, vol. 26, no. 2, pp. 82–88, Jan. 1983, doi: 10.1179/pom.1983.26.2.82.
- [102] A. R. Khoei, “APPLICATION OF CAP PLASTICITY MODELS,” in *Computational Plasticity in Powder Forming Processes*, Elsevier, 2005, pp. 128–174.
- [103] A. R. Khoei, “INTRODUCTION,” in *Computational Plasticity in Powder Forming Processes*, Elsevier, 2005, pp. 1–18.
- [104] M. Qian and G. B. Schaffer, “Sintering of aluminium and its alloys,” in *Sintering of Advanced Materials*, Elsevier, 2010, pp. 291–323.
- [105] J. Tomas, “Fundamentals of cohesive powder consolidation and flow,” *Granul. Matter*, vol. 6, no. 2–3, pp. 75–86, Oct. 2004, doi: 10.1007/s10035-004-0167-9.
- [106] E. Arzt, “The influence of an increasing particle coordination on the densification of spherical powders,” *Acta Metall.*, vol. 30, no. 10, pp. 1883–1890, Oct. 1982, doi: 10.1016/0001-6160(82)90028-1.
- [107] S. Kondo, Y. Kume, M. Kobashi, and N. Kanetake, “Densification Behavior of Different Metal Powders by Compression and Shear Combined Loading,” *Procedia Eng.*, vol. 81, pp. 1175–1179, 2014, doi: 10.1016/j.proeng.2014.10.284.
- [108] M. Blackmore, “Strain Path Effects on Timetal 834 Under Hot Working Conditions,” University of Sheffield, 2009.
- [109] V. P. Severdenko and V. Z. Zhilkin, “Heat treatment in drawing of titanium wire,” *Met. Sci. Heat Treat. Met.*, vol. 1, no. 10, pp. 21–24, 1959, doi: 10.1007/BF00811658.
- [110] W. W. Milligan, “Mechanical Behavior of Bulk Nanocrystalline and Ultrafine-grain

- Metals,” in *Comprehensive Structural Integrity*, Elsevier, 2003, pp. 529–550.
- [111] M. Szymula, K. Muszka, J. Majta, M. Paćko, and J. Dybich, “Study of the effect of Accumulative Angular Drawing deformation route on grain refinement in 304L stainless steel,” *Procedia Manuf.*, vol. 50, pp. 350–354, 2020, doi: 10.1016/j.promfg.2020.08.065.
- [112] K. Muszka, L. Madej, and J. Majta, “The effects of deformation and microstructure inhomogeneities in the Accumulative Angular Drawing (AAD),” *Mater. Sci. Eng. A*, vol. 574, pp. 68–74, Jul. 2013, doi: 10.1016/j.msea.2013.03.024.
- [113] S. W. Williams, F. Martina, A. C. Addison, J. Ding, G. Pardal, and P. Colegrove, “Wire+Arc Additive Manufacturing,” *Mater. Sci. Technol.*, p. 1743284715Y.000, 2015, doi: 10.1179/1743284715Y.0000000073.
- [114] J. W. Elmer and G. Gibbs, “The effect of atmosphere on the composition of wire arc additive manufactured metal components,” *Sci. Technol. Weld. Join.*, vol. 24, no. 5, pp. 367–374, Jul. 2019, doi: 10.1080/13621718.2019.1605473.
- [115] A. K. Sachdev, K. Kulkarni, Z. Z. Fang, R. Yang, and V. Girshov, “Titanium for automotive applications: Challenges and opportunities in materials and processing,” *JOM*, vol. 64, no. 5, pp. 553–565, 2012, doi: 10.1007/s11837-012-0310-8.
- [116] Y. Kosaka, S. P. Fox, and K. Faller, “Recent developments of titanium and its alloys in automotive and motorcycle applications,” *Ti-2007*, pp. 1383–1386, 2007, [Online]. Available: papers3://publication/uuid/63F7088C-8146-4DE8-BA49-DFBDF59271C.
- [117] M. Jackson and R. R. Boyer, “Titanium and its Alloys: Processing, Fabrication and Mechanical Performance,” *Encycl. Aerosp. Eng.*, 2010, doi: 10.1002/9780470686652.eae199.
- [118] H. M. Flower, *High Performance Materials in Aerospace*. 2011.
- [119] B. A. Szost *et al.*, “A comparative study of additive manufacturing techniques: Residual stress and microstructural analysis of CLAD and WAAM printed Ti-6Al-4V components,” *Mater. Des.*, vol. 89, pp. 559–567, 2016, doi: 10.1016/j.matdes.2015.09.115.
- [120] H. Miura, “Direct laser forming of titanium alloy powders for medical and aerospace applications,” *KONA Powder Part. J.*, no. 32, pp. 253–263, 2015, doi: 10.14356/kona.2015017.
- [121] O. Yilmaz and A. A. Uglá, “Shaped metal deposition technique in additive manufacturing: A review,” *Proc. Inst. Mech. Eng. Part B J. Eng. Manuf.*, vol. 230, no.

- 10, pp. 1781–1798, 2016, doi: 10.1177/0954405416640181.
- [122] D. A. Hollander *et al.*, “Structural, mechanical and in vitro characterization of individually structured Ti-6Al-4V produced by direct laser forming,” *Biomaterials*, vol. 27, no. 7, pp. 955–963, 2006, doi: 10.1016/j.biomaterials.2005.07.041.
- [123] S. Leuders *et al.*, “On the mechanical behaviour of titanium alloy TiAl6V4 manufactured by selective laser melting: Fatigue resistance and crack growth performance,” *Int. J. Fatigue*, vol. 48, pp. 300–307, 2013, doi: 10.1016/j.ijfatigue.2012.11.011.
- [124] R. Baker, “Method of Making Decorative Articles,” 1 533 300, 1920.
- [125] D. Ding, Z. Pan, D. Cuiuri, and H. Li, “Wire-feed additive manufacturing of metal components: technologies, developments and future interests,” *Int. J. Adv. Manuf. Technol.*, vol. 81, no. 1–4, pp. 465–481, Oct. 2015, doi: 10.1007/s00170-015-7077-3.
- [126] S. Katsas, R. Dashwood, G. Todd, M. Jackson, and R. Grimes, “Characterisation of Conform™ and conventionally extruded Al-4Mg-1Zr. Effect of extrusion route on superplasticity,” *J. Mater. Sci.*, vol. 45, no. 15, pp. 4188–4195, 2010, doi: 10.1007/s10853-010-4513-5.
- [127] J. A. Slotwinski, E. J. Garboczi, P. E. Stutzman, C. F. Ferraris, S. S. Watson, and M. A. Peltz, “Characterization of Metal Powders Used for Additive Manufacturing,” *J. Res. Natl. Inst. Stand. Technol.*, vol. 119, p. 460, Oct. 2014, doi: 10.6028/jres.119.018.
- [128] A. Mullis, “the Physical Mechanism Formelt Pulsation During Close-Coupled Atomization,” *At. Sprays*, vol. 29, no. 2, pp. 143–159, 2019, doi: 10.1615/atomizspr.2019030110.
- [129] P. Sun, Z. Z. Fang, Y. Zhang, and Y. Xia, “Review of the methods for production of spherical Ti and Ti alloy powder,” *J. Mater.*, vol. 69, no. 10, pp. 1853–1860, 2017.
- [130] J. Dawes, R. Bowerman, and R. Trepleton, “Introduction to the Additive Manufacturing Powder Metallurgy Supply Chain,” *Johnson Matthey Technol. Rev.*, vol. 59, no. 3, pp. 243–256, Jul. 2015, doi: 10.1595/205651315X688686.
- [131] C. Hoyle, “Critical Capabilities,” *Flight International*, 2019. <https://finreader.flightglobal.com/publications-dist/1263/7943/2708/31204/article.html>.
- [132] T. Childerhouse and M. Jackson, “Near Net Shape Manufacture of Titanium Alloy Components from Powder and Wire: A Review of State-of-the-Art Process Routes,” *Metals (Basel)*, vol. 9, no. 6, p. 689, Jun. 2019, doi: 10.3390/met9060689.
- [133] M. Furukawa, Z. Horita, M. Nemoto, and T. G. Langdon, “Processing of metals by

- equal-channel angular pressing,” *J. Mater. Sci.*, vol. 36, no. 12, pp. 2835–2843, 2001, doi: 10.1023/A:1017932417043.
- [134] N. Llorca-Isern, T. Grosdidier, and J. M. Cabrera, “Enhancing Ductility of ECAP Processed Metals,” *Mater. Sci. Forum*, vol. 654–656, pp. 1219–1222, Jun. 2010, doi: 10.4028/www.scientific.net/MSF.654-656.1219.
- [135] S. C. Yoon, S. I. Hong, S. H. Hong, and H. S. Kim, “Densification and conolidation of powders by equal channel angular pressing,” *Mater. Sci. Forum*, vol. 534–536, no. PART 1, pp. 253–256, 2007, doi: 10.4028/www.scientific.net/MSF.534-536.253.
- [136] R. D. Haghighi, S. A. J. Jahromi, A. Moresedgh, and M. T. Khorshid, “A Comparison Between ECAP and Conventional Extrusion for Consolidation of Aluminum Metal Matrix Composite,” *J. Mater. Eng. Perform.*, vol. 21, no. 9, pp. 1885–1892, Sep. 2012, doi: 10.1007/s11665-011-0108-9.
- [137] L. Olejnik and A. Rosochowski, “Scaled-up ecap with enhanced productivity,” *Steel Res. Int.*, vol. 79, no. 2, pp. 439–446, 2008.
- [138] H. Zhao, Y. Ren, B. Yang, and G. Qin, “Microstructural evolution of equal channel angular drawn purity titanium at room temperature,” *J. Alloys Compd.*, vol. 811, p. 152002, Nov. 2019, doi: 10.1016/j.jallcom.2019.152002.
- [139] Y. Yagi, T. Yukawa, and H. Kusamichi, “Characteristics of Work Hardening and Anneal Softening of Titanium Base Ti-Al Alloy Wires,” *J. Japan Inst. Met. Japan Inst. Met. Mater.*, vol. 21, no. 5, pp. 360–363, 1957, doi: 10.2320/jinstmet1952.21.5_360.

Appendix 1: Recycling of Titanium Alloy Powders and Swarf through Continuous Extrusion (Conform™) into Affordable Wire for Additive Manufacturing

This chapter includes a published paper written during the course of the project. The format of the chapter will be as the paper was written but formatted in the style of the thesis, rather than the journal. The paper [7]: S.A. Smythe, B. Thomas and M. Jackson (2020), Recycling of Titanium Alloy Powders and Swarf through Continuous Extrusion (Conform™) into Affordable Wire for Additive Manufacturing, *Metals*, 10(6), p. 843 (<http://doi.org/10.3390/met10060843>).

11.1 Abstract

Over the last 20 years, there has been growing research and development investment to exploit the benefits of wire deposition additive manufacturing (AM) for the production of near-net shape components in aircraft and space applications. The wire feedstock for these processes is a significant part of the overall process costs, especially for high value materials such as alloyed titanium. Powders for powder-based AM have tight specifications regarding size and morphology, which results in a significant amount of waste during the powder production. In the aerospace sector, up to 95% of forged billet can be machined away, and with increasing aircraft orders, stockpiles of such machining swarf are increasing. In this study, the continuous extrusion process – Conform™ – is employed to consolidate waste titanium alloy feedstocks in the forms of gas atomised powder and machining swarf into wire. Samples of wire were further cold drawn down to 40% reduction using conventional wire drawing equipment. As close to 100% of the waste powder can be converted to wire using the Conform™ process. This technology offers an attractive addition to the circular economy for manufacturers and with further development could be an important addition as industries move towards more sustainable supply chains.

11.2 Keywords

solid-state processing, wire drawing, direct energy deposition, waste recycling

11.3 Introduction

In recent years, there has been significant attention on the use of powder based additive manufacturing in the production of components in the aerospace, medical and automotive sectors. The ability to produce near-net shape components, at a faster rate and with less material waste is a clear advantage of these processes, however, they require high quality, spherical powders [127] to produce high quality components. An increase in powder production to supply the AM sector comes with the inevitable generation of unusable waste material. Typically, this relates to powders which are non-spherical, too small/large for the process, or it has already been AM processed and therefore cannot be reused due to an increase in interstitial elements such as oxygen and nitrogen. Examples of the size ranges required for various AM processes, compared to other powder metallurgy routes and to typical gas atomized (GA) powder sizes [29], are shown in Figure 90. In the case of gas atomisation, up to 65% of the powder [128] could be out of specification for powder based additive manufacturing processes. Many AM powder producers are stockpiling powder and need alternative recycling options in order to make AM processes more sustainable.

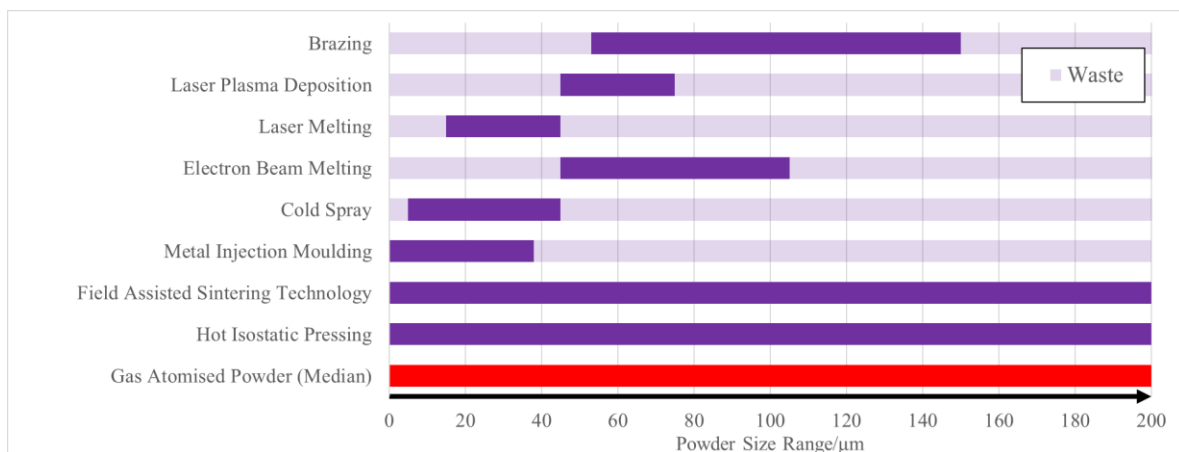


Figure 90 Examples of powder size ranges in powder metallurgy processes. Reproduced from [29], [129], [130]

One of the most desirable materials for use in AM is titanium. This is because near-net-shape components produced via AM could result in reduced costs, due to the reduction in the amount of wasted material: up to 95% of a forged billet can be machined off during the production of aerospace components [131]. In summary, AM is beneficial in that it can produce

high quality, near-net shape components at a much improved buy-to-fly ratio [13]. The increase in waste material from the production of powders specifically required for AM processes is a potential issue that could be mitigated through recycling and the use of wire deposition additive processes, such near net shape manufacturing processes for titanium were reviewed in Ref [132].

Recycling titanium waste is a common practice but it is not reverted to high performance products due to its strong affinity to embrittling interstitial elements, lack of cleanliness and the high chance for contamination with high density inclusions. Current recycling processes include additions in the form of lumps of cored wire into steelmaking, where any contamination can be reduced by the steelmaking processes. More novel methods utilise severe plastic deformation (SPD) to produce a higher quality material from the waste, that can be produced at a low cost. One such example is equal-channel angular pressing (ECAP). ECAP is an SPD process that takes a solid metal billet and forces it through a 90° channel in the ECAP die [133]. The resulting material has been reported to have improved hardness and strength than those produced using traditional methods such as forging and extrusion [134]. There have been examples of ECAP where the feedstocks have been particulate, rather than a solid billet, allowing for the recycling of waste [135], [136]. Despite this, one of the largest drawbacks of ECAP is that it is a batch process and can only be operated on small samples [137], which reduces the attractiveness of the process on industrial scales. Recently, it has been demonstrated that titanium alloy swarf can be recycled and fully consolidated into near net shapes using the emerging solid-state FAST-*forge* process [31].

This paper describes a solid-state method for consolidating out-of-specification titanium powders and waste swarf titanium directly into wire, which after subsequent wire drawing could be used in metal wire deposition AM processes or as a consumable filler wire in fusion welding, such as tungsten inert gas (TIG) welding. For wire deposition AM technologies, a major mechanical property requirement is wire ductility that permits the feedstock to be coiled and unwound without fracturing.

The direct consolidation, solid state continuous process – ConformTM – was first developed by Green for the UKAEA (United Kingdom Atomic Energy Authority) in Preston, UK in the early 1970s and has been in use since [1], [74]. It was invented to recycle electrical components

from waste aluminium and copper electrical conductors. Research into the ConformTM process has recently turned towards the use of both titanium and powder feedstocks. Palan et al. [4], [84] have reported ultra-fine grained commercially pure titanium wire produced through multiple pass ConformTM, coupled with rotary swaging. Wilson et al. [89] attempted to use ConformTM to produce titanium alloy wire from powders at 900°C in an argon atmosphere. The main drawback is that an inert atmosphere is expensive to implement and use. For the ConformTM process there has been no evidence to date to suggest that an inert atmosphere for feedstocks increase the product quality. The heating of the powder is also an additional step that may be unnecessary to the process; as the process increases pressure and heat through friction, the preheating of the material would be obsolete. Work at The University of Sheffield with commercially pure titanium (CP-Ti) hydride-dehydride (HDH) powder [3] demonstrated successful ConformTM extrusion without the need for feedstock preheating or an inert atmosphere.

Knowledge of how particulate materials are processed through a ConformTM machine is still an immature field when compared to conventional metalworking processes. It has been suggested that powder particles are sheared in the grip region of the wheel groove, which then generates the heat and pressure for the particles to weld together and material to be extruded. This process is a continuous extrusion process and follows a similar layout, as shown in Figure 91. The powder is fed into the groove of the wheel at its apex. As the wheel rotates, the particulate feedstock flows into the groove until it meets the abutment tool, which protrudes into the groove. As more powder is processed, it heats up through the inter-particle friction, adiabatic heating of compressed particles and conduction from the tooling. This causes the titanium alloy particles to soften and deform, increasing the density of material above the abutment. Once the pressure and temperature are high enough, the material is extruded through a shaped die positioned radially to the wheel. Although it could be assumed that the continuous nature of the process means that a steady state is achieved, it is entirely feasible that this may not be the case.

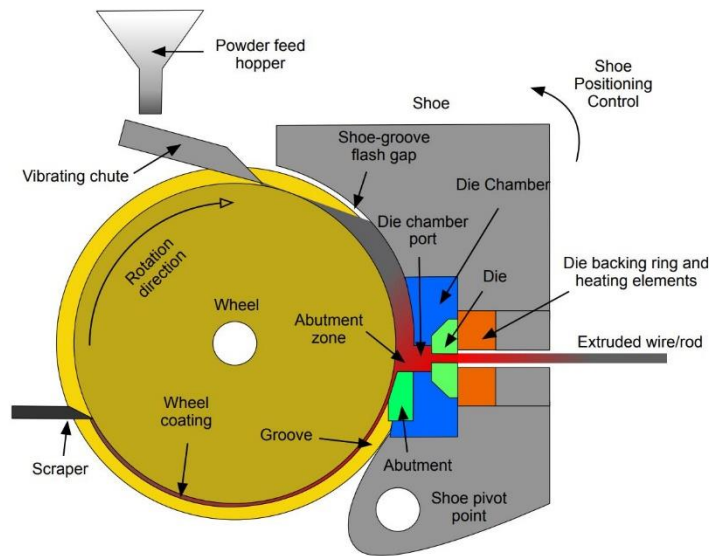


Figure 91 Schematic of a Conform™ machine used to consolidate powder directly into wire.

Conform™ is often found coupled with ECAP in the literature [69] and the combination of the two methods allows for an increase in the productivity of the ECAP process. However, it is possible to use Conform™ as a standalone process and therefore, it is advantageous over processes such as ECAP, as it is continuous, can be used with a vast array of feedstocks and can produce ultra-fine grained material. Ultimately, the Conform™ process is a disruptive technology as it is a potential recycling process that would result in a high-quality wire for laser metal AM or welding processes. Currently, the production of conventional titanium wire is an expensive, multi-step, batch process involving: the Kroll extraction process (titanium sponge), vacuum arc melting, multi-step rolling and drawing, as highlighted in Figure 92. Conform is a disruptive technology, in that it provides a single-step continuous process for recycling waste from gas atomisation, the machining of forged billets (swarf) and additive manufacturing.

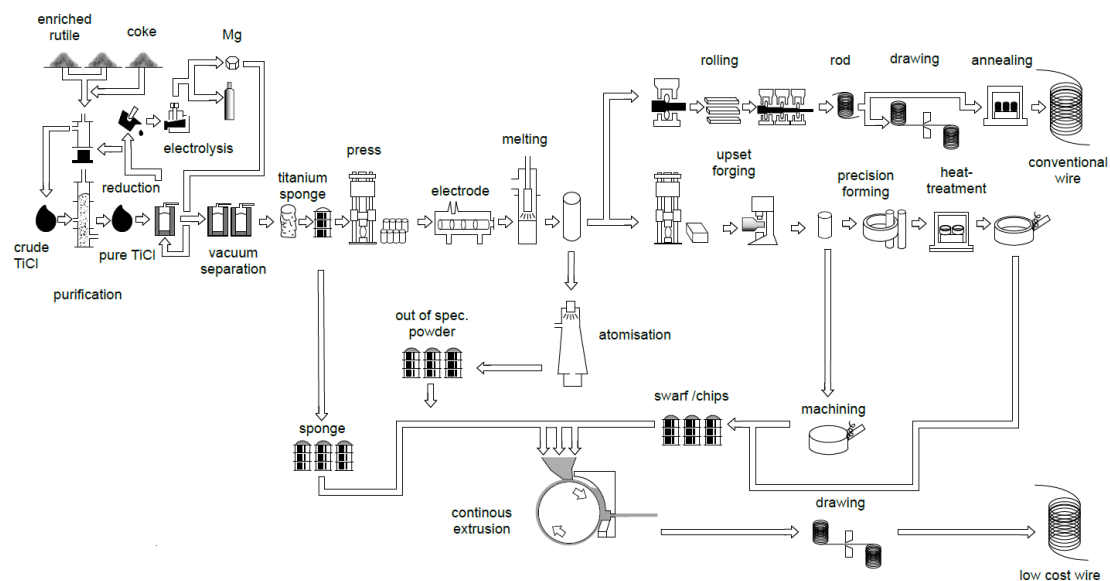


Figure 92 Schematic demonstrating the various wire production routes commonly used and the potential feedstocks identified for investigation into low-cost wire production using the disruptive technology of Conform™.

The aim of this paper is to outline the process and parameters used to consolidate oversized gas atomised Ti-6Al-4V (GA), CP-Ti HDH and machining swarf waste into wire using Conform™. Furthermore, in the case of CP-Ti HDH especially, additional cold wire drawing could produce affordable, wire feedstock for fusion welding processes and direct energy deposition AM processes.

11.4 Materials and Methods

11.4.1 Powder Characteristics

Three materials were used during this work; grade 2 commercially pure titanium hydride-dehydride (CP-Ti Gr 2 HDH) powder with a 45 – 150 µm size fraction from Phelly Materials Inc., USA, Ti-6Al-4V gas atomised (GA) powder with a size fraction of 67 – 750 µm from Puris LCC, USA and Ti-6Al-4V (ASTM Grade 5) machining swarf from Airbus, St Eloi, Toulouse, France. The Ti-6Al-4V GA powder was made up from three different sieve fractions remaining from previous batches of powder from additive manufacturing collaborators, which was then reblended into a single batch. All of these recycled sieve fractions were from the same

original atomisation batch. The material was used as received, with any cleaning completed by the suppliers using proprietary cleaning methods. Oxygen analysis via inert gas fusion was provided by the Ti-6Al-4V GA supplier, 0.15 ± 0.02 %. The CP-Ti Gr 2 HDH powder was also found through inert gas fusion by the supplier, Phelly Materials Inc. and found to be between 0.14% and 0.20%.

The size ranges of the powder were determined via laser scattering using a Malvern MasterSizer 3000 and estimated by sieving the swarf. The morphology of the powder was determined from SEM and light microscopy.

CP-Ti Gr 2 HDH, has an irregular and angular morphology, due to the hydride-dehydride process where the metal is mechanically crushed into a powder. The Ti-6Al-4V GA powder contains primarily spherical particles from the gas atomisation process with a high percentage, also observed to have attached satellite particles. The particle size distributions for the feedstocks are given in Figure 93. The swarf was of various sizes, in both length and width, ranging from 0.3-1.0 mm in thickness, through to 10 mm in length with some curvature to the structure typical of material generated through machining processes.

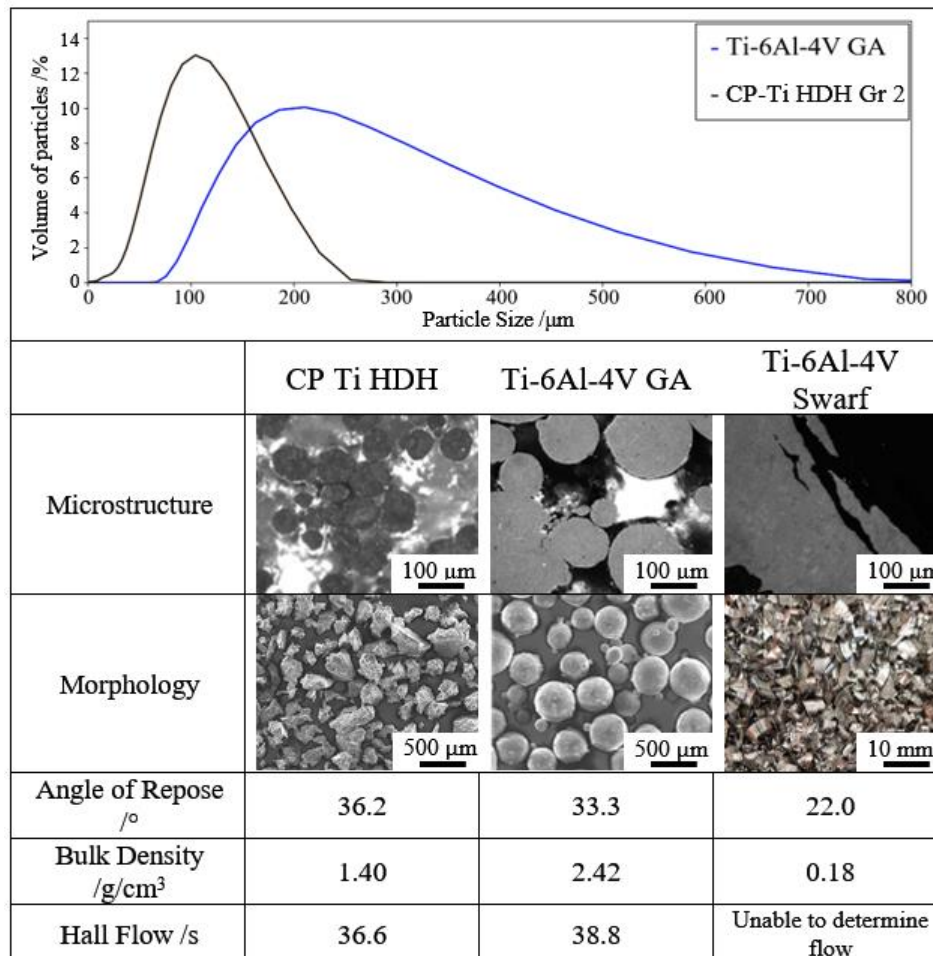


Figure 93 Summary of particle characteristics for titanium alloy feedstocks used in this study. No particle size distribution was recorded for the swarf owing to a lack of valid techniques for determining this.

11.4.2 Conform Extrusion

A BWE ConformTM 350i machine situated at BWE Ltd, Ashford, UK was used for the trial extrusions (Figure 94). Bespoke tooling was designed specifically for the processing of titanium powders based on theoretical calculations by Thomas [90]. The primary reason for different tool dimensions was to account for the larger particle size of the machining swarf, to allow sufficient material to be fed effectively into the wheel groove. The key geometry parameters are listed in Table 12 and are scaled from conventional BWE tool geometries. Abutment materials were chosen for their high hot strength following previous extrusion trials conducted by Thomas et al. [3], where StelliteTM abutments were used. While an extremely hard material, StelliteTM can be brittle and abutments made from this can fracture early in the process, preventing successful extrusion from titanium powders. In the case of softer, weaker

metals such as aluminium and copper, Stellite™ and cheaper tool materials can be used effectively. For the extrusion of titanium in this study, abutments were machined from more exotic materials.

The die and die chamber were preheated to 500°C, but the wheel was not preheated, as it was believed that the heat generated from friction between the feedstock and tooling during the Conform™ process was sufficient to heat the wheel during the initial stages of the trial. Typically, the temperature at the abutment face furthest away from the feedstock can increase to a temperature between 600°C to 900°C. The as-received powders/swarf were manually poured into a vibrating chute at the top of the wheel where it was conveyed into a groove. The powder feed was moderated according to the observed extrusion pressure, as determined from the current draw by the machine's drive motor.

It is worth noting that this process was conducted without the preheating of powder/particulate feedstock and without inert gas shielding.

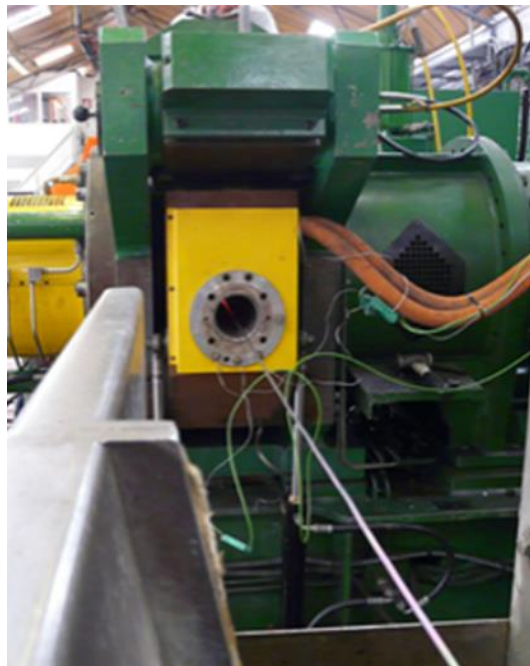


Figure 94 Photograph of the titanium alloy wire being extruded from the Conform™ machine. The wire glows white/red as it emerges from the back of the extrusion die in the centre of the photograph.

Table 12 Geometries of the tooling used in the trials and the abutment materials used.

| Trial Feedstock | Abutment Material | Abutment dimensions (l x w) /mm | Wheel Groove (h x l) /mm | Die Diameter /mm |
|-----------------|-------------------------|---------------------------------|--------------------------|------------------|
| Ti-6Al-4V GA | W-26 wt.% Re-2 wt.% HfC | 10.0 x 12.0 | 11.0 x 13.0 | 6.00 |
| Ti-6Al-4V Swarf | Inconel 718 | 14.0 x 14.0 | 15.0 x 15.0 | 10.00 |

CP-Ti Gr 2 HDH powder was fed into the machine first and used to preheat the wheel, coat the groove and to achieve an initial build-up of pressure for extrusion without contaminating the product or prematurely abrading the tools. Previously, preliminary investigations have shown that using Ti-6Al-4V from the start of the trial resulted in tooling wear and premature abutment failure. During this heat up phase, the powder feed rate was at its highest - 0.5-1.0 kg/min - before being reduced, as the titanium wire started to extrude. The main process feedstock was added when it was determined that the extrusion was beginning to reach a steady state, as determined from measured tool temperatures and the wheel motor current. The wheel speed was kept at a constant 6 RPM for the full duration of each trial. Once clear of the die, the extruded wire was guided through a water trough for quenching. Sample 1 was extruded early in the process when the feedstock was 100% CP-Ti and sample 5 was extruded last when the feedstock was 100% Ti-6Al-4V. The samples between these points, were taken equidistantly across the length of the extruded material.

11.4.3 Cold Drawing

As-extruded CP-Ti Gr 2 HDH from the smaller toolset was cold wire drawn with the intention of performing additive manufacturing trials in the future. The dies used were 4.09, 3.50 and 3.00 mm in diameter to give an average 28% reduction for each pass. After each pass, the wire was stress-relieved at 700°C for 30 minutes without a protective atmosphere. A thin (approx. 50 µm), oxide layer formed during heat treatment aided the cold wire-drawing process, as the thin oxide layer spalled off as the wire entered the drawing die and added to the applied zinc stearate lubricant. This resulted in a bright, smooth surface finish in the final wire which can be seen in Figure 95.



Figure 95 Photograph of as-Conformed CP-Ti Gr 2 wire with blue oxide film (top) and ϕ 3.00 mm cold-wire drawn wire with bright surface (bottom) from the same extruded product.

11.4.4 Characterisation

Samples 1-5 for each trial were prepared using a standard preparation routine until a final mechanical-chemical polish with a silica/H₂O₂ suspension and the microstructure was investigated using cross-polarised light microscopy. Porosity and grain size were determined from the light micrographs using image analysis and the linear intercept method, respectively. Higher resolution microscopy was conducted using a FEI Inspect F50 scanning electron microscope in backscattered electron imaging mode. Tensile specimens were machined from the as-extruded wire and tested to failure at ambient temperature according to ASTM E8/E8M-15a. Due to the surface finish of the material, the samples were prepared with a 2.50 mm gauge diameter and a 15.00 mm gauge length. An example is shown in Figure 96. The tensile specimens were taken from the area directly adjacent to the metallographic specimens so can be assumed to have been processed under the sample conditions. It should be noted that in the case of the swarf extruded wire, the poor surface finish, which is demonstrated in Figure 97, and high curvature restricted the extraction of tensile specimens to three due to difficulties in gripping the wire during machining. Additionally, error has been determined for the results of the tensile testing and measurement of the final samples based on tensile testing errors. Microhardness was recorded in an array across the sample cross-sections (see example in Figure 97) using HV1 with a dwell time of 15 s and indents every 0.5 mm. This was conducted using a Struers DuraScan 70.

11.5 Results

The as-extruded wire has a distinctive macrostructure in its cross-section, which is particularly visible early in the process when temperatures and extrusion speeds are relatively low. Figure 8 gives an example of this structure, where two distinct areas can be identified, the inner equiaxed microstructure (Figure 98a) and the outer rings/layers (Figure 98b).

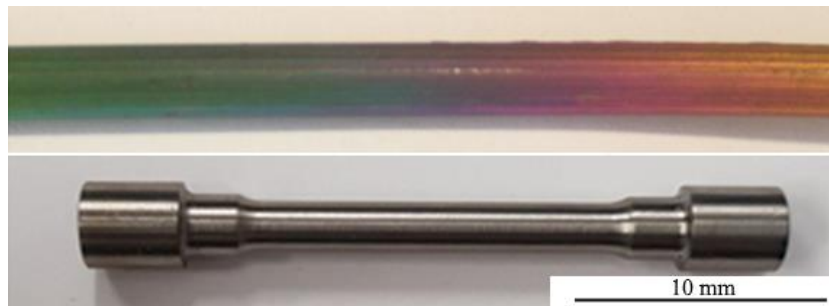


Figure 96 Photographs (at the same magnification) of as-extruded Ti-6Al-4V wire derived from GA powder with multi-coloured oxide film (top) and a sub-size tensile specimen with 15.00 mm gauge length (bottom) tested according to ASTM E8/E8M-15a.

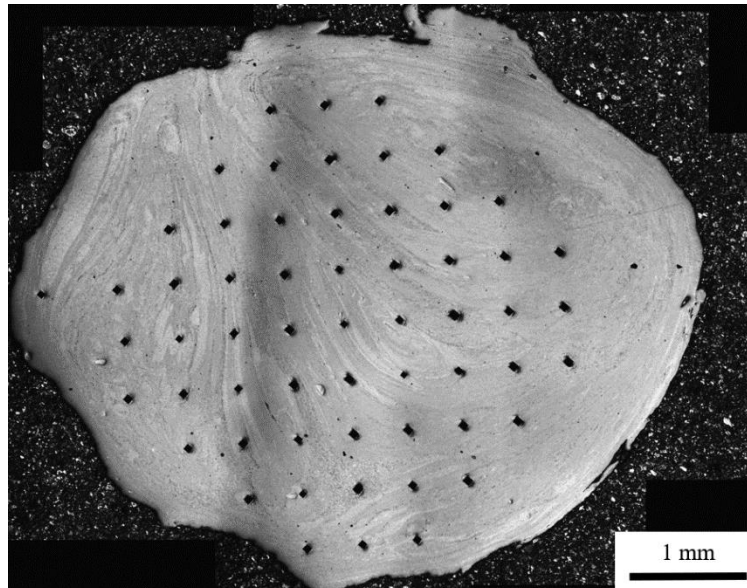


Figure 97 Polarised light micrograph of as-extruded wire from CP-Ti Gr2 HDH powder in the swarf tooling. The indents are result of microhardness testing (and correlates with the data for sample 2a in Fig 15).

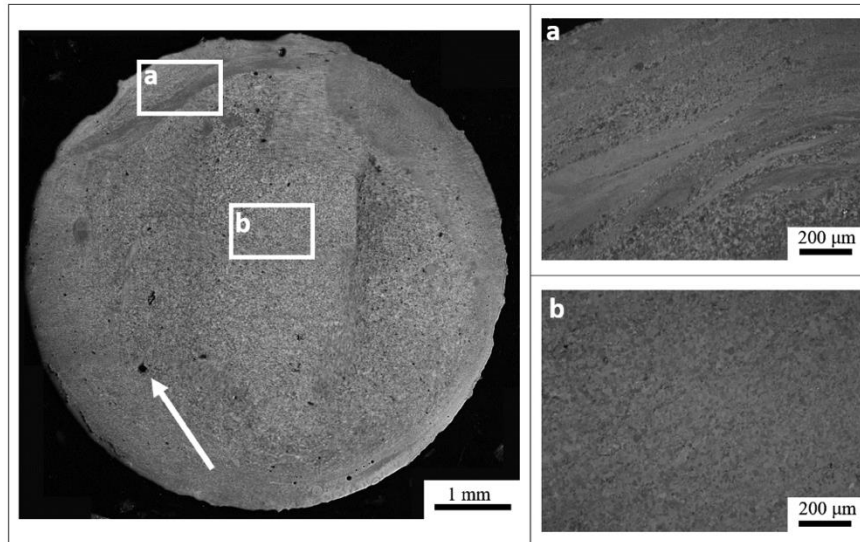


Figure 98 Polarised light micrograph of as extruded wire from Ti-6Al-4V GA powder. (a) Shows the distinct layered structure around the outside of the wire. b) A more uniform microstructure in the inner core of the wire). The arrow denotes an example of the porosity.

Previous work has shown that the viscoplastic behaviour of aluminium alloys in the region of the abutment and die in Conform™ results in flow behaviour similar to that of fluid in a pipe [2], [126]. This flow results in a shell-core structure where material moves fastest through the centre of the die creating a shear between the core and shell helping to refine the microstructure. Further evidence of this flow is observed in work completed by Etherington in 1978 [75], where a transverse-section of the rod produced from the extrusion of OFHC (oxygen-free high conductivity copper) demonstrates flow lines, much like those found in this work. This suggests that material is not necessarily extruded in the same order it entered the process. The transverse direction further demonstrates this flow structure, with evidence of flow direction as demonstrated by the wave like structure across the sample (Figure 99). This same structure is replicated in the swarf material, as can be seen in the cross-section of material shown in Figure 97.

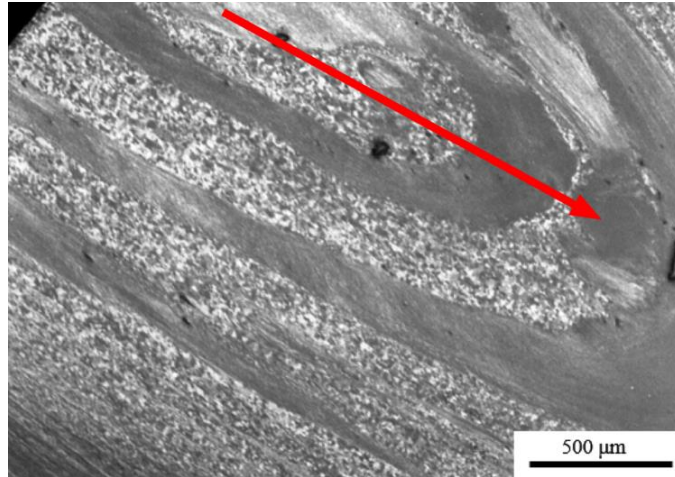


Figure 99 Cross polarised light micrograph of a transverse section of as-extruded Ti-6Al-4V GA wire. The flow direction, as indicated by the arrow is evident based on the flow lines across the material.

The evolution in grain size and porosity for the GA powder and swarf derived Ti-6Al-4V wire at different sample locations varied significantly from the initial extruded wire through to the back end of the extrusion (i.e., samples 1 through to 5, respectively). The grain sizes and porosity levels were measured from high magnification light micrographs shown in Figure 100 and plotted in Figure 101.

The initial microstructure in the Ti-6Al-4V GA wire is moderately fine-grained with average grain sizes below 20 μm (as shown in Figure 101a). There are some areas of very fine grains (2-5 μm) and others of larger 30-50 μm grains that are segregated in areas that mirror the macrostructure flow patterns seen in Figure 97. Some samples exhibit prior particle boundaries, indicating inconsistent consolidation of the powder, and these are more pronounced in samples extruded earlier in the process where temperatures and pressures are lower. As Figure 101b demonstrates, there is a small amount of porosity which could be attributed to there being insufficient pressure to fully consolidate the material early in the process. During the warm-up phase with CP-Ti powder (samples 1-3), there was a slight increase in the both the average and variance of the grain size observed in wire produced during the Ti-6Al-4V GA trial. This contrasts with wire produced early in the swarf trial, which was more homogenous with a much smaller average grain size during the early stages. Once the Ti-6Al-4V GA powder was fed into the machine (samples 4-5), the average grain size of the wire dropped sharply, primarily due to the inherent smaller initial grain size of the powder feedstock. However, it also continued to reduce as the extrusion progressed and further Ti-6Al-4V powder

was fed into the machine. A similar trend occurred once the swarf feedstock was fed into the machine, with the initial grain size at sample 4 reducing as the processed progressed to sample 5.

A single sample of wire containing the Ti-6Al-4V swarf was heat treated at 1010°C for three hours in order to qualitatively determine the degree of diffusion bonding between swarf particles and the matrix material. The microstructure of the starting material (in Figure 102a) shows a swarf particle consisting of α laths surrounded at the bottom of the micrograph by equiaxed α grains in a β matrix. The heat treatment resulted in annihilation of the α laths and production of the more homogenous equiaxed microstructure without any visible prior particle boundaries (Figure 102b).

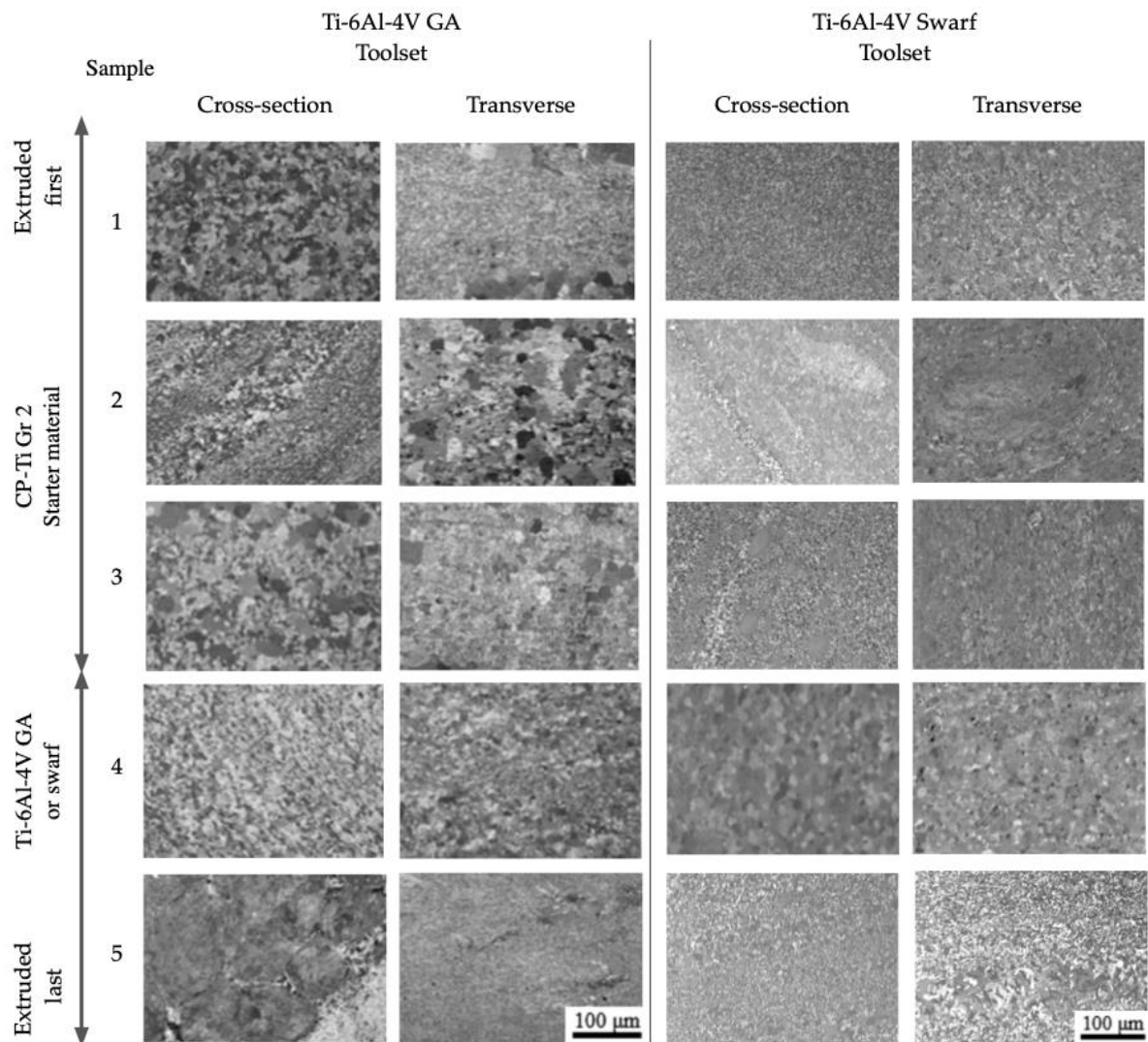


Figure 100 Polarised light micrographs of the extruded wire for both trials. The micrographs are ordered as they exited the Conform™ die, where sample 1 was extruded first and sample 5 last. All micrographs were taken at the same magnification.

Using the sample geometry shown in Figure 96, the room temperature tensile behavior of the Ti-6Al-4V extruded wires was measured at different locations, from the initial extruded wire (sample 1) through to the back end of the extrusion (sample 5). The measured tensile properties for GA powder and swarf derived wires are plotted and compared in Figure 103.

Material taken from the first couple of metres of the extruded Ti-6Al-4V GA wire is made up of CP-Ti Gr 2 (samples 1-3) and has a UTS of 550 ± 40 MPa which is much higher than expected for CP-Ti Gr 2 (340 MPa [ASTM B265-15]) and is closer to the UTS for CP-Ti Gr 4 (shown in Figure 103). There is an early peak in strength for sample 1, which is contrasted with the sample also having very low ductility, 4.8% elongation to failure. As the process continues and heats up the yield strength and UTS initially reduce but ductility improves, correlating with the porosity results shown in Figure 101b. As the process continues, the yield and UTS gradually increase further. For the Ti-6Al-4V swarf trial, all of the initial tensile samples exhibit excellent static strength characteristics when compared with the early samples in the Ti-6Al-4V GA trial with a 64% increase in 0.2% yield strength and 42% increase in UTS. Despite improvements in these properties, the tensile ductility of samples was significantly lower for the swarf trial than the GA trial. This could be attributed to the generally lower grain sizes demonstrated in the microstructure and/or a higher interstitial content in the swarf derived wire compared to the GA derived wire.

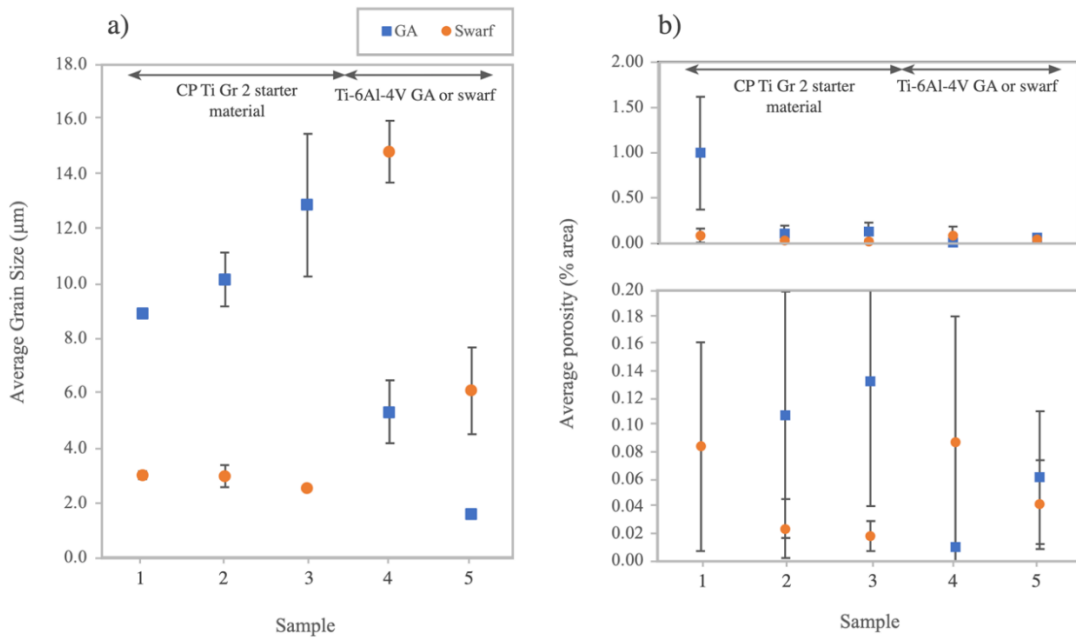


Figure 101 a) Graph showing the change in the average grain size as the trial progresses. b) Graph showing the change in the porosity in the material as the trial progresses.

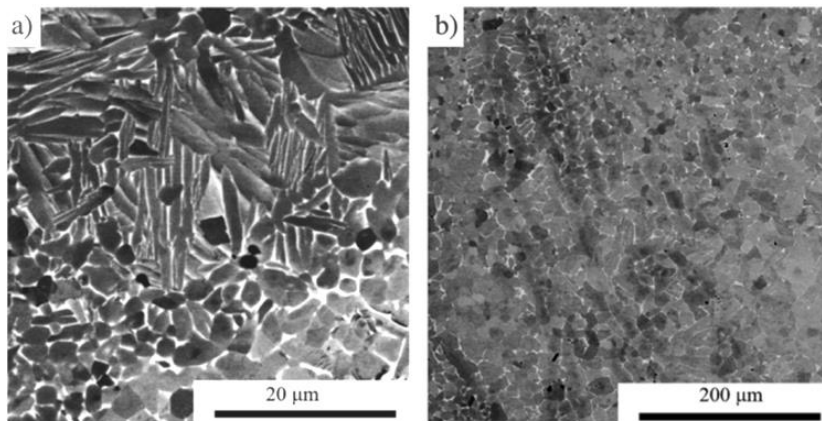


Figure 102 Backscattered electron micrographs of the swarf wire (a) before and (b) after heat treatment of wire containing extruded Ti-6Al-4V swarf.

The Ti-6Al-4V GA wire microhardness shown in Figure 104 exhibited a similar trend to the tensile results with no significant variation between samples extruded early and late in the process. There is also very little difference in the hardness observed across the cross section of the wires. The initial results are taken from the first metre of material where the extrusion has not yet reached steady state. The average hardness falls at 180 ± 20.32 HV1. The later results are lower at 177 ± 12.33 HV1, however, the result is much more consistent. The swarf wire has much larger results overall, with an average hardness of 241 ± 35.2 HV1 in the initially extruded material (2a in Figure 104) and an even greater average of 334 ± 23.9 HV1 for material at the back-end of the extrusion (2b in Figure 104). Any areas in the initially extruded

material with larger values can be attributed to undeformed particles or impurities, which can be seen in the microstructure of sample 1 in Figure 100.

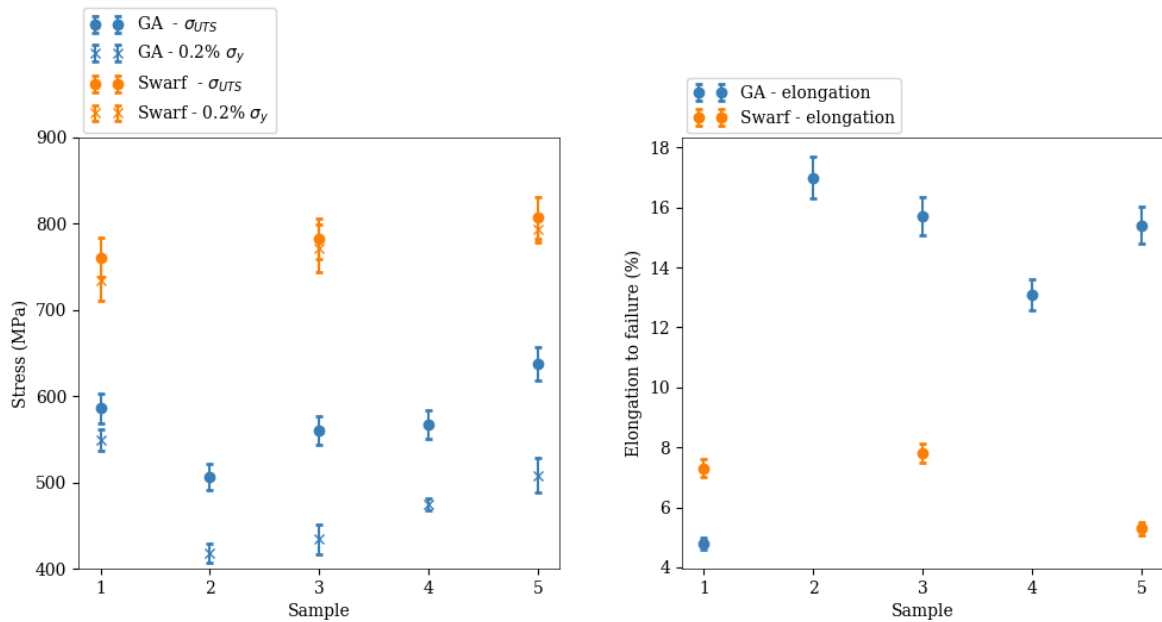


Figure 103 Room temperature tensile mechanical properties for the as-extruded wire produced from the gas atomised and swarf titanium alloy feedstocks.

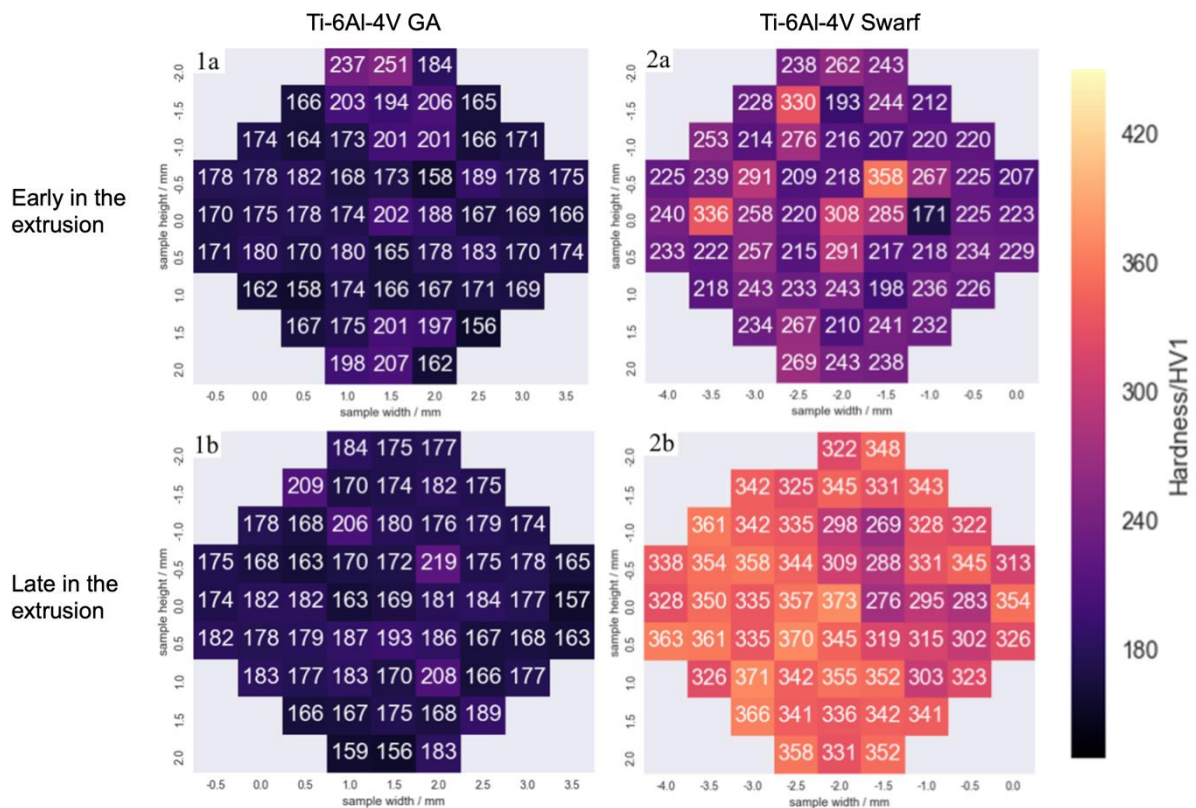


Figure 104 The microhardness of the cross-section material. 1a/b are recorded from the cross-section of the Ti-6Al-4V GA wire and 2a/b are taken from the Ti-6Al-4V swarf wire. a is from the initial extrusion; b is the last material to be extruded during a trial.

11.5.1 Wiredrawing

Conform™ extruded CP-Ti Gr 2 HDH wire from the smaller toolset was cold drawn down into a wire with a 37% reduction in diameter after 3 passes. There is a distinct variation in the grain sizes across the material, with some grains upwards of 50 µm and other less than 10 µm. This is similar to that observed in the parent material. The microstructural evolution during the wiredrawing is shown in Figure 105. There is a clear trend that as the number of passes increase, there is a more homogeneous microstructure. This can be seen in Figure 106, where the grain size increases but the deviation is much smaller.

Previous wire drawing work has established that through equal channel angular drawing (ECAP), it is possible to draw titanium wire with an ultra-fine grained structure [138]. It should be noted that between each pass, there was no heat treatment, which would ultimately result in grain growth. This ultra-fine grained structure had also previously been observed through multiple Conform™ passes followed by rotary swaging [65]. The rotary swaged wire was successfully cold drawn down with an average 29% cross-sectional reduction, giving an overall reduction of ~64% from the initial wire diameter. Although this did not result in an overall reduction in the grain size, there was an improved uniformity of grains, resulting from static recrystallisation during the heat treatments. This recrystallisation has been demonstrated in previous work and it has been shown that at around a 56% reduction, recrystallisation of pure titanium can occur at temperatures of 500°C and above [139].

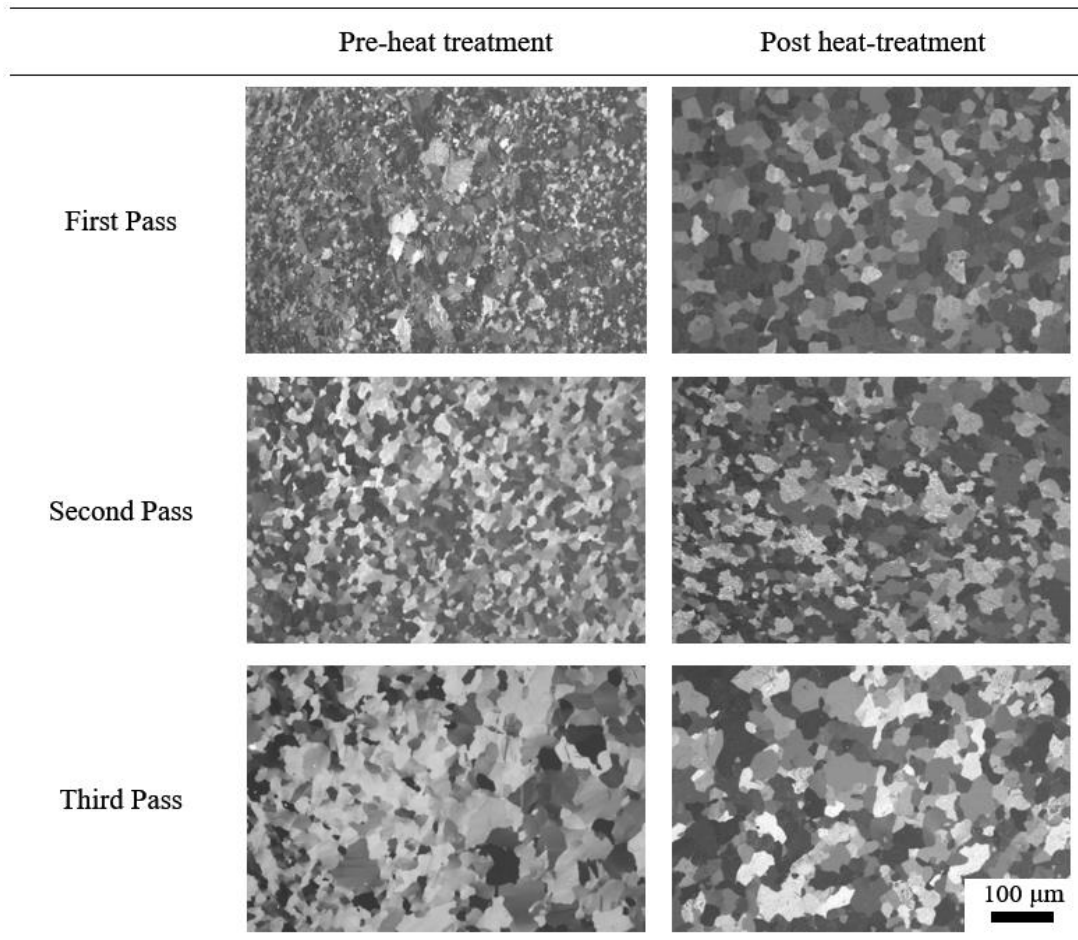


Figure 105 Polarised light micrographs of the cold drawn CP-Ti Gr 2 wire cross section after each pass, before and after heat treatment. The first pass reduction from 5.00 mm to 4.09 mm, second pass 4.09 mm to 3.50 mm and the third pass from 3.50 mm to 3.00 mm.

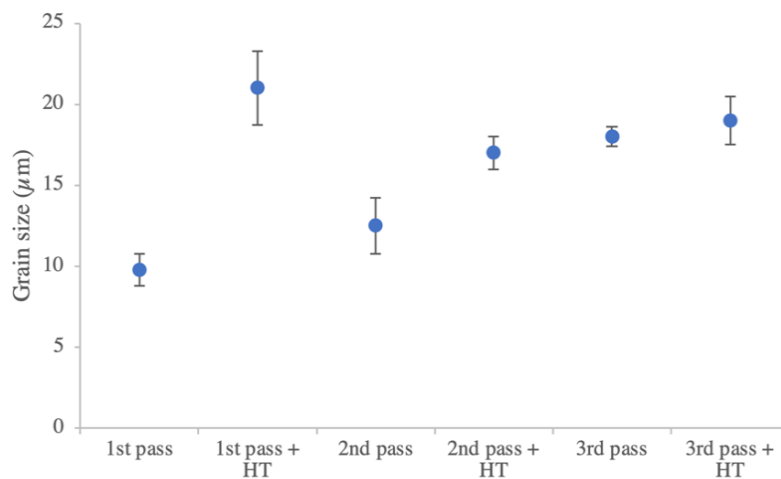


Figure 106 Graph showing the change in the grain size of the cold drawn CP-Ti Gr 2 wire through each of the three drawing passes with intermediate annealing heat treatments (HT).4.

11.6 Discussion

The results presented here show the evolution of three different material throughout two different extrusion trials. Both trials were initiated by extruding CP-Ti Gr 2 HDH powders to heat up the tools and wheel as well as providing suitable back pressure for the following materials of Ti-6Al-4V GA powder and Ti-6Al-4V machining swarf. Samples 1, 2 and 3 were found to be contain 100% CP-Ti Gr 2 as expected from the feedstocks. During this early extrusion phase, tool temperatures are lower (at approx. 600 - 700°C) as the wheel is coated in deformed powder and material builds up above the abutment; here powder or solid material has a relatively long residence time in the tools, allowing powder particles time to bond together and for significant grain growth to occur. Fresh powder that is fed on top of existing consolidated material is incorporated into the bulk, further contributing to the material gripped by the wheel groove, which increases the extrusion pressure.

The reader should be reminded that each trial had a different tool set up and hence different potential extrusion pressures. The larger swarf tooling set had a required extrusion pressure of about 180 MPa lower than that for the gas atomised powder when CP-Ti Gr 2 HDH powder was extruded. For the larger toolset (i.e., swarf trial), it is clear that a far more homogenous extrusion product was generated with the CP-Ti Gr 2 HDH feedstock when compared with the smaller toolset for the gas atomised powder trial. The product was also produced at a steadier state as indicated by the low variation in grain sizes, low porosity and excellent tensile properties presented above. In contrast, the CP-Ti extruded with the smaller toolset exhibited an unsteady product with an increasing average grain size as well as inhomogeneous microstructure. This causes the increased porosity to have a deleterious effect on the tensile properties. In both trials, the CP-Ti grain structure has differed from the material produced in other work. This is of particular interest in the trial that used the larger of the two tool sets where the extruded product had a much higher than expected, yield strength and UTS when compared with the CP-Ti Gr 2 ASTM standard.

The reasons for these observations could stem from the extrusion toolsets, where the design for the GA powder required a higher extrusion pressure and generated higher process temperatures in an attempt to overcome this. This was observed as an ever-increasing abutment temperature during the process when samples 1-3 were produced. A hotter consolidated bulk

metal in the tooling would have a lower flow stress and hence less resistance to extrusion. Fresh powder particles fed in behind this at room temperature would be able to embed themselves into the hotter matrix and pass through the process with minimal deformation as strain would mainly be localised in the hotter, lower strength areas of the product. This shear localisation would generate smaller grains observed in the wire cross section while other, less deformed regions would have primarily experienced grain growth caused by the high local temperatures. This would lead to the observed bimodal equiaxed microstructures being more prominent in samples 1, 2 and 3 from the GA powder trial. In contrast to this, the larger tooling with 10 mm die required lower extrusion pressures and evolved less frictional and adiabatic heat during the extrusion process. This meant that the process was far more stable and more homogeneous deformation occurred through the wire during extrusion.

The outer edge of the wires in both materials were made up of a small oxide layer (< 20 μm thick) and some larger grains up to 80 μm in diameter. These larger grains are in a region subjected to a high degree of shear between extruded material and the die surface, resulting in more deformation and a longer residence time in the tools. These two factors couple together to increase the recrystallisation kinetics of grains around the outside of the wire when compared with the central core.

Once the titanium alloy particulates were poured into the ConformTM machine, there was a sudden change in the wires average grain size from samples 3 to 4. While each of the feedstocks initial grain sizes were different, all were < 10 μm so such differences between samples 3 and 4, 5 cannot solely be down to this factor. It can be seen in the Ti-6Al-4V GA sample 5 cross section that there are some slightly deformed spherical particles embedded in a matrix of secondary material. When a stronger alloy, such as Ti-6Al-4V is fed in behind a softer material, in this case CP-Ti, it is able to embed itself in the matrix and move through the tooling with relative ease. If the new Ti-6Al-4V particles are in the centre of the die flow they undergo minimal deformation and hence the heat of the matrix material and the tooling goes primarily into growing the grains. The stronger alloy also caused extrusion temperatures to increase, from about 700 to 950°C in the case of CP-Ti and Ti-6Al-4V when measured at the abutment. When sample 5 was extruded, as the softer CP-Ti matrix is fed out of the die with an increasing proportion of Ti-6Al-4V behind it, more and more of the wire becomes pure Ti-6Al-4V. When the wire composition is dominated by this second material, a more homogenous

deformation can take place across each of the powder/swarf particles. This causes the more particles to undergo severe plastic deformation and the average grain size to being to reduce as observed for sample 5 in Figure 101a. For these reasons is it clear that not all of the wire in samples 4 and 5 for each trial were 100% Ti-6Al-4V but instead a mixture of CP-Ti and Ti-6Al-4V.5.

11.7 Conclusions

Several metres of 6 mm wire, consisting of CP-Ti Gr 2 HDH and Ti-6Al-4V GA was continuously extruded using ConformTM. As-extruded CP-Ti wire was subsequently cold drawn using a conventional wiredrawing process down to diameters acceptable for conventional wire-arc additive machines. Additionally, several metres of 10 mm wire, consisting of CP-Ti Gr 2 HDH and Ti-6Al-4V swarf was also extruded demonstrating the potential of a recycling process for creating cost-effective feedstock for use in other processes.

The as-extruded material had a fine-grained microstructure, especially as extrusion progresses and a steady state is reached. Once the process has reached the steady state, there was a significant improvement in many of the static mechanical properties as porosity reduced and extrusion temperature and speed became more consistent. There was significant variation in the process and extruded product from the two tooling designs used when extruding CP-Ti Gr 2 HDH powder. The tooling that required a lower extrusion pressure (10 mm die) produced a more homogenous product microstructure due to the process having a more stable thermal history. Despite having a more homogeneous product, the extruded wire from the swarf trial had a poor surface finish and did not consistently have sufficient die filling. As this is preliminary work, it is clear that further work is needed to ensure the production of a consistent, high quality product from the swarf tooling and feedstock.

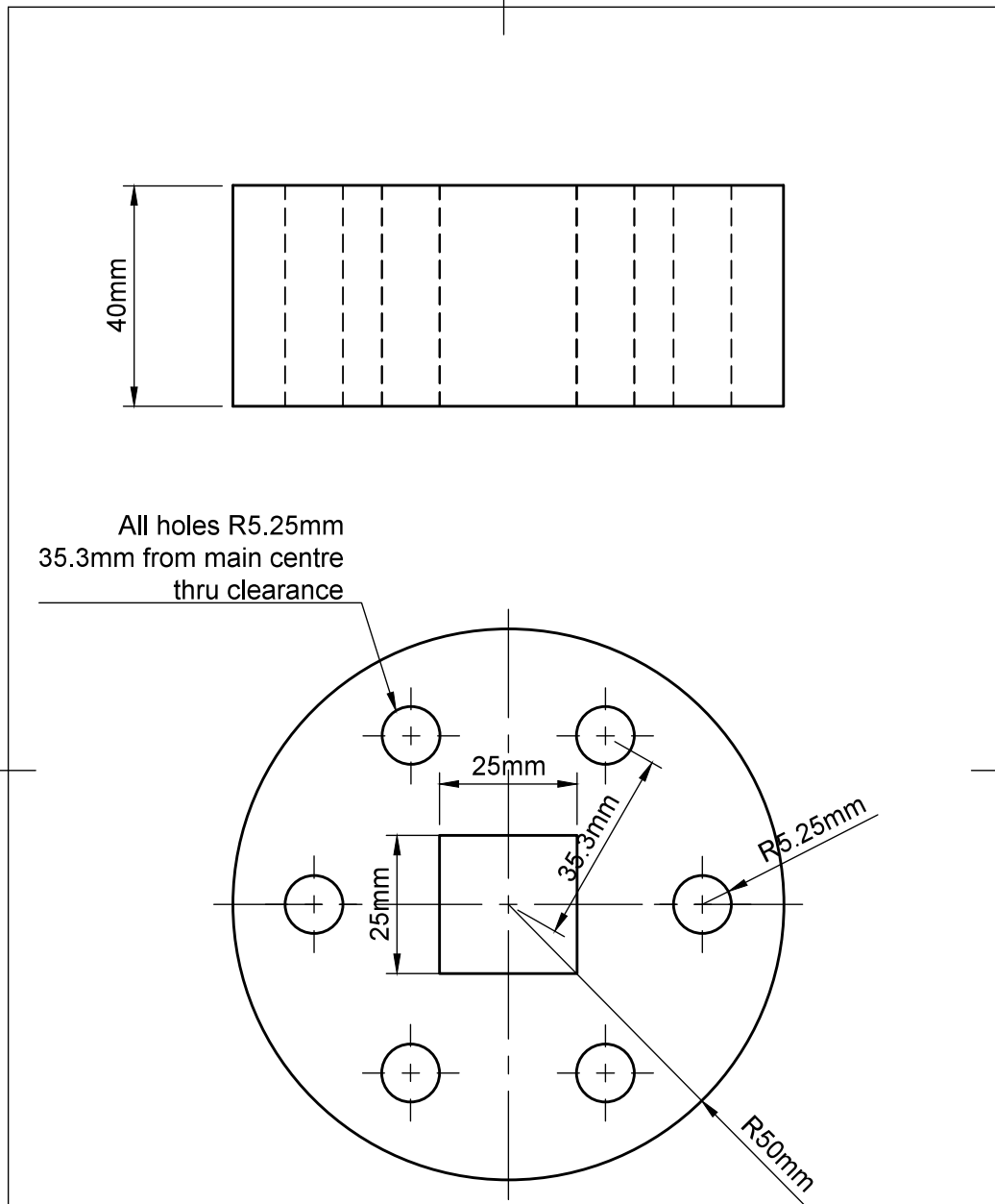
The mechanical performance of the as-Conformed wire and its ability to be cold drawn demonstrates a strong potential for use in wire deposition AM processing. Further work will need to be done to ensure the repeatability of the process and to ensure the chemical purity of the final product, a critical requirement for high quality wire deposition processing. The wire extruded late in the process when the feedstock consisted of purely Ti-6Al-4V (GA powder or swarf) was found to not contain 100% Ti-6Al-4V as expected. It was known that material can

have a long residence time in the Conform™ tooling and can be fed out slowly with fresh material. This was also found to be the case in this work where CP-Ti infiltrated the Ti-6Al-4V wire. While this is not desirable it might be possible to harness this as a method for either in-situ alloying, functionally grading materials or joining dissimilar wire materials. Whilst we have a mixture of CP-Ti and Ti-6Al-4V in the product, it is believed that with extended trial times, a wire consisting of 100% Ti-6Al-4V could be produced. Further work will need to be conducted to improve the wear resistance of abutment materials, in order to extend trial times and extrude longer sections of wire.

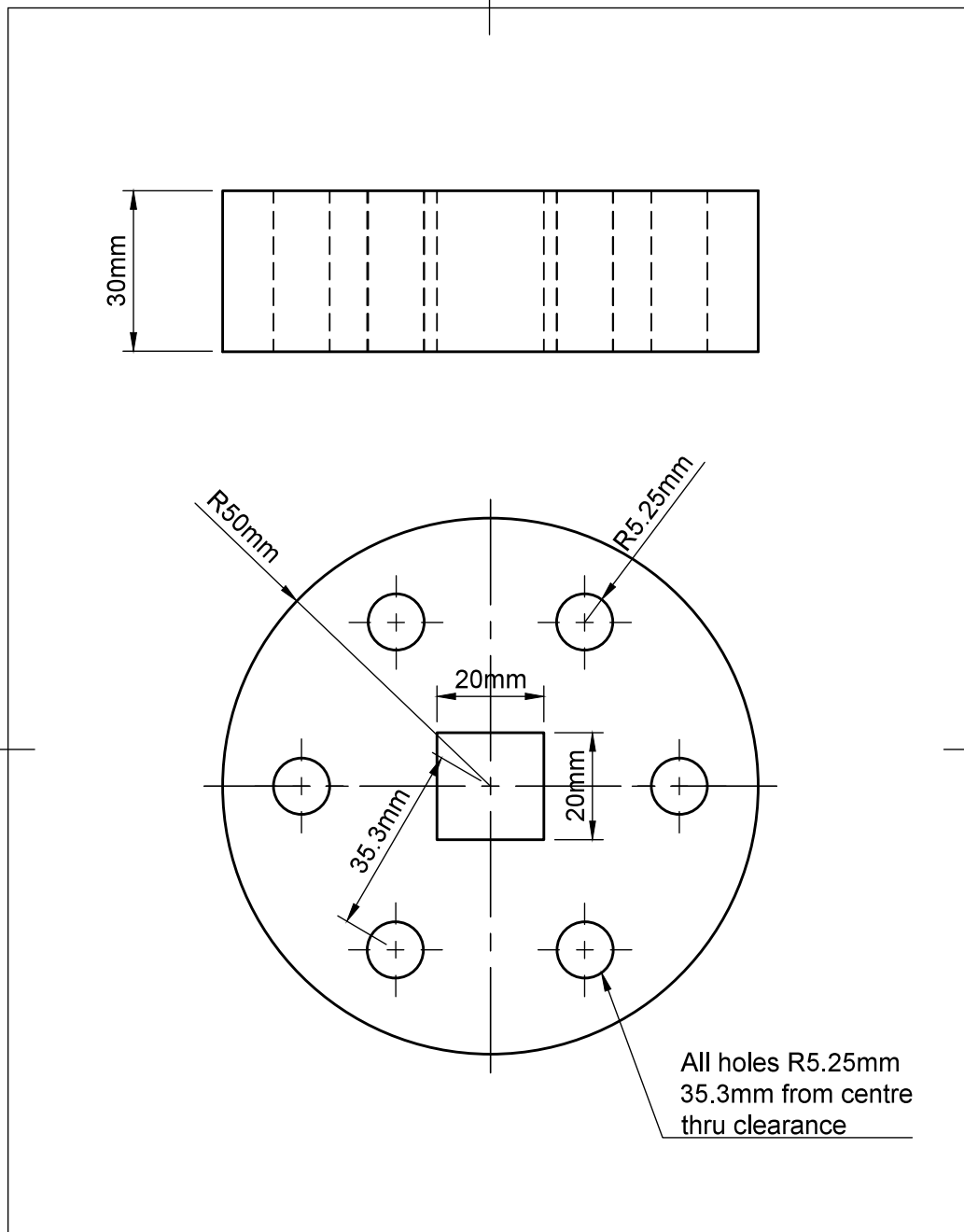
11.8 Acknowledgements

The authors gratefully acknowledge Samuel Robinson and Daniel Suarez Fernandez from the University of Sheffield and Darren Davison, Xin Fang and Kevin Bennett from BWE Ltd. for their technical support during the Conform™ trials. We also acknowledge Benoit Marguet from Airbus Ltd. and Jeff Bernath (formerly of Arconic) for additional funding and for supply of titanium feedstocks.

Appendix 2 CAD Drawings – ASP Tools



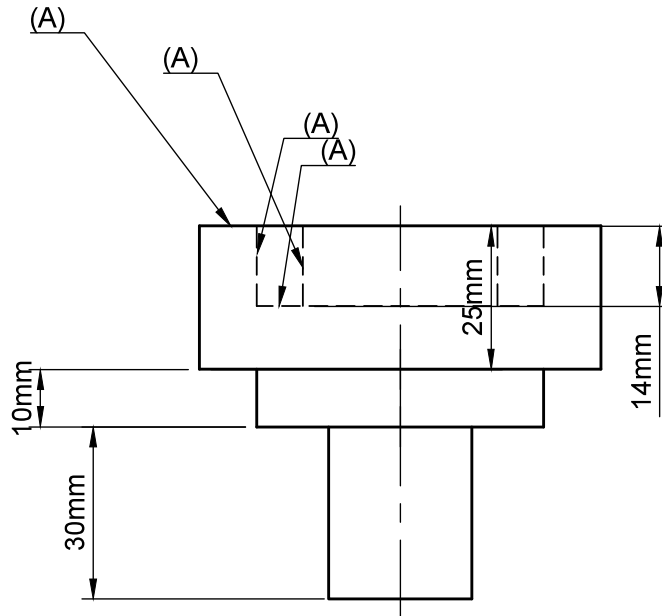
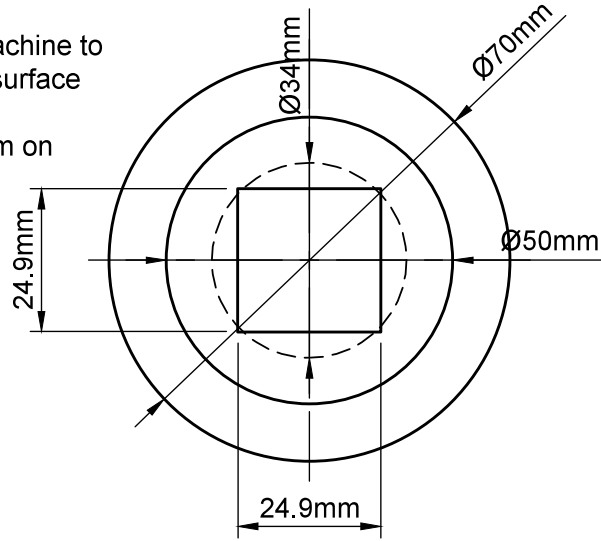
| | | | |
|----------------------------|--------------------------------|---|----------------------------------|
| Dept. Materials Science | Technical reference Science | Created by Ben Thomas 26/02/2016 | Approved by |
| | | Document type | Document status |
| | | Title ASP Shear Tool Bottom adapter | DWG No. |
| | | Rev. 1 | Date of issue Sheet 1 of 1 |



All holes R5.25mm
35.3mm from centre
thru clearance

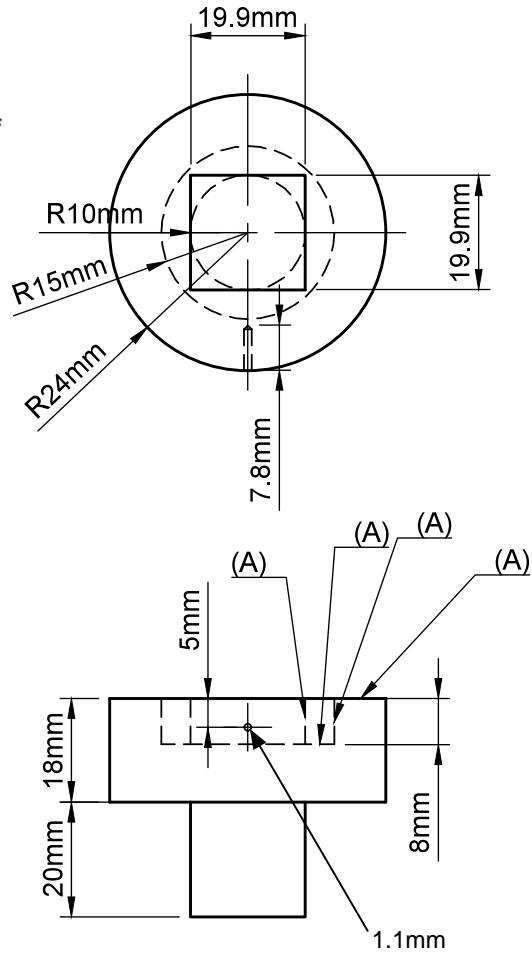
| | | | |
|-----------------------------------|---------------------|---|------------------------------------|
| Dept. Materials Science | Technical reference | Created by Ben Thomas 18/04/2016 | Approved by |
| | | Document type | Document status Final |
| | | Title ASP Shear Tools Bottom Adapter v2 | DWG No. |
| | | Rev. 2 | Date of issue 18/04/2016 |
| | | | Sheet 1 of 1 |

- Rough machined
- Hardened to 38HRC
- Finish machine to achieve surface finish of $Ra=1.6\mu m$ on faces (A)

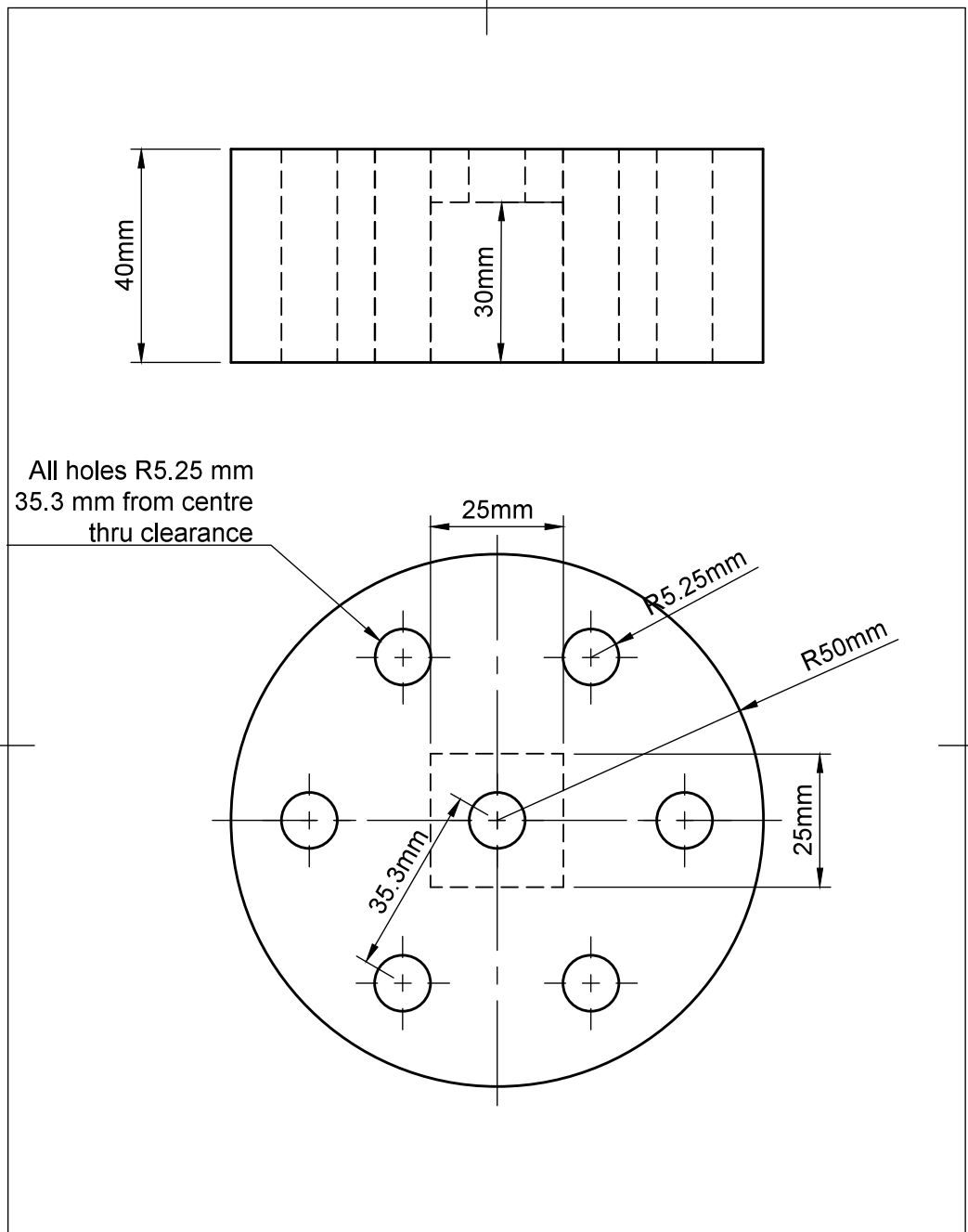


| | | | |
|----------------------------|---------------------|---|----------------------------------|
| Dept. Materials Science | Technical reference | Created by Ben Thomas 26/02/2016 | Approved by |
| | | Document type | Document status |
| | | Title ASP Shear Tools Bottom Tool | DWG No. |
| | | Rev. 1 | Date of issue Sheet 1 of 1 |

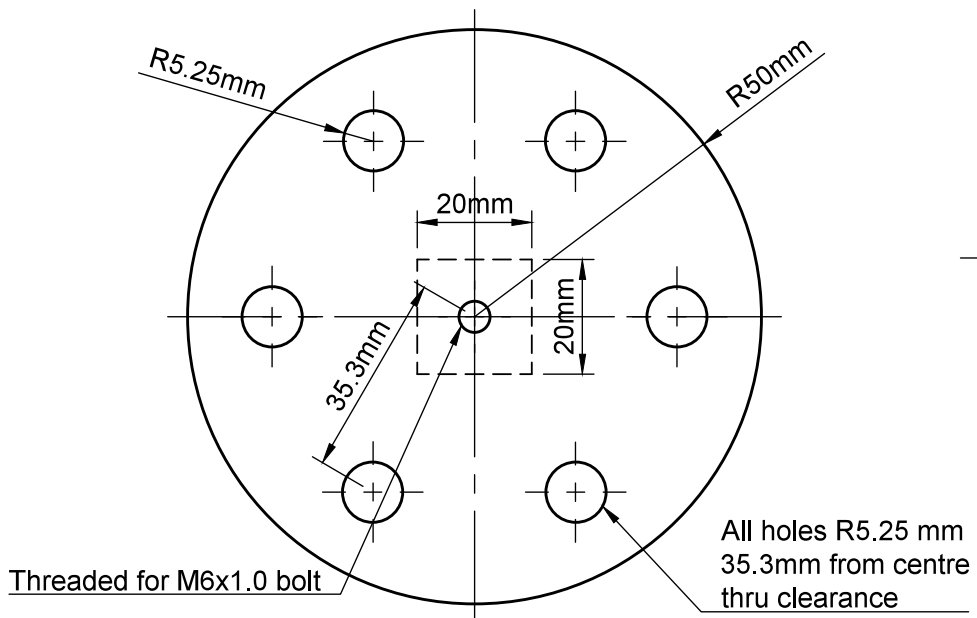
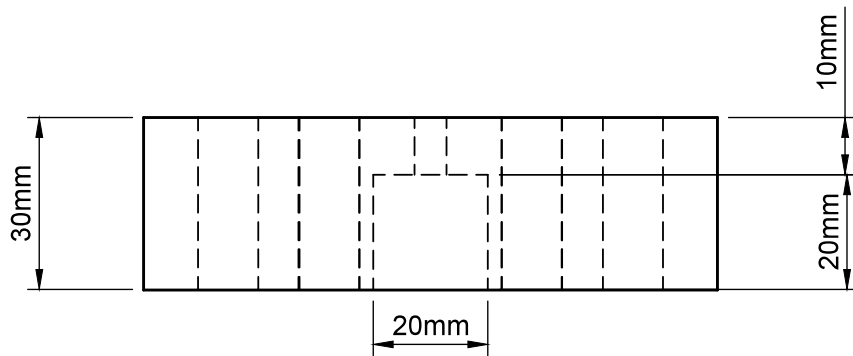
- Rough machined
- Hardened to 45 HRC
- Finish machined to achieve desired surface finish of $1.6\mu\text{m}$ on all faces marked (A)



| | | | |
|-----------------------------------|---------------------|--|------------------------------------|
| Dept. Materials Science | Technical reference | Created by Ben Thomas 18/04/2016 | Approved by |
| | | Document type | Document status Final |
| | | Title ASP Shear Tools Bottom tool v2 | DWG No. |
| | | Rev. 2 | Date of issue 18/04/2016 |
| | | | Sheet 1 of 1 |

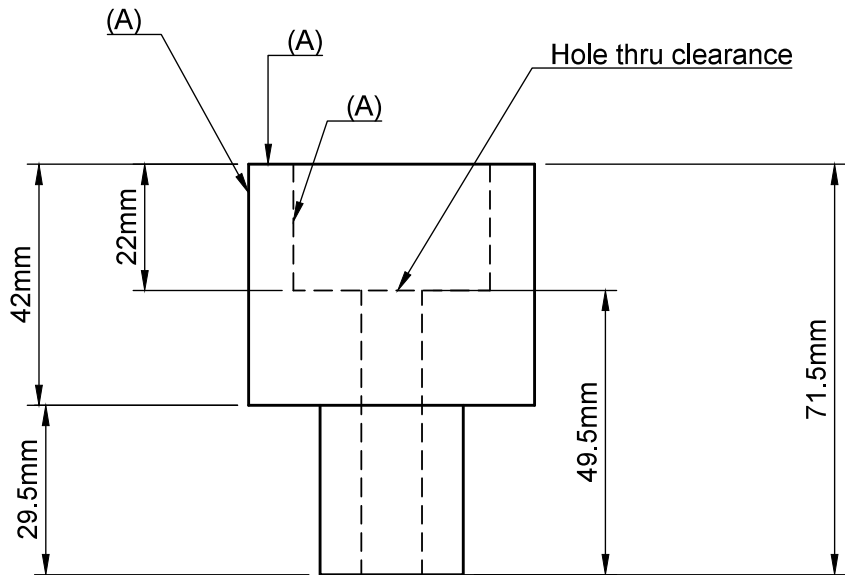
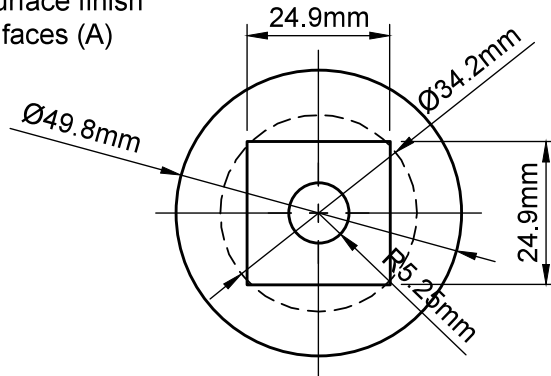


| | | | |
|-----------------------------------|---------------------|---|---|
| Dept. Materials Science | Technical reference | Created by Ben Thomas 26/02/2016 | Approved by |
| | | Document type | Document status |
| | | Title ASP Shear Tools Top adapter | DWG No. |
| | | Rev. 1 | Date of issue Sheet 1 of 1 |



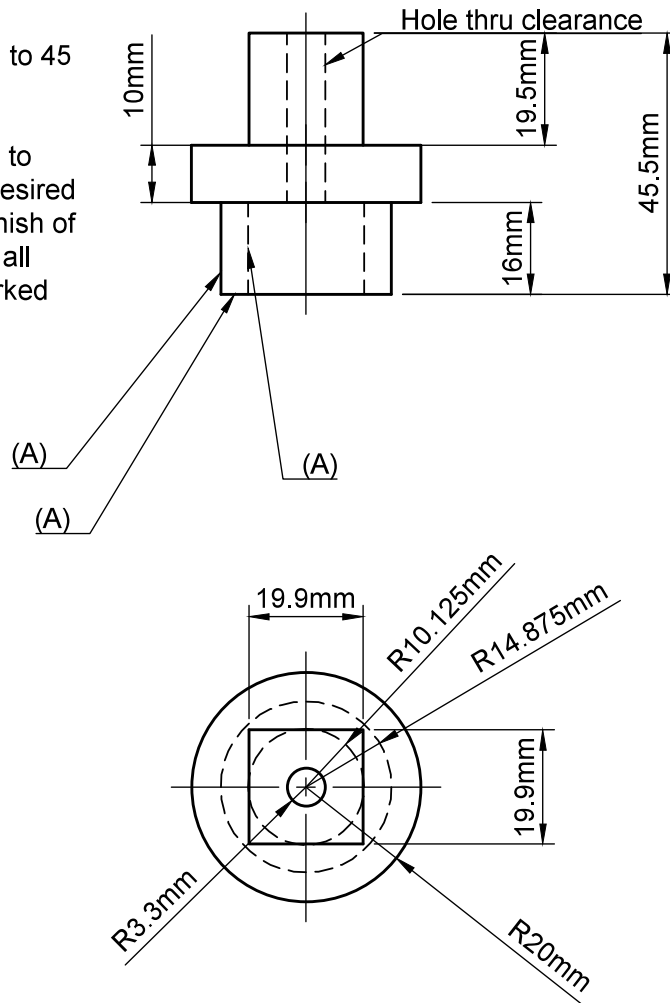
| | | | |
|-----------------------------------|---------------------|---|------------------------------------|
| Dept. Materials Science | Technical reference | Created by Ben Thomas 18/04/2016 | Approved by |
| | | Document type | Document status Final |
| | | Title ASP Shear Tools Top Adapter | DWG No. |
| | | Rev. 2 | Date of issue 18/04/2016 |
| | | | Sheet 1 of 1 |

- Rough machined
- Hardened 38HRC
- Finish machine to achieve desired surface finish 1.6µm on faces (A)



| | | | |
|-----------------------------------|---------------------|--|---|
| Dept. Materials Science | Technical reference | Created by Ben Thomas 26/02/2016 | Approved by |
| | | Document type | Document status |
| | | Title ASP Shear Tools Top tool | DWG No. |
| | | Rev. 1 | Date of issue Sheet 1 of 1 |

- Rough machined
- Hardened to 45 HRC
- Finish machined to achieve desired surface finish of $1.6\mu\text{m}$ on all faces marked (A)



| | | | |
|-----------------------------------|---------------------|---|------------------------------------|
| Dept. Materials Science | Technical reference | Created by Ben Thomas 09/05/2016 | Approved by |
| | | Document type | Document status Final |
| | | Title ASP Shear tools Top tool v2 | DWG No. |
| | | Rev. 2 | Date of issue 18/04/2016 |
| | | | Sheet 1 of 1 |